Multifunctional Self-Healing Hydrogels Based on Natural Polymers for Biomedical Applications

by

Weijuan Huang

A thesis submitted in partial fulfillment of the requirements for the degree of

Doctor of Philosophy

in

Food Science and Technology

Department of Agricultural, Food & Nutritional Science
University of Alberta

Abstract

Hydrogel is a chemically or physically cross-linked hydrophilic three-dimensional (3D) polymer network. Classic hydrogels with irreversibly cross-linked polymer networks cannot heal after rupture, leading to degradation and deterioration in their functions over time. In contrast, self-healing hydrogels could be spontaneously restored after damage, which could extend the longevity. Because self-healing hydrogels from synthetic chemicals generate environmental issues, self-healing hydrogels from natural polymers would be more desirable. Chitosan is a cationic polysaccharide derived from the partial deacetylation of chitin, which is the main constituent of exoskeleton of crustaceans (e.g. shrimp, lobster, crayfish, and crab) and is the second abundant natural polysaccharide after cellulose on the earth. Besides its abundance, chitosan also possesses many superior physicochemical and biological properties, which is the ideal precursor to fabricate hydrogels. One major challenge is that self-healing hydrogels based on reversible interactions usually exhibit poor mechanical properties and slow self-healing process. In addition, most self-healing hydrogels could only heal under harsh conditions such as high temperature and low pH. Consequently, there is a demand for the development of new natural polymers-based self-healing hydrogels, which could quickly self-heal under physiological conditions and possess good mechanical strength.

This research developed carboxymethyl chitosan (CMC) based self-healing hydrogels by crosslinking with benzaldehyde-terminated four-arm polyethylene glycol (PEG-BA) and dialdehyde cellulose nanocrystals (DACNC). Both the CMC/PEG-BA and CMC/DACNC hydrogels exhibited good mechanical strength and rapidly healed within 5 min at room temperature without external stimuli. Afterwards, a second network crosslinked through covalent bonds were introduced to the chitosan based self-healing network to increase their stretchability and toughness.

Furthermore, chitosan were grafted with catechol moieties and crosslinked with DACNC to construct self-healing hydrogels with bioadhesive capacity. The three-dimensional (3D) cell encapsulation demonstrated that the hydrogel possessed excellent cytocompatibility and could be used for 3D cell culture. *In vivo* tests indicated that the hydrogels could be employed as non-compressive hemostatic material and be injected to internal tissues (e.g. liver) to rapidly and effectively stop massive hemorrhage. In addition, the self-healing hydrogels could be precisely injected to irregular and deep injuries to fully cover the wound beds, and then be painlessly removed by on-demand dissolving using amino acid solution, which prevented complex surgical procedures. The self-healing hydrogels have been used as deep partial thickness burn wound dressing to facilitate burn healing with reduced scar formation.

This research opens up novel pathways to fabricate self-healing hydrogels with desired properties including facile to prepare and use, rapid self-healing, high mechanical strength and strong tissue adhesive capacity. These benefits support their potential applications in biomedical field, such as 3D cell encapsulation, hemostasis and wound healing.

Preface

This dissertation is an original work by Weijuan Huang under the supervision of Prof. Lingyun Chen.

Chapter 3 of this thesis has been published as **Weijuan Huang**, Yixiang Wang, Yun Chen, Yanteng Zhao, Qiang Zhang, Xiang Zheng, Lingyun Chen*, Lina Zhang. Strong and Rapidly Self-healing Hydrogels: Potential Hemostatic Materials. ***Advanced Healthcare Materials***, 2016, 5, 2813–2822. In this chapter, I designed and conducted majority of the experiments, analyzed the data and wrote the manuscript. Assistance was received from Dr. Yixiang Wang and Prof. Lina Zhang in designing the experiments and revising the manuscript. The *in vivo* tests were conducted at Wuhan University led by Prof. Yun Chen, together with Dr. Yanteng Zhao, and Qiang Zhang. Prof. Lingyun Chen was the supervisory author and contributed to the experimental design, data discussion, manuscript composition, submission and revisions.

Chapter 4 of this thesis has been published as **Weijuan Huang**, Yixiang Wang, Zhiqiang Huang, Xiaolan Wang, Lingyun Chen*, Yu Zhang, Lina Zhang. On-Demand Dissolvable Self-Healing Hydrogel Based on Carboxymethyl Chitosan and Cellulose Nanocrystal for Deep Partial Thickness Burn Wound Healing. ***ACS Applied Materials & Interfaces***. 2018, 10 (48), 41076–41088. In this chapter, I designed and conducted majority of experiments, analyzed the data and wrote the manuscript. Assistance was received from Dr. Yixiang Wang in conducting the rheology testing as well as revising the manuscript. The *in vivo* tests were conducted at South China University of Technology led by Dr. Yu Zhang, together with Zhiqiang Huang, and Xiaolan Wang. Prof. Lina Zhang assisted with the synthesis of modified cellulose nanocrystals and contributed to manuscript edits. Prof. Lingyun Chen was the supervisory author and contributed to the experimental design, data discussion, manuscript composition, submission and revisions.

Chapter 5 of this thesis has been submitted as Weijuan Huang, Yixiang Wang, Lynn M. McMullen, Mark T. McDermott, Hongbing Deng, Yumin Du, Lingyun Chen*, Lina Zhang, Stretchable and Tough Nanocomposite Hydrogels with Excellent Self-Recovery and Cytocompatibility. In this chapter, my primary responsibility was to design experiments, collect and analyze data, as well as to write the manuscript. Prof. Lynn M. McMullen and Prof. Mark T. McDermott were my supervisory committee members and were involved with research design and manuscript edits. Dr. Yixiang Wang and Prof. Lina Zhang guided the test of mechanical properties, and they also both contributed to manuscript review and revisions. Prof. Hongbing Deng and Prof. Yumin Du helped with the synthesis of modified chitosan. Prof. Lingyun Chen was the supervisory author and contributed to the experimental design, data discussion, manuscript composition, submission and revisions.

Another manuscript was generated based on the data in **Chapter 6**. In this chapter, I was responsible for experimental design, data collection and analysis, as well as manuscript composition. Prof. Lingyun Chen was the supervisory author and contributed to the experimental design, data discussion, manuscript composition, and revisions.

Acknowledgements

I feel incredibly lucky to have Dr. Lingyun Chen as my Ph.D. supervisor at the University of Alberta and I am deeply grateful to her. I truly enjoyed working with Dr. Chen. She always encouraged me to try some new ideas and offered a lot of support. Particularly, I appreciated her training in academic writing and communication skills. Thanks to her guidance and patience, I could be a better scientist. I would also like to thank my supervisory committee members Dr. Lynn M. McMullen and Dr. Mark T. McDermott for their excellent suggestions to my research project at every committee meeting. I sincerely thank Dr. Yun Chen (Wuhan University, China) and Dr. Yu Zhang (South China University of Technology, China) for their help and support in the *in vivo* tests.

I would also like to thank all the past and present members in the laboratory. It is because of them that I've had such a great life during my Ph.D. study. I really appreciate all the time we worked together. My special gratitude gives to Dr. Yixiang Wang for his assistance in designing and conducting experiments as well as academic writing. His attitude toward research has significant effect on me.

Last but not least, I want to express the depth of my gratitude to my family. It is their unconditional love and support that encourage me to start the Ph.D. study and hold on straight to the end. They are the best parents anyone could ever ask for. I couldn't have finished my study without them.

This whole journey has made me into something different, but a better version of myself.

Table of Contents

List of Tables

List of Figures

List of Abbreviations

Abbreviation	Full name
AAm	Acrylamide
APS	Ammonium persulfate
CHI-C	Catechol-conjugated chitosan
CMC	Carboxymethyl chitosan
CNC	Cellulose nanocrystal
CS	Chitosan
DACNC	Dialdehyde modified cellulose nanocrystal
DCC	*N, N'*-Dicyclohexylcarbodiimide
DMAP	4-(Dimethylamino)pyridine
DN	Double network
DPBS	Dulbecco's phosphate buffered saline
EDC	*N*-(3-Dimethylaminopropyl)-*N'*-ethylcarbodiimide hydrochloride
FDA	Fluorescein diacetate
FE-SEM	Field emission scanning electron microscopy
FT-IR	Fourier transform infrared spectrometer
G'	Storage modulus
G''	Loss modulus
HCA	Hydrocaffeic acid or 3-(3,4-Dihydroxyphenyl) propionic acid
^{1}H NMR	Proton nuclear magnetic resonance spectrometer
MBAA	*N, N'*-Methylenebis (acrylamide)
MTT	Thiazolyl blue tetrazolium bromide
NHS	*N*-Hydroxysuccinimide
PAAm	Polyacrylamide
PEG	Polyethylene glycol
PEG-BA	Benzaldehyde-terminated telechelic four-armed polyethylene glycol
PI	Propidium iodide
TEM	Transmission electrical microscopy
TEMED	Tetramethyl-ethylenediamine
THF	Tetraphydrofuran
TNBSA	2, 4, 6-Trinitrobenzenesulfonic acid or Picrylsulfonic acid
XRD	X-ray diffractometer

Chapter 1

Introduction, Research Hypotheses and Objectives

1.1 Introduction

1.1.1 Self-healing hydrogels

Hydrogels are chemically or physically cross-linked hydrophilic three-dimensional (3D) polymer networks. Nowadays, the synthetic methods to fabricate hydrogels have been extensively investigated and current hydrogels have exhibited excellent properties such as ultrahigh mechanical strength,[1-3] stimuli-responsiveness,[4-5] biocompatibility,[6] and biomimetic.[7] However, the classic hydrogels with irreversibly cross-linked polymer networks are unable to heal after rupture, leading to degradation and deterioration in their functions over time and shortened lifetime.[8] In contrast, self-healing hydrogels have emerged as a novel type of hydrogels whose mechanical integrity and functions could be autonomously restored after physical damage, which could extend the longevity and increase the durability of the hydrogels.[9-11] The formation of self-healing hydrogels relies on reversible interactions, which refers to spontaneous formation of new interactions when old crosslinks are broken within a hydrogel network, endowing self-healing capacity (**Figure 1-1**).

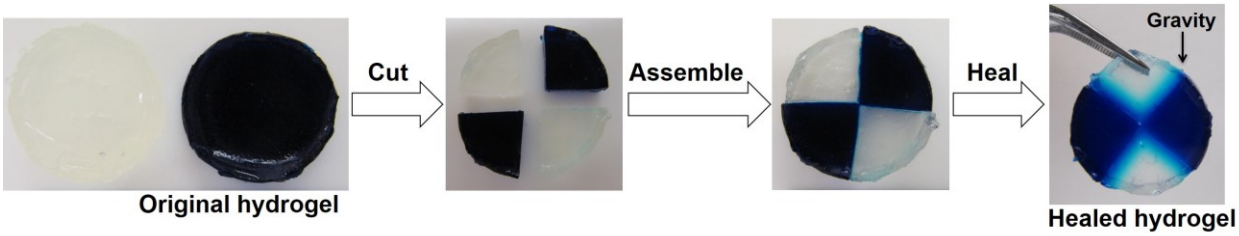

Figure 1-1. Pictures of self-healing hydrogel.

Over the past decade, self-healing hydrogels have rapidly gained in popularity due to their great potential in diverse fields with promise in biomedical engineering. Research trends for self-healing hydrogels have shifted from extrinsic healing to intrinsic healing, from synthesized polymers to natural polymers, from weak hydrogels to robust elastomers, and from toxic hydrogels to biocompatible hydrogels in order to improve the user experience.[12] Many strategies have been explored to synthesize new self-healing hydrogels, especially rapid self-healing hydrogels. The quicker the self-healing occurs, the better it is in most cases. For applications in regenerative medicine, self-healing hydrogels could respond to cell-induced stress by rapidly breaking and reforming bonds. Such systems prompt complex cellular functions, while maintaining the overall mechanical environment. Cell spreading, proliferation, and osteogenic differentiation of mesenchymal stem cells were improved in hydrogels with high self-healing efficiency.[13-14] The efficient self-healing is driven by the mobility of polymer chains and the reversible nature of dynamic interactions,[15] which results in poor mechanical properties as hydrogels with high stiffness are commonly held together by strong and stable interactions.[16]. The application of the self-healing hydrogels is often severely limited by their mechanical behavior. Therefore, self-healing hydrogels often exhibit a trade-off between mechanical strength and self-healing efficiency. The development of a mechanically robust hydrogel with rapid self-healing under facile conditions is yet to be fully realized. Although several studies have been carried out to improve the mechanical strength of self-healing hydrogels, the complicated materials synthesis and gel formation process, as well as harsh healing conditions limit their development and application. Thus, it is required to fabricate strong self-healing hydrogels that exhibit high self-healing capacity at neutral pH and ambient temperature without any external stimuli for biomedical applications.

1.1.2 Adhesive self-healing hydrogels

Tissue adhesive property is important for practical applications of self-healing hydrogels as biomedical materials such as for implantation and hemostasis. Most reported self-healing hydrogels usually lack wet tissue adhesive capacity for effective localization of transplanted cells *in vivo* and flow around due to tissues and cells actions, which may result in inflammation or damage of surrounding tissues.[17] Moreover, self-healing hydrogels with poor tissue adhesion cannot be fixed with the surrounding tissues during surgical operation.[18] There is significant need for effective medical adhesives that function reliably on wet tissue surfaces. However, currently approved commercial adhesives (e.g. fibrin glues, cyanoacrylate glues) suffer from many limitations, such as poor adhesion in the presence of biological fluids, sensitization and allergic response, and inflammation.[19]

Given the shortage and poor biocompatibility of synthetic adhesives for wet tissue surfaces, extensive effort has been directed to developing adhesives derived from nature. Marine mussels can tightly adhere onto various substrates under high-flow, wet, and saline conditions because of 3,4-dihydroxy-L-phenylalanine (DOPA).[20-21] The functional group on DOPA is catechol, which is prone to be chemically or enzymatically oxidized to quinone. Quinone is highly reactive with diverse functional groups including thiol, amine, and imidazole on tissue surface via Michael-type additions and Schiff-base reactions.[22] Recently, it has been reported that mussel-inspired catechol moieties conjugated polymers have significant potential in biomedical applications as tissue adhesive, sealant, and drug delivery carrier.[23] Lee et al synthesized a catechol-conjugated hyaluronic acid (HA-CA) and developed a HA-CA based tissue adhesive hydrogel via oxidative crosslinking.[24] The adhesiveness of HA-CA hydrogel allowed the cell-laden hydrogel to simply be painted directly onto tissues. The hydrogel was easily deposited onto liver and heart surfaces

and adhered well to the tissues even after one month. The hydrogel exhibited great therapeutic and regenerative capacity of transplanted cells for angiogenesis and hepatic function. Most previously reported mussel-inspired hydrogels were formed through oxidation or metal chelation, but the toxicity of oxidants (e.g. $NaIO_4$) and metals (e.g. Fe^{3+}) might be a serious concern for biomedical applications. In addition, rapid formation of a strong bond on the tissue is another essential requirement for tissue adhesives. It remains a major challenge to develop a hydrogel with both excellent self-healing ability and strong tissue adhesive capacity, which at the same time is non-toxic and biocompatible.

1.1.3 Chitosan and chitosan derivatives

Given the concerns over environmental protection and sustainable development, more attention has been paid to naturally occurring polymers. Application of renewable polymers for production of new materials can have both economic and environmental benefits. Biopolymers, such as chitosan and cellulose, have been applied to fabricate self-healing hydrogels.[16, 25-26]

Chitosan is a cationic polysaccharide derived from the partial deacetylation of chitin, which is the main constituent of exoskeleton of crustaceans (e.g. shrimp, lobster, crayfish, and crab) and is the second abundant natural polysaccharide after cellulose on the earth. Chitosan is a linear copolymer, consisting of (1-4)-linked D-glucosamine and N-acetyl-D-glucosamine (**Figure 1-2**).[27] Chitosan possesses many superior physicochemical and biological properties, such as abundant amino groups, biocompatibility, biodegradability, as well as mucoadhesive, antibacterial, and hemostatic ability. Therefore, it has been widely applied in biomedical fields, including drug/cell/gene delivery, hemostasis, wound healing, and tissue engineering.[28-31] Currently, chitosan-based hemostatic materials and wound healing dressings (e.g. Celox™, HemCon®) have been widely

applied in clinic. Chitosan is a promising candidate to construct self-healing hydrogels based on Schiff-based linkages owing to the abundant amino groups on its backbone.[25, 32]

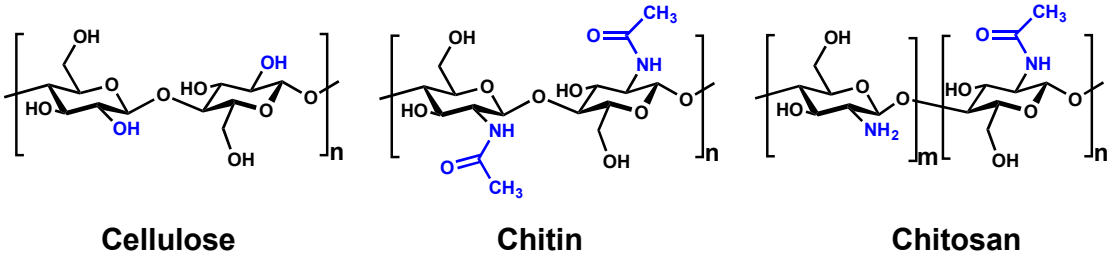

Figure 1-2. Chemical structures of cellulose, chitin and chitosan.

One major drawback of chitosan is its poor solubility in neutral solutions due to its semicrystalline nature, as a result of inter- and intra-molecular hydrogel bonds.[33-34] The insolubility of chitosan in aqueous solution at pH > 6 restricts its potential applications in biomedical fields. To address this problem, various hydrophilic moieties have been grafted to the chitosan backbone to synthesize chitosan derivatives with improved solubility in neutral water for more desired properties and wide applications. Generally, chitosan carries two types of reactive functional groups, namely an amino group at C(2) positions, and primary and secondary hydroxyl groups at the C(3) and C(6) positions, respectively.[35] These groups allow introduction of various functional groups to chitosan, such as carboxymethyl, carboxyethyl, quaternary ammonium salt, and catechol moieties.

Carboxymethylation of chitosan (**Figure 1-3**a) is a very attractive method among the various chemical modifications due to the introduction of active carboxyl groups (-COOH) into the molecules. Carboxymethyl chitosan (CMC) is an amphiprotic ether derivative with carboxyl groups and amino groups in the molecule. The introduction of carboxymethyl groups with negative charges to chitosan reduced the positive charged amino groups and affected the isoelectric point of chitosan. Moreover, the degree of carboxymethylation and grafting sites (*N, O*-

carboxymethylated chitosan and *O*-carboxymethylated chitosan) could be controlled by adjusting the modifying conditions.[36] Furthermore, CMC is non-toxic and biocompatible as chitosan. Therefore, hydrogel/film/nanoparticles made from CMC have been widely used as drug/cell carrier and wound healing dressing.[37-40] Not only does the CMC dissolve in neutral aqueous system, but also the abundant amino groups remained for crosslinking. In spite of the progress made by other researchers, at this moment, the research on CMC-based self-healing hydrogel is still very limited.

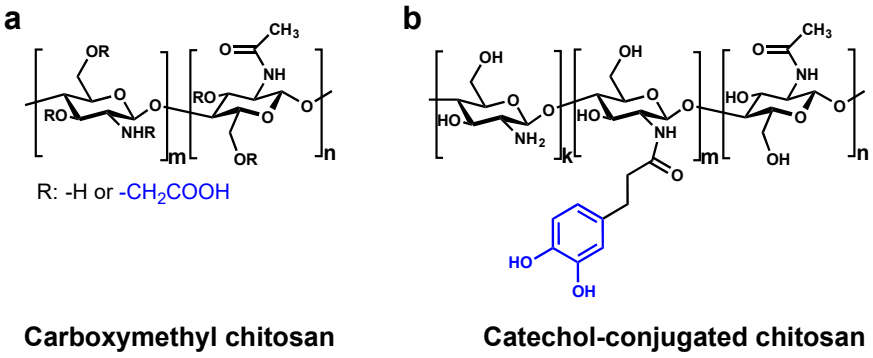

Figure 1-3. Chemical structure of (a) carboxymethyl chitosan and (b) catechol-conjugated chitosan.

Chitosan has bio-adhesive ability owing to its cationic nature, which provides strong electrostatic interaction with negatively charged components of tissue surface (e.g. mucosa).[41] However, its limited tissue adhesive strength and poor water-solubility at neutral system restrict its application. Mussels demonstrate robust wet-resistant adhesion due to abundant catecholamine in mussel adhesive proteins.[42-44] Inspired from adhesion behaviors of mussel, Lee group developed a chitosan derivative that possessed both excellent solubility in neutral pH solutions and strong adhesiveness on tissue surfaces by introducing catechol moieties to chitosan backbone.[45-48] Catechol-conjugated chitosan (**Figure 1-3**b) demonstrates tissue adhesion due to covalent

reactions of oxidized catechol groups with diverse nucleophiles (e.g. amine, thiol, and imidazole groups) present on tissue surface.[24] The amino groups and catechol moieties have synergistic effect for wet-resistant adhesion via covalent/non-covalent interactions.[46, 49] Therefore, biocompatible catechol-conjugated chitosan is a promising adhesive polymer to fabricate wound healing patches, tissue sealants, and hemostatic materials for biomedical applications.[46] It would be interesting to introduce catechol-conjugated chitosan into self-healing hydrogels to enable the bio-adhesive properties to broaden their applications. However, such system has been seldom reported in previous work.

1.1.4 Cellulose and cellulose nanocrystal

Over the past few decades, materials derived from bio-based resources instead of fossil fuel-based polymers are gaining attention both in industry and academia owing to their minimized impacts on ecosystems and environment. Among various natural materials, cellulose, the most abundant biopolymer available on the earth, has drawn much attention thanks to its superior properties, such as abundance, versatility, renewability, sustainability, and biocompatibility.[50-51] Cellulose is ubiquitous and takes up about 1.5 trillion tons of total annual biomass productions.[52] Cellulose mainly comes from plants, especially wood and cotton. Apart from plants, cellulose can also be obtained from a wide range of living species, such as algae, fungi, bacteria, and even in some sea animals like tunicates.[51, 53] Cellulose is composed of several hundreds to thousands of linear glucose molecules linked through β (1→4) glycolsidic bonds (**Figure 1-2**).[54] Cellulose fibers with hierarchical structure contain both amorphous and crystalline structures, which can be broken down to nanoscale building blocks through either strong acid hydrolysis or oxidation.[50] The strong acid hydrolysis removes the amorphous regions of cellulose fibers and produces cellulose nanocrystals (CNCs). Natural fibers consist of three major components, including cellulose,

hemicellulose, and lignin.[55] It is impossible to obtain the completely pure cellulose, and the residual hemicellulose and lignin have impacts on the properties and applications of CNCs.[56] The purification of cellulose and hydrolysis conditions affect the morphology, crystallinity, and thermal stability of CNCs. Sulfuric and hydrochloric acids are commonly used in the hydrolysis process. Sulfuric acid hydrolysis brings about abundant negatively charged sulfate ester groups on the surface of CNCs, which enables the CNCs to well disperse in water through the attraction/repulsion forces of electrical double layers.[57-58]

CNCs, also known as nanocrystaline cellulose, consist of rod-like or needle-like crystals with widths of 3-70 nm (typically less than 10 nm) and length 25-500 nm (typically between 100-200 nm).[59-60] CNCs have many unique characteristics, such as the high aspect ratio (10-30 for CNCs derived from cotton and ~70 for tunicate), high elastic modulus, high strength, low density, and reactive surfaces that could be functionalized. The theoretical tensile strength and elastic moduli of CNCs were measured to be 7.5-7.7 GPa and 100-140 GPa, respectively, which are much higher than those of steel wire and Kevlar.[53, 57] Therefore, CNCs are attractive high-performance reinforcing materials. Cooperation of CNCs into material matrices increases their strength and stiffness. In most reports about CNC-reinforced hydrogels, pristine CNCs are only physically entrapped within the hydrogel matrix for mechanical strength improvement. Nevertheless, there has been very few attempts so far on the employment of modified cellulose nanocrystals as both cross-linkers and reinforcing nanofillers to develop self-healing hydrogels with improved mechanical properties.

1.2 Hypotheses and objectives

The overall objective of this research was to develop novel multifunctional self-healing hydrogels using natural biopolymers and explore their applications in biomedical fields such as hemostasis and wound healing.

This research aims to test the following hypotheses:

(1) Self-healing hydrogels with high mechanical strength and self-healing efficiency can be prepared by combining water-soluble chitosan derivatives and benzaldehyde-terminated four-arm polyethylene glycol (PEG-BA) or dialdehyde cellulose nanocrystals (DACNC);

(2) Cooperation of a self-healing network and a covalent bonds crosslinked network can increase the toughness, stretch, and self-recovery rate of the self-healing hydrogels;

(3) Chitosan-based self-healing hydrogels with tissue adhesive properties can be achieved by introducing catechol moieties.

The specific objectives are:

Objective I: To prepare new self-healing hydrogels with both high mechanical strength and self-healing efficiency by combining benzaldehyde-terminated four-arm polyethylene glycol (PEG-BA) and carboxymethyl chitosan (CMC), and apply the CMC/PEG-BA self-healing hydrogel as 3D cell capsule and hemostatic material (Chapter 3);

Objective II: To fabricate on-demand dissolvable self-healing hydrogels based on CMC and dialdehyde cellulose nanocrystals (DACNC), and to apply it as wound dressing to facilitate deep partial-thickness burns healing (Chapter 4);

Objective III: To further improve the mechanical properties of the self-healing hydrogels by integrating reversible Schiff-base crosslinked CMC/DACNC and covalently crosslinked network, thus to construct a stretchy and tough hydrogel with high self-recovery rate (Chapter 5);

Objective IV: To improve tissue adhesion of the self-healing hydrogels by introducing catechol-conjugated chitosan to the hydrogel network (Chapter 6);

This research will generate new knowledge to understand what factors influence mechanical properties, self-healing efficiency and bio-adhesive properties of chitosan-based self-healing hydrogels at molecular and supramolecular levels. This knowledge allows rational design of advanced hydrogels for biomedical applications potentially. Additionally, this research will explore new applications of self-healing hydrogels including 3D cell encapsulation, hemostasis, and wound healing. These applications will create value-added opportunity for chitosan and cellulose as a by-product of seafood and wood industry.

Chapter 2

Multifunctional Self-Healing Hydrogels Based on Chitosan: A Review of Advances in Design, Evaluation, and Biomedical Applications

2.1 Development of self-healing hydrogels

One unique feature of all intelligent living organisms is that they are capable to heal spontaneously once damaged.[61] Self-healing is ubiquitous in the incredibly bio-diverse populations, from DNA and cell wall in unicellular organisms to skin and bone in human bodies.[62-63] Self-healing is an intrinsic ability of living things, but classic man-made materials usually cannot self-recover when break occurs. Since White et al (2001) have successful developed a healing agent-laden epoxy matrix that can be triggered to repair upon crack intrusion by the released healing agent from microcapsules embedded in the matrix,[64] the property of self-healing has been considered as a desirable function for synthesized materials. Apparently, various industries can benefit from self-healing materials owing to their long lifecycle and sustainability. In the past two decades, widespread effort to explore new design strategies and approaches to develop self-healing materials for a variety of applications have been executed. Self-healing materials were regarded as an alternative approach to 20 centuries of materials science in the first international conference on self-healing materials (Netherlands, 2007).[65]

The fantastic self-healing property has motivated the research and development of self-healing hydrogels in biomedical fields, such as cell and drug delivery, tissue engineering and regeneration, hemostasis, and wound healing.[66-68] The dynamic nature of interactions enables self-healing hydrogels to exhibit shear-thinning characteristic. Consequently, self-healing hydrogels could be utilized as injectable vehicles. Recently, self-healing hydrogels with injectable ability have drawn growing attention because they could effectively and homogeneously encapsulate and protect

sensitive biological cargos (e.g. cells), and then be minimally invasively injected to the target sites in a gel state instead of solution state, which could reduce the loss of loads in the hydrogels. Because of these properties, self-healing hydrogels show great promise as cell and drug carrier for cell therapy and drug delivery.[69-73] Furthermore, self-healing hydrogel could serve as ink for 3D printing due to their shear-thinning behavior with rapid self-healing after injection.[74] Hydrogels have been found to induce wound contraction and healing because they could absorb wound exudate, protect wounds from infection, and provide a moist wound environment, leading to rapid granulation and reepithelialization.[75-76] However, conventional hydrogels only can cover the top surface of wounds. On the contrary, self-healing hydrogels can be easily injectable to deep and irregular wounds and then recover to an integrate hydrogel that can three dimensionally fill the wounds, which prompts wound healing.[77]

Self-healing hydrogels refer to hydrogels that can autonomously restore mechanical integrity and functions after damage. Here, we only discuss intrinsic self-healing hydrogels that could heal without any external stimuli, which were triggered by noncovalent and dynamic covalent interactions. Extrinsic self-healing hydrogels relying on external stimuli or introduction of microcapsules and microvascular networks are out of the scope of this review. Self-healing hydrogels are being explored for a variety of applications and research in this field is rapidly expanding, especially over the past two years. A literature survey for self-healing hydrogels based on Sci-Finder Scholar search in the past decade is shown in **Figure 2-1**. Several reviews have been recently published on the topic of self-healing hydrogels, which focus on the self-healing mechanism of each type of self-healing hydrogels.[8, 10-11, 25, 32, 66-68, 78-79] In the beginning, researches about self-healing hydrogels focused on exploring new mechanisms for self-healing and new substrates to construct self-healing hydrogels. At that moment, self-healing hydrogels took long

time to heal (e.g. 24 h) and the mechanical properties were very poor, which restricted their practical applications. Recently, researchers have paid more attention to prepare rapidly self-healing hydrogels with superior mechanical properties together with other functions (e.g. conductivity, biocompatibility, adhesive ability).

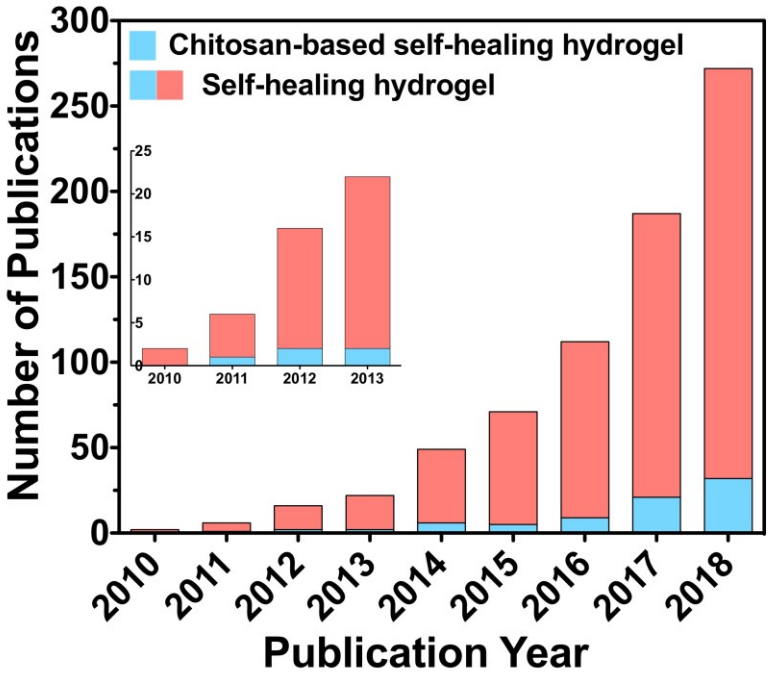

Figure 2-1. Number of research articles published in recent years. These numbers were analyzed by SciFinder using key words *self-healing hydrogel or self-repairing hydrogel* (), *self-healing hydrogel and chitosan* (). The graph clearly demonstrates the growing research interest in self-healing hydrogels.

Currently, a variety of different crosslinking mechanisms have been utilized to synthesize self-healing hydrogels, including reversible physical interactions and dynamic covalent bonds. Reversibly physically crosslinked hydrogels are cross-linked by either molecular entanglements or secondary forces, such as host-gust interactions, hydrophobic interactions, hydrogen bonding,

and electrostatic interactions.[8, 10] Dynamic covalent bonds are able to be broken and reformed reversibly under equilibrium control. Recent reports involving in dynamic covalent chemistry include Schiff-base linkages, reversible hydrazine bonds, oxime bonds, disulfide bonds, boronate ester bonds, and Diels-Alder reactions.[10, 80] Dynamic covalent bonds exhibit stronger but slower dynamic equilibrium compared to reversible physical interactions.[67] Self-healing hydrogels crosslinked by dynamic covalent bonds have much stronger linkages in the hydrogel network, endowing the quicker self-healing process and higher mechanical strength than those of physical interactions based self-healing hydrogels.

2.2 Chitosan-based self-healing hydrogels

In recent years, chitosan-based self-healing hydrogels are becoming more and more popular due to their facile preparation, rapid self-healing under mild conditions, and biocompatibility.

Chitosan is a natural cationic polysaccharide composed of *N*-acetyl glucosamine and glucosamine with abundant amino groups, which could be used to form Schiff-base linkages and for further modifications. Chitosan has been widely used in the wound management field for its antibacterial and hemostatic properties due to the positive charge of amino groups, which can interact with anions on the red blood cells through electrostatic interactions, thus inducing platelet aggregation and stopping blood.[28, 81-82] Moreover, it also can accelerate the cytokine production from macrophages which can promote wound healing.[83] It also has the ability to stimulate cell proliferation and histoarchitectural tissue organization by activating macrophages at the wound sites.[84] The hydrophilic surface of chitosan also contributes to cell adhesion, proliferation and differentiation.[85] These properties make chitosan-based hydrogels good candidates for the development of hemostatic agent, wound healing dressing, and tissue engineering matrix. Recently, there is growing interest in chitosan-based self-healing hydrogels in biomedical field.

In the following sections, recent advances in the development of chitosan based self-healing hydrogels towards biomedical applications are introduced. The first part consists of the design strategies for chitosan based self-healing hydrogels. Following this, the typical methods to evaluate the self-healing efficiency are discussed. Finally, the potential biomedical applications of chitosan-based self-healing hydrogels are analyzed.

2.3 Design strategies of chitosan-based self-healing hydrogels

A variety of strategies have been designed and applied to form chitosan-based self-healing hydrogels. **Table 2-1** summarized the typical healing mechanisms in chitosan-based self-healing hydrogels, including Schiff-base linkage (i.e. imine bond), enamine bond, metal coordination, hydrogen bond, and hydrophobic interaction (**Figure 2-2**). They have been generally utilized separately or synergistically.

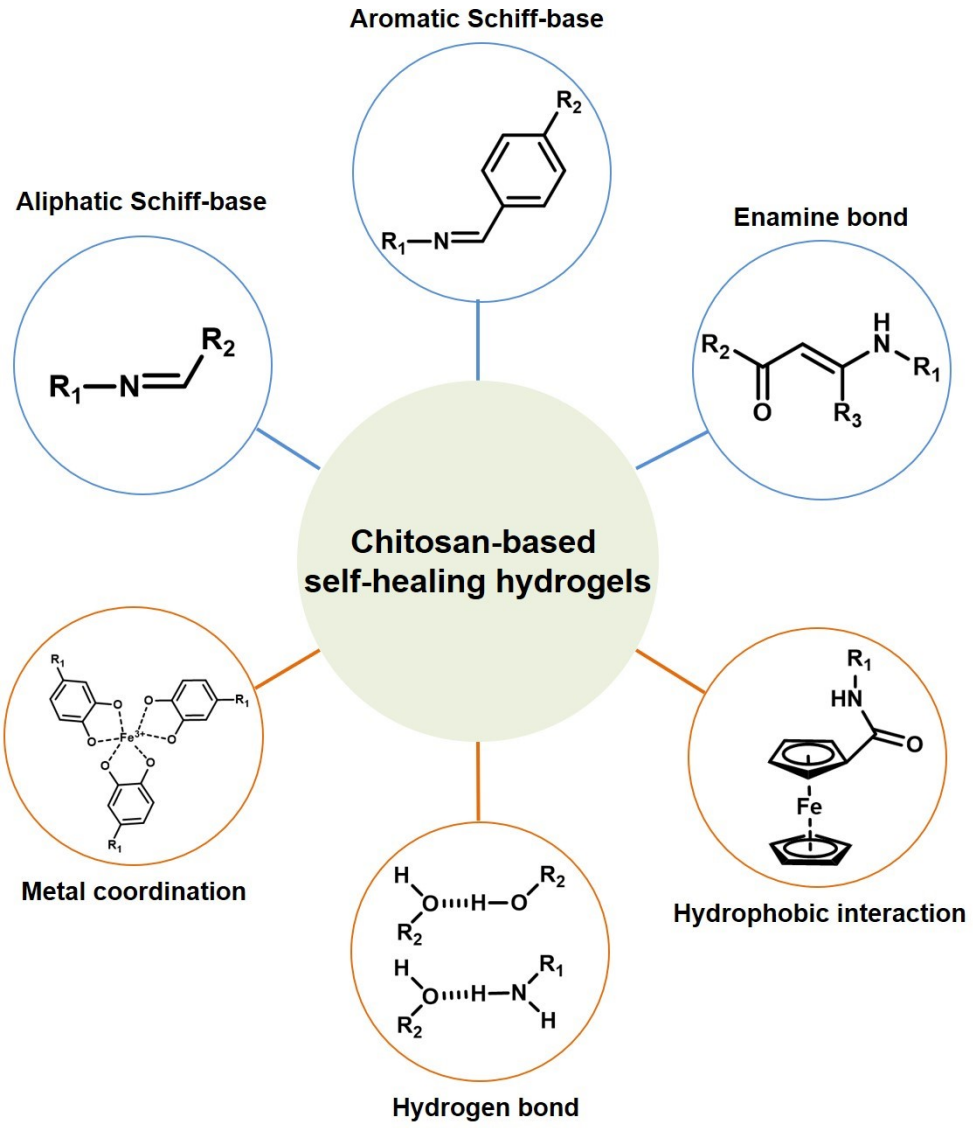

Figure 2-2. Various strategies used to synthesize chitosan-based self-healing hydrogels.

Table 2-1. General overview of chitosan-based self-healing hydrogels: substrates, healing conditions and efficiency, mechanical properties and applications.

Healing mechanisms	Substrates		Gelation conditions	Healing conditions	Mechanical properties	Multi-functions	Biomedical applications	Refs.
	Chitosan/ Chitosan derivatives	Polymers with -CHO						
Schiff-base linkages 2-A	Chitosan	Dibenzaldehyde-terminated telechelic poly(ethylene glycol) (DF-PEG)	RT, 30~40 s	RT[a], 2 h	G'=1 kPa	Multi-responsive	Control release of bioactive molecules	86
	Chitosan	DF-PEG	--[b]	RT, 12 h	G' = 1.5 kPa	--	Cell (neutral stem cells) encapsulation, repair the central nervous system	71
	Chitosan	DF-PEG Fe_3O_4	A few seconds	RT, 2 h	G' = ~2 kPa	Magnetic	Asynchronous control release of doxorubicin and docetaxel to treat triple-negative breast cancer	87-88
	Glycol chitosan (GCS)	DF-PEG	RT, ~60 s	RT, 15 min	G'=1~2 kPa	--	Injectable cell therapy carrier	89
	GCS	DF-PEG	--	--	G' = 1~4 Pa	--	Localized release of colistin, antimicrobial treatment of burn wound	90
	GSC	DF-PEG	--	--	G' = 500 Pa	Self-adapting	Wound healing	91
	GSC	DF-PEG	--	--	G' = ~10 kPa	--	Injectable drug carrier for in vivo intra-tumor therapy	92
	GCS	DF-PEG	--	--	~1.2 kPa	--	Neural stem cells delivery carrier	93
	QCS Fibrinogen	DF-PEG	--	--	--	--	Induce blood capillary formation	94
	N-Succinyl-chitosan (SCS)	DF-PEG	--	--	--	--	Fibroblast growth factor 2 delivery system for tissue repair applications.	95
	GCS	Dibenzaldehyde terminated poly(N-isopropylacrylamide)-co-poly(acrylic acid)	RT, 80 s	RT, 40 min	G' = 900 Pa	pH and temperature responsive	Drug delivery and 3D cell cultivation	96

	Chitosan-graft-aniline tetramer (CS-AT)	DF-PEG	37 ℃, ~1 min	37 ℃, 3 h	G'=~2 kPa (CS-AT10 hydrogel)	Conductive Antibacterial Tissue adhesive Anti-oxidative	Cardiac cell delivery carrier	97
	N-carboxyethyl chitosan (CEC)	DF-PEG	RT, ~ 2 min	25 ℃, 3 h	G' = 12 kPa (CEC/PEG-DA20)	pH-responsive	Drug delivery vehicles for liver cancer treatment	98
Schiff-base linkages M-A	Quaternized chitosan-g-polyaniline (QCSP)	Benzaldehyde group functionalized poly(ethylene glycol)-co-poly(glycerol sebacate) (PEGS-FA)	37 ℃, 105 s	25 ℃, 2 h	G'=251 Pa (QCSP3/PEGS-FA1.5 hydrogel)	Conductive Antibacterial Tissue adhesive	Hemostasis and wound healing	99
	CEC	Dextran-graft-aniline tetramer-graft-4-formylbenzoic acid (Dex-AT-FA)	--	37 ℃, 12 h	G' = ~ 700 Pa	Conductive	Injectable carriers for myoblast cell therapy Muscle regeneration	100
Schiff-base linkages 4-A	Chitosan	Tetra-aldehyde functionalized zinc phthalocyanine (TA-ZnPc)	RT, ~ 30 s	RT, 15 min	G' = 2 kPa	Super self-healing High strength Electrical properties Injectable pH-stimuli responsive	Photo-sensitizer carrier Effective cancer therapy	101-102
	carboxymethyl chitosan (CMC)	PEG-BA	RT, ~2 min	RT, 5 min	G' = 3.5 kPa	--	3D cell encapsulation Hemostasis	103
	Chitosan-g-L-glutamic acid (chi-glu)	PEG-BA	RT, ~ 60 s	RT, 3 h in PBS	Compress stresss = 10 kPa	--	--	104
	Dodecyl-modified chitosan	PEG-BA	--	--	G' = 300 Pa	Tissue adhesive Anti-infective	Vascular endothelial growth factor (VEGF) encapsulation, wound healing	105
Schiff-base linkages Star-A	Quanternized chitosan (QCS)	Benzaldehyde-terminated Pluronic F127 (PF127-CHO)	37 °C, ~90 s	37 °C, 2 h	G'=4000 Pa~ (QCS/PF 1.0) Tensile stress = 14.3 kPa Compressive stress at 90% = ~250 kPa	Antibacterial Adhesive Rapid self-healing Stretchable Compressive Double network	Joints skin wound healing	77
Schiff-base linkages Oxidized Polysaccharide	N -carboxyethyl chitosan (CEC) Adipic acid dihy-drazide (ADH)	Oxidized sodium alginate (OSA)	RT, ~ 20 s	37 °C, 12 h, 95%	G' = 6 kPa	Injectable Biocompatible	Cell encapsulation and release	15
	CEC	OSA	37 °C, 25 min	37 °C, 24 h	G' = 577 Pa	Injectable Biocompatible	Injectable carrier for the delivery of neutral cell stems	106
	CEC	Oxidized acrylated hyaluoronic acid (OAHA)	37 °C, 0.6 min	37 °C, 20 min	G' = 775 Pa	--	Modular gradient hydrogel	107

	Acrylamide-modified chitosan (AMCS)	OSA	--	RT, 1 h	G' = ~ 100 Pa	Remodeling	--	[108]
	CEC	OSA	RT, 47 s	--	G' = ~ 100 Pa	--	Enable diffusive transport of carbon quantum dots across gel-gel interface Scavenge reactive oxygen species	[109]
	N-succinyl-chitosan (SC).	Oxidized chondroitin sulfate (CSMA)	--	RT, 2 h	G' = 3.5 kPa (CSMA3/SC3)	--	Cell encapsulation	[110]
	Quanternized chitosan (GCS)	Oxidized dextran (Odex)	37 °C, 114 s	37 °C, 120 min	G'=400 Pa (Odex/GCS 2)	--	Protein delivery	[111]
	Chitosan	Oxidized konjac glucomannan (OKGM)	37 °C, 30 s	25 °C, 4 h	G'=1000 Pa (CS-OKGM-4)	Antibacterial Adhesive	Wound healing	[112]
	CEC	Oxidized hyaluoronic acid (OHA)	--	RT, 3 min	G' = 2 kPa	--	pH responsive drug release	[113]
Schiff-base condensation reaction	Chitosan	Formaldehyde	RT, 7 min	RT, 30 min	G' = 1150 Pa	pH dependent swelling	radiochemical separation	[114]
Small moleculer with aldehyde groups crosslinker	Chitosan	3,5-Diformyl-4,4-difluoro-4-bora-3a,4a-diaza-s-indacene (BDP)	RT, ~30 min	RT, 3 h	G' = 30~270 Pa	Photophysical and photochemical	Extend fluorescence lifetime	[115]
	Chitosan	4-hydroxy-3-methoxybenzaldehyde (Vanillin)	RT, 6 min	RT, 5 h	G' = 10 kPa	--	--	[116]
Enamine bonds	Chitosan	Cellulose acetoacetate (CAA)	RT,	37 °C, 40 min	G' = 500 Pa (1% CAA+1% Chitosan)	pH responsive	--	[117]
Metal-coordination	DOPA-chitosan	Fe^{3+}	pH: 1-8	RT, 2-7 min	G' = ~30 kPa	--	--	[118]
Metal-coordination	Catechol-Chitosan	Fe^{3+}	pH 5	--	G' = 1 kPa	--	Drug delivery (DOX, DTX) Localized combination cancer therapy	[119-120]
Metal-coordination and hydrogen bonds	PPy-chitosan (DCh-PPy)	Poly(acrylic acid) (PAA) Fe^{3+}	--	RT, 2 min	G' = 1.1 Pa	Conductive Pressure sensitive Stretchable 3D printable	Stretchable wireless human motion detector	[121]
Metal-coordination and hydrogen bonds	Chitosan	PAA Fe^{3+}	--	12 h	Compressive stress = 10~ MPa Tensile stress=~0.15 MPa G'= 20~ kPa (CS- PAA-Fe (III)-4)	Double-network Stretchable Compressive Conductive	--	[122]

Metal-coordination and chain entanglement	Chitosan	PAA Fe^{3+} NaCl	--	70 ℃, 24 h	Tensile stress=3.7 MPa	Strong Tough Double network	--	[123]
Metal coordination	CMC	Zinc ions (Zn^{2+})	~ 60 s	RT, a few seconds	G' = 100 Pa (CMC-Zn1)	Antibacterial	--	[124]
Metal coordination	Catechol-Chitosan/ Chitosan/ Genipin	Fe^{3+}	37 ℃, 2-24 h	RT, 5 min	Compressive stress = 3 MPa	Ultratough Fast recovery Injectable	--	[125]
Metal coordination and Diels-Alder reaction	Catechol-modified N-(furfural) chitosan (CFC)	Fe^{3+}, Dimaleimide poly (ethylene glycol) (Mal-PEG-Mal)	--	RT, 3 h	G' = 1 kPa	Thermodynamic Anti-EDTA	--	[126]
Hydrogen bonds	Chitosan-PVA	Glutaraldehyde	37 ℃, 10 min	RT, 1 h	--	Thermo-reversible	pH sensitive controllable drug release	[127]
Hydrogen bonds	Chitosan carbon dots	Poly(vinyl alcohol)	Freezing/thawing	RT, 12 h	G' = 10 kPa	Thermal stable	--	[128]
Hydrogen bonds and electrostatic interaction	Chitosan	Iron oxide coated graphene oxide (GIO)	--	--	--	Antibacterial Noncytotoxic	Antimicrobial biofilms	[129]
Hydrogen Bonding and supramolecular interactions	Chitosan	Graphene oxide (GO) nanosheets	RT	RT, 1 min	G'=100 Pa	Thermo-reversible	--	[130]
	Chitosan, Dopamine	Graphene oxide	--	--	--	Adhesive Conductive		[131]
Hydrophobic interactions	Ferrocene-modified chitosan (FcCS)		2% acetic acid	RT, 4 h	G' = 1 kPa	Multi-responsive (pH, redox, ions)	Control release	[132]
Endothermic interactions between polyelectrolytes	2-hydroxypropyltrimethyl ammonium chloride chitosan	Alginate (ALG)	RT, 12 h	RT, 7 h	G' = 13 kPa	Adhesive	Potential candidate for cell and drug delivery	[133]

[a] RT refers to room temperature.

[b] – means no description in the corresponding article.

2.3.1 Schiff-base linkages

A Schiff-base is a compound with a structure of -C=N- formed by nucleophilic attack of amine to aldehyde or ketone.[67] The dynamic equilibrium between the Schiff-base linkages and the aldehyde groups and amino groups in the hydrogel network endows the hydrogel with self-healing ability.[86] Self-healing hydrogels crosslinked by Schiff-base linkages are the most important motif of chitosan-based self-healing hydrogels because chitosan intrinsically has abundant amino groups on its backbone and the imine bonds can be rapidly formed between amino and aldehyde groups under physiological conditions, which is beneficial to biomedical applications. To date, several self-healing hydrogels have been developed through dynamic Schiff-base linkages.[25, 78] The poor mechanical performance and long self-healing time impede their use in practical applications that require great mechanical performance, such as artificial cartilage and hemostasis. Therefore, the development of strong and rapidly self-healing hydrogels based on Schiff-base linkages remains a challenge, especially for those driven from natural polymers in which the types of functional groups are limited.

Based on different sources of aldehyde groups, there are two kinds of Schiff-base linkages, namely aromatic Schiff-bases and aliphatic Schiff-base.[8, 86] Both linkages have been utilized to construct chitosan-based self-healing hydrogel and the aliphatic Schiff-base linkages are less stable than the aromatic Schiff-base linkages. The cross-linking agents with aldehyde groups were summarized in **Figure 2-3**, including (1) linear polymer with benzaldehyde groups at both end of polymer chain, (2) linear polymer with multiple aldehyde group as pendant group, (3) star-shaped polymer (4-arm polymer and micelle) with benzaldehyde group at end of each arm, and (4) oxidized polysaccharide with aldehyde groups. By using different types of crosslinking agents, the mechanical and self-healing properties of the hydrogel can be tailored.

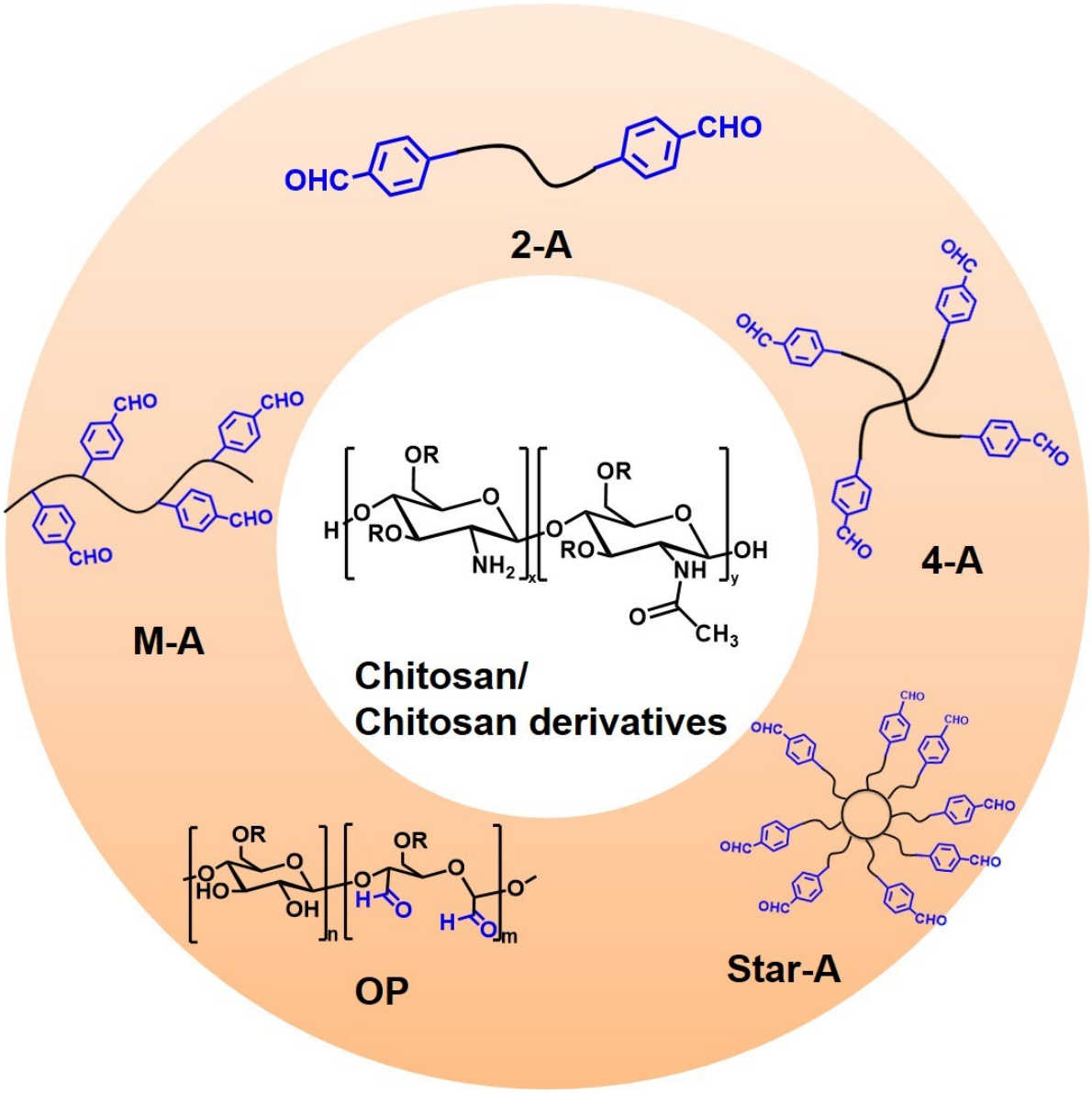

Figure 2-3. Typical crosslinking agents used for making chitosan-based self-healing hydrogels formed through Schiff-base linkages: (2-A) Linear polymer with benzaldehyde groups at both end of polymer chain. (M-A) Linear polymer with multiple aldehyde group as pendant group of polymer backbone chain. (4-A) Four-arm polymer with benzaldehyde group at end of each arm of polymer. (Star-A) Micelle with pendant benzaldehyde groups at outside layer. (OP) Oxidized polysaccharide with aldehyde groups.

2.3.1.1 Linear polymer with two aldehydes at end of polymer chain

The most popular polymer with aldehyde groups is dibenzaldehyde-terminated poly(ethylene glycol) (DF-PEG). Polyethylene glycol (PEG) is widely applied in tissue engineering due to good biocompatibility.[134] Since Zhang et al. synthesized DF-PEG and applied it to build self-healing hydrogels,[86] there are at least thirteen articles that reported self-healing hydrogels derived from chitosan/chitosan derivatives and DF-PEG (**Table 2-1**). DF-PEG was synthesized by esterification of hydroxyl-terminated PEG with 4-formylbenzoic acid (**Figure 2-4**). The mixture of chitosan solution and DF-PEG solution formed gel within 2 mins at room temperature. The hydrogel network was constructed through dynamic Schiff-base linkages between amino groups on chitosan and benzaldehyde groups at PEG chain ends. The chitosan/DF-PEG hydrogels exhibited good self-healing capacity due to intrinsic dynamic equilibrium. Two pieces of freshly cut chitosan/DF-PEG hydrogels healed within 2 h at room temperature. They prepared a series of hydrogels with different solid contents and ratios of CHO/NH_2, which made the hydrogels show storage modulus from 700 Pa to 30 kPa. In addition, the chitosan/DF-PEG hydrogels were sensitive to many biochemical-stimuli, such as pH and amino acids, suggesting the potential application for controlled-release of drugs because acidic condition and amino acids can trigger the cleavage of Schiff-base linkages.[135] Due to the poor neutral water solubility of chitosan, it was later replaced by glycol chitosan (GSC) with better solubility in neutral pH. Upon mixing glycol chitosan and DF-PEG solution, a hydrogel was facilely prepared at 25 ℃ within 1 min. The storage modulus (150 Pa~2000 Pa) and loss modulus could be adjusted by changing the concentration of glycol chitosan and DF-PEG. The GSC/DF-PEG hydrogel could smoothly pass through the syringe needle (21-gauge) and the broken hydrogel fragments were reformed a completely homogeneous hydrogel in 30 mins, suggesting good injectable and self-healing ability. Although these reports

provided inspiration for using Schiff-base linkages to obtain self-healing hydrogels, they have encountered challenges because the mechanical strength and self-healing efficiency have not satisfied practical applications.

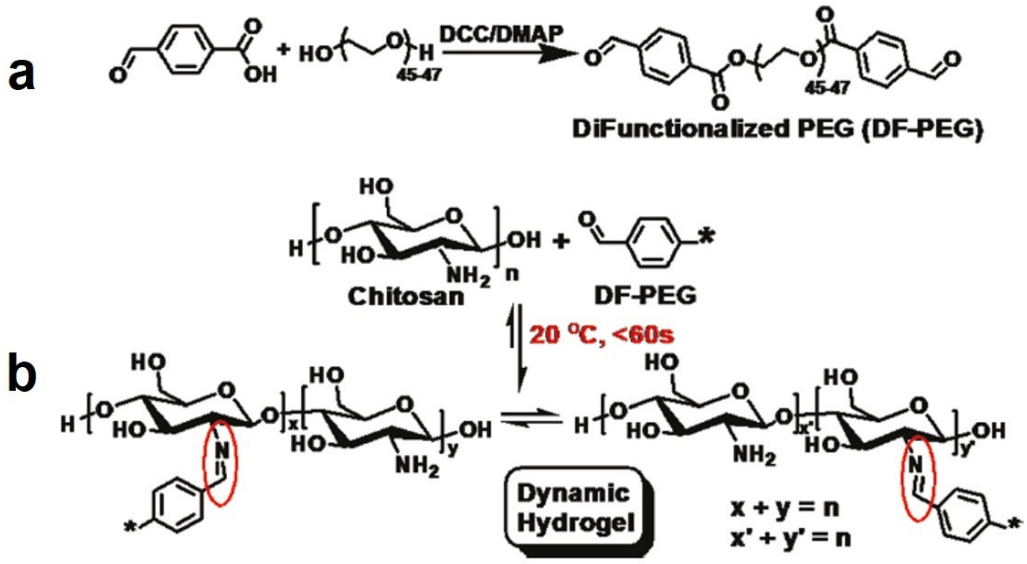

Figure 2-4. (a) Synthesis of DF-PEG and (b) formation of chitosan-based self-healing hydrogel based on Schiff-base linkages. Reprinted with permission from ref.[86] Copyright (2011) American Chemical Society.

2.3.1.2 Linear polymer with multiple aldehydes as pendant group

Compared with dialdehyde modified polymers, multi-aldehyde modified polymers have more potential cross-linking sites with chitosan to improve the efficiency and tunability of the gelation and recovery of hydrogels, as well as mechanical properties. Zhao et al developed a self-healing hydrogel composed of quaternized chitosan-g-polysaniline (QSP) and benzaldehyde group functionalized poly(ethylene glycol)-co-poly(glycerol sebacate) (PEGS-FA).[99] First, poly(ethylene glycol)-co-poly(glycerol sebacate) (PEGS) was synthesized through polycondensation of sebacic acid (SAA), poly (ethylene glycol) (PEG), and glycerol. Following this, 4-formylbenzoic acid (FA) was grafted onto the PEGS by an esterification reaction to

synthesize the benzaldehyde functionalized PEGS (PEGS-FA) (**Figure 2-5**A). The hydrogel was prepared by mixing the quaternized chitosan-g-polysaniline solution and PEGS-FA solution. Increasing the PEGS-FA crosslinker concentration from 0.5 wt.% to 2 wt.%, the gelation time decreased from 374 s to 86 s, and the storage modulus of the hydrogels increased from 58 Pa to 368 Pa, which was caused by the enhanced crosslinking density of the hydrogel network. Four pieces of freshly cut hydrogel became a whole piece of hydrogel with obscure boundaries at 25 ℃ after 2 h and the healed hydrogel could be lifted by holding one end of the hydrogel, which suggested that the hydrogel exhibited self-healing ability due to PEGS-FA's branched structure and higher molecular weight. Guo and co-workers prepared a self-healable conductive injectable hydrogels based on *N*-carboxyethyl chitosan (CEC) and dextran-graft-aniline tetramer-graft-4-formylbenzoic acid (Dex-AT-FA) (**Figure 2-5**B).[100] Carboxyethyl chitosan solution and Dex-AT-FA solution with various molar ratio of -NH_2 to -CHO were mixed together to form hydrogels through dynamic Schiff-base bond between the amino groups from carboxyethyl chitosan and the aldehyde groups from Dex-AT-FA. The gelation occurred within 2 min under physiological conditions, and the storage modulus of Dex/CEC hydrogel was 300-600 Pa. After 12 h at 37 ℃ in a humid atmosphere, the cut hydrogel pieces fused together and the storage modulus of the self-healed hydrogel was almost the same value as that of the original hydrogel, suggesting good self-healing properties. In spite of the progress made by the researchers, the synthesis of PEGS-FA and Dex-AT-FA were complicated and the aldehyde substitutions were low, which limited the development and applications of these self-healing hydrogels.

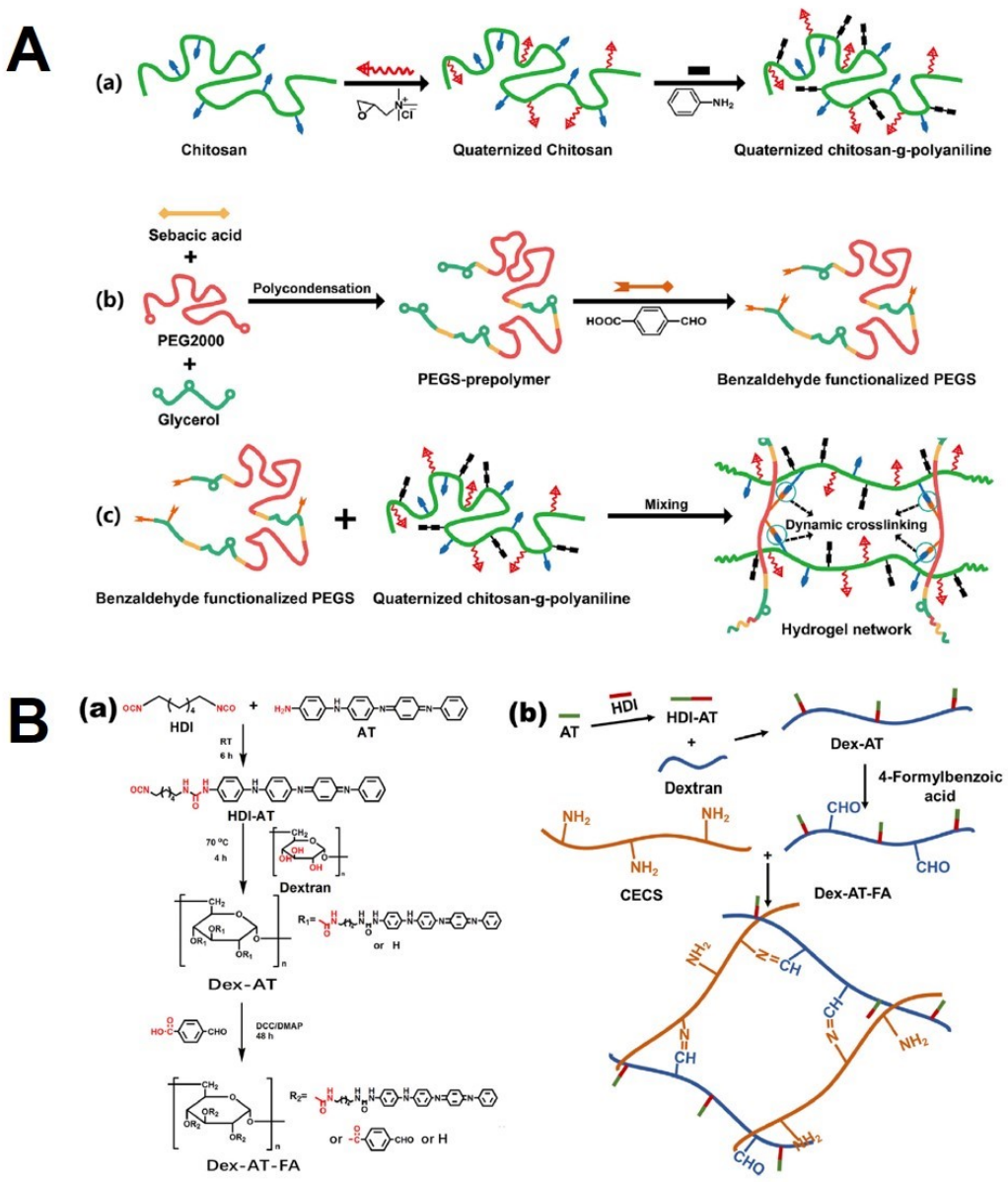

Figure 2-5. (A) Schematic of QCSP/PEGS-FA hydrogel synthesis: (a) Synthesis of QCSP copolymer, (b) synthesis of PEGS-FA copolymer, and (c) preparation of QCSP/PEGS-FA self-healing hydrogel. Reprinted with permission from ref.[99] Copyright (2017) Elsevier. (B) Schematic of Dex/CEC hydrogel synthesis: (a) Synthesis of Dex-AT-FA polymer, and (b) preparation of the Dex-AT/CECS self-healing hydrogel. Reprinted with permission from ref.[100] Copyright (2019) Elsevier.

2.3.1.3 Star-shaped polymers with aldehydes at end of each arm of polymer

Compared with linear polymers, star-shaped polymers (e.g. 4-arm polymers and micelle with functional groups at outside layer) crosslinked hydrogel networks are more resistant to fracture because star-shaped polymer is an impenetrable space-filled sphere and has compact structure, smaller hydrodynamic size, and lower internal viscosities, compared to linear analogues of identical molecular weight and monomer composition.[103] More arms corresponds to a greater probability of a macromolecule to participate simultaneously in multiple crosslinks and increases the cross-linking density.[136] Therefore, star-shaped polymers are particularly popular cross-linkers to form strong hydrogels. Benzaldehyde-terminated four-arm poly(ethylene glycol) (PEG-BA) (**Figure 2-6**) and carboxymethyl chitosan (CMC) were used to prepare the dynamic hydrogels,[103] and the mechanical strength and self-healing efficiency could be adjusted according to the molar ratio of -NH_2/-CHO and the total solid content of hydrogels. Owing to the dynamic Schiff-base linkages and the branched structure of the cross-linker, the cut hydrogel lines healed to an integrated hydrogel film after 5 min at room temperature without any external intervention. The hydrogels had good storage modulus up to 3.2 kPa, which was higher than the chitosan/DF-PEG hydrogels (1 kPa). Following this work, Khan et al fabricated an injectable self-healing hydrogel composed of water-soluble chitosan-g-L-glutamic acid (WSC) and PEG-BA.[104] The hydrogel was formed within 60 s by mixing WSC and PEG-BA solution. The compressive modulus of the WSC/PEG-BA hydrogel could be easily tuned between 4 to 31 kPa by adjusting the PEG-BA cross-linker and total solid content. Chen et al utilized PEG-BA as the cross-linker to construct a multifunctional hydrogel with dodecyl-modified chitosan.[105] The hybrid hydrogel exhibited multi-functions, such as strong tissue adhesion, blood cell coagulation, and anti-infective properties. Although several examples of star-shaped PEG crosslinked networks have been described recently,

the influence of number of arms and arm molecular weight on hydrogel network formation, mechanical properties, and self-healing ability have not been fully investigated.

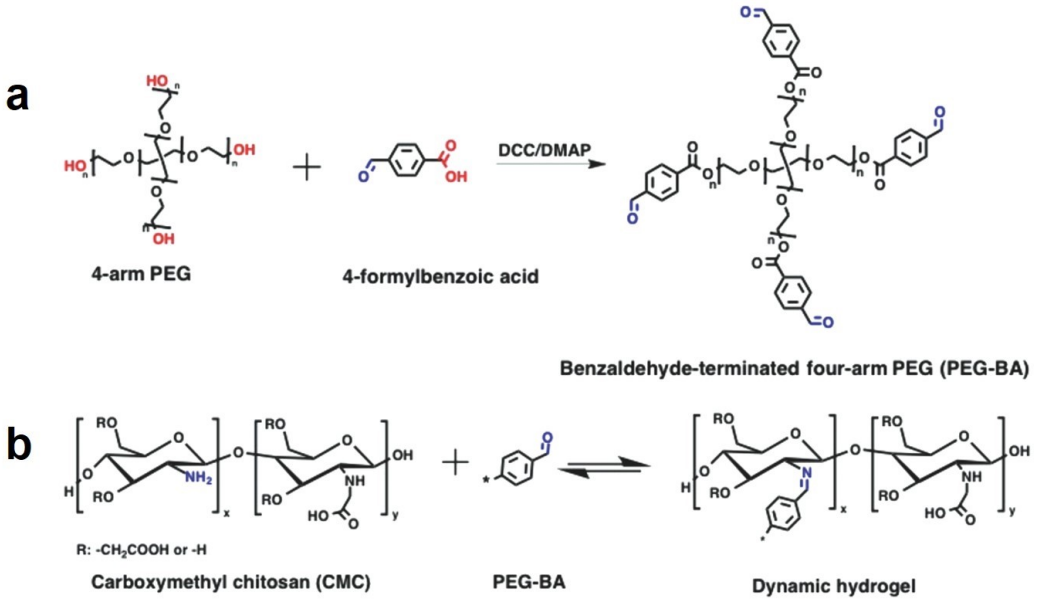

Figure 2-6. (a) Synthesis scheme of benzaldehyde-terminated four-arm PEG (PEG-BA), and (b) benzaldehydes at ends of PEG-BA conjugated amino groups of CMC to form dynamic CMC/PEG-BA hydrogel. Reprinted with permission from ref.[103] Copyright (2016) John Wiley and Sons.

Qu et al designed a self-healing injectable micelle/hydrogel composites with multi-functions by mixing quaternized chitosan (QCS) and benzaldehyde-terminated Pluronic®F127 (PF127-CHO) solution under physiological conditions (**Figure 2-7**).[77] PF127 could self-assemble into micelle in water because it is an amphiphilic triblock copolymer. Double dynamic networks in the QCS/PF127-CHO hydrogel network endow the hydrogel with unique mechanical properties and self-healing performance. PF127 micelles function as dynamic micro-crosslinker in forming the first network and dynamic Schiff-base linkages between benzaldehyde groups from PF127-CHO micelles and amine groups from quaternized chitosan act as the second network in the hydrogel. A hybrid physically–chemically crosslinked double network hydrogel was formed by combining

the micelle cross-linking and dynamic Schiff-base linkages in one system. The hydrogel exhibited good mechanical properties (tensile stress = 9.8-25.7 kPa, Compressive stress at 90% = 240 kPa) and self-healing ability (2 h at 25 ℃). Compared with 4-arm PEG, PF127 micelles not only had more crosslinking joints, but also could encapsulate and controlled release bioactive components.

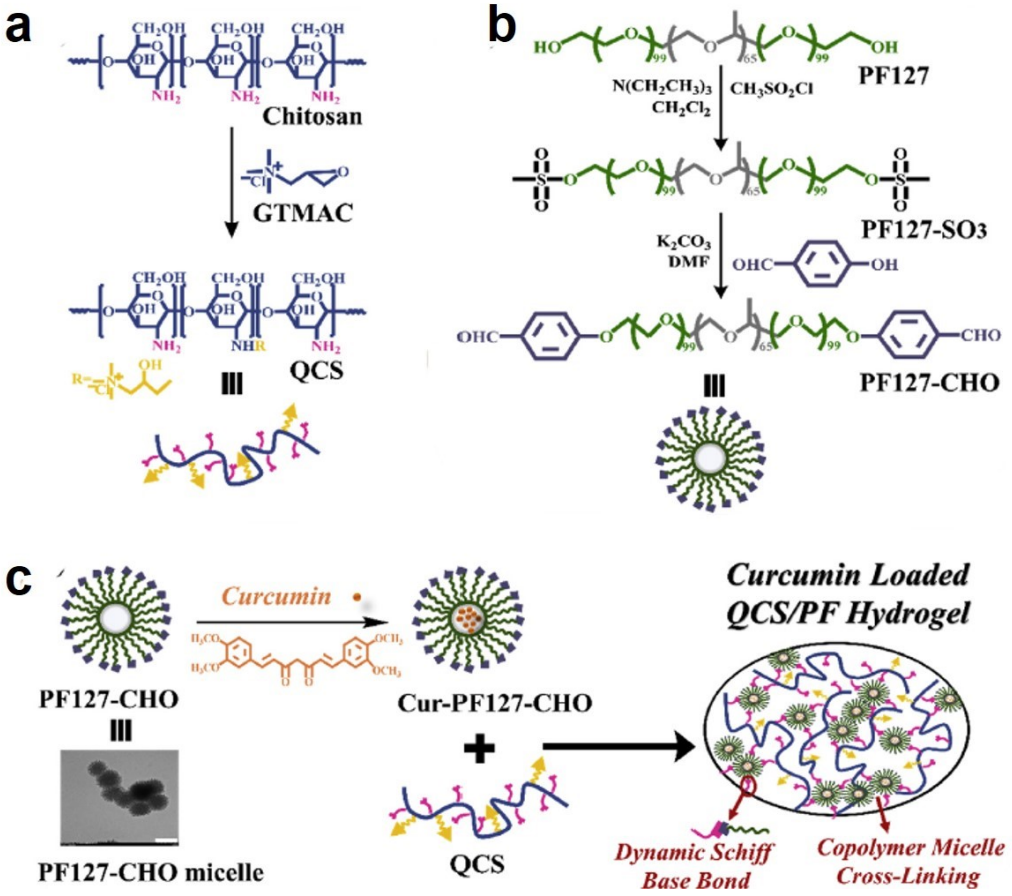

Figure 2-7. Schematic of Cur-QCS/PF hydrogel synthesis: (a) Synthesis of QCS polymer, (b) synthesis of PF127-CHO polymer, (c) schematic illustration of Cur-QCS/PF hydrogel. Reprinted with permission from ref.[77] Copyright (2018) Elsevier.

2.3.1.4 Oxidized polysaccharide (OP)

Naturally occurring polysaccharides, such as alginate, hyaluronic acid, and chondroitin sulfate, have been widely applied to fabricate hydrogels for biomedical applications due to abundant sources, biodegradability, and biocompatibility.[137] Oxidized polysaccharides also attract extensive attention as cross-linker to prepare self-healing hydrogels. Sodium periodate could oxidize the vicinal hydroxyl groups of polysaccharides to dialdehydes, which opens the sugar ring to form dialdehyde derivatives.[138] Aldehyde groups can generate chemical crosslinking action with amino functions via Schiff-base linkages. A variety of oxidized polysaccharides, including oxidized dextran,[111, 139] oxidized chondroitin sulfate,[110] oxidized cellulose,[140] oxidized hyaluronic acid,[113, 141] and oxidized konjac glucomannan,[112] have been synthesized and applied to prepare self-healing hydrogels with chitosan and chitosan derivatives (**Table 2-1**). For instance, Wei et al developed a polysaccharide-based self-healing hydrogel composed of *N*-carboxyethyl chitosan (CEC), adipic acid dihydrazide (ADH), and oxidized sodium alginate (OSA) (**Figure 2-8**). Gelation occurred shortly after homogeneously mixing OSA with CEC and ADH solution for ~20 s at room temperature. The formation of hydrogel was attributed to the coexistence of dynamic Schiff-base linkages (OSA and CEC) and acylhydrazone bonds (OSA and ADH) in the hydrogel networks. The storage modulus of the hydrogel could be as high as 6 kPa because of the double crosslinkings. The separated hydrogel pieces healed to an integrate hydrogel disk after 6 h at 25 °C without any external intervention.

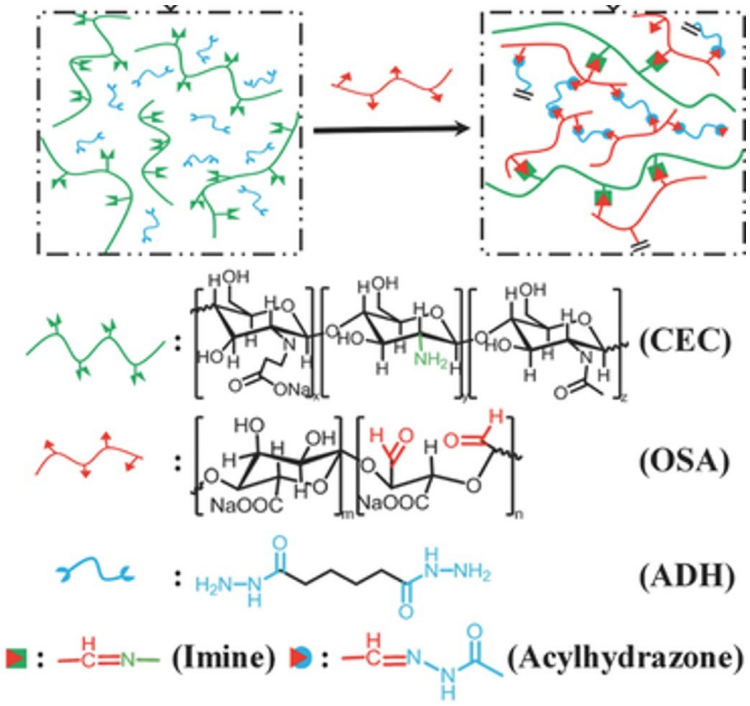

Figure 2-8. Schematic of CEC-OSA-ADH hydrogel synthesis. Reprinted with permission from ref.[15] Copyright (2015) John Wiley and Sons.

2.3.2 Other interactions

Enamine bonds are similar to the imine and hydrazone dynamic covalent bonds. Therefore, the enamine bonds could also be utilized in construction of dynamic hydrogel networks, which can be synthesized by the reaction of acetoacetate groups with amine groups.[142] Enamine bonds could reversibly break and recover under appropriate conditions. To demonstrate the application of enamine bonds in the development of dynamic hydrogel, Liu et al introduced the acetoacetates into the cellulose chain by trans-esterification of hydroxyl with tert-butyl acetoacetate (t-BAA) in an ionic liquid 1-allyl-3-methylimidazolium chloride (AMIMCl).[117] A polysaccharide hydrogel was prepared by simply mixing cellulose acetoacetate (CAA) aqueous solution with chitosan aqueous solution (**Figure 2-9**). The hydrogel network was constructed through the formation of dynamic enamine bonds between carbonyl groups from CAA and amine groups from chitosan.

The gelation occurred quickly at room temperature and the storage modulus could reach 1 kPa. The self-healing experiment showcased that separated hydrogel pieces could heal autonomously after about 40 min at 25 °C, suggesting the CAA/chitosan hydrogel demonstrated self-healing behavior due to the dynamic enamine bonds in the hydrogel network. This study reported a new design strategy to develop polysaccharide-based self-healing hydrogel. Besides, the hydrogel showed good stability under physiological conditions and pH-responsive properties.

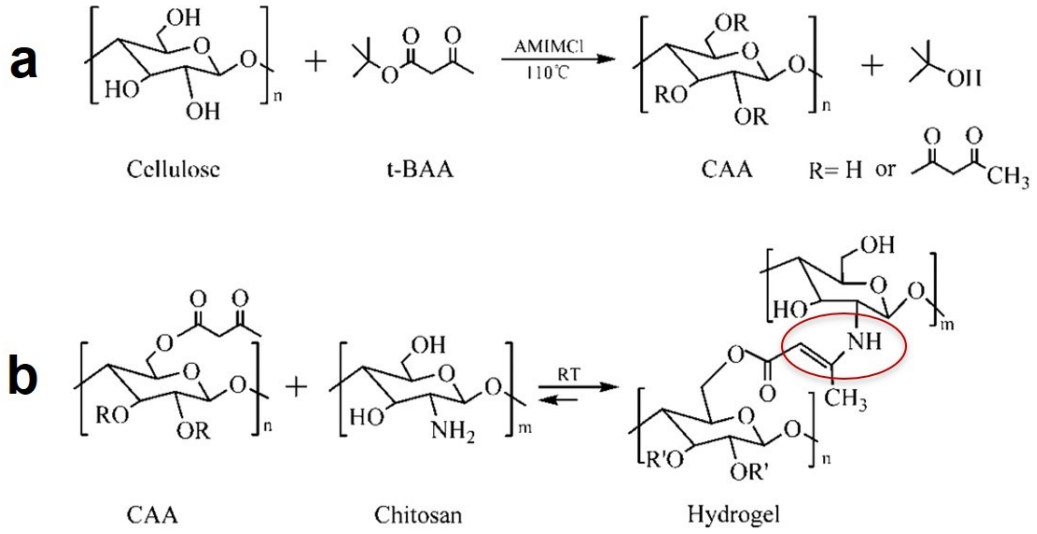

Figure 2-9. (a) Synthesis of CAA, and (b) formation of enamine bond linkage between CAA and chitosan. Reprinted with permission from ref. [117] Copyright (2016) John Wiley and Sons.

Recently, inspired by mussel adhesion, self-healing hydrogels have been prepared based on metal-coordination bonds, which mimicked the coordination bonds found in mussel byssal threads.[23] Coordination between Fe^{3+} and catechol ligands has been proposed to endow self-healing properties.[143-144] Yavvari et al grafted catechol ligands to chitosan backbone to synthesize the catechol-conjugated chitosan.[119-120] The hydrogels were assembled through catechol-Fe^{3+} coordinative interactions (**Figure 2-10**). The storage modulus of the hydrogel was about 1 kPa.

The self-healing nature of the catechol-chitosan based hydrogel enabled it to be injected to the target sites while retaining its gel status.

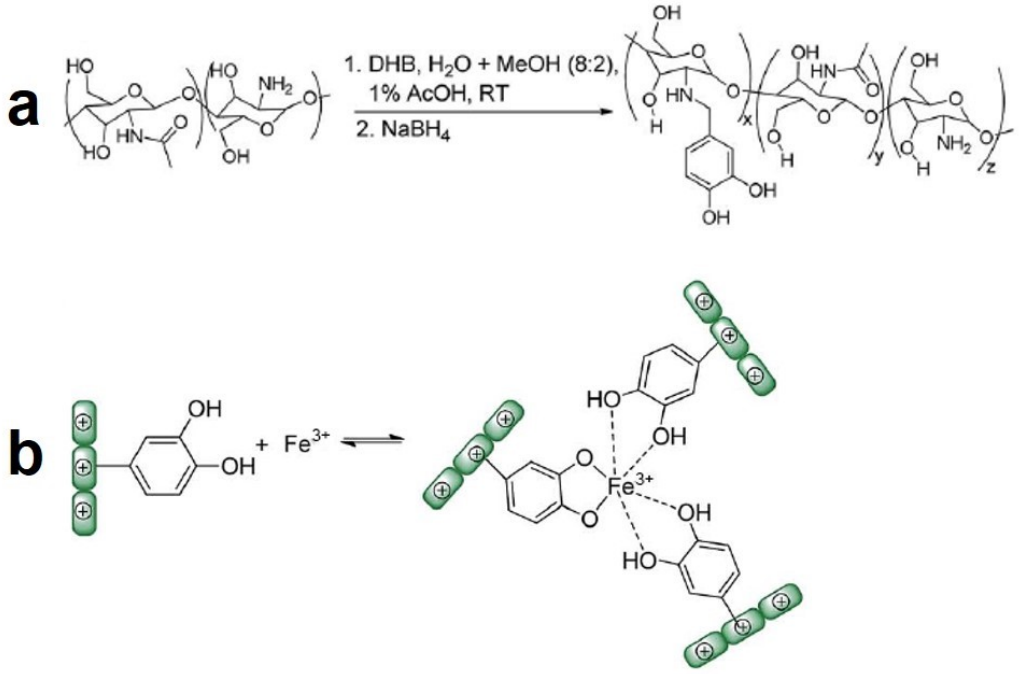

Figure 2-10. (a) Schematic of catechol-conjugated chitosan synthesis, and (b) schematic of monocomplex formation between catechols and Fe^{3+}. Adapted with permission from ref.[119] Copyright (2015) Royal Society of Chemistry.

Hydrogen bonding is a type of non-covalent interaction that is much weaker than dynamic covalent and ionic crosslinks.[11] Chitosan is rich in hydroxyl and amine groups, which are favorable for the formation of reversible hydrogen bonds to construct the self-healing hydrogel network. Chang et al reported a reversible and self-healable chitosan (CS)/polyvinyl alcohol (PVA) hydrogel by adding a small amount of glutaraldehyde into the CS/PVA precursor solution.[127] The gelation occurred at 37 ℃ in 10 mins based on hydrophobic interactions and hydrogen bonds. The self-healing ability of the CS/PVA hydrogel was demonstrated by punching a hole in the hydrogel, which closed gradually and finally disappeared within 1 h without any external stimuli.

Intermolecular and intramolecular hydrogen bonds made the PVA and CS chains move and cross-link at the damage interface, which led to healing of the broken hydrogen network. In addition, Zhang et al. prepared a supramolecular polymer hydrogel composed of chitosan carbon dots (CDs) and PVA based on hydrogen bonds.[128] The separated pieces of hydrogel healed to an integrate hydrogel at room temperature after 12 h without any external stimuli and it showed good thermal stability and pH sensitivity.

Hydrophobic interactions usually occur during the aggregation of hydrophobic surfaces or hydrophobes in aqueous system.[11] Hydrophobic interactions crosslinked networks are readily to form, break, and re-form. Hydrophobicity has played a powerful role in forming supramolecular hydrogels, and hydrophobic segments could re-aggregate after damage, which caused the self-healing of hydrogel based on hydrophobic interactions.[145] Ferrocene (Fc) has drawn much attention to prepare supramolecular hydrogels owing to the unique sandwich structure, hydrophobic feature, redox property, and low toxicity.[146] Fc was grafted to chitosan through amide linkages between amino group of chitosan and carboxyl group of ferrocenecarboxylic acid (FcA).[132] The hydrogel was formed via the self-assembly of ferrocene-modified chitosan (FcCS) in an acid aqueous solution, which was based on the equilibrium of hydrophilic and hydrophobic interactions. The cut hydrogel pieces healed to a united hydrogel disk after 4 h without any external stimuli because the hydrophobic aggregation of Fc group acted as reversible cross-linking. Moreover, the hydrogel also presented stimuli-responses towards pH, redox, and different ions.

2.4 Major properties of self-healing hydrogels and their evaluations

Practical application of self-healing hydrogels as smart materials requires a combination of rapidly self-healing process, great mechanical properties, and strong tissue adhesive ability. In addition, biocompatibility is required for biomedical applications.

2.4.1 Self-healing performance

Self-healing ability is the most important index to evaluate a self-healing hydrogel. The external environmental conditions (e.g. temperature, pH), geometries and mechanical strength of hydrogels, as well as gap distance all affect the self-healing process. For example, increasing temperature can enhance the dynamic kinetics of the reversible bonds, thus improving self-healing efficiency.[15] Self-healing hydrogels crosslinked through Schiff-base linkages could recover under neutral and basic conditions, whereas they lose self-healing ability under acidic conditions.[135] However, there is not a universal method to assess the self-healing efficiency of self-healing hydrogels yet.

Currently, several methods have been employed to determine the self-healing ability, including macroscopic observation, microscopic observation, SEM observation, rheological recovery test, and mechanical strength recovery test.

It is conventional to evaluate the self-healing ability of hydrogels by macroscopic observation. Briefly, two freshly prepared disk-shaped hydrogels with different colors were cut in halves. Then two equal halves taken from each of the original hydrogels were brought together. After a period, the boundary between the different colored hydrogels became obscure and the two semicircles merged into a united hydrogel (**Figure 2-11**a). The healed hydrogel could be lifted using tweezer or be stretched from both ends.[109-110, 117-118, 132-133] This hydrogel merging method is suitable for almost all self-healing hydrogels. Another method is to punch a hole in the center of hydrogels. Photographs at different time intervals were taken to record the self-healing process of the hole in

the hydrogel. The hole in the hydrogel closed gradually, and finally disappeared completely (**Figure 2-11**b). The self-healed hydrogel exhibited similar appearance to the original hydrogel.[86-87, 127, 147] This hole contracting method is suitable for the weak self-healing hydrogels because the polymer chains have high mobility in the weak hydrogel system. The strong hydrogels have relatively stable shape. It takes long time for strong hydrogel to contract the hole.

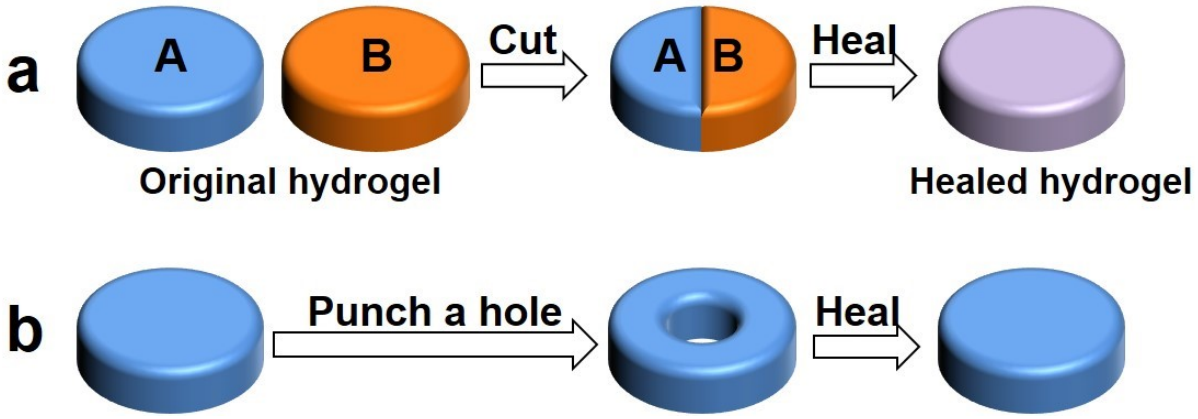

Figure 2-11. Schematic illustration of macroscopic observation of self-healing process.

Besides the macroscopic observation, microscope could also be used to observe the gradual disappearance of the boundary between the combined hydrogels (**Figure 2-12**a) on microscopic scale. Owning to the mobility of polymer chains and regeneration of cross-linking interactions, the crack distance decreased along with time. To further illustrate the disappearance of crack between the hydrogels and conform the complete healing of hydrogels, scanning electron microscope (SEM) was used to observe the boundary (**Figure 2-12**b). It was clearly seen that no crack existed between the hydrogels when the broken hydrogels healed to an integrate piece.

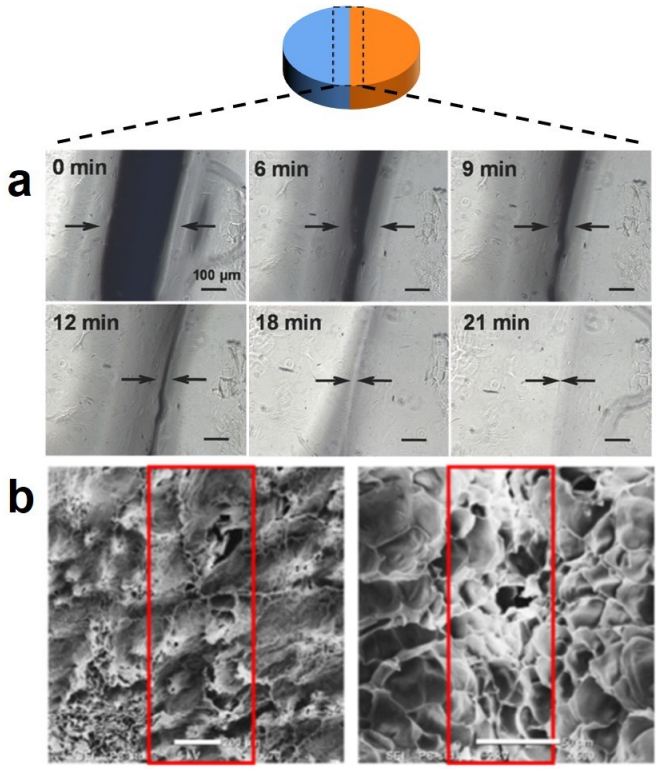

Figure 2-12. Schematic illustration of self-healing process: (a) Optical microscopic images of original hydrogel and healed hydrogel. Adapted with permission from ref.[107] Copyright (2017) John Wiley and Sons. (b) Scanning electron microscope (SEM) images of healed hydrogel. Adapted with permission from ref.[110] Copyright (2015) American Chemical Society.

The self-healing properties were quantitatively investigated using rheometer and universal test machine to more precisely determine the rheological self-healing efficiency. The storage modulus (G') and loss modulus (G'') versus frequency of original and healed hydrogel were measured to assess the self-healing performance of the hydrogels (**Figure 2-13**a1). The G' and G'' values of the healed hydrogels increased to the values of the original hydrogels, indicating the recovery of the inner structure of the network. The continuous step strain measurements were also performed to test the rheology recovery behavior of self-healing hydrogels (**Figure 2-13**a2). The alternate step strain sweep of hydrogel was measured at a fixed angular frequency (e.g. ω = 10 rad/s).

Amplitude oscillatory strains were switched from small strain (e.g. $\gamma = 1.0\%$) to subsequent large strain with 100 s for every strain interval. As the strain stepped from low strain to high strain and maintained for 100 s, the storage modulus (G') and loss modulus (G'') overlapped, while they immediately restored their original values once the strain moved back to low strain. The G' immediately recovered after the breaking strain was removed, suggesting the polymer network of the hydrogels exhibited rapid recovery ability.

Tensile and compression test of the self-healing hydrogels were also performed by universal test machine to quantitatively determine the self-healing efficiency. Hydrogels with elasticity were molded to rod or dumbbell shape to measure the tensile properties. The tensile stress-strain curves were recorded (**Figure 2-13**b), and the tensile self-healing efficiency (THE) was defined to the ratio of tensile strength of healed hydrogels to original hydrogels. Weak and brittle self-healing hydrogels could also be applied to test the tensile strength. Their self-healing efficiency was calculated by beam-shaped strain compression measurements (**Figure 2-13**c). Two identical hydrogel samples were prepared. One of them was cut in halves and then healed for a period of time. Both the original and the healed hydrogels were compressed by the beam-shaped mold (inset in **Figure 2-13**c1) until rupture occurred and the fracture strength of the original (S_0) and healed (S_h) samples were recorded. The compressive self-healing efficiency (CHE) was calculated as the ratio of fracture strength of healed hydrogel to original hydrogel ($CHE = S_h/S_0$).

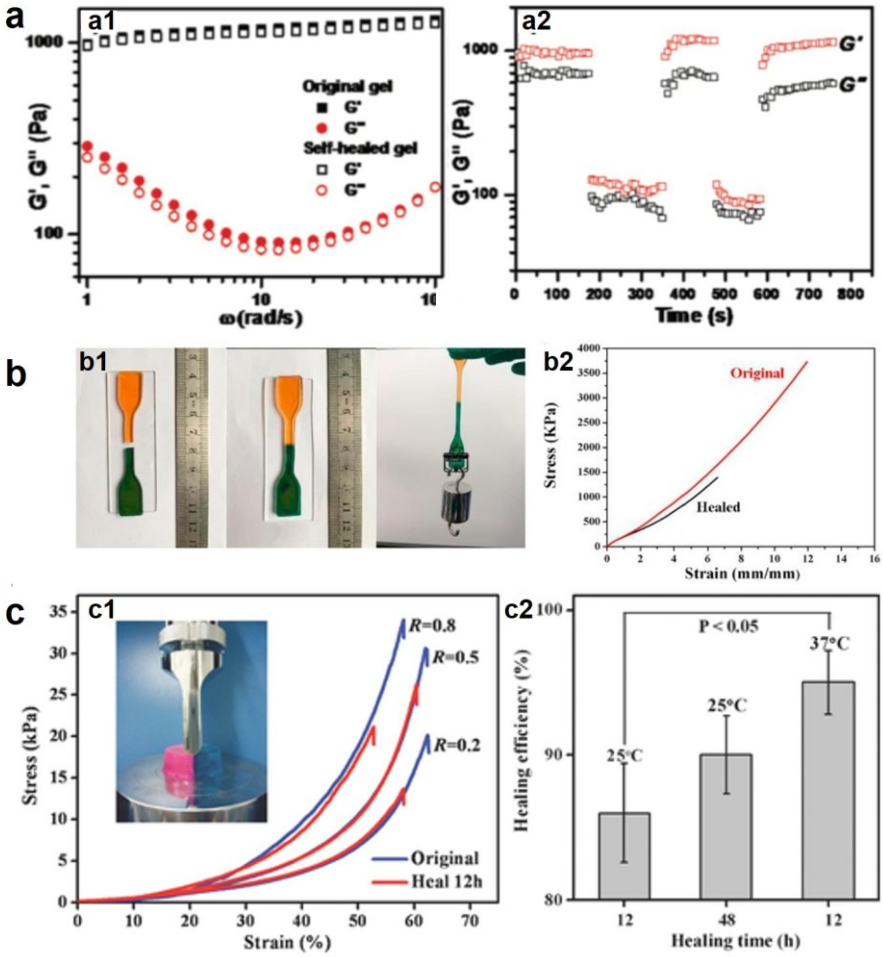

Figure 2-13. Schematic of self-healing process: (a) Rheological recovery test: (a1) Storage modulus G' and loss modulus G'' of original and self-healed hydrogels, and (a2) G' and G'' in continuous step strain (alternative high and low strain) measurements. Reprinted with permission from ref.[86] Copyright (2011) American Chemical Society. (b) Tensile stress recovery test: (b1) Optical images illustrating self-healing of a dumbbell-shaped hydrogel sample, and (b2) tensile stress-strain curves of original and healed hydrogels. Reprinted with permission from ref.[123] Copyright (2018) Elsevier. (c) Compressive stress recovery test: (c1) The beamed-shape compressive stress-strain curves of original and healed hydrogels, and (c2) healing efficiency (HE) of hydrogels. Reprinted with permission from ref.[15] Copyright (2015) John Wiley and Sons.

2.4.2 Mechanical properties

The mechanical property of self-healing hydrogels plays an essential role for their applications as biomaterials. For example, the mechanical properties of a self-healing hydrogel affect the proliferation and functions of cells encapsulated in the hydrogel matrix. The fate of neural stem cells (NSCs) relies on the hydrogel matrix's stiffness. NSCs neither survive well in very soft hydrogel (G' < 0.1 kPa) nor very hard hydrogels (G' > 100 kPa). Reasonably soft hydrogel (0.1-1 kPa) and slightly stiffer hydrogels (7-10 kPa) are beneficial to neuronal differentiation and glial differentiation, respectively.[71] A tough hydrogel that can bear load has potential use as a cartilage substitute, while a skin substitute not only requires stiffness but also elasticity.[148] The mechanical properties of self-healing hydrogels mainly depend on the composition and crosslinking density of the hydrogel network. The strategies to improve the self-healing hydrogels' mechanical properties involved the addition of star-shaped polymers, nanoreinforcing agents (e.g. cellulose nanocrystals), and a second network into the hydrogel system.

Employing CNCs as reinforced materials in hydrogels has been reported previously due to their fantastic features, such as large surface area, high mechanical strength, high aspect ratio, hydrophilicity, non-toxicity, low bulk density, biocompatibility, and biodegradability.[149-150] In the past few decades, the investigation and utilization of CNCs in functional materials has become an active field. In particular, Canada, as the world's leading producer of CNCs, ranks first in research in this area. The North American market for CNC may reach $250 million.[151] CNCs have been approved as the safest nanomaterials on Environment Canada's domestic substance list.[26] Compared with pristine CNC, the modifying and functionalizing CNCs are promising as they enable the creation of advanced materials with new or improved properties. Although several publications have demonstrated that CNCs with surface modification could function as both

nanofillers and cross-linkers to reinforce hydrogels, there are limited studies that reported self-healing hydrogels composed of modified CNCs. The oxidation of CNCs by sodium periodate can generate aldehyde groups for crosslinking reactions or for further modification, which can extend application of CNCs. Sodium periodate can selectively oxidize the hydroxyl groups in cellulose to 2,3-dialdehyde.[152] These aldehyde groups could act as potential cross-linkers since they will react with free amine groups of polymers (e.g. chitosan, gelatin) through Schiff-base linkages. Many oxidized polysaccharides (e.g. oxidized alginate, oxidized dextran) have been utilized to build self-healing hydrogels owing to their abundant aldehyde groups for Schiff-base formation.[15, 135, 153] However, limited works reported the self-healing hydrogels derived from chitosan and aldehyde modified CNCs. Dash et al developed a gelatin hydrogel crosslinked by oxidized cellulose nanowhiskers, and they observed a significant improvement in mechanical and thermal properties of the cross-linked hydrogels compared to neat gelatin hydrogels.[154] Yang and co-workers prepared an injectable polysaccharide hydrogel reinforced with cellulose nanocrystals. Oxidized CNCs (CHO-CNC) acted as both fillers and chemical cross-linkers, making the CHO−CNC-reinforced hydrogels more elastic and more dimensionally stable without sacrificing mechanical strength.[26] Research within this field has grown over recent years but modified CNCs only acted as additives in these hydrogel systems. A comprehensive study should be conducted to investigate the modified CNCs reinforced and crosslinked self-healing hydrogels.

Since Gong et al reported a general method to prepare extremely tough and strong hydrogels by inducing a double-network (DN) structure,[2] DN hydrogels have drawn much attention as a new class of hydrogels with high mechanical strength and toughness.[1, 155] The mechanical properties of DN hydrogels are comparable to those of rubbers and soft load-bearing tissues (e.g. cartilage).[155] Double network (DN) hydrogels comprise two different polymer networks. The first network is

rigid and brittle, which contains sacrificial bonds to break and dissipates energy under large deformation. The second network is soft and stretchable, endowing the hydrogels with elasticity.[156] However, the first-generation chemically linked DN hydrogels could not recover after break, which shortens their lifespan and increases product cost. Afterwards, reversible physically crosslinked first network has been introduced to DN hydrogels to extend their lifetime and improve the mechanical properties.[157] In contrast to the stable covalent bonds, the reversible interactions can break and reform at deformation to dissipate energy, which endows the hydrogels with high toughness and self-recovery properties. However, it is still challenging to develop a hydrogel exhibiting both high toughness and brilliant self-healing properties. Recently, dual physically crosslinked DN hydrogels have been developed with favorable mechanical properties, fast self-recovery properties, and good self-healing properties.[158-159] The dual physically crosslinked DN hydrogels usually need harsh conditions (e.g. high temperature) and long time to achieve self-healing. To address these problems, DN hydrogels consist of a dynamic covalent crosslinked network and a covalent crosslinked network may self-heal at room temperature in short time, because the dynamic covalent crosslinked network (e.g. Schiff-base linkages) can break and recover under moderate conditions.

The mechanical properties of self-healing hydrogels are usually determined by a rheometer or universal test machine.[74, 160-161] The mechanical strength of a hydrogel is quantified by determining the stress-strain relationship depending on the types of applied loads, including shear stress (**Figure 2-14**a), axial compressive stress (**Figure 2-14**b), and axial tensile stress (**Figure 2-14**c).[162] Viscoelastic properties are measured with a rheometer using parallel plates in the oscillatory mode. Firstly, the hydrogels are loaded to the sample plate, and then the upper rotating plate is lowered to a measuring gap size, and the test is started (**Figure 2-14**a-middle).[163] Oscillatory frequency

sweep measurements are carried out within the viscoelastic region to quantify the mechanical strength of hydrogels, in which the storage modulus (G') and loss modulus (G'') are measured as a function of time (**Figure 2-14**a-right). G' represents the elastic part of the hydrogel, while the G'' associates with the viscous part.[164] Self-healing hydrogels usually display an elastic characteristic with G' larger than G'' at a high frequency region. Higher storage modulus refers to stiffer hydrogel network.[110] Determining the mechanical properties of self-healing hydrogels under dynamic conditions is necessary when applying the self-healing hydrogel to living tissues because they are dynamic. On the contrary, compressive and tensile test are performed under static strain.[165] Compressive tests can be performed to obtain the compress stress-strain curve (**Figure 2-14**b-right). A self-healing hydrogel with high compressive stress (σ) means it has good fatigue resistance, while a hydrogel that fractures at low strain is brittle. Furthermore, tensile tests are conducted to examine the strength, extensibility, and elastic modulus of the self-healing hydrogels (**Figure 2-14**c-right). The elastic modulus is calculated from the slope of the linear section of the stress-strain curve.[166] Strong hydrogels exhibit high failure stress (tensile strength), whereas elastic hydrogels possess large elongation length. The toughness of a hydrogel can also be calculated from the tensile stress-strain curve, which equals to the area under the stress-strain curve.[167] A tough self-healing hydrogel shows high value of toughness. The tensile test is more suitable to the stretchable hydrogels than the brittle hydrogels which cannot be fixed by the clamps of a universal test machine.

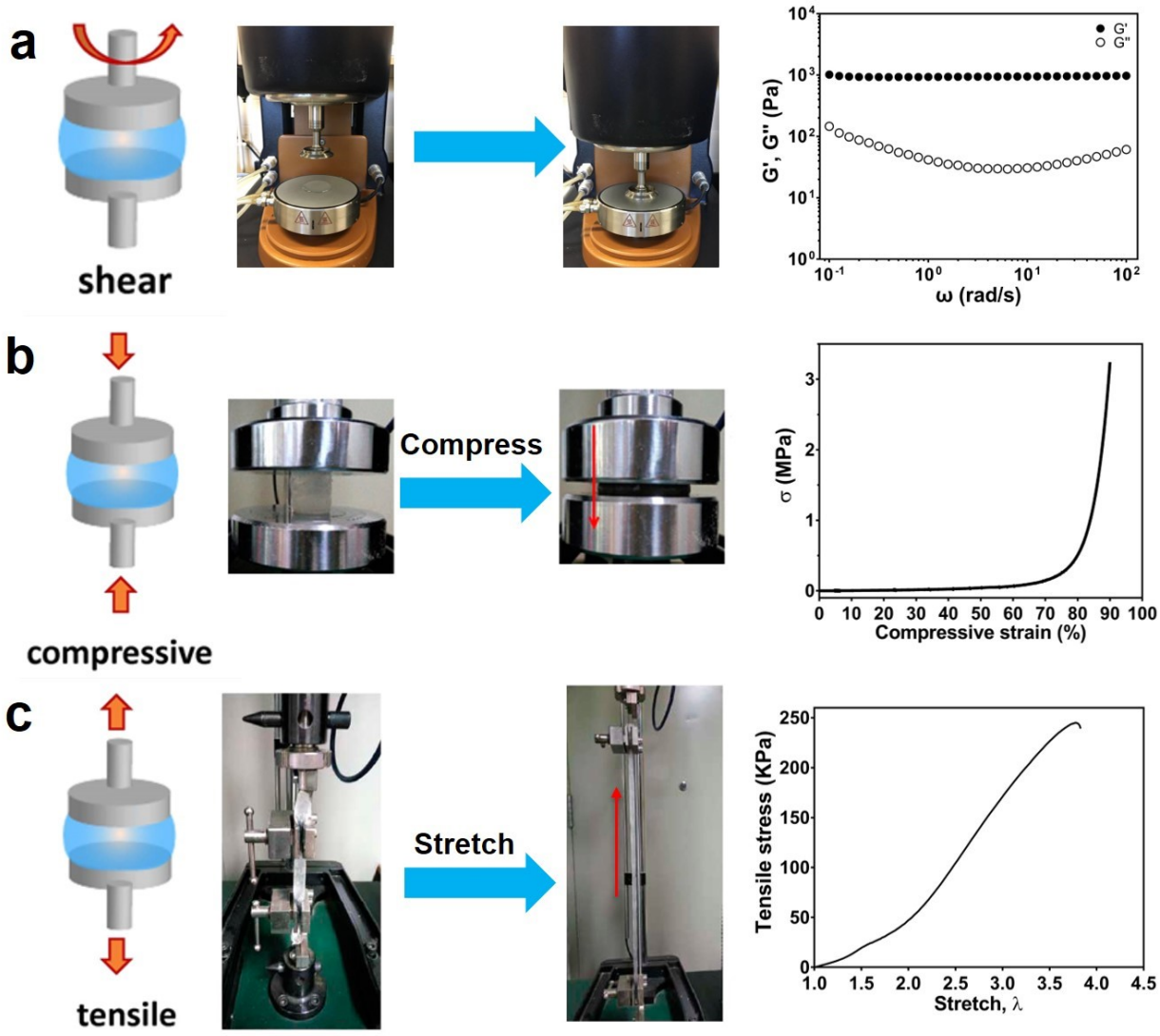

Figure 2-14. Schematic representation of methods for characterizing the mechanical properties of self-healing hydrogels: (a) Rheological test, (b) uniaxial tensile test, and (c) unconfined compressive test. (Left: test mechanism. Middle: test process. Right: typical results). Adapted with permission from ref.[161] Copyright (2017) American Chemical Society, and ref.[162] Copyright (2019) Springer Nature.

2.4.3 Adhesive capacity

There is a significant medical need for hydrogel adhesives that can self-heal while remaining strongly attached to tissues. Tissue adhesive capacity enables the hydrogels to attach to the target tissue surface after implantation, which avoids disruption by the movement of surrounding tissues. [168] Tissue adhesives are used for would sealing instead of suture to prompt hemostasis and wound healing.[169] Besides, the application of tissue adhesive could simplify complex suturing procedures, minimize damage, and reduce risk of infection.[170]

The cyanoacrylate tissue adhesives as a medical grade topical tissue adhesive have been extensively used for almost seven decades. They can strongly bond the apposed wound edges through polymerization of liquid monomers.[171] Nevertheless, the synthesized cyanoacrylates and derivatives demonstrated potential toxicity within patients and among doctors and nurses who are occupationally exposed when applying cyanoacrylates.[172-173] Thus, there is an urgent medical need for tissue adhesives that are biocompatible. Fibrin tissue adhesive obtained from autologous preparations showed good biocompatibility, but they lack the strength due to poor cohesive properties.[174]

It is a considerable clinical challenge to develop tissue adhesives with both good biocompatibility and high tissue adhesive strength, especially for wet tissues. Researchers turn their attention to nature. It is well known that a lot of living organisms (e.g. gecko, marine mussel, slugs) can strongly adhere themselves to various surface. Mahdavi et al developed a gecko-inspired adhesive by modifying the surface of a poly(glycerol-co-sebacate acrylate) elastomer to mimic the nanotopography of gecko feet, which has the ability to adhere to vertical and inverted surfaces through fibrillar arrays.[175] Furthermore, the nanomolded pillars were coated with a thin layer of oxidized dextran, which dramatically enhanced the interfacial adhesion strength on porcine

intestine tissue in vitro. Moreover, the mussel-inspired biocompatible hydrogel adhesives that covalently bond to wet tissues have been used in biomedical field.[22] Marine mussels can attach to various types of inorganic and organic surfaces in underwater environments, which lies in the mussel foot proteins rich in catecholic 3,4-dihydroxy-L-phenylalanine (DOPA) and lysine amino acids.[176] Shin et al developed a bioinspired, tissue-adhesive catechol modified hyaluronic acid (HA-CA) hydrogel via oxidative crosslinking. Cell encapsulated in HA-CA hydrogel could be easily and efficiently transplanted onto various tissues due to the strong tissue adhesiveness of HA-CA hydrogels.[24] Additionally, inspired by a defensive mucus secreted by slugs (*Arion subfuscus*) that can strongly adhere to wet surfaces, Li et al prepared a tough tissue adhesive that consisted of an adhesive surface and a dissipative matrix.[177] The adhesive surface comprised an interpenetrating positively charged polymer, so it could strongly attach to the substrate through electrostatic interactions, covalent bonds, and physical interpenetration. The matrix dissipates energy through hysteresis under deformation.

The most widely used approach to measure the tissue adhesive strength is lap shear strength tests (**Figure 2-15**A). Fresh pig skin is cut into small pieces, and the adhesive is spread to one end of a piece of pigskin. Another pigskin piece is immediately covered onto the previous one to make the overlapping area. The adhered samples are then processed for the tensile test. The adhesive strength is calculated as the ratio of the tensile stress to the overlapping area. Additionally, pressure testing has been used to evaluate the sealant capacity and adhesive properties of the tissue adhesives. An incision has been made on an intact tissue (e.g. heart) and then sealed with the adhesive (**Figure 2-15**B). The pressure within the system increases until the adhesive is broken.

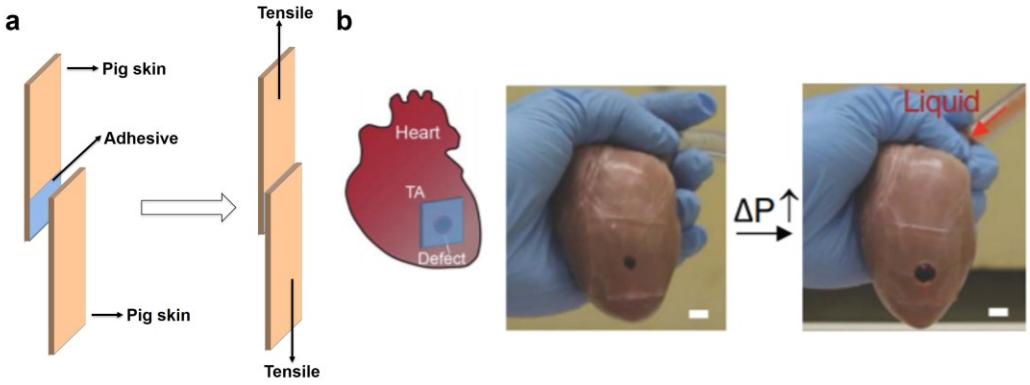

Figure 2-15. (a) Schematic illustration of lap shear strength tests, and (b) tissue adhesives served as heart sealants. The tissue adhesive sealant could prevent liquid leakage as the porcine heart was inflated. Reprinted with permission from ref.[177] Copyright (2017) The American Association for the Advancement of Science.

In spite of high potential to develop multi-functional self-healing hydrogels for biomedical applications, incorporating good mechanical properties, rapidly self-healing process, and strong tissue adhesive capacity into one self-healing hydrogel system is still a daunting challenge. Self-healing hydrogels possess poor mechanical properties as a consequence of the weaker nature of the reversible interactions compared to that of covalent bonding. It seems that the self-healing and mechanical properties are two contradictory characteristics, which makes it difficult to optimize them simultaneously. Moreover, adhesion to wet and dynamic biological tissues is important in biomedical fields but has proven to be extremely challenging. Thus, innovative design is still required to improve these properties of self-healing hydrogels.

2.5 Biomedical applications of chitosan-based self-healing hydrogels

Over the past decade, there has been a growing interest in chitosan-based self-healing hydrogels due to the prolonged lifetime, rapid self-healing process, tunable mechanical properties, injectability, biodegradability, and biocompatibility. They have demonstrated potential applications in biomedical field, such as controlled drug release,[88, 98, 113] three-dimensional cell encapsulation and delivery,[89, 103] tissue engineering,[71, 139] hemostasis,[99, 103] and wound healing.[90, 100]

2.5.1 Drug delivery

Chitosan-based self-healing hydrogels are promising candidates as cargo delivery vehicles for controlled release mainly due to the injectability and pH-sensitivity. The slow gelation of the traditional injectable hydrogels resulted in cargos loss and diffusion from the target sites, while the rapid gelation may lead to undesired premature solidification and blocking of needle. The traditional injectable hydrogels are injected as liquids and then formed gel *in situ*, in contrast, self-healing hydrogels loaded with cargos that are homogeneously mixed in the pre-gel solution are injected to target sites as a gel status, which protects the sensitive drugs/cells in the hydrogel.[178] The self-healing hydrogels could smoothly pass through the narrow needle due to the shear-thinning property, avoiding the risk of needle clogging.[69] After injection, the broken self-healing hydrogels could recover the integral network and remain at the target site.[179] Therefore, self-healing hydrogel as a new drugs/cells delivery system can increase the cargos delivery efficiency and improve the therapeutic effect. Self-healing hydrogels instead of traditional injectable hydrogel are becoming increasingly popular in biomedical field.

A series of self-healing hydrogels with injectability and pH-sensitivity have been applied as drug delivery vehicles. pH-responsive hydrogels exhibited pH-dependent gel degradation and release

of antitumor drugs, which are suitable for chemotherapy. A chitosan (CS)/polyvinyl alcohol (PVA) self-healing hydrogel was developed and used as an injectable drug carrier for localized chemotherapy.[127] The self-healing hydrogel exhibited good biocompatibility and could be easily and rapidly formed. Moreover, the CS/PVA self-healing hydrogel could swell and degrade easily in acidic environment, so the acidic environment of tumor cells could promote drug release, which relied on the pH sensitivity of the Schiff-base linkages. The Schiff-base linkages are unstable under acidic conditions, while they could be reconstructed by regulating the pH to neutral, leading to recovery of the mechanical integrity of the hydrogel.[108] The CS/PVA self-healing hydrogel loaded with fluorouracil (5-FU, a thymidylate synthase inhibitor and an antineoplastic) showed good drug retention ability at pH 7 (60.8% 5-FU was retained in the hydrogel after 6 days), which could prevent 5-FU from diffusing to normal cells and reduce the side effect. While the hydrogel exhibited continuous and controllable drug release at pH 5, and the final cumulative releasing amount reached to 84.8%. The CS/PVA self-healing hydrogel maintained a higher antineoplastic concentration around tumor cells to improve the antitumor effect and achieved pH-sensitive controllable drug release at the target sites.

Combination of two or more drugs into one delivery system has been considered to have significant impact on cancer treatment due to their efficient synergistic effect. An injectable and self-healing thermosensitive magnetic hydrogel, consisting of chitosan and DF-PEG, was applied for asynchronous control release of doxorubicin (DOX) and docetaxel (DTX) to treat triple-negative breast cancer.[88] Iron oxide for magnetic hyperthermia could induce stimuli responsive drug release. The DOX/DEX-laden chitosan/DF-PEG/Fe_3O_4 hydrogels not only exhibited self-healing and injectable ability, but also good biocompatibility and asynchronous control release property. Yavvari et al also utilized a chitosan-catechol/Fe^{3+} based self-healing hydrogel loaded with both

DOX and DTX for localized combination therapy in murine lung and breast cancer models.[120] They also found synergistic therapeutic effect from the sequential and sustained release of the entrapped DOX and DTX from the hydrogel.

2.5.2 Cell therapy

Chitosan-based self-healing hydrogels have received increasing attractions in cell therapy. Self-healing hydrogels as extracellular matrix mimics are suitable for the proliferation of cells encapsulated in the hydrogel scaffold.[180] Moreover, gelation of most chitosan-based self-healing hydrogels readily occurred under physiological conditions. In addition, cell-laden self-healing hydrogels could be injected to desired sites through a minimally invasive way and accommodate irregular shaped defects, which could protect cells from damage and deliver cells to the target sites. Recent reports have demonstrated growth of cells encapsulated in self-healing hydrogels without extra added growth factor.[15, 89, 181-182] 3D cell proliferation is a critical factor for cell therapy, especially, after injection.

Yang et al demonstrated the proliferation regulation of the 3D-embedded HeLa cells in a modulus-tunable and injectable self-healing hydrogel before and after injection without adding specific growth factor.[89] HeLa cells were suspended in culture media and mixed with glycol chitosan (GSC) solution dissolved in the same media. Then the DF-PEG solution was added into the HeLa-GSC suspension and gently mixed to induce gelation (**Figure 2-16**). The cell viability after one day and three days was ~97% and ~87%, respectively, suggesting HeLa cells could tolerate the 3D encapsulation in the hydrogels and live well in the hydrogel. To further investigate the effects of injection through a needle on the cell viability, the cell-laden GSC/DF-PEG self-healing hydrogels were prepared in a syringe and then extruded through a 21-gauge needle. The cell viability was as high as ~87% after injection and self-healing processes, which indicated HeLa cells could only

tolerate 3D encapsulation, but also the following injection and self-healing processes. After 24 h, there were ~85% of cells living in the hydrogel. The cell viability and the distribution are the most important two aspects when determining the potential of self-healing hydrogels as cell delivery vehicles. As shown in the 3D confocal microscopy image, the cells were homogenously distributed in the hydrogel. The authors suggested that the GSC/DF-PEG self-healing hydrogel might have potential for 3D cell culture and cell therapy. Lü et al encapsulated HeLa cells in a self-healing hydrogel composed of chondroitin sulfate multiple aldehyde (CSMA) and *N*-succinyl chitosan (SC). Cells encapsulated in the hydrogel remained viable and metabolically active.[110] The mouse NIH 3T3 fibroblasts were encapsulated in a polysaccharide-based self-healing hydrogel comprising *N*-carboxyethyl chitosan (CEC), adipic acid dihydrazide (ADH), and oxidized sodium alginate (OSA). The cell viability of NIH 3T3 fibroblasts encapsulated in the hydrogel was 98.5% ± 1.2%, 97.6% ± 4.0%, and 95.3% ± 3.4% after 12, 24, and 48 h *in vitro* culture, respectively.[15] CEC-OSA self-healing hydrogels were also applied to encapsulated neural stem cells (NSCs). The NSCs were uniformly dispersed in CEC-OSA hydrogels and exhibited ~90% cell viability after cultivation for 1, 3 and 5 days. After injection, the cell viability of NSCs loaded inside the self-healed CEC-OSA hydrogel was ~80% after cultivation for 1, 3 and 5 days.[106]

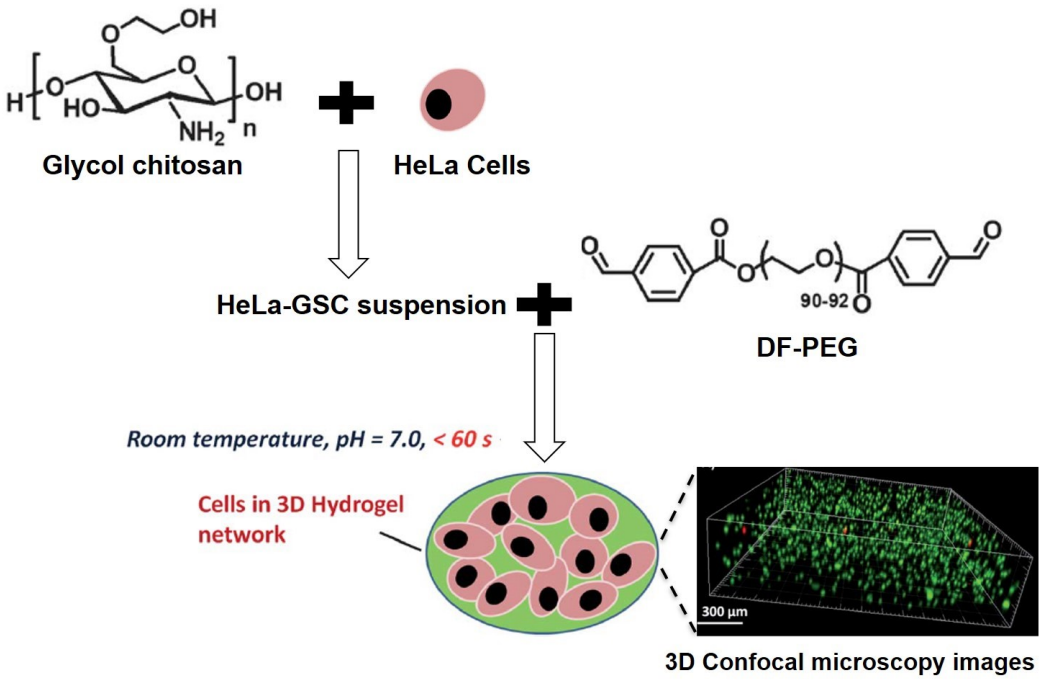

Figure 2-16. Schematic of preparation of cell-laden self-healing hydrogel, and 3D confocal microscopy images of cells encapsulated in hydrogel scaffold. Adapted with permission from ref.[89] Copyright (2012) Royal Society of Chemistry.

2.5.3 Tissue engineering

Self-healing hydrogels have shown potential for tissue engineering application. Neurological disorders are diseases of the body nervous system. They have not yet been completely recovered, especially for central nervous system disorders. Transplantation of neural stem cells (NSCs) is a promising therapeutic strategy to treat neurological disorders. Chitosan-based self-healing hydrogels have been developed to repair the central nervous system.[71, 106] Neural stem cells were encapsulated in the glycol chitosan(GSC)/aldehyde functionalized PEG (DF-PEG) self-healing hydrogel. The neurospere-like aggregates of NSCs proliferated twice faster and had a much greater tendency to differentiate neuron-like cells in the self-healing hydrogels than those in alginate hydrogel. In the zebrafish embryo neural injury model, injection of the self-healing hydrogel alone

partially rescued the neural nerous system (≈ 38% recovery), while injection of the self-healing hydrogel encapsulated with neurosphere-like progenitors produced a much better healing effect on neural development (≈ 81% recovery). The chitosan-based self-healing hydrogel encapsulating aggregated neuro-progenitors represents a promising vehicle for treating the central nerve system deficits due to their good injectable and self-healing properties. Self-healing hydrogels rapidly break and reform according to cell activities, while retaining the physical integrity, which are beneficial to the proliferation of cells encapsulated in the hydrogel.

A major challenge in tissue engineering is to generate a functional microvasculature that ensures proper blood perfusion and connection with surrounding microenvironment. Although various strategies have been applied to construct vascular network in a tissue engineering construct, they are yet to be fully realized. Chitosan can promote angiogenesis in corneal and skin tissue, and fibrin is a biological polymer in vertebrates that accounts for arterial endothelial cell adherence and induces angiogenesis at the site injury.[94] Vascular endothelial cells seeded in chitosan-fibrin/DF-PEG based self-healing hydrogels were able to form capillary-like structures, which was associated with the self-healing ability, the interpenetrating polymer network structure, and the appropriate stiffness (~1.2 kPa) of the hydrogel.[94] In addition, the chitosan-fibrin/DF-PEG self-healing hydrogel alone promoted angiogenesis in the perivitelline space of zebrafish and rescued the blood circulation in ischemic hindlimbs of mice. This self-healing hydrogel offers new possibilities for future applications to vascular repair.

2.5.4 Hemostasis

Chitosan possesses good hemostatic properties mainly due to the positive charge, which can interact with anions on the red blood cells, thus inducing platelet aggregation and finally stopping bleeding.[81-82, 183] Chitosan-based self-healing hydrogels could be injected to inner and irregular

bleeding sites to promote the hemostatic process. An injectable conductive self-healing hydrogels, consisting of quaternized chitosan-g-polyaniline (QCSP) and benzaldehyde group functionalized poly(ethylene glycol)-co-poly(glycerol sebacate) (PEGS-FA), were chosen for *in vivo* hemostatic study because it simultaneously possessed rapid gelling, autonomously self-healing ability, and good blood compatibility, antibacterial activity, and adhesive property.[99] The hemostatic ability of the QCSP/PEGS-FA self-healing hydrogel was evaluated using a hemorrhaging liver mouse model. The amount of blood loss after either applying the hydrogel or without treatment (control group) on the hemorrhaging site was determined by macroscopic observation and quantitatively weighing the lost blood. Hydrogel group and control group had a total blood loss of 214.7 ± 65.1 mg and 2025.9 ± 507.9 mg, respectively. The QCSP/PEGS-FA self-healing hydrogels showed good blood clotting capacity. The authors proposed that a synergistic hemostatic effect from the natural hemostatic activity of chitosan, positive-charged quaternary ammonium groups and polyaniline segments and the adhesive property of the hydrogel might contribute to the hemostatic performance. Chen et al prepared a self-healing hydrogel composed of dodecyl modified chitosan (DCS) and four-armed benzaldehyde-terminated polyethylene glycol (PEG-BA) exhibited good hemostasis function because the dodecyl tails on the DCS could be inserted into and be anchored onto the lipid bilayer of the cell membrane, thus, the blood cells could coagulate on the interface of bleeding sites and hydrogels, forming clots to stop bleeding.[105] Although the use of self-healing hydrogels has promoted hemostasis to a certain degree, the recently developed self-healing hydrogels could only contribute to venous bleeding rather than hemorrhaging, which remains the primary cause of prehospital trauma deaths.[184-185] The low mechanical strength made self-healing hydrogels easily be flushed away by the intensive blood pressure. A strategy that holds great

potential to overcome this problem is the development of strong adhesive self-healing hydrogels, which can stably adhere and stanch the injure.

2.5.5 Wound healing

Wound healing dressing could promote wound healing and reduce scar formation.[186] Chitosan-based self-healing hydrogels as wound healing dressing present many unique properties, such as injectability, self-adapting property (**Figure 2-17**), *in situ* encapsulating drugs and biocompatibility. Conventional wound dressings like bandage faces considerable problems in deep and irregular wounds as well as joint wounds. The unstable connection between dressings and wound site weakens their availability and reliability. The self-healing hydrogels could be adjusted to differently shapes according to the wound contour,[187] thus, the injectable self-healing hydrogels can be simply injected into the deep and irregular wound beds and then recover to an integrate hydrogel that fully fill the wound.

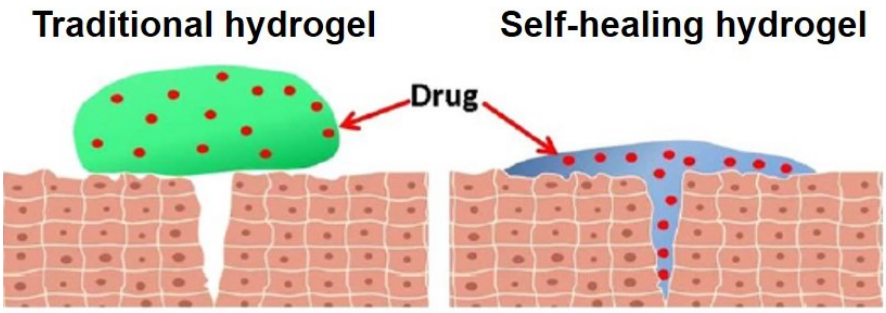

Figure 2-17. Schematic illustration of wound-healing by a traditional hydrogel and a self-healing hydrogel. The traditional hydrogel just could cover the top surface of wound beds, while the self-healing hydrogel could self-adapt to fully fill the irregular and deep wound beds. Adapted with permission from ref.[91] Copyright (2018) American Chemical Society.

Chitosan (CS)/oxidized konjac glucomannan (OKGM) based self-healing hydrogels with inherent antibacterial capacity significantly shortened wound recovery time in a full-thickness skin defect model.[112] Wounds treated with the CS/OKGM hydrogel and chitosan solution exhibited closure on day 12 and 16, respectively, but wounds without any treatment were not fully closed on day 16. The QCSP/FEGS-FA self-healing hydrogel exhibited better wound healing effect than commercial dressing (Tegaderm™ film) in a full-thickness skin defect model.[99] Guo et al demonstrated that Dex-AT-FA/CEC hydrogels could efficiently enhance the regeneration of the skeletal muscle tissue in a volumetric muscle loss injury model.[100] In addition to hemostasis, the DCS/PEG-BA self-healing hydrogel encapsulated with vascular endothelial growth factor (VEGF) could also be used as a wound dressing for chronic wound healing.[105] The GCS/DF-PEG hydrogels with thrombin have been used to treat hemorrhaging livers in rats and exhibited excellent therapy effect of wound-healing.[91] Qu et al applied the QCS/PF127-CHO based self-healing injectable micelle/hydrogel composites with multi-functions, including moderate stretchability, compressibility, excellent self-healing ability and pH-responsive ability, as wound dressing for joint skin damage. Curcumin was encapsulated in the hydrogel, which showed good antioxidant ability and pH responsive release profiles. Curcumin-laden hydrogels accelerated wound healing rate with high granulation tissue thickness and collagen disposition and upregulated VEGF in a full-thickness skin defect model.[77] Most of these hydrogels could only repair a simple wound, which restricted their wide applications in the clinic. Compared with regular wounds induced by mechanical factors, burn wounds, especially deep partially thickness burn wounds, are more difficult to treat because they usually produce massive wound exudate and are easily infected, as well as the wound area is large and irregular. Additionally, it is painful to remove the wound dressing by mechanical and physical peeling at the wound dressing changes. Although the burn

wounds can eventually heal, but it forms scars. Thus, the creation of new self-healing hydrogels that can prompt burn wound healing without scarring and be painlessly removed is still anticipated.

2.6 Conclusions and outlook

Self-healing hydrogels is a smart material with reversible interactions that endow the hydrogel with self-healing ability. Over the past few decades, there has been a growing interest in self-healing hydrogels. Compared to conventional hydrogels, self-healing hydrogels have extended life-times and improved product safety because they can autonomously repair hydrogel networks following damage. The rise of self-healing hydrogels has created new opportunities and challenges in materials area. Currently, most of researchers have focused on developing new self-healing mechanisms and polymers to prepare self-healing hydrogels. Diverse chitosan derivatives and cross-linkers have been utilized to form the chitosan-based self-healing hydrogels. Nevertheless, as the self-healing hydrogels are just emerging, their poor mechanical performance restricts the practical applications. Efforts should be made towards improving both the mechanical properties and self-healing efficiency of self-healing hydrogels derived from natural polymers. In addition, adhesion to biological tissues is a highly challenging task because the adhesive hydrogels should possess an adhesive strength in the presence of physiological fluids. Endowing self-healing hydrogels with adequate tissue adhesive capacity will widen their applications.

Currently, efforts have been focused on applications of self-healing hydrogels in industrial fields, such as electronics, automotive and chemical production. The published papers on their applications in biomedical areas are much less. Self-healing hydrogels derived from natural polymers are biodegradable and biocompatible for biomedical applications, thus these areas of applications such as hemostatic materials and wound healing dressing should be further addressed. Moreover, current reports on self-healing hydrogels barely focused on synthesis and self-healing

mechanisms of self-healing hydrogels, limited studies investigated the structure-function relationship of the self-healing hydrogels. The compositions and interactions of the self-healing hydrogels have significant effect on the self-healing efficiency and mechanical properties. A deeper understanding of structure-function relationships of self-healing hydrogels will pave the way for innovative strategies for synthesizing new self-healing hydrogels with desired features and applying them in biomedical field.

Chapter 3

Strong and Rapidly Self-healing Hydrogels: Potential Hemostatic Materials

3.1 Introduction

Self-healing hydrogels are a new class of emerging "smart" hydrogels with the ability to repair a broken network without external stimuli. These hydrogels maintain and reconnect their integrated network and mechanical properties even after being damaged. Currently, most researches on self-healing hydrogels have focused on their synthesis and characterization, but very few practical applications of self-healing hydrogels have been reported, especially for biomedical applications. Until now, self-healing hydrogels have only been explored as biomaterials for three-dimensional (3D) cell encapsulation and transplantation. This is because these self-healing hydrogels can repair a fractured network destroyed by cellular actions. Self-healing efficiency and mechanical strength are the most critical and limiting properties for their practical application. For example, the dynamic behaviors of hydrogels show promise as extracellular matrix mimics for 3D cell encapsulation. Normally, cell behavior, such as movement, growth, and proliferation, can degrade the hydrogel network, and thus deteriorate its mechanical strength and even result in hydrogel disappearance in long-term cell culture. This is not a problem in self-healing hydrogels because they can spontaneously repair a broken network. Good self-healing systems can quickly re-form broken matrices and well maintain the structure stability and mechanical strength of the hydrogel. The spatial integrity and mechanical properties of hydrogels have a profound influence on cell functions.[8, 71, 188] For example, living cartilage tissue is a kind of multi-functional hydrogel. Cartilage is strong and the resident chondrocytes do not live well in a very soft hydrogel, and their fate depends on the mechanical strength of hydrogel.[189] However, it is difficult to combine high

self-healing efficiency with high mechanical strength. On the one hand, mechanical strength normally comes from strong and stable cross-linking interactions, but on the other hand these forces may restrict the mobility of polymer chains necessary for the recovery of a gel network.

Due to good biodegradability and biocompatibility, chitosan has been widely applied in hemostasis, wound healing, and tissue engineering.[183, 189-190] Chitosan can only dissolve in water under acidic conditions, which limits its application as matrices of living cells and tissues that prefer a neutral microenvironment. Thus the water-soluble derivative of chitosan, carboxymethyl chitosan (CMC) presents a more appropriate material to form extracellular matrix mimics for three-dimensional cell encapsulation.[188] Chitosan or glycol chitosan cross-linked with dibenzaldehyde-terminated telechelic polyethylene glycol (DE-PEG) can form a self-healing hydrogel through dynamic Schiff-base linkages between amino groups on chitosan backbone and aldehyde groups at the end of DF-PEG chains.[86, 89] However, the self-healing efficiency is slow and the mechanical strength is not ideal. Polyethylene glycol (PEG) is also biocompatible and has been widely applied in tissue engineering.[134] Star-shaped PEGs are especially popular cross-linkers for forming hydrogels with good mechanical strength.[191-192] Hence, compared with linear PEG, the four-arm PEG is a good potential material to form strong hydrogels since the four-arm polymers behave as impenetrable space-filled spheres and there are only a few entanglements frozen into the network. This is markedly different from that of conventional linear polymer-based networks. Therefore, four-arm based networks are more resistant to fracture than equivalent two-arm polymer based networks of the same average crosslink density.[193-194]

In this project, in order to simultaneously improve both mechanical strength and self-healing ability, benzaldehyde-terminated four-arm poly (ethylene glycol) (PEG-BA) was synthesized by Steglich esterification of hydroxyl-terminated four-arm PEG with 4-formylbenzoic acid. A molar

ratio of CMC to PEG-BA and the total solid content of hydrogels were optimized to obtain strong and rapidly self-healing hydrogel. The gelation performance of the optimized CMC/PEG-BA hydrogels was investigated by rheological analysis. Their self-healing behaviors were systematically demonstrated by rheological recovery, macroscopic and microscopic observation of self-healing process, and beam-shaped strain compression measurements. Furthermore, cytotoxicity and biocompatibility were evaluated using normal adult human primary dermal fibroblasts model via MTT assay and three-dimensional (3D) cell encapsulation, respectively. To date, self-healing hydrogels have not been reported as hemostatic materials. Strong and rapidly self-healing hydrogels are potential hemostatic materials, because they can be directly injected to a trauma or surgical site and form a tough barrier to entrap platelets and stop bleeding. Therefore, their hemostatic property was investigated *in vivo* using rabbit liver injury model.

3.2 Experimental section

3.2.1 Materials

Chitosan (viscosity-average molecular weight: 12.4×10^5, degree of deacetylation: 80%), sodium hydroxide (NaOH, ACS reagent, ≥97.0%), sodium chloroacetate ($ClCH_2COONa$, 98%), 4-formybenzoic acid (97%), *N, N'*-dicyclohexylcarbodiimide (DCC), diethyl ether (anhydrous, ACS reagent, ≥99.0%), 4Å molecular sieves, rhodamine B (≥95% (HPLC)), thiazolyl blue tetrazolium bromide (MTT, ≥97.5% (HPLC)), dimethyl sulphoxide (DMSO, Hybri-max®), fluorescein diacetate (FDA), and prodidium iodide (PI, ≥94.0% (HPLC)) were purchased for Sigma-Aldrich Canada Ltd. (Oakville, ON, Canada) and were used without further treatment. Isopropanol (Optima®), 4-(dimethylamino)pyridine (DMAP, 99%, Acros Organics), tetraphydrofuran (THF, THF was dried prior to use), ethyl alcohol and methylene blue were purchased from Fisher Scientific (Markham, ON, Canada) and were used as received unless otherwise described. Four-

arm polyethylene glycol (4-arm PEG, Mw 10K Da, 99%) was supplied by Creative PEGWorks (Chapel Hill, NC, USA). 1×Dulbecco's phosphate buffered saline (DPBS, GIBCO®) was obtained from GIBCO (Burlington, ON, Canada). The normal adult human primary dermal fibroblasts cell line (ATCC® PCS-201-012™), fibroblast basal medium (ATCC® PCS-201-030™), fibroblast growth kit-low serum (ATCC® PCS-201-041™), trypsin-EDTA (ATCC® PCS-999-003™, 0.05% trypsin and 0.02% EDTA in phosphate buffered saline without calcium or magnesium), and trypsin neutralizing solution (ATCC® PCS-999-004™) were purchased from American Type Culture Collection (ATCC, Manassas, VA, USA).

3.2.2 Synthesis of carboxymethyl chitosan (CMC)

Chitosan (10 g) was dispersed in 120 g 50 wt.% NaOH aqueous solution and then was kept at -20 °C for 12 h. The frozen alkali chitosan was transferred to a 500 mL three-neck glass flask and 100 mL isopropanol was poured into it. Subsequently, sodium chloroacetate (35 g) was added in portions within 30 min and reacted for 2 h at room temperature (22 °C) with mechanical stirring, and then reacted at 60 °C (water bath) for another 2 h. The reaction was stopped by adding 70% ethyl alcohol (150 mL). The crude CMC was washed with 500 mL 70% ethanol and 500 mL ethanol, and was dried at 60 °C. The dried crude CMC was dissolved in 300 mL deionized water and then adjusted to pH 7 by adding 6 mol/L HCl aqueous solution. After dialyzing against deionized water for one week, the CMC product was freeze-dried and stored at 4 °C for further use. The synthesis of CMC was studied by Fourier transform infrared spectrometer (FT-IR) and proton nuclear magnetic resonance spectrometer (^{1}H NMR, 400 MHz, D_2O).

3.2.3 Synthesis of benzaldehyde-terminated four-arm PEG (PEG-BA)

Four-arm PEG (2.00 g, 0.2 mmol), 4-formylbenzoic acid (0.24 g, 1.6 mmol), and DMAP (0.049 g, 0.4 mmol) were dissolved in 100 mL dry THF, followed by the addition of DCC (0.41 g, 2 mmol) in a 250 mL three-neck flask under nitrogen atmosphere. The system was stirred at room temperature for 24 h and the solid powder was filtered. The product was obtained as white solid powder after repeated dissolution in THF and precipitation in diethyl ether for three times. The chemical structure of PEG-BA was invested via FT-IR and ^{1}H NMR (^{1}H NMR, 400 MHz, D_2O).

3.2.4 Preparation of CMC/PEG-BA hydrogel

CMC (400 mg) was dissolved in 10 mL of ultrapure water to prepare the 4% (w/v) CMC solution. The 8% (w/v) PEG-BA solution was obtained by dissolving 800 mg of PEG-BA in 10 mL of ultrapure water. As a typical hydrogel preparation, PEG-BA solution was added to CMC solution at room temperature. The gelation occurred within ~100 s of vortex. **Table 3-1** shows hydrogel samples with various total concentrations of polymers (T) and mass ratios of CMC/PEG-BA (R).

Table 3-1. Components of various self-healing CMC/PEG-BA hydrogels.

Samples	Mass ratio of CMC/PEG-BA (R)	Molar ratio of $-NH_2$/-CHO*	Total solid content (T)
CMC/PEG-BA (R = 1/2, T = 4)	1:2	0.73	4 wt.%
CMC/PEG-BA (R = 1/2, T =5)	1:2	0.73	5 wt.%
CMC/PEG-BA (R = 1/1, T = 5)	1:1	1.45	5 wt.%
CMC/PEG-BA (R = 2/1, T = 5)	2:1	2.91	5 wt.%
CMC/PEG-BA (R = 3/1, T = 5)	3:1	4.36	5 wt.%
CMC/PEG-BA (R = 1/2, T = 6)	1:2	0.73	6 wt.%

* Molar ratio of amino groups to aldehyde groups was calculated based on ^{1}H NMR of CMC and PEG-BA, there are 1.16×10^{-3} mol amino groups in 1 g CMC, and 0.8×10^{-3} mol aldehye groups in 1g PEG-BA.

3.2.5 Characterizations

FT-IR spectra of the samples were recorded on a Nicolet 6700 spectrophotometer (Thermo Fisher Scientific Inc., MA, USA). The chitosan powder, CMC powder, 4-arm PEG powder, PEG-BA powder and freeze-dried CMC/PEG-BA hydrogel were vacuum-dried for 24 h and were pressed into pellets with KBr powder for testing. Spectra were recorded as the average of 64 scans at 4 cm^{-1} resolution and 25 °C, using the pure KBr pellet as blank. During measurements the accessory compartment was flushed with dry air.

3.2.6 Rheological analysis

Dynamic rheological test was carried out on a DHR-3 rheometer (TA Instruments, DE, USA) at 25 °C unless otherwise description with a 40 mm diameter flat plate attached to a transducer. The gap was set to 1 mm. (1) The storage modulus G' and loss modulus G'' of CMC/PEG-BA hydrogel discs (20 mm in diameter) with different weight ratios and total weight contents were tested under a 1.0% strain level, and the angular frequency (ω) was swept from 0.1 rad s^{-1} to 100 rad s^{-1}; (2) The CMC/PEG-BA hydrogel (R = 1/2, T = 6) was measured under strain amplitude sweep (γ=1%-1000%) at 10 rad s^{-1} angular frequency. (3) The alternate step strain sweep of CMC/PEG-BA hydrogel (R = 1/2, T = 6) was measured at 10 rad s^{-1} angular frequency, and amplitude oscillatory strains were switched from γ = 1% strain to large strain (γ = 180%, 300%, 800%) with 100 s for every strain interval. (4) Similar to step (3) experiments were carried out for γ = 800% with loading time changed from 100 s to 200 s for each strain level. (5) G' and G'' versus time were tested to obtain the gelation time at 25 °C and 37 °C. The CMC solution was loaded onto test plate and then the PEG-BA solution was added into CMC solution to form gel (time t = 0).

3.2.7 Self-healing performance test

(1) Macroscopic hydrogel recovery experiment: CMC/PEG-BA hydrogel (R = 1/2, T = 6) was added into 1 mL syringe (BD, Franklin lakes, NJ, USA) and injected to be strips on the surface of a PTFE plate. Seven hydrogel strips were prepared successively and placed side by side. They were then kept in a desiccator containing KNO_3 saturated solution (HR = 93% (25 °C)) to avoid dehydration for 30 min at room temperature and taken pictures after 0 min, 5 min, and 30 min to test the self-healing properties. Self-healing was confirmed by the capacity of the healed hydrogel to hold its structure when suspended under gravity.

(2) Microscopic hydrogel recovery experiment: A crack was created with a knife on CMC/PEG-BA hydrogel (R = 1/2, T = 6). At various time intervals (1 h, 2 h), optical microscopy (ZEISS Primovert, Carl Zeiss, Inc., Germany) images were taken to record the microscopic self-healing process of the hydrogel.

(3) Healing efficiency of the CMC/PEG-BA hydrogel (R = 1/2, T = 6) was calculated by beam-shaped strain compression measurement on an Instron 5967 universal testing machine (Instron Corp., MA, USA).[21] A hydrogel cylinder (diameter = 1 cm, thickness = 0.5 cm) was cut by razor in half, put together physically, and healed for 6 h or 12 h at 25 °C or 37 °C in a desiccator (KNO_3 saturated solution, RH = 93% (25 °C)). Both the original hydrogel and the self-healed hydrogels were compressed at a speed of 1 mm min^{-1} by the beam-shaped mold until rupture occurred, and the compressive load-strain curves were recorded. For the self-healed hydrogel compression, the compression site was at the boundary between two semicircular hydrogels. The healing efficiency was calculated by dividing the compressive load at breaking point of the healed hydrogel into that of original hydrogel. This experiment was replicated at least three times.

3.3.8 CMC/PEG-BA self-healing hydrogel injectability

(1) Two pieces of CMC/PEG-BA hydrogels (R = 1/2, T = 6) stained by rhodamine B and methylene blue were separately put into two 3 mL Luer-Lok^{TM} tip syringes with needle (20 gauge) and injected into a 10 mL glass beaker. The hydrogel pieces in the bottom of the beaker formed a whole hydrogel keeping for 5 min at room temperature, and then the composite hydrogel was removed from the beaker. (2) A piece of blue hydrogel was added into 3 mL Luer-Lok^{TM} tip syringe with needle (20 gauge) and extruded on a PTFE plate to write words *ABCD* to test the injectability of the hydrogel.

3.2.9 *In vitro* cytotoxicity evaluation of CMC/PEG-BA hydrogel

Normal adult human primary dermal fibroblast cells were grown in T-75 flasks at 37 °C in a humidified atmosphere of 5% CO_2. The cells were cultured in complete growth media (fibroblast basal medium with fibroblast growth kit-low serum). The medium was changed every other day until the cells reached 80% confluence. The cells were detached with 4 mL trypsin-EDTA solution at 37 °C for 3-4 min, and then were neutralized with equal volume of the trypsin neutralizing solution and passaged with fresh medium.

Cytotoxicity of CMC/PEG-BA hydrogel (R = 1/2, T = 6) on normal adult human primary dermal fibroblast cells was examined by MTT assay. Cells were seeded in 96-well plates at a density of 10^4 cells per well in 100 μL culture medium. The cells were grown for 24 h to allow attachment before the experiment. Hydrogel was added into each well to reach the final concentrations of 50 mg mL^{-1} and 100 mg mL^{-1}, respectively, and incubated with the cells for another 24 h. Then hydrogel was removed and cells were washed with 100 μL DPBS. 100 μL of MTT solution (0.5 mg mL^{-1} in DPBS) was then added to each well and incubated for 4 h at 37 °C. The above MTT solution was aspirated off and 100 μL of DMSO was added into each well followed by the

measurement of the absorbance at 570 nm using a microplate reader (SpectraMax, Molecular Devices, USA). The viability was expressed by the percentage of living cells with respect to the control cells. Five replicate wells were used for each control and test concentrations per microplate, and the experiment was repeated three times. Results are presented as mean ± standard deviation (SD).

3.2.10 Three-dimension (3D) cell encapsulation

Normal adult human primary dermal fibroblast cells were encapsulated in CMC/PEG-BA hydrogel (R = 1/2, T = 6). Firstly, 8% (w/v) PEG-BA solution and 4% (w/v) CMC solution were prepared by dissolving PEG-BA and CMC in complete growth media. The fibroblasts were suspended in above PEG-BA solution (cell concentration = 8.64×10^5 cells/mL, viability = 97.8 ± 1.8%). Subsequently, 1 mL CMC solution and 1 mL cells/PEG-BA solution were pipetted into a well of 12-wells plate and mixed gently by a pipette to induce gelation. No additional media was added into the well. The hydrogels were incubated at 37 °C in the humidified atmosphere of 5% CO_2, and took confocal images after 0 d, 1 d, 2 d, and 7 d incubation. To evaluate the viability of cells encapsulated in hydrogel, each piece of hydrogel was rinsed in 2 mL FDA/PI solution (FDA stock solution was prepared by dissolving 5 mg of FDA in 1 mL acetone, PI stock solution was prepared by dissolve 2 mg of PI in 1 mL DPBS. The FDA/PI staining solution was prepared by mixing 8 μL and 50 μL in 5 mL DPBS) for 10 min in the dark and observed by a CLSM 710 Meta confocal laser scanning microscope (Carl Zeiss, Jena, Germany). Images were processed with ZEN 2009LE software (Carl Zeiss MicroImaging GmbH, Germany) and 3D confocal stacks were processed with Imaris 8.0.1 Software (Bitplane AG, Zurich, Switzerland).

3.2.11 CMC/PEG-BA hydrogel hemostatic ability

A rabbit hemorrhaging liver model was used to test *in vivo* hemostatic properties of CMC/PEG-BA hydrogel. This animal study was performed at School of Basic Medical Sciences of Wuhan University and all animal experiments in this study were carried out in accordance with the guidelines and the ethics approval of the Laboratory Animal Center of Wuhan University. A total of twelve adult white New Zealand rabbits with weight of about 2.5 kg (random distribution of male and female) were used in this study. CMC/PEG-BA hydrogel was tested (n = 4) and compared to negative control of no treatment (n = 4) and positive control of sterile gauze with compression (n = 4). An intravenous injection of sodium pentobarbital, at a dose of 35 mg/kg, was administered as a general anesthetic. Rabbit was immobilized on a surgical corkboard and fur surrounding the intended surgical area was removed. The exposed surgical area was wiped with povidone iodine, followed by 75% ethanol. The liver of the rabbit was exposed by abdominal incision, and then an incision (length of 1 cm) was prepared in liver lobe using a scalpel. The pre-weighted sterile gauze was placed under the liver to absorb blood. Upon bleeding, site of bleeding was treated with hydrogel, or gauze with compression for hemostasis or no treatment. Time taken for hemostasis was recorded and total blood loss was weighted in each case. After bleeding stopped completely, liver tissue around incision site was harvested and stained with hematoxylin-eosin (H&E) for evaluation using light microscopy. The test was repeated three times in one rabbit liver at different liver lobes.

3.3.12 Statistical analysis

All experiments were performed at least in three independent batches. Data were represented as the mean ± standard deviation (SD). For data in figures, error bars showed standard deviations. Statistical evaluation was conducted by Student's t-test and analysis of variance (ANOVA). The

multiple-comparisons were evaluated by Duncan's multiple-range test. Statistical differences between samples were performed with a level of significance as $p < 0.05$.

3.3 Results and discussion

3.3.1 CMC and PEG-BA synthesis

Water-soluble carboxymethyl chitosan (CMC) was prepared by reacting chitosan with monochloroacetic acid under alkaline condition. FT-IR (**Figure 3-1b**) and ^{1}H NMR (**Figure 3-2A**) in supporting document demonstrated the successful preparation of CMC. The FT-IR spectrum of CMC showed a characteristic peak at 1603 cm^{-1} corresponding to carboxylic acid group ($-COO^{-}$ asymmetric stretch).[38] Besides, the chemical shifts in ^{1}H NMR at 3.3 and 3.8-4.0 ppm belonged to the protons of $–CH_2–COO^{-}$ at the N-position at C2 and the O-position at C3 and C6 of CMC, respectively, which indicated that carboxymethyl substituents took place on both the amino and hydroxyl sites of chitosan structure.[195] The total degree of substitution (DS) of carboxymethyl was 0.26 as calculated from ^{1}H NMR spectrum.[195]

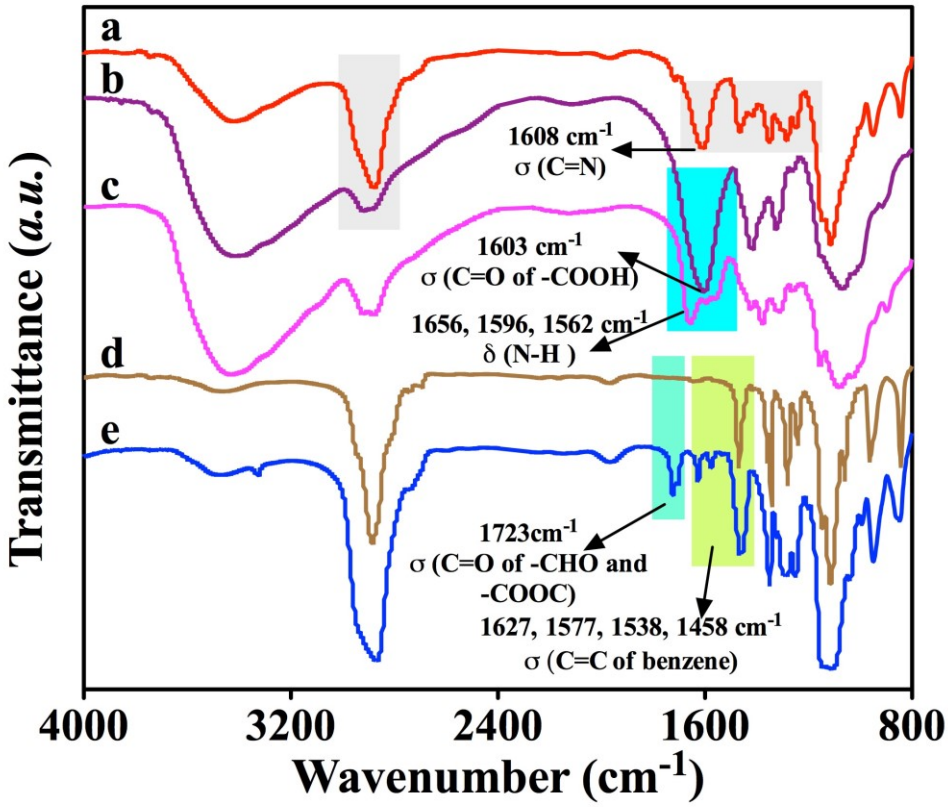

Figure 3-1. FT-IR spectra of (a) CMC/PEG-BA Hydrogel, (b) CMC, (c) chitosan, (d) four-arm PEG, and (e) PEG-BA.

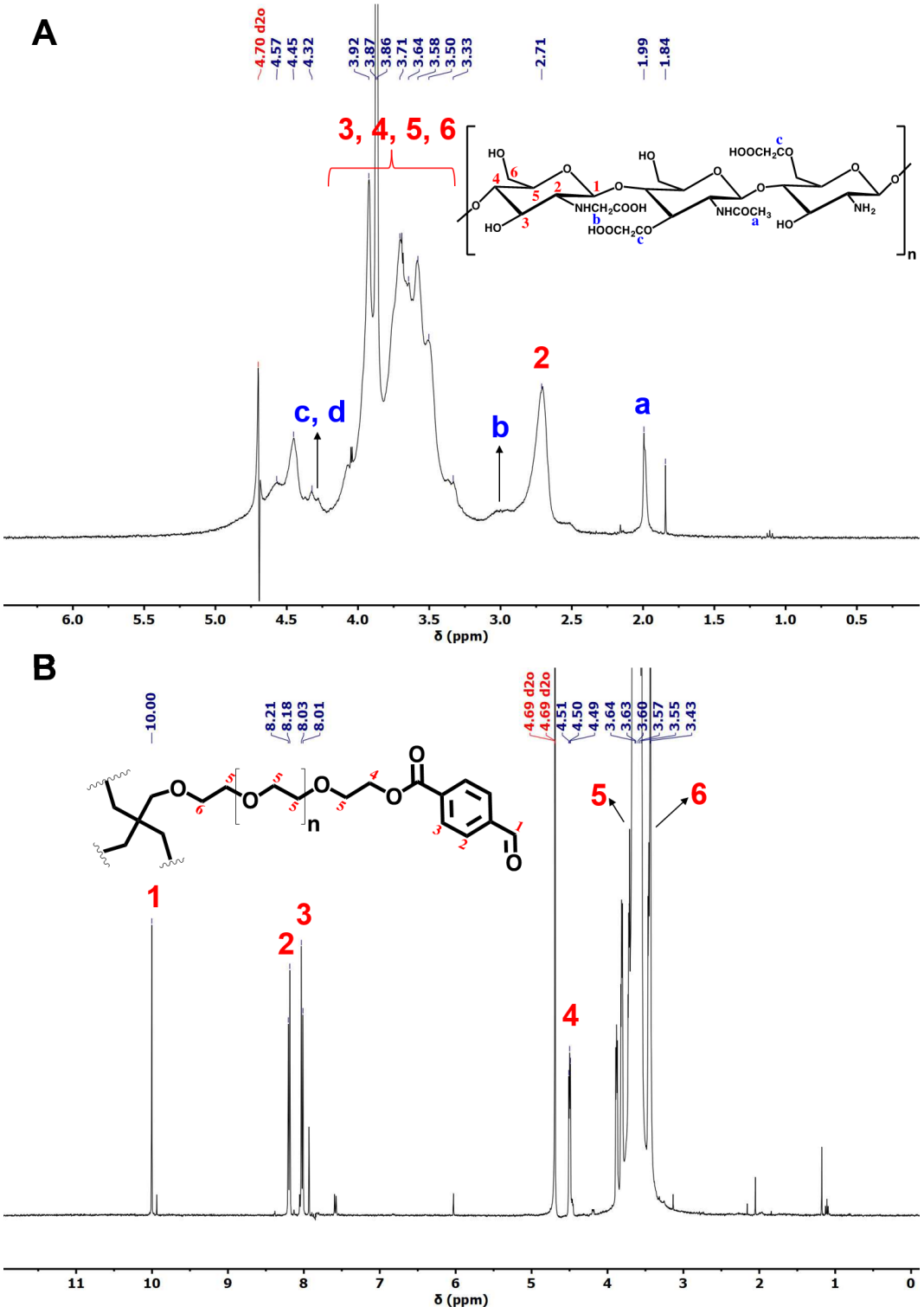

Figure 3-2. ^{1}H NMR spectra of (A) carboxymethyl chitosan (CMC), and (B) benzaldehyde-terminated four-arm polyethylene glycol (PEG-BA).

The benzaldehyde-terminated four-arm polyethylene glycol (PEG-BA) was synthesized by conjugating 4-formylbenzoic acid to the terminal hydroxyl of 4-arm PEG via carbodiimide coupling reaction (**Figure 3-3**).[86, 196] The aldehyde and ester carbonyls at 1723 cm^{-1} and benzene at 1627, 1577, 1538, 1458 cm^{-1} were identified in FT-IR spectrum (**Figure 3-1**e) in a supporting document. In ^{1}H NMR spectrum of PEG-BA (**Figure 3-2**B), the protons of ether methylene (-CH_2-O-CH_2-) on polymer backbone showed signal at 3.6 ppm, and new peaks of the protons of aldehyde (–CHO) at 10.0 ppm, benzene ring at 8.0 ppm and 8.2 ppm, ester methylene (-CH_2-COO^-) at 4.5 ppm were clearly observed. All polymer chains were terminated with benzaldehyde groups at four ends according to the integration ratio from ^{1}H NMR spectrum.

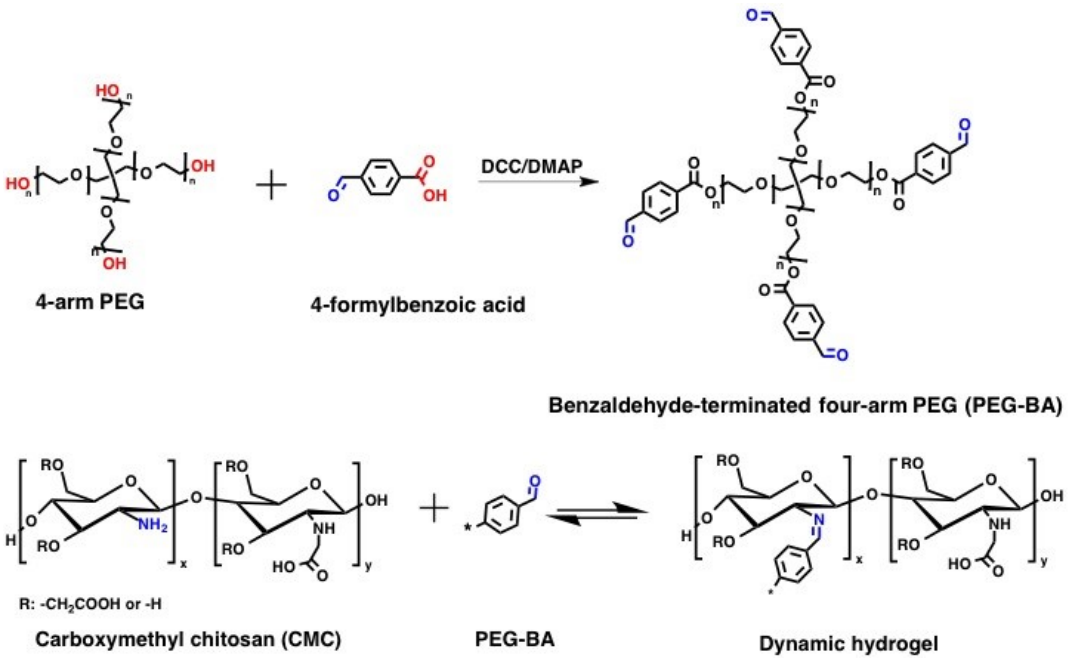

Figure 3-3. Synthesis scheme of benzaldehyde-terminated four–arm PEG (PEG-BA), and benzaldehydes at ends of PEG-BA conjugated amino groups of CMC to form dynamic hydrogel (CMC/PEG-BA hydrogel).

3.3.2 CMC/PEG-BA hydrogel formation

The CMC/PEG-BA hydrogels were prepared through homogeneously mixing CMC solutions with PEG-BA solutions at room temperature. The fluidic mixtures transformed into transparent hydrogels within 2 min (**Figure 3-4A** and **Figure 3-5B**). The amino groups on CMC backbone were cross-linked by aldehyde groups at the terminal of PEG-BA to form reversible imine bonds (**Figure 3-3**). The dynamic hydrogel networks were based on the equilibrium between aromatic Schiff-base linkages and the disassociated aldehyde and amino groups. FT-IR spectrum of CMC/PEG-BA hydrogel (**Figure 3-1**a) showed a characteristic absorption of imine stretching vibration (-C=N-) at 1608cm^{-1}, which indicated the condensation reaction between CMC and PEG-BA to form the Schiff-base linkages.

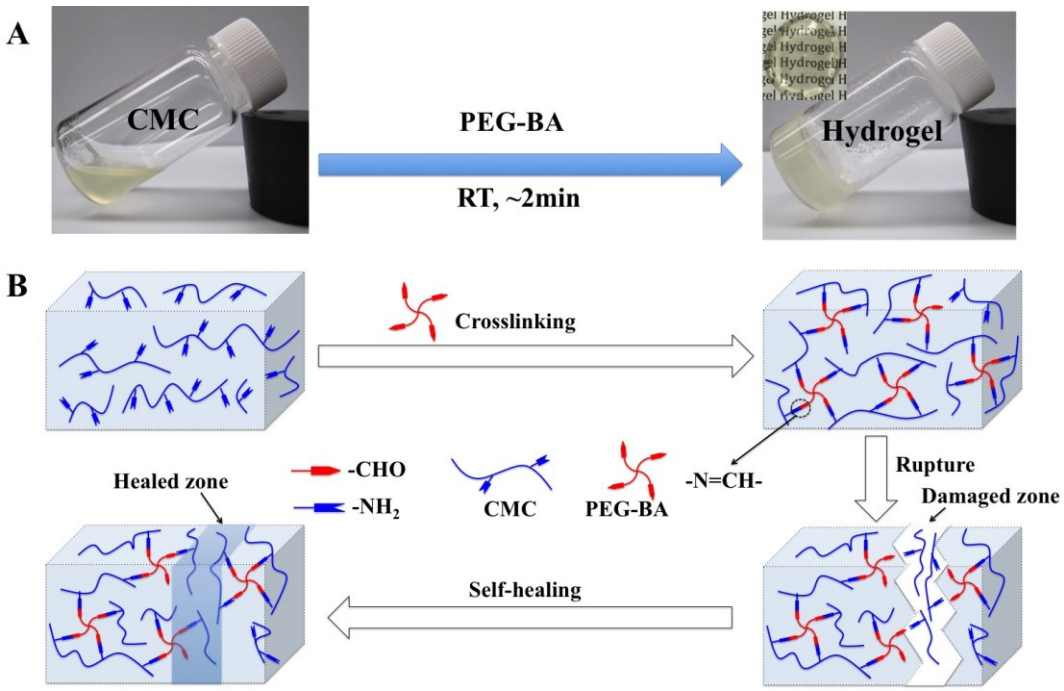

Figure 3-4. Preparation and self-healing process of CMC/PEG-BA hydrogel. (A) Gel formation of CMC/PEG-BA self-healing hydrogel (The inset image showed the visibility of the hydrogel with 0.5 cm thickness). (B) Schematic illustration of the gelation and self-healing process.

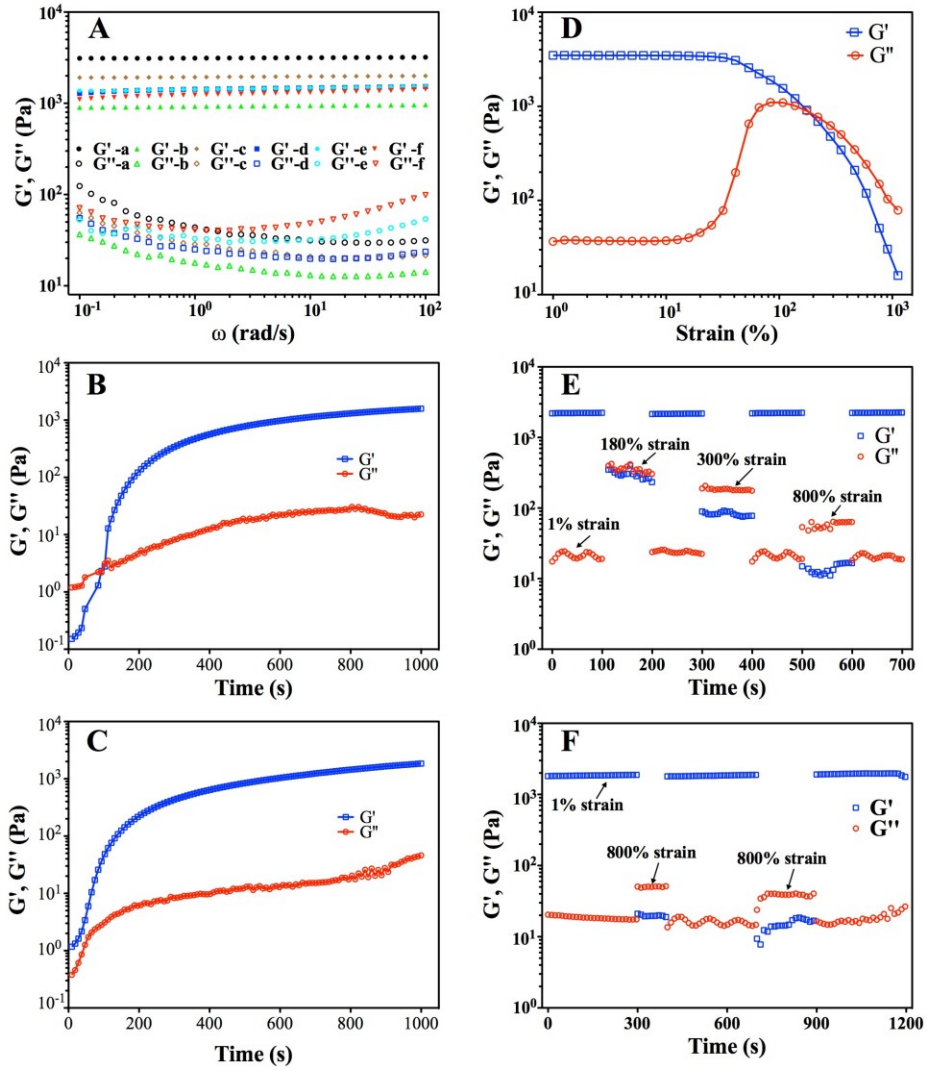

Figure 3-5. Rheological properties of CMC/PEG-BA hydrogels. (A) Storage modulus (G') and loss modulus (G'') of the hydrogels with different weight ratios of CMC and PEG-BA, and different total solid contents: (a) CMC/PEG-BA (R = 1/2, T = 6), (b) CMC/PEG-BA (R = 1/2, T = 4), (c) CMC/PEG-BA (R = 1/2, T = 5), (d) CMC/PEG-BA (R = 1/1, T = 5), (e) CMC/PEG-BA (R = 2/1, T = 5), and (f) CMC/PEG-BA (R = 3/1, T = 5). Sweeps were performed at 1% strain. Gelation kinetics of CMC/PEG-BA hydrogel (R = 1/2, T = 6) at (B) 25 °C and (C) 37 °C. (D) G' and G'' of CMC/PEG-BA hydrogel (R = 1/2, T = 6) on strain amplitude sweep (γ = 1%-1000%) at a fixed angular frequency (10 rad/s). (E) G' and G'' of CMC/PEG-BA hydrogel (R = 1/2, T =

6) when alternate step strain switched from small strain (1%) to large strain (γ = 180%, 300%, 800%) in continuous step strain measurements at a fixed angular frequency (10 rad/s). (F) Cyclic G' and G'' values of CMC/PEG-BA hydrogel (R = 1/2, T = 6) for a large strain level (γ = 800%) and different loading period from 100 to 200 s.

As shown in **Table 3-1**, hydrogels samples with various total concentrations of polymers (T) and mass ratios of CMC/PEG-BA (R) were prepared because they may impact the network density so that may influence the mechanical strength and self-healing efficiency of hydrogels. The viscoelastic properties of the CMC/PEG-BA were measured and the results are shown in **Figure 3-5** and **Figure 3-6.** Components of various self-healing CMC/PEG-BA hydrogels. In the whole frequency range tested (0.1-100Hz, **Figure 3-5**A), storage modulus (G') was consistently greater than loss modulus (G''), indicating that the CMC/PEG-BA hydrogels were stable and behaved like a viscoelastic solid. When CMC/PEG-BA ratio was 1:2 (R = 1/2), the storage modulus increased from 944.55 Pa to 3162.06 Pa with the total solid content increased from 4% to 6% (**Figure 3-6**), because of the formation of a denser polymer network with increasing of the polymer concentration. When the total solid content was fixed at 5%, the storage modulus decreased slightly with CMC/PEG-BA ratio increasing from 1/2 to 3/1, due to the decrease amount of large molecular weight CMC. It is recognized that the hydrogel with shear modulus greater than 10^2 Pa can potentially be used for stopping bleeding, and the stronger hydrogel is better for rapid hemostasis.[45, 197] The CMC/PEG-BA hydrogel (R = 1/2, T = 6) that exhibited the strongest mechanical properties was selected for further tests.

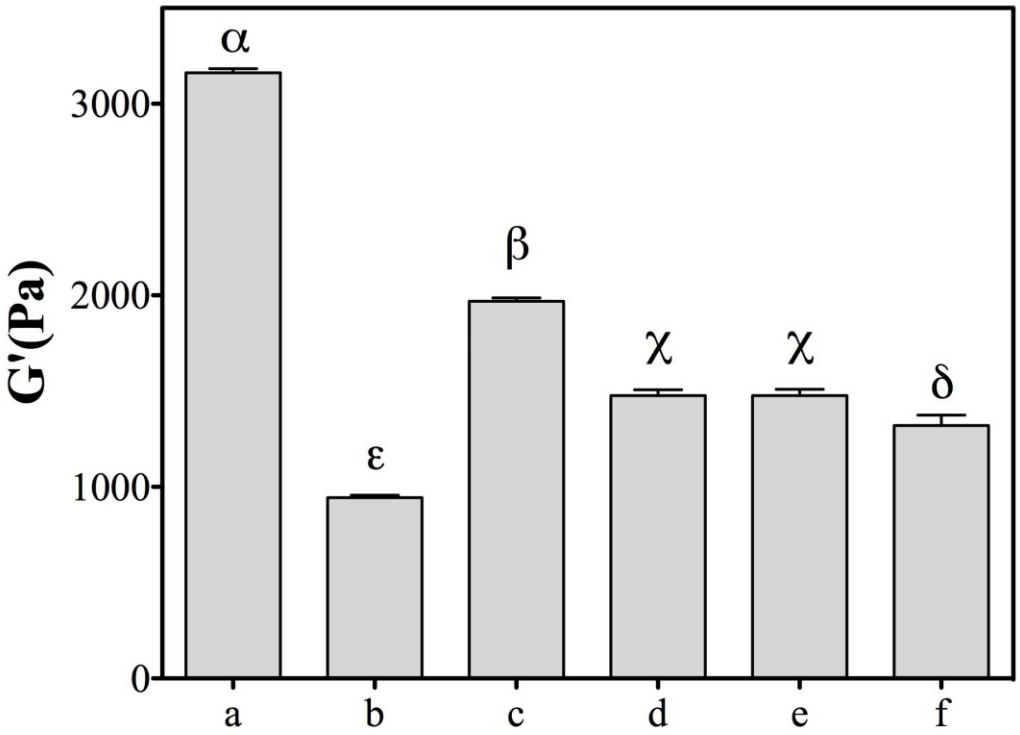

Figure 3-6. The storage modulus (G') of CMC/PEG-BA self-healing hydrogels calculated from Figure 3−5: (a) CMC/PEG-BA (R = 1/2, T = 6), (b) CMC/PEG-BA (R = 1/2, T = 4), (c) CMC/PEG-BA (R = 1/2, T = 5), (d) CMC/PEG-BA (R = 1/1, T = 5), (e) CMC/PEG-BA (R = 2/1, T = 5), and (f) CMC/PEG-BA (R = 3/1, T = 5). (Bars with the same alphabetical letters are not significantly different at $p < 0.05$ according to one-way ANOVA, and the error bars represent standard deviation.).

Gelation kinetics at 25 °C and 37 °C were evaluated in dynamic time sweep mode to test the gelation time. The CMC and PEG-BA solutions were gradually mixed during the test, and CMC/PEG-BA (R = 1/2, T = 6) formed hydrogel within 100 s at 25 °C, as indicated by the crossover point of G' and G'' curves (**Figure 3-5**B). The solution instantly formed gel at physiological temperature (37 °C) (**Figure 3-5**C), which allowed the rapid solidification when

applied *in vivo*. Although at molecular level, Schiff bases were formed nearly instantaneously, it took minutes to form strong gel networks because it took time for amino groups and aldehyde groups to diffuse and mix in the bulk system. Zhang et al reported chitosan/dibenzaldehyde-terminated telechelic polyethylene glycol solution formed gel within 20 s at 20 °C.[86] Gelation time of hydrogel is important for practical applications because slow gelation would result in liquid hydrogel precursors and cargos (i.e. cells/drugs) diffusing away from the injection site. In contrast, it is difficult to homogeneously mix the raw materials if gelation process takes place rapidly, and there is not enough operation time.

3.3.3 Self-healing performance

The rheological recovery tests were performed to evaluate the elastic response and self-healing behaviors of CMC/PEG-BA (R = 1/2, T = 6) hydrogel. As shown in **Figure 3-5**D, the G' curve intersected the G'' curve at the strain of 180%. When the strain was larger than this critical value, the G' was lower than G'', which indicated the collapse of the hydrogel, and solid hydrogel transformed to fluid state. This can be attributed to the imine bonds that broke after being exposed to large shear strain. With the increase of strain from 20% to 800%, the G' steeply went down from *ca.* 3485 Pa to *ca.* 37 Pa due to the dissociation of Schiff-base linkages.[86, 135] Subsequently, the hydrogel was subjected to alternate step strain sweep experiment. As the oscillatory shear strain took steps from 1% to 180% for 100 s, the G' overlapped G''. When high strain was discontinued and a low strain (1%) was applied, the hydrogel exhibited total recovery of both G' and G'' within a few seconds after strain-induced failure (**Figure 3-5**E), since the broken imine bonds re-formed due to their reversible properties. Analogously, when large strains (300% and 800%) and a small strain (1%) were alternatively applied, the G' could rapidly restore to the initial value. The influence of the duration at the breaking strain on the rheological recovery behavior was studied

by fixing step strain to 800% but increasing the loading time from 100 s to 200 s (**Figure 3-5**F). Here the G' was immediately recovered after the amplitude strain was removed, regardless of loading time. The imine bonds between them are highly reversible and act as sacrificial bonds that are ruptured under high stress, but readily reform upon the remove of stress. During the test, the amino groups and aldehyde groups were at their positions, and those Schiff bases broke at large strain level and reformed at small strain level nearly instantaneously, showing a quick recovery. This dynamic equilibrium helps to rapidly stabilize the gel network under stress and allows for the quick reformation of the gels.

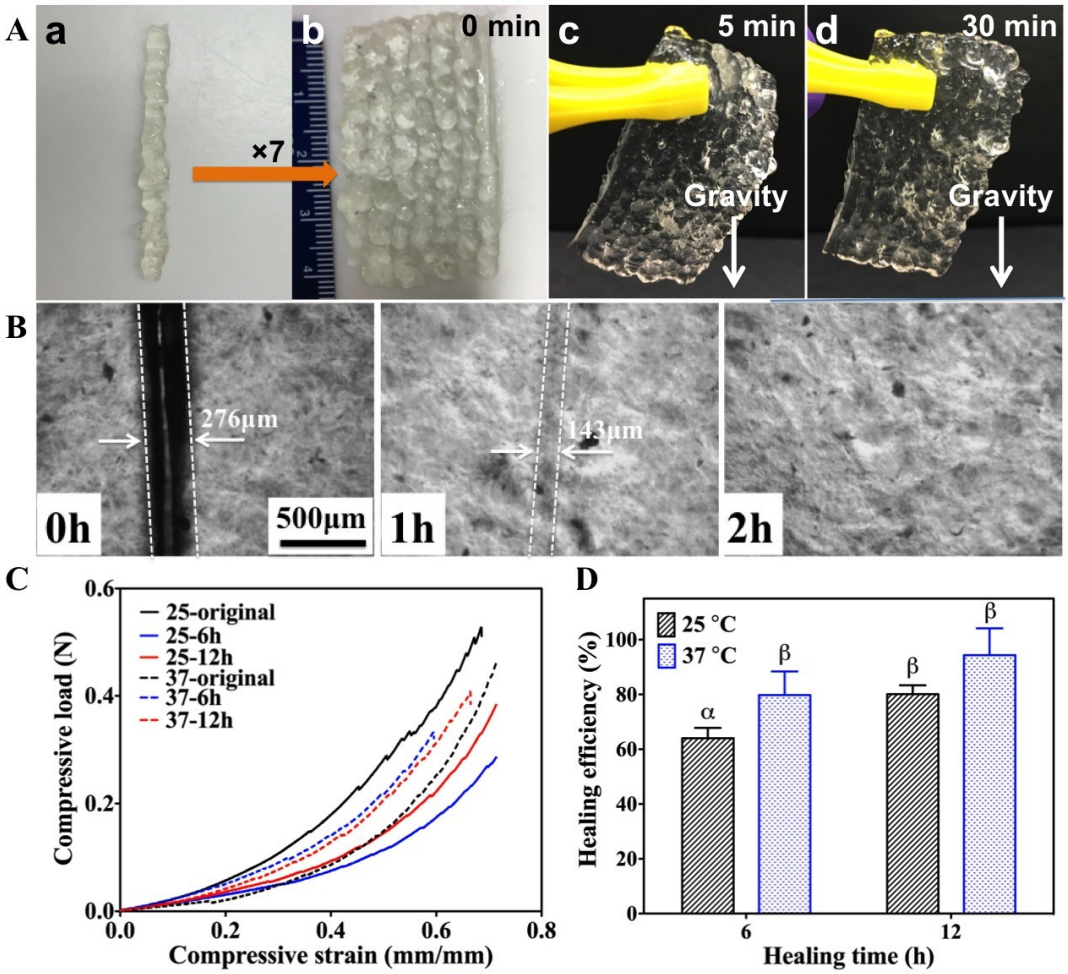

Figure 3-7. Self-healing properties of CMC/PEG-BA hydrogel (R=1/2, T=6). (A) Macroscopic hydrogel recovery process: (a) one hydrogel strip extruded from syringe, (b) hydrogel strips drawn by a syringe and separated hydrogel stripes couldn't stand by themselves and laid on a surface, (c) hydrogel stripes healed to a whole piece and suspended under gravity, (d) the boundaries between hydrogel stripes disappeared gradually. (B) Optical microscope images of hydrogel after healing for 0 h, 1 h, and 2 h at room temperature. (C) The beamed-shaped strain compression curves of the original hydrogel and the hydrogels after healing for 6 h and 12 h at 25 °C and 37 °C. (D) Healing efficiency of the hydrogel after healing for 6 h and 12 h at 25 °C and 37 °C, respectively. (Bars with the same alphabetical letters are not significantly different at $p < 0.05$ according to one-way ANOVA, and the error bars represent standard deviation.)

Macroscopic self-healing test was carried out by strip-to-film method to further evaluate the self-healing ability of the CMC/PEG-BA (R = 1/2, T = 6) hydrogel. As shown in **Figure 3-7**A, seven hydrogel strips were successively extruded from the syringe onto a PTFE plate and placed side by side. At t = 0 min, the 'whole' piece could not be grabbed and held by the clips due to the lack of enough interactions among the strips. After 5 min at room temperature without any external intervention, the hydrogel strips were rapidly connected together and became an integrated film, so the hydrogel suspended under gravity, indicating an efficient self-healing. Besides, the boundaries between the adjacent hydrogel strips turned obscure gradually because of healing. It was expected that the intimate contact of the separated hydrogel strips would promote new imine bonds formation across the interface to affect covalent healing as the aldehyde groups at the chain end of PEG-BA and amino groups on CMC backbone gradually diffused across the interface. As mentioned earlier, it is usually difficult to combine high self-healing efficiency and mechanical strength together, since the high mechanical strength comes from strong and stable cross-linking interactions that restrict the mobility of polymer chains and slow down the recovery of gel network. In previous work, it took 2 h to recover the chitosan/DF-PEG hydrogel when gel storage modulus was 1150 Pa.[86] In this study, the CMC/PEG-BA hydrogel with significantly higher storage modulus (3162 Pa) took much less time (5 min) to heal since fewer imine bonds were required to re-form with the same network density.

The self-healing process of the CMC/PEG-BA (R = 1/2, T = 6) hydrogel was monitored in real-time using optical microscope as well. Optical images (**Figure 3-7**B) showed that the crack (width 276 μm) made by a knife gradually disappeared after 1 h (width 143 μm) and no gap was observed after 2 h, suggesting the rebuilding of the cross-linked gel network. Once a crack occurred, a "mobile phase" was generated at the damaged interfaces, where the imine bonds were cleaved and

free aldehyde and amide groups were exposed. The crack was then recovered by directed polymers move towards the damaged interfaces, and local new imine bonds formed through reconnection of crack planes due to their dynamic and reversible properties. As illustrated in **Figure 3-4**, once CMC solution was mixed with PEG-BA, amino groups at carboxymethyl chitosan backbone react with aldehyde groups at the chain end of benzaldehyde-terminated four-arm PEG to form dynamic imine bonds, which in turn form a gel network. The gel network was damaged when cross-linking imine bonds were cleaved and amino groups and aldehyde groups were exposed in the interface of damage area. The exposed amino groups and aldehyde groups could re-form new imine bonds due to their reversibility, which induced gel network reformation. In the end, the fragments of hydrogel were recovered to form an integrated hydrogel like the original one.

To quantitatively analyze the self-healing efficiency of the CMC/PEG-BA (R = 1/2, T = 6) hydrogel, beam-shaped strain compression test was performed.[15, 198] As shown in **Figure 3-7**C and D, after healing for 6 h at 25 °C, the healing efficiency was 64 ± 3.8%, and it increased to 80 ± 3.2% when the healing time prolonged to 12 h. However, the healing efficiency of the hydrogel at physiological temperature (37 °C) reached as high as 80 ± 8.6% and 94 ± 9.8% after 6 h and 12 h, respectively. It indicated that the hydrogel exhibited better self-healing property at physiological temperature than room temperature, likely since the higher temperature enhanced the dynamic kinetics of the reversible bonds and resulted in a faster recovery of the hydrogel network at the molecular level.

3.3.4 Hydrogel injectability

According to the results of the rheological recovery tests (**Figure 3-5**E and F), the self-healing hydrogel behaved like liquid under high shear strain and recovered when stress was removed, thus can be used as injectable gel material. To confirm this, the CMC/PEG-BA hydrogel was loaded

into syringe and extruded through 20-gauge needle. As shown in **Figure 3-8**A, four smooth letters 'ABCD' were successfully written, suggesting that the hydrogel was injectable. Moreover, two pieces of hydrogel stained with different colors were injected through 20-gauge needles without clogging into a beaker, respectively. After injection, the extruded CMC/PEG-BA hydrogel strips healed to a holdable cylindrical hydrogel in 5 min (**Figure 3-8**B). This result further confirmed the self-healing capability of CMC/PEG-BA hydrogel. When the hydrogel was compressed in the syringe, pressure induced the dissociation of Schiff-base linkages and made the hydrogel deform and 'flow' like liquid to pass through the thin needle. The extruded hydrogel came together to form an integrated piece again due to its rapid self-healing ability. This means the hydrogel may be used to encapsulate cells/drugs homogeneously and implant to tissue with a minimally invasive strategy.

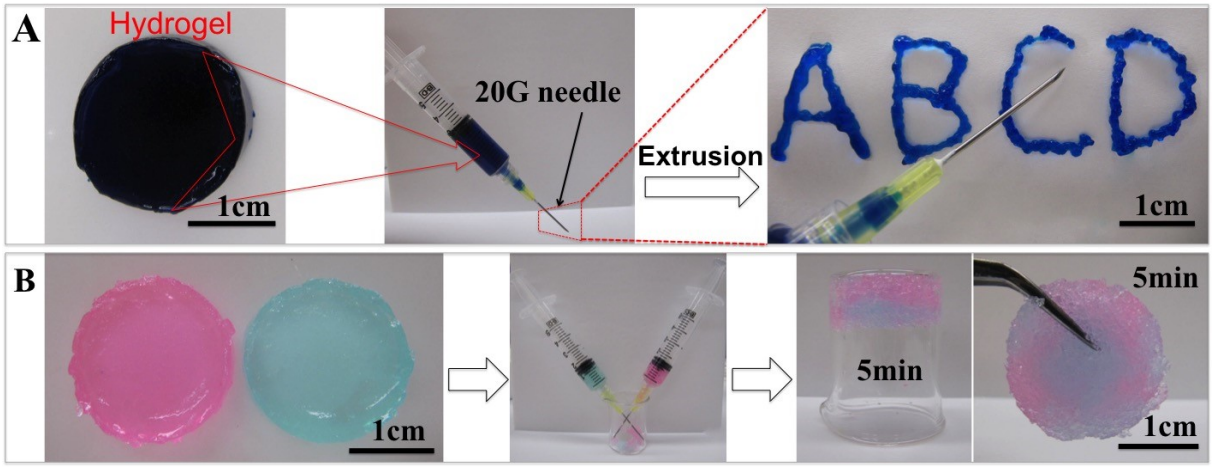

Figure 3-8. The injectable process of the self-healing CMC/PEG-BA hydrogel (R=1/2, T=6). (A) The self-healing hydrogel passed through a 20 G needle without clogging. (B) Two disk-shaped hydrogels (diameter = 2 cm, height = 1 cm) stained with rhodamine B and methylene blue were separately injected into a 10 mL beaker from 20 G needles and then combined into one piece after 5 min.

3.3.5 Cytotoxicity and 3D cell encapsulation

To study the cytotoxicity of the CMC/PEG-BA (R = 1/2, T = 6) hydrogel, the viability of normal adult human primary dermal fibroblast was measured by MTT assay after incubation with hydrogel. Fibroblasts have been widely used as an *in vitro* model to investigate the cytotoxicity and biocompatibility of biomaterials.[199] As shown in **Figure 3-9**, the cell viability was 99.21 ± 11.98% and 99.86 ± 9.85% for cells incubated with 50 mg mL^{-1} and 100 mg mL^{-1} hydrogel for 1 d, respectively. These results suggested that the CMC/PEG-BA (R = 1/2, T = 6) self-healing hydrogel was relatively nontoxic even at higher polymer concentration.

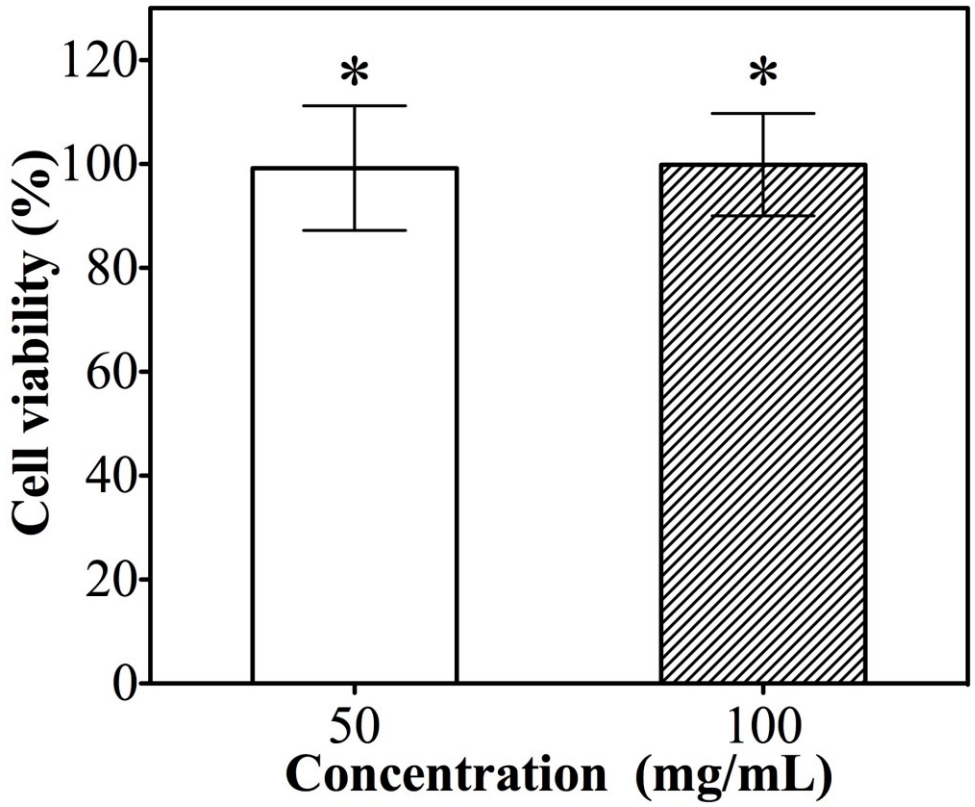

Figure 3-9. Percentage of the viable cells evaluated by MTT assay on normal adult human primary dermal fibroblast treated with increasing concentration of CMC/PEG-BA (R = 1/2, T = 6) self-healing hydrogel for 24 h. Same symbol above the column indicate no significant difference ($p < 0.05$).

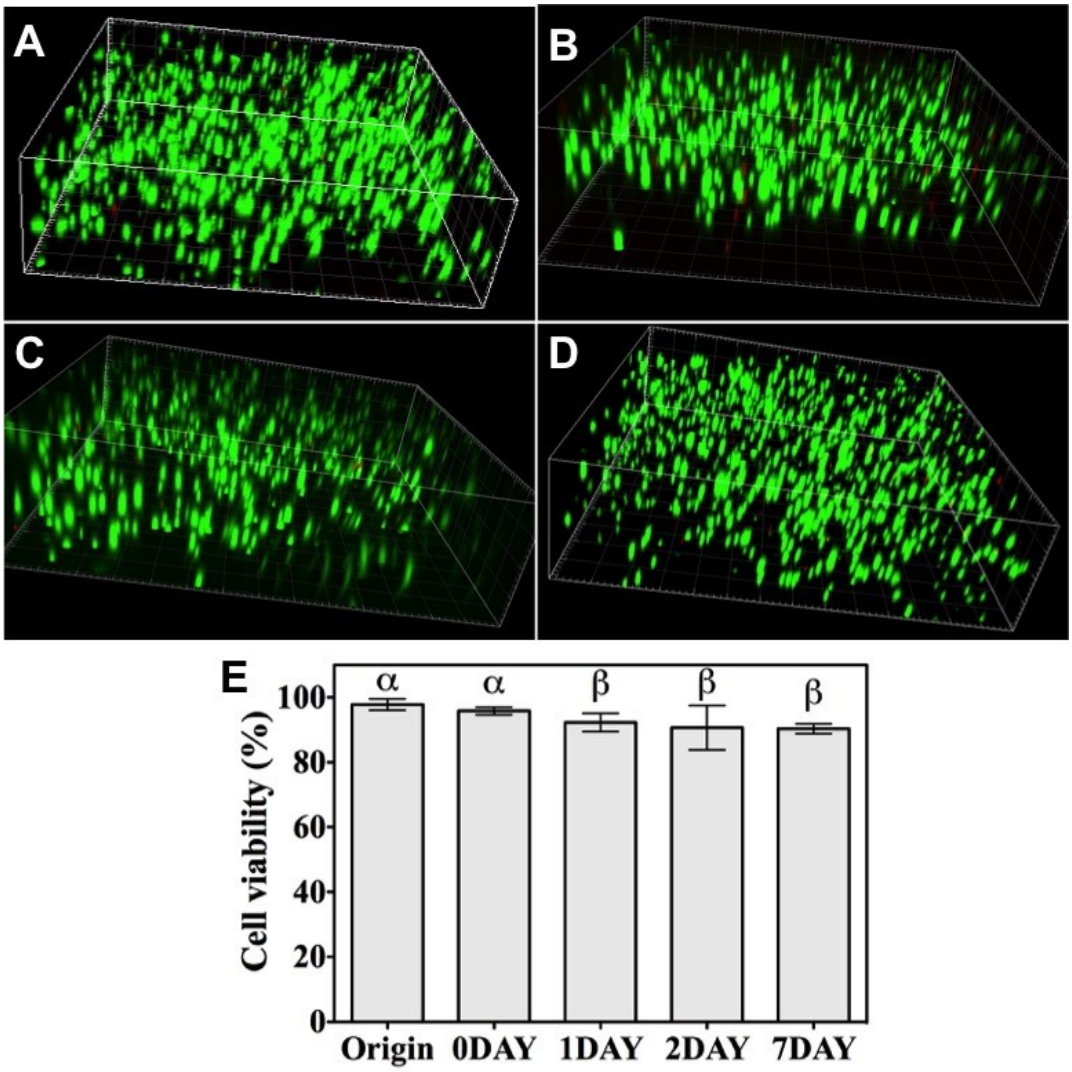

Figure 3-10. 3D confocal microscopy images of cells encapsulated in CMC/PEG-BA hydrogel (R = 1/2, T = 6) (viable cells: green spots, dead cells: red spots): (A) 0 day, (B) 1 day, (C) 2 days, and (D) 7 days culture after encapsulation. (E) Cell viability versus different culture time. (Bars with the same alphabetical letters are not significantly different, and different alphabetical letters are significantly different at $p < 0.05$ according to one-way ANOVA, and the error bars represent standard deviation.)

Cell therapy is a very promising treatment strategy for many diseases, such as spinal cord injury[200] and cartilage disorder.[201] However, most of primary cells easily lose their viability and functionality after isolation, especially as a single cell. *In vivo*, cells live inside extracellular matrix, and self-healing hydrogels are the potential mimics due to their dynamic behavior. Therefore, self-healing hydrogels have been widely applied for cell encapsulation, culture, and transplantation.[15, 71, 89] Three-dimensional encapsulation of normal adult human primary dermal fibroblast cells was performed to test the cytocompatibility of the CMC/PEG-BA (R = 1/2, T = 6) self-healing hydrogel. The cell viability of free fibroblast cells before encapsulation was 97.8 ± 1.8%. Fluorescent confocal microscopy images (**Figure 3-10**) of cells stained with fluorescein diacetate/propidium iodide (FDA/PI) reagent showed fibroblast cells tolerated the 3D encapsulation in the hydrogel, and it made no significant difference after encapsulation (95.8 ± 1.2% viability), indicating that the fibroblast cells lived well in the hydrogel network. The cell viability was as high as 92.3 ± 2.8% and 90.7 ± 6.8 % after 1 d and 2 d culture, respectively. Moreover, the cell viability maintained at 90.3 ± 1.5%, which didn't significantly decrease after one week culture, indicating cells still live well inside hydrogel, such an extended survival period and good viability in the hydrogel are vital for cells to play their role *in vitro*.[15, 89] Cells could live well inside hydrogel for a long time probably because the hydrogel not only acted as extracellular matrix mimic and provided a microenvironment for cell living, but also transported nutrition to cells for living.

3.3.6 Hemostasis ability

The application of the CMC/PEG-BA (R = 1/2, T = 6) hydrogel as hemostatic material was evaluated in rabbit hemorrhaging liver model. **Figure 3-11** showed the amount of blood loss and hemostasis time after applying hydrogel, gauze pad, or no treatment at the hemorrhaging site. The

total blood loss after applying the CMC/PEG-BA (R = 1/2, T = 6) hydrogel without compression was 0.29 ± 0.11 g, much less than the sample treated by the sterile gauze with compression and the negative control (no treatment), which showed blood loss of 0.65 ± 0.10 g and 1.33 ± 0.45 g, respectively. The hemostasis time was 120 ± 10 s when the hydrogel was applied, which was much shorter than those of gauze (167 ± 21 s) and negative control group (311 ± 62 s). After treating with hydrogel at the bleeding site, the total blood loss steeply decreased and hemostasis time significantly shortened, which indicated that the CMC/PEG-BA (R = 1/2, T = 6) hydrogel treatment significantly improved hemostasis over gauze pad. The negative control group stopped bleeding finally because of the body's normal physiological response for the prevention and stopping of hemorrhage. After directly injecting the CMC/PEG-BA (R = 1/2, T = 6) hydrogel onto the bleeding site, it was very small pieces of hydrogel and act as fluid, thus it could quickly flow into the injury and tightly cover the surface and reach into the incision to act as a bleeding-arrest barrier to stop bleeding. The hydrogel was strong enough to remain at the bleeding site and wasn't swept away by the flowing blood. Additionally, chitosan is known to have a hemostatic ability due to its positive charge.[202] However, the gauze could only contact the outside wound surface with the assistance of physical compression. Histological assessment (**Figure 3-12**) of the injured liver surface showed that the gap in the incision of the negative control group was narrow because the interfaces connected together during hemostatic process. In the positive group, sterile gauze was applied on the incision with compression and adsorbed the blood, which resulted in a broad gap between wound interfaces. However, a gap filled with blood cells was observed in the image of hydrogel group. After applying hydrogel on the bleeding site, the hydrogel filled the incision and trapped blood cells between the wound interfaces. This strong physical barrier resulted in the shorter bleeding time and less blood lost compared to the traditional gauze treatment.

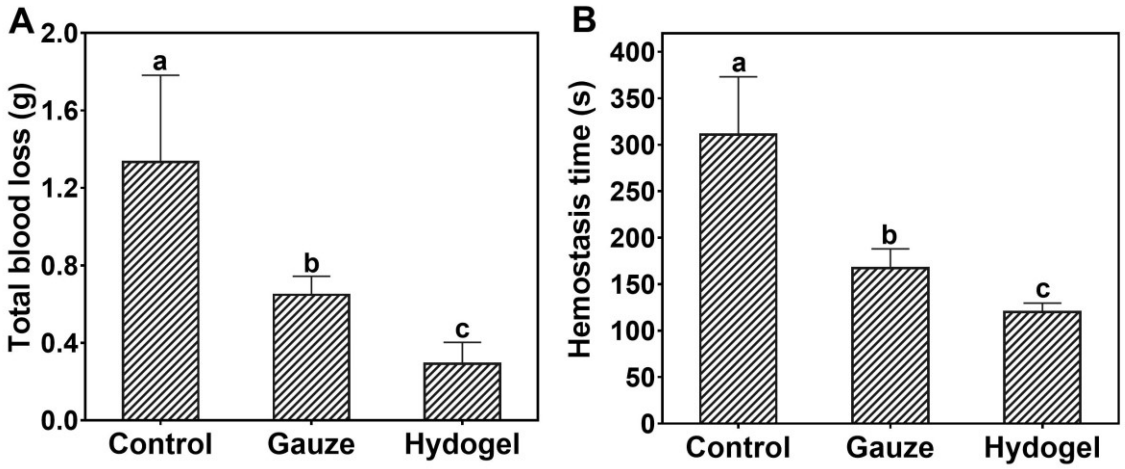

Figure 3-11. The quantitative analysis of hemostatic ability of CMC/PEG-BA hydrogel (R = 1/2, T = 6wt.%) compared with negative control (no treatment) and positive control (gauze with compression) against a rabbit liver injury: (A) Total blood loss until bleeding stopped completely, and (B) hemostasis time. (Different letters indicate significant differences between groups)

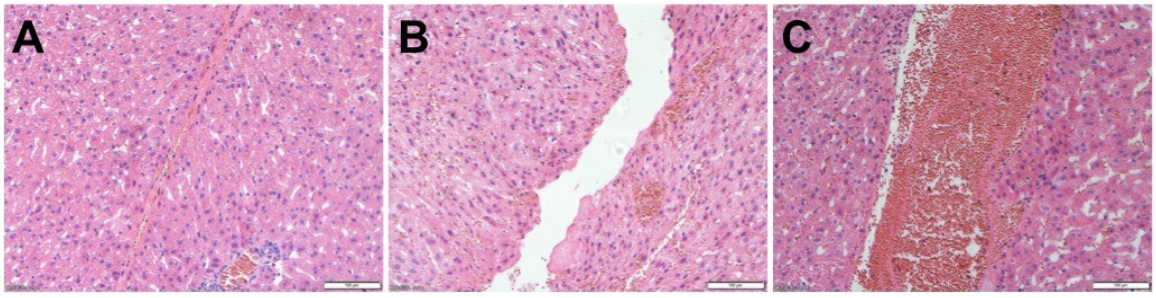

Figure 3-12. Histological Assessment: Representative tissue sections stained with hematoxylin and eosin (H&E). (A) Untreated group (negative control group), (B) gauze group with compression (positive control group), and (C) CMC/PEG-BA hydrogel (R = 1/2, T = 6wt.%).

3.4 Conclusion

In this study, we developed self-healing and injectable CMC/PEG-BA hydrogel which possessed both excellent self-healing efficiency and strong mechanical strength. The dynamic and reversible Schiff-base linkages in the hydrogel structure conferred the ability to spontaneously reconnect or be "self-healing". The resultant hydrogel showed the strong storage modulus of 3162.06 ± 21.06 Pa, and excellent healing efficiency of 94 ± 9.8% after 12h under physiological temperature. The four-arm based networks of the hydrogel are more resistant to fracture than the equivalent two-arm polymer based on the same average crosslink density. All the hydrogels could pass through 20 G needle without clogging because of the dissociation of dynamic Schiff-base linkages under large shearing forces. The hydrogel was nontoxic based on the MTT assay when the gel concentration reached to 100 mg ml^{-1}, and showed good cytocompatibility as a 3D cell carrier. Moreover, the hydrogel exhibited good ability to stop bleeding after direct application to a rabbit liver incision; it could be potentially used as a hemostatic material.

Chapter 4

On-Demand Dissolvable Self-healing Hydrogels Based on Carboxymethyl Chitosan and Cellulose Nanocrystal for Deep Partial Thickness Burn Wound Healing

4.1 Introduction

Annually, more than 300, 000 people die or suffer from injuries caused by thermal, chemical, electrical, radiation and other burns.[203-205] The deep partial thickness burn wounds are extremely complicated in many cases, which would affect the tissues underneath the skin and internal organs. Keeping the burn wound under a sterilized and moist wound dressing is highly desirable which will facilitate faster healing.[206] However, it is challenging to manage the burn injuries due to extensive burn size, irregular wound shape, difficult-to-access areas, and massive wound exudate, etc.[207] Therefore, the desirable wound dressing should be well adapted to the irregular wound shapes and conveniently applied to the extensive wound area. Besides, wound dressing should be replaced when the fluids soak through it, otherwise, the infection will occur.[208] Considering that the dressing tends to adhere to the wound once the absorbed blood and exudate dry out, it is laborious and painful to surgically peel the old dressing from the wound area at wound dressing changes. Consequently, the newly formed skin or tissue may be destroyed, causing re-injury of the wounds and probably bleeding. In this context, a wound dressing that can be readily operated and painlessly removed would be ideal to speed up healing and improve burn patient outcomes and decrease mortality.

Hydrogels are promising materials as burn wound dressings to facilitate wound healing because they absorb and retain the wound exudate, and sustain an ideal moisture environment for healing while protecting the wound. However, the currently available hydrogel sheets cannot quite match

the deep and irregularly shaped burn wounds, neither can they reach to some special areas, such as joint and cavity wounds. To this end, self-healing hydrogels represent a new class of emerging "smart" hydrogel, which can repair a broken network without any external stimuli.[8] Self-healing hydrogels with injectable properties provide a solution to address the burn wound healing issues more ideally because they can be quickly and directly injected to the large and irregular wounds and even certain areas with difficult access. Subsequently, the hydrogel fragments can self-heal to form a single piece of hydrogel with desirable shape and thoroughly fill the wounds. Once the hydrogels possess both good mechanical strength and short self-healing time, they will efficiently generate a mechanical barrier to protect the wounds from infections. Ideally, the hydrogels would have on-demand dissolvable capacity to be removed easily and painlessly. This can be achieved by self-healing hydrogels cross-linked by Schiff-base linkages. Zhang et al reported that primary amines from amino acids could compete with amines of chitosan chain to react with aldehydes, enabling shift of Schiff-base linkages and dissolution of the hydrogel.[86] Despite the high potential, the injectable self-healing hydrogel with on-demand dissolvable ability applied in deep partial thickness burn wound healing has never been reported in the previous works.

Because of the growing environmental trends to switch from synthetic petroleum-based polymers towards macromolecules obtained from renewable and sustainable sources, as well as the potential of naturally occurring polymers in biomedical and pharmaceutical applications,[209-211] hydrogels made out of natural polymers, such as chitosan and cellulose, have attracted much attention in the past few decades. Chitosan is a natural polysaccharide from renewable resource, for example shell of crab and shrimp, which has been widely applied in the biomedical fields due to its biodegradability and biocompatibility.[212-213] However, one of the most critical drawbacks regarding the use of chitosan in biomedicine is its poor solubility in neutral water. Carboxymethyl

chitosan (CMC) is a chitosan derivative with high solubility under physiological conditions, and hydrogels made of CMC demonstrate good biocompatibility and moisture retention capacity.[39] One of the most important features of chitosan and its derivatives is that the primary amine groups are abundant. The amine groups from CMC can react with aldehyde groups of polymers to form dynamic and reversible Schiff-base linkages which can be readily broken and re-formed, allowing the hydrogel to self-heal rapidly. However, the swelling property of self-healing hydrogel composed of chitosan derivatives is not favorable to burn wounds with massive wound exudate, because the fluid uptake rate is low and the hydrogel degrades easily in aqueous system.

Cellulose nanocrystal (CNC), a natural biopolymer originated from natural renewable resources, have drawn much attention as a promising biomaterial because of their good biocompatibility,[214] high specific surface area and aspect-ratio and high mechanical strength and stiffness.[154, 215] CNCs are commercially available in Canada, U.S.A. and India et al., and have been approved as the first safe nanomaterials on Environment Canada's domestic substance list.[26, 57] These outstanding characteristics enable CNCs to be widely incorporated in polymeric hydrogel matrices as reinforcing nanofillers. However, in most of the CNC-reinforced hydrogels, the pristine CNCs are only physically entrapped within the matrices and yield to mechanical properties improvement. More recently, aldehyde-modified rigid rod-like cellulose nanocrystals were reported with maintained crystal structure.[216] The aldehyde groups allow the cellulose nanocrystal to chemically cross-link with the polymer chains in the matrix for improved reinforcing effect. Dash et al prepared a gelatin hydrogel cross-linked by aldehyde-modified cellulose nanowhiskers, in which the aldehyde groups could react with amine groups from gelatin through Schiff-base linkages to reinforce the network.[154] However, the procedures to form gel are laborious (24 h at room temperature and then 10 day at 4 °C) and self-healing capacity was not reported. Nevertheless, this

has provided opportunities to develop self-healing hydrogels by combining aldehyde-modified CNCs (DACNCs) and CMC via Schiff-base linkages. The CNCs can be easily transformed to a highly reactive cross-linker by using aldehyde-modification. It is hypothesized that the self-healing hydrogels comprised of CMC and DACNC quickly form gel, and rapidly self-heal upon breaking under physiological conditions considering that the abundant amine groups in CMC and large specific surface area and massive active aldehyde groups of DACNC, as well as the DACNCs in the hydrogel can support and protect the network structure when immerse in aqueous system.

With these considerations in mind, herein, we reported the design and synthesis of the CMC/DACNC nanocomposite self-healing hydrogels. The hydrogel's mechanical strength and self-healing efficiency were modulated by adjusting the substitution degree of aldehyde of the modified cellulose nanocrystal and the molar ratio of the amine to aldehyde. The hydrogels' injectable performance, swelling capacity and on-demand dissolving capacity were systematically investigated, as well as the biocompatibility using cell models. In addition, these hydrogels were evaluated for their applications for deep partial thickness burn wound healing through *in vivo* models.

4.2 Experimental section

4.2.1 Materials

Chitosan (viscosity-average molecular weight: 12.4×10^5, degree of deacetylation: 72%), monochloroacetic acid (ACS reagent, ≥99.0%), 2, 4, 6-trinitrobenzene sulfonic acid (TNBSA, 5 (w/v)% in water), D-glucosamine, sodium bicarbonate ($NaHCO_3$), sodium (meta) periodate ($NaIO_4$, ≥99.0%), hydroxylamine hydrochloride ($NH_2OH{\cdot}HCl$, 99%), glycine (ACS reagent, ≥98.5%), deuterium oxide (D_2O), deuterium chloride solution (DCl, 35wt.% in D_2O), hydrochloric acid (HCl, ACS reagent, 37%), ethylene glycol (≥99.0%), and thiazolyl blue tetrazolium bromide

(MTT, 98%) were purchased from Sigma-Aldrich (St. Louis, MO, USA). Sodium docecyl sulfate (SDS), sodium acetate trihydrate, potassium bromide (KBr, 99+%, for spectroscopy, IR grade, Acros Organics), 2-propanol, sulfuric acid (H_2SO_4, certified ACS plus), and glacial acetic acid (certified ACS) were purchased from Fisher Scientific (Markham, ON, Canada). Spruce cellulose (bleached kraft pulp, $M_w = 4.10 \times 10^5$ g mol^{-1}) with α-cellulose content of 87.3 % was provided by Alberta Pacific Forest Industries Inc. (AB, Canada). Spectra/Por dialysis membranes with a molecular weight cut off (MWCO) of 3.5 kDa were supplied from Spectrum Labs. Primary dermal fibroblasts (Normal, Human, Adult, ATCC® PCS-201-012™), fibroblast basal medium (ATCC® PCS-201-030™), fibroblast growth kit-low serum (ATCC® PCS-201-041™), trypsin-EDTA for primary cells (ATCC® PCS-999-003™), and trypsin neutralizing solution (ATCC® PCS-201-004™) were purchased from American Type Culture Collection (ATCC, Manassas, VA, USA).

4.2.2 Synthesis of carboxymethyl chitosan

Carboxymethyl chitosan (CMC) was synthesized by a procedure described in our previous work with slight modifications.[103, 217-218] Chitosan powder (20.0 g) was dispersed in 100 g 50 wt.% NaOH aqueous solution and kept at -20 °C overnight for alkalization. After thawing, the alkaline chitosan was transferred to a 1000 mL round-bottom flask, followed by addition of 100 mL isopropanol. With vigorous mechanical stirring at room temperature (22 °C), monochloracetic acid (57.0 g) dissolved in another 100 mL isopropanol was then added dropwise to the flask over 30 min. Stirring was continued for one and half more hours. Then, the mixture was refluxed at 60 °C water bath under stirring for another 2 h. At end of the reaction, the residual solvent was discarded. The solid product was washed with 70% (v/v) ethanol aqueous solution and ethanol, and then dried in a fume hood at room temperature. The dried crude CMC was dissolved in distilled water (1500 mL) and neutralized with 6 mol/L HCl aqueous solution. The crude CMC solution was centrifuged

(5000 g, 10 min) to remove the undissolved residue. Refined CMC product was obtained after dialyzing the supernatant against distilled water for 5 days at room temperature and freeze-drying. The content of primary amino group in CMC was 0.56 mmol/g CMC as determined by the 2, 4, 6-trinitrobenzenesulfonic acid (TNBSA) assay.[219-220] The degree of carboxymethyl substitution (DS) of CMC was 0.31, which was determined from the ^{1}H NMR spectra using the method reported in the literature.[195, 221]

4.2.3 Synthesis of dialdehyde cellulose nanocrystal

The cellulose nanocrystal (CNC) was prepared by sulfuric acid hydrolysis of wood cellulose, followed by periodate oxidation to obtain dialdehyde cellulose nanocrystal (DACNC).[152, 222-223] Briefly, wood cellulose pulp sheets were ground to small fibers in a mill (Retsch GmbH, Haan, Germany) with screen aperture size of 0.75 mm. The ground wood cellulose fibers (10 g) were mixed with 65 wt.% sulfuric acid solution (100 mL) and stirred at 45 °C for 1 h. Immediately following hydrolysis, the suspension was diluted with 10-fold iced water to stop the reaction, centrifuged (10 000 rpm, 10 min) and washed several times with distilled water until the supernatant became turbid. The resulting product was loaded in dialysis tubing (MWCO 3.5 KDa) and dialyzed against distilled water. The resulting suspension was then dispersed via sonication for 30 min in an ice bath. Subsequently, the CNC suspension (pH 3, 333 g) was transferred to a 500 mL beaker and 3.33 g $NaIO_4$ was added. The beaker was covered with aluminum foil to prevent the entry of light. The mixture was stirred at room temperature for a certain period of time (12, 24, and 48 h) before the oxidation reaction was quenched by addition of ethylene glycol. The oxidized product was washed several times with distilled water by centrifugation (10 000 rpm, 10 min). The product in dialysis tubing (MWCO 3.5 kDa) was dialyzed against distilled water for several days to remove residuals and freeze-dried to obtain DACNC. DACNC was coded as

DACNC-12, DACNC-24, and DACNC-48, corresponding to periodate oxidation time of 12 h, 24 h, and 48 h, respectively.

4.2.4 Determination of aldehyde content

The dialdehyde content of the DACNC was determined by an oxime reaction. The above never-dried DACNC solution (20 g) and 1.39 g of NH_2OH HCl dissolved in 100 mL of 0.1 M acetate buffer (pH 4.5) were added into a beaker (250 mL) and stirred at room temperature for two days. Product was centrifuged and washed with distilled water, and then freeze-dried. The nitrogen content of the oxime derivate of DACNC was measured with an elemental analyzer (LECO CN628, USA). One mol of aldehyde reacts with one mol of NH_2OH HCl and the amount of aldehyde groups was obtained directly from the measured nitrogen content.

4.2.5 CMC/DACNC hydrogel formation

CMC solution (4 wt.%) was prepared by dissolving CMC powder in distilled water and stirring at room temperature overnight. Suspensions of 4 wt.% DACNC were prepared by dispersing 400 mg of DACNC powder in 9.6 g distilled water and stirring at 80 °C water bath for 4 h.[224] The CMC/DACNC hydrogels were made through homogeneously mixing CMC solution with the solution of DACNC at room temperature at different molar ratios (MR = n (amines from CMC)/n (aldehydes from DACNC)) of 5, 4, 3, 2, 1, 0.5, 0.33, 0.25, 0.2, respectively. Gelation was confirmed using the vial tilting method.[225] The hydrogels were named as CMC/DACNC-t (MR = x), where t and x are the values of oxidation time (12, 24, 48 h) and molar ratio (5, 4, 3, 2, 1, 0.5, 0.33, 0.25, 0.2), respectively.

4.2.6 Characterizations

Fourier transform infrared (FT-IR) spectra of samples were recorded on a Nicolet 6700 spectrophotometer (Thermo Fisher Scientific Inc., MA, USA) in the range from 4000 to 800 cm^{-1}

with 64 scans and 4 cm^{-1} resolution. Samples used for FT-IR analysis was vacuum-dried for 24 h pressed into pellets with KBr.

The proton nuclear magnetic resonance (^{1}H NMR) spectra of chitosan and CMC were acquired at 25 °C by using a 400 MHz spectrometer (s400). Chitosan (10 mg/mL) was dissolved in 2% DCl/D_2O and CMC (10 mg/mL) was dissolved in D_2O.

The morphologies of CNC, DACNC-12, DACNC-24, and DACNC-48 were observed by transmission electrical microscopy (TEM, Morgagni 268, Philips-FEI, Hillsboro, USA) at an accelerating voltage of 80 kV. The dimensions of CNC and DACNC were measured using the ImageJ image analysis software (NIH, USA).[226]

To understand the crystal structure of DACNC, the XRD measurements were carried out using a wide-angle X-ray diffractometer (Ultimate IV, Rigaku, Japan) in symmetric reflection mode,[227] and samples were scanned from 2θ = 4° to 40° at a scanning rate of 1°/min. The crystallinity index (CI) was calculated using the following equation:

$$\mathrm{CI} = \frac{I_{002} - I_{am}}{I_{002}} \times 100\% \qquad (4\text{-}1)$$

Where I_{002} refers to the height intensity of the crystalline peak for the (002) cellulose plane around 22.8. I_{am} refers the height intensity of the minimum between the 002 and 101 peaks around 18.7, which is attributed to the amorphous cellulose peak.[228]

Morphologies of hydrogel were characterized by utilizing field emission scanning electron microscopy (FE-SEM). The hydrogels were frozen in liquid nitrogen and freeze-dried before test. Cross-sections of hydrogels were coated with carbon. The cross-sectional morphologies were observed using a Zeiss Sigma FE-SEM operated at 5 kV accelerating voltage.

4.2.7 Rheological properties test

All rheological studies were performed on a DHR-3 rheometer (TA Instruments, DE, USA) using a 40 mm parallel plate and a 1.0 mm gap distance at 25 °C, unless otherwise specified. Although the pre-gel solution gelled quickly in all cases, the hydrogels were allowed to equilibrate for another 30 min before testing to ensure each sample was analyzed under comparable conditions. Frequency sweeps were performed at 1% strain and at oscillation frequencies from 0.1-100 rad s^{-1}. Strain sweeps had a fixed oscillation frequency of 10 rad s^{-1} and variable applied strain of 1-1000%. For the cyclic strain measurements, the alternate step strain sweep was measured at a fixed oscillation frequency of 10 rad s^{-1}, and amplitude oscillatory strains were switched from γ = 1% strain to large strain (γ = 100%, 200%, 800%) with 100 s for every strain interval.

4.2.8 Self-healing assay and injectable analysis

The self-healing ability of the CMC/DACNC hydrogel was tested by macroscopic observations and quantitative method. In the macroscopic self-healing experiment, the CMC/DACNC-48 (MR = 2) hydrogel was used as a representative. Two pieces of cuboid-shaped hydrogels (20 mm length, 5 mm width and 4 mm thickness) stained with rhodamine B and methylene blue were cut into halves, respectively. Then the cut interfaces of each piece were put together immediately without any external stimuli at room temperature. Pictures were taken to record the self-healing process of the hydrogel. Healing was confirmed by stretching the healed hydrogel with fingers from both ends.[161, 229-230] Furthermore, the rheology analysis of hydrogel was performed to monitor qualitatively the self-healing process. Based on the strain amplitude sweep results, the continuous alternate step strain measurement was carried out to test the rheology recovery behavior of the hydrogel.[98, 101] To test the injectable capability of the CMC/DACNC hydrogel, the CMC/DACNC-48 (MR = 2) hydrogel was chosen as an example. CMC solution and DACNC-48 solution were

mixed for 20 s by a vortex mixer to obtain a homogenous mixture. After gelation, the hydrogel was loaded into a 5 mL syringe with a 20-gauge (20 G) needle and injected out to draw letters on a plate.

4.2.9 Swelling test

To study the swelling kinetics of the CMC/DACNC-48 (MR = 2) hydrogels, cylindrical hydrogels (20 mm in diameter, 6 mm in height) were immersed in 10 mL of distilled water at room temperature. At specific time intervals, the samples were removed from the water and were blotted with a piece of paper towel to absorb excess water on the surfaces. The weight of the samples was measured and compared with initial weight. The swelling ratio was calculated as the following equation:

$$\text{Swelling ratio (\%)} = \frac{W_t - W_0}{W_0} \times 100 \qquad (4\text{-}2)$$

Where W_t and W_0 are the weights of hydrogel at time t and the weight of hydrogel right after gelation, respectively.[231-232]

4.2.10 On-demand dissolution of hydrogel with amino acid

The dissolution of CMC/DACNC hydrogel was studied by using amino acid as the stimuli. Typically, glycine aqueous solution (100 mg/mL) was added to CMC/DACNC-48 (MR = 2) hydrogels (Diameter = 20 mm, Height = 4 mm) in a 20 mL of disposable scintillation vial. The mixture was kept at room temperature with gentle shake. The dissolution of hydrogel was confirmed by turning the vial upside down.[86] Furthermore, quantitative rheological measurement was used to test the dissolution of hydrogel. A time sweep was run on the DHR-3rheometer under the same conditions as described in section 4.2.7, except for the exposure of the hydrogel to glycine solution.[233]

4.2.11 *In vitro* cytotoxicity of hydrogel and dissolved hydrogel products

Normal adult human primary dermal fibroblasts were cultured in fibroblast basal medium supplemented with fibroblast growth kit and grown at 37 ℃ incubator with 5% CO_2. The *in vitro* cytotoxicity of hydrogel and dissolved hydrogel products was assessed by MTT method. Fibroblasts were plated in a 96-well plate at 8000 cells/well and cultured for 24 h in fresh complete growth media at 37 ℃ incubator with 5% CO_2. Afterwards, the medium was replaced with 100 μL of fresh media, and hydrogel disks (2.5 mg, and 5.0 mg) and dissolved hydrogel products were introduced into the wells, followed by further 24 h culture. After incubation, spent media and hydrogel disks were discarded and cells were washed with DPBS followed by adding 100 μL MTT (0.5 mg/mL) into each well. After 4 h of incubation at 37 ℃ in the dark, remove out the MTT solution and add 100 μL DMSO into each well, absorption at 570 nm was detected by a microplate reader (SpectraMax, Molecular Devices, USA). The viability was expressed by the percentage of living cells with respect to the control cells. Five replicate wells were used for each control and test concentrations per microplate, and the experiment was repeated three times. Results are presented as mean ± standard deviation (SD).

4.2.12 Three-dimensional (3D) cell encapsulation and cytotoxicity essay

Normal adult human primary dermal fibroblasts were cultured in fibroblast complete growth media (fibroblast basal medium supplemented with fibroblast growth kit) and grown at 37 °C incubator with 5% CO_2. For preparing the CMC/DACNC-48 (MR = 2) hydrogel encapsulated cells, the CMC and DACNC powder were dissolved in the complete growth media in a biosafety cabinet first and then the cells were suspended in the DACNC solution. The CMC solution and DACNC solution containing cells were loaded into a 24-well plate and mixed by a pipette to form hydrogel (2×10^5 cells/mL hydrogel). The plate was cultured in a 37 °C incubator with 5% CO_2 and 100%

relative humidity. The cell viability inside the hydrogel was evaluated by living/dead staining after 0, 1, 4, and 7 days.[103] The cells encapsulated in the hydrogel were also observed by a CLSM 710 Meta confocal laser scanning microscope (Carl Zeiss, Jena, Germany). Images were processed with ZEN 2009LE software (Carl Zeiss MicroImaging GmbH, Germany) and 3D confocal stacks were processed with Imaris 8.0.1 Software (Bitplane AG, Zurich, Switzerland). Cell density in the hydrogel is defined as the number of cells per unit hydrogel volume. Additionally, cytotoxicity assay was conducted for the dissolved hydrogel using the same cell model. After incubating for seven days, the hydrogel was dissolved by glycine for releasing the encapsulated cells. The free cells were cultured in the plate for another 12 h, and then stained as the cells encapsulated in the hydrogel.

4.2.13 *In vivo* deep partial-thickness burns healing test

The burn wound healing capacities of hydrogels were evaluated using a rat model. All animal experiments were performed under the approval of the Institutional Animal Care and Use Committee of General Hospital of Guangzhou Military Command of PLA. White female Sprague Dawley (SD) rats, aged 6-8 weeks (200-300 g) were purchased from Laboratory Animals Center of General Hospital of Guangzhou Military Command of PLA. All rats were housed in standard cages, and they had *ad libitum* access to food and water throughout the experiment. Animals were allowed to adapt to the laboratory for one-week prior to experiment.

Rats were firstly anaesthetized with intraperitoneal injection of 10% chloral hydrate (300 mg/kg), and the dorsal hair of rat was shaved by an electric shaver and the skin was cleaned with sterile normal saline and disinfected using 70% ethanol. Two deep partial thickness burns (Diameter = 2 cm), one on either side of the mid-dorsal line, were created with a pre-heated soldering iron (50 g) at the temperature of 100 °C for 15 s the dorsal area of each rat. Twelve rats were randomly divided

into four groups with different treatments, namely (1) Control group in which no treatment was applied to the wounds. (2) Gauze group in which sterile petrolatum gauzes were applied to cover the wounds. (3) Hydrogel group in which the CMC/DACNC-48 (MR = 2) hydrogels were loaded into a syringe and then injected to the wound sites. For group (2) and (3), the petrolatum gauze and the hydrogel were surgically debrided from the wounds when they were changed. (4) D-Hydrogel group in which the hydrogels were applied to the wound as described in (3), but removed by dissolving the hydrogel with the aid of glycine solution at hydrogel changes. Specifically, sterile glycine solution (100 mg/mL, 5 mL) was sprayed to the hydrogel surface to dissolve the gel and make it painless to remove from the wounds. After treatment, a piece of Vaseline® petrolatum gauze was applied to cover the hydrogel, and the rat body was further wrapped in a reticular elastic bandage to protect the hydrogel and gauze from moving. The wound dressings and covers were replaced every two days until wound healing or sacrifice. The residents on wounds were gently cleaned by gauze and the wounds were gently washed by sterilized saline to remove the residents thoroughly at every wound dressing change. The appearance of the wound was photographed.Wound area was measured by ImageJ software (NIH, USA) to trace the wound margin, and the unclosed wound rate was calculated as follows.

$$\text{Unclosed wound rate (\%)} = \frac{A_t}{A_0} \times 100 \qquad (4\text{-}3)$$

Where A_0 and A_t are the initial wound area and wound area at day t, respectively.

The rats were anesthetized at day 14 after burn induction and the full-thickness skin around the wound sites was dissected, washed with normal saline solution, fixed in 4% phosphate-buffered polyformaldehyde solution, embedded in paraffin and sectioned in 5 mm increments. The sections were made perpendicular to the surface of the wound and were fixed on a slide and stained with

hematoxylin-eosin (H&E) reagents and Masson's trichrome staining reagents for histological analysis.

4.2.14 Statistical analysis

All experiments were performed at least in three independent batches. Data were represented as the mean ± standard deviation (SD). Statistical evaluation was conducted by Student's t-test and analysis of variance (ANOVA). The multiple-comparisons were evaluated by Tukey's multiple comparison tests. Statistical differences between samples were performed with a level of significance as $p < 0.05$.

4.3 Results and discussion

4.3.1 Formation of CMC/DACNC hydrogels

The molecular structure of the carboxymethyl chitosan (CMC) was identified by Fourier transform infrared spectroscopy (FT-IR) (**Figure 4-1**) and proton nuclear magnetic resonance (^{1}H NMR) spectra (**Figure 4-2**). Compared with chitosan, the FT-IR spectrum of CMC shows characteristic peaks at 1601 cm^{-1} for ν_{as} (COO) and 1410 cm^{-1} for ν_s (COO) attributed to carboxylate band of $–COO^-$, indicating that carboxymethyl groups were successfully introduced to chitosan molecular chains.[38] In the ^{1}H NMR spectrum of CMC, the chemical shifts at 3.06 and 4.28 ppm are the protons of $–CH_2$-COO- introduced to N-position at C_2 and O-position at C_3/C_6 of the CMC, respectively. These results suggest that carboxymethyl substitution occurs at both the amino and primary hydroxyl sites of the chitosan molecules.

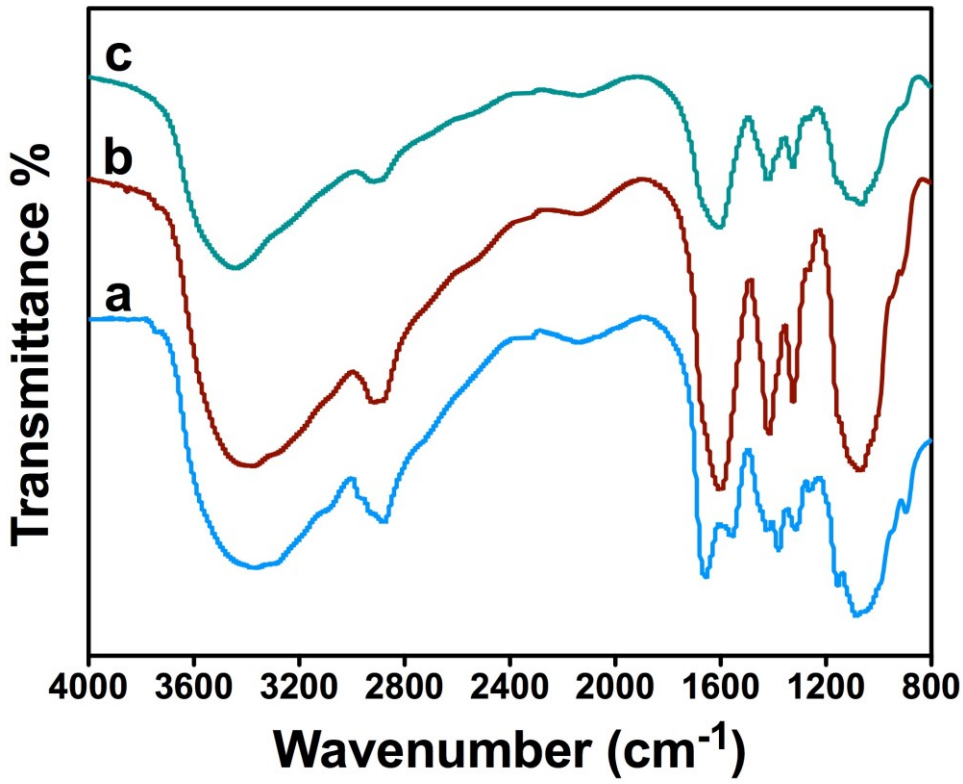

Figure 4-1. FT-IR spectra: (a) Chitosan, (b) CMC, and (c) CMC/DACNC hydrogel.

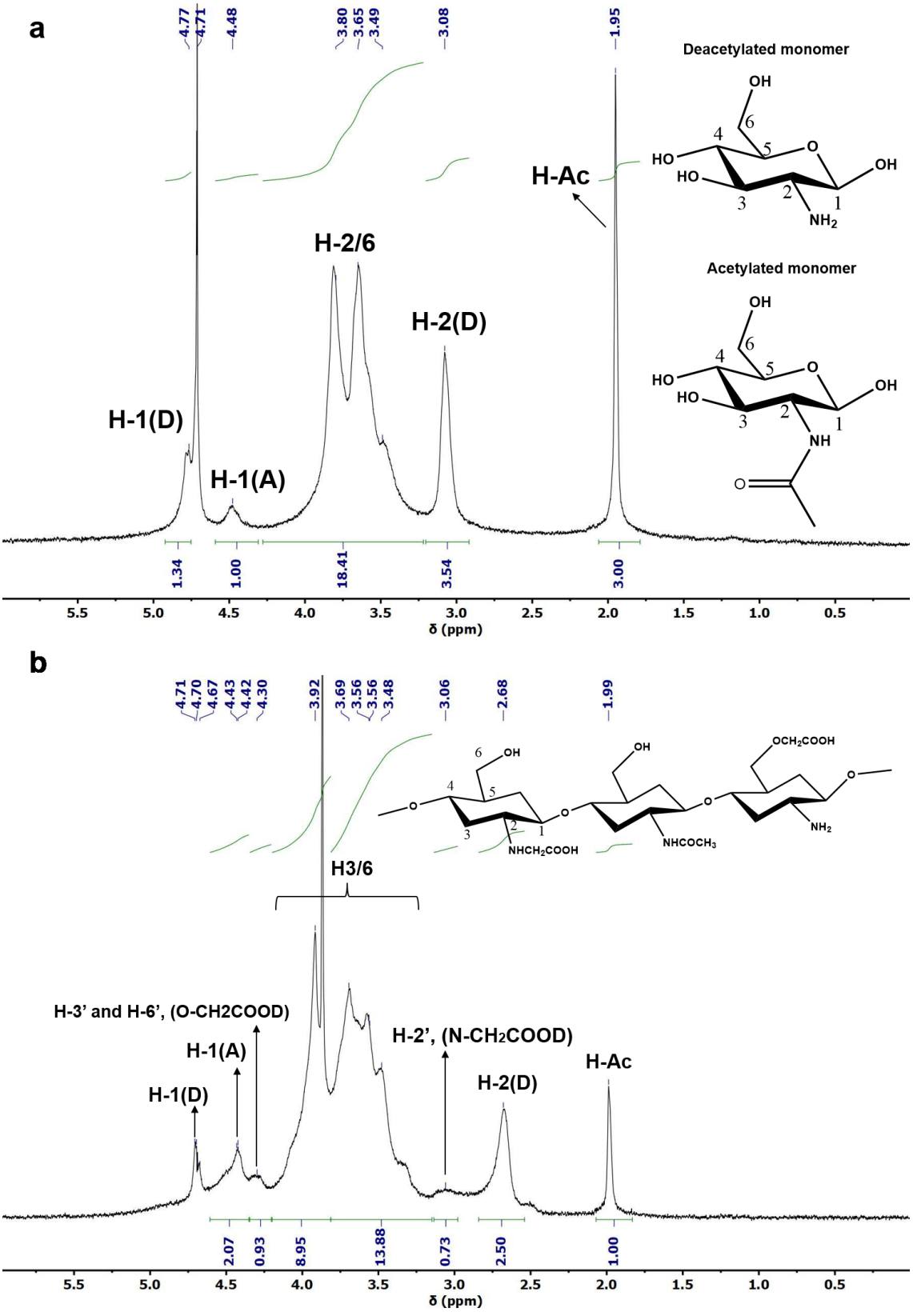

Figure 4-2. ^{1}H NMR spectra of (a) chitosan, and (b) CMC.

Rod-like CNCs with 122 ± 36 nm in length (**Figure 4-3**b) were directly obtained from wood cellulose fibers using sulfuric acid-catalyzed hydrolysis. The stable suspension of CNCs were obtained because the negative sulfate groups were introduced into the outer surface of cellulose during the hydrolysis process. CNCs were oxidized in presence of sodium periodate to yield the corresponding C2/C3 dialdehyde modified CNCs (DACNC) and the aldehyde content was quantified from the nitrogen content of the corresponding oximes.[154, 234-235] The aldehyde groups in turn could function as cross-linkers to react with free amine groups of polymer chains through Schiff-base linkages. The introduction of aldehyde groups reduced the dispersibility of CNCs, so three DACNCs with different aldehyde content were synthesized in this study. The aldehyde content of DACNC increased with oxidation time, which was calculated to be 0.80, 1.12 and 1.71 mmol/g DACNC for DACNC-12, 24 and 48, respectively, and their lengths slightly decreased to 114 ± 29 nm, 112 ± 16 nm and 100 ± 18 nm, but the morphology of DACNC was almost the same as CNC. In comparison to CNC (**Figure 4-3**b), the FT-IR spectrum of DACNC exhibits a new peak at 1732 cm^{-1} (**Figure 4-3c**), which is the characteristic peak of the carbonyl (-C=O-) group. The result confirms that the aldehyde groups were successfully introduced into CNC by periodate oxidation. Furthermore, the crystallographic properties of DACNC were analyzed by X-ray diffraction (XRD) using CNC as the control. As shown in **Figure 4-3**d, CNC possesses typical peaks of cellulose with main peaks at 2θ of 16.5° and 22.6°, which are assigned to (110) and (200), respectively.[216] Although the cellulose crystallinity decreased to certain extent after oxidation depending on the reaction time, there was no significant change in angles of the diffraction peaks, suggesting the DACNC still maintained the cellulose nanocrystal structure.

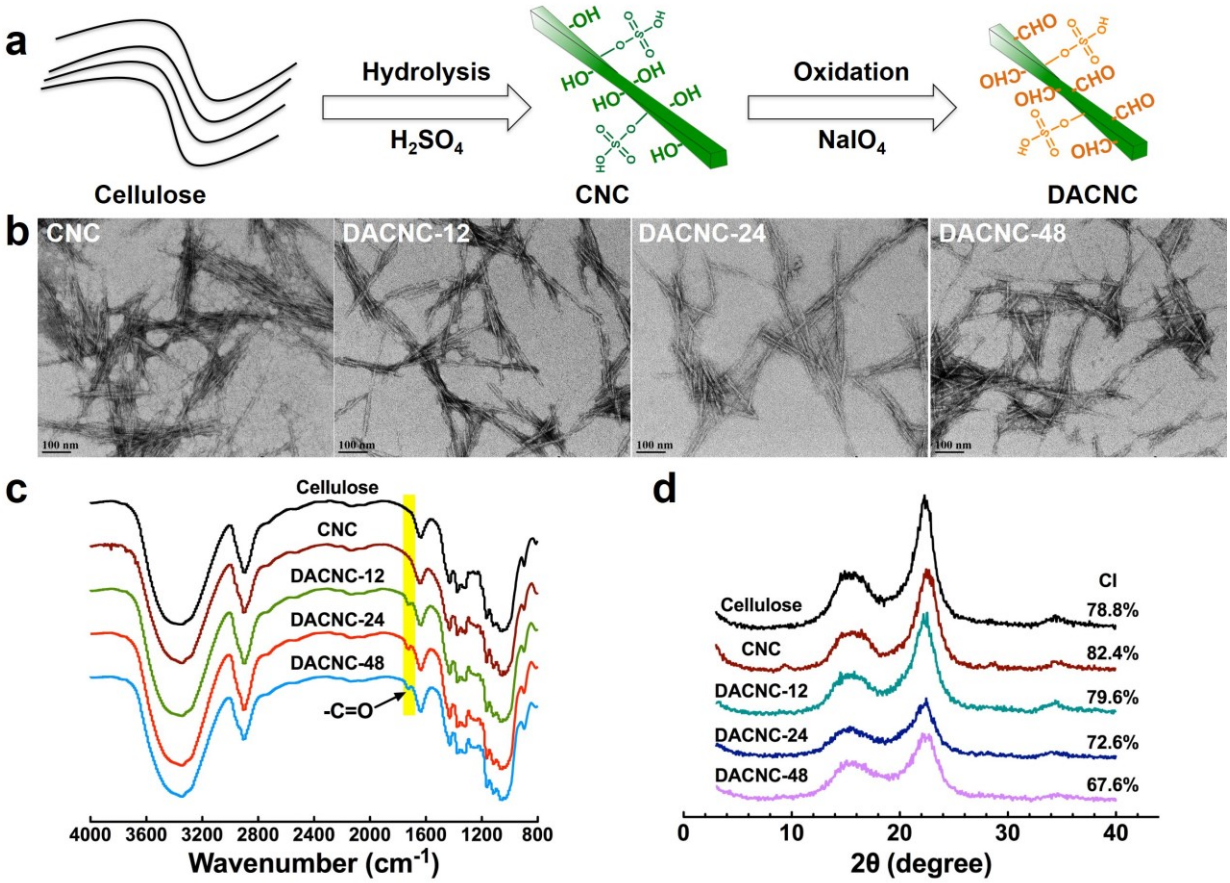

Figure 4-3. Synthesis and structural characterizations of DACNC: (a) Schematic of fabrication of DACNC by hydrolyzing and oxidizing. (b) TEM images of CNC and DACNC with different oxidation time (12, 24, 48 h). (c) FT-IR spectra and (d) XRD patterns of cellulose, CNC, DACNC-12, DACNC-24, and DACNC-48. (Inset numbers in (d) are the corresponding crystallinity indexes).

An array of hydrogels was formulated by homogeneously mixing CMC aqueous solution and suspensions of DACNC containing varying number of aldehydes at room temperature under physiological pH (**Figure 4-4**). When the MR (molar ratio of amines to aldehydes) was larger than 5, the mixture could not form self-standing hydrogels, whereas when MR was less than 0.2, the mixture quickly formed hydrogel before sufficient mixing. Thus, the MR range of 0.2~5 was selected for this work. It is worth highlighting that only water was used as the solvent to prepare the hydrogel, the gelation time is short (less than 2 min), and no stimuli (e.g. pH, temperature, light) are needed for gelation, which enable the CMC/DACNC hydrogels suitable for biomaterials. The gelation mechanism of the CMC/DACNC hydrogel was attributed to the formation of reversible and dynamic Schiff-base linkages (-C=N-) between amine groups ($-NH_2$) from flexible CMC polymer chain and aldehyde groups (-CHO) from rigid rod-like DACNC (**Figure 4-3**b). In the hydrogel network, rigid rod-liked DACNCs not only function as cross-linkers, but also nano-reinforcing fillers. The large specific surface area and aspect ratio of DACNC provide massive active junctions in the network. This highly reactive cross-linker gives a fast gelation to the hydrogel. The SEM images (**Figure 4-5**) revealed the inner structure morphologies of CMC/DACNC hydrogel. The hydrogel displays a honeycomb-like macro-porous structure with a pore size distribution of 50-300 μm. Moreover, there is a small second nano-net inside the macro-pores. As shown in **Figure 4-5**d, the rod-like DACNC could be clearly observed in the hydrogel.

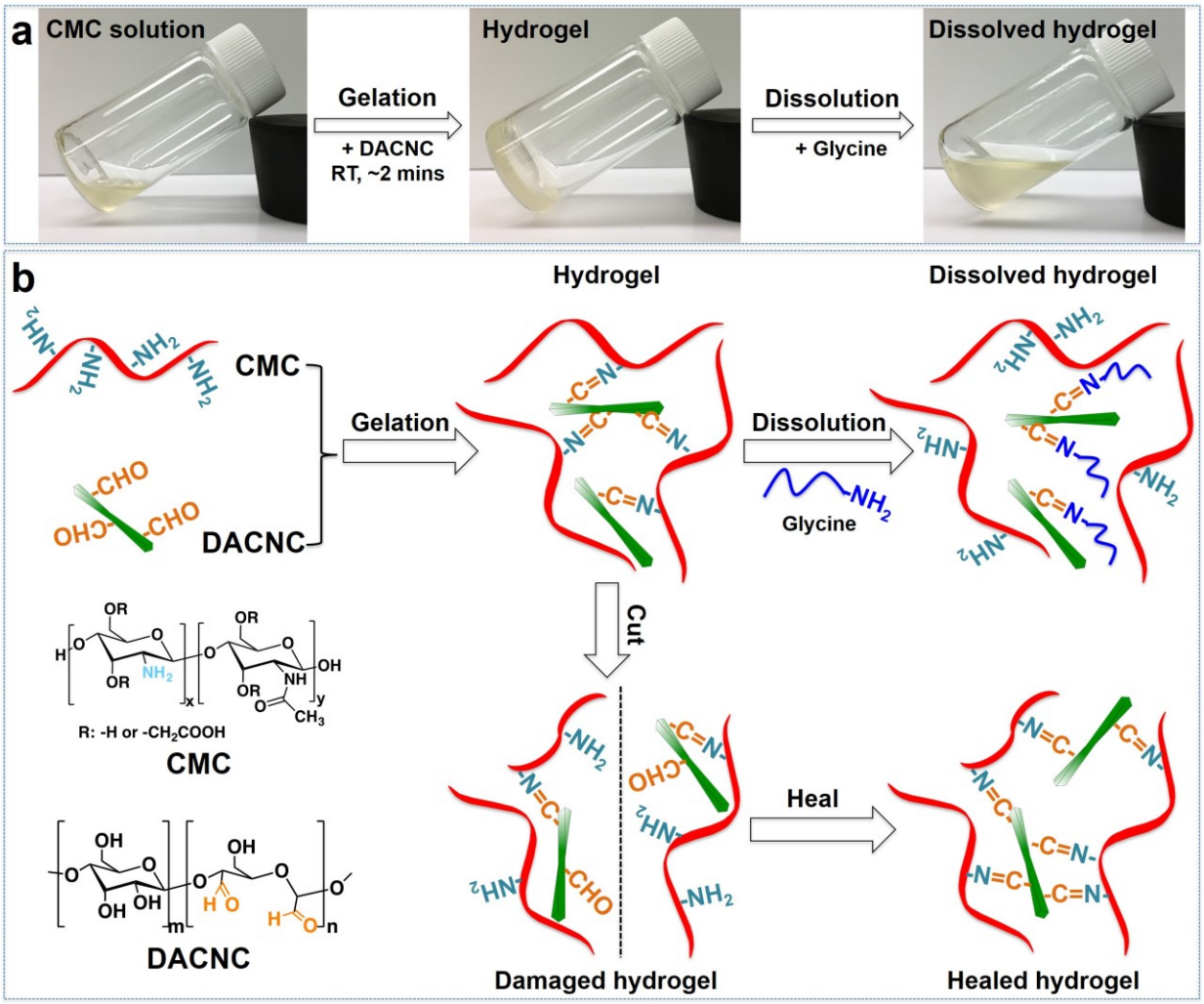

Figure 4-4. Gel formation: (a) Pictures of hydrogel gelation and dissolution process. Adding DACNC solution into CMC solution and mixing, the mixture gelled within 2 min at room temperature. The CMC/DACNC hydrogel dissolved after the addition of glycine solution. (b) Schematic illustration for gelation and on-demand dissolution of CMC/DACNC hydrogel. Amine groups (-NH_2) of CMC reacted with aldehyde groups (-CHO) of DACNC to form reversible and dynamic Schiff-base linkages (-C=N-). After adding glycine into the dynamic CMC/DACNC hydrogel, the amine groups of glycine replaced the amino groups of CMC and reacted with aldehyde groups of DACNC to form new Schiff-base linkages, and finally the hydrogel network was broken.

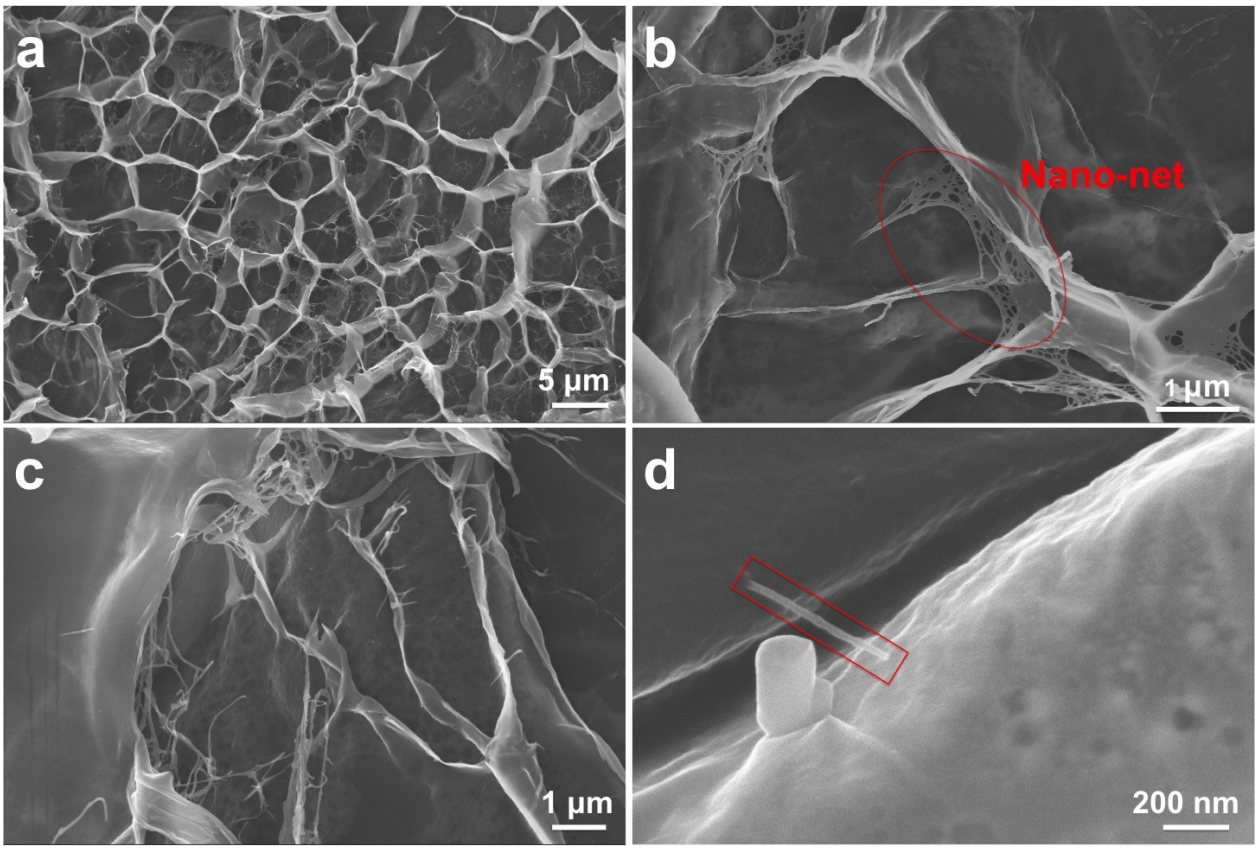

Figure 4-5. SEM images of CMC/DACNC-48 (R = 0.33) hydrogel: Cross-sectional morphologies of hydrogels with different magnifications of (a) 2 000 ×, (b) 15 000 ×, (c) 10 000 ×, and (d) 60 000 ×.

4.3.2 Viscoelastic behaviors and mechanical strength

Substitution degree of aldehyde group on DACNC and molar ratio of the amine to aldehyde are two essential parameters to determine the network structures and properties of CMC/DACNC hydrogels. Thus, their impacts on the hydrogel mechanical properties were first studied by measuring the storage modulus (G'). The tested samples included DACNC-12, DACNC-24, and DACNC-48 and the molar ratios (MR) were 5, 4, 3, 2, 1, 0.5, 0.33, 0.25, and 0.2. Generally, with the same molar ratio, the storage modulus of CMC/DACNC-48 hydrogel is higher than CMC/DACNC-24 hydrogel followed by CMC/DACNC-12 hydrogel (**Figure 4-6** and **Figure 4-**

7). This indicates that increasing substitution degree of aldehyde group results in stronger hydrogel, because there is higher probability for aldehyde groups in DACNC-48 than in DACNC-12/24 to interact with amine groups from CMC, leading to more compact networks to sustain stress. For CMC/DACNC-48 hydrogel, the storage modulus increased with molar ratio decreasing until MR = 0.33, followed by a decrease in modulus below the critical molar ratio. This is probably because the excessive DACNCs tended to aggregate to reduce their dispersion ability, resulting in the decrease of active junctions in the network and cross-linking density of hydrogel.[26, 236] Specifically, the maximum storage modulus (G') for CMC/DACNC-48 hydrogel was around 4 kPa at 0.33 molar ratio of amines to aldehydes, which improved by 17 times compared with hydrogel at molar ratio of 5. This is higher than many other chitosan based self-healing hydrogels reported in literatures due to the reinforcing effect of DACAC in addition to its role as chemical crosslinker, such as chitosan/dialdehyde poly(ethylene glycol) (DF-PEG) and glycol chitosan/DF-PEG self-healing hydrogels (G' = 0.2-1 kPa),[71, 86, 89] as well as the acrylamide-modified chitosan/oxidized alginate (G' = 0.5 kPa).[135] The mechanical strength of the CMC/DACNC hydrogel could be tailored by adjusting the aldehyde contents of DACNCs and molar ratio of amines to aldehydes, which implies potential applications for these CMC/DACNC hydrogels for tissue engineering of soft tissues, whose elasticity scales range from 0.1 to 10 kPa.[237-238] Moreover, gelation time is important when designing hydrogels for biomedical applications, such as injectable gels and gels for cell/drug encapsulations. Slow gelation leads to uneven distribution of components, whereas too fast gelation results in insufficient handle time.[239] The gelation time shortened as the molar ratio of amine to aldehyde decreased, while the strength of hydrogel increased until MR reached to 0.33 and then decreased. Usually, the strength of hydrogels for burn wound healing dressing is

about or less than 1 kPa.[76] Given the rapid gelation time (2-5 min) and mechanical strength (1 kPa), we chose CMC/DACNC-48 (MR = 2) hydrogel for the following experiments.

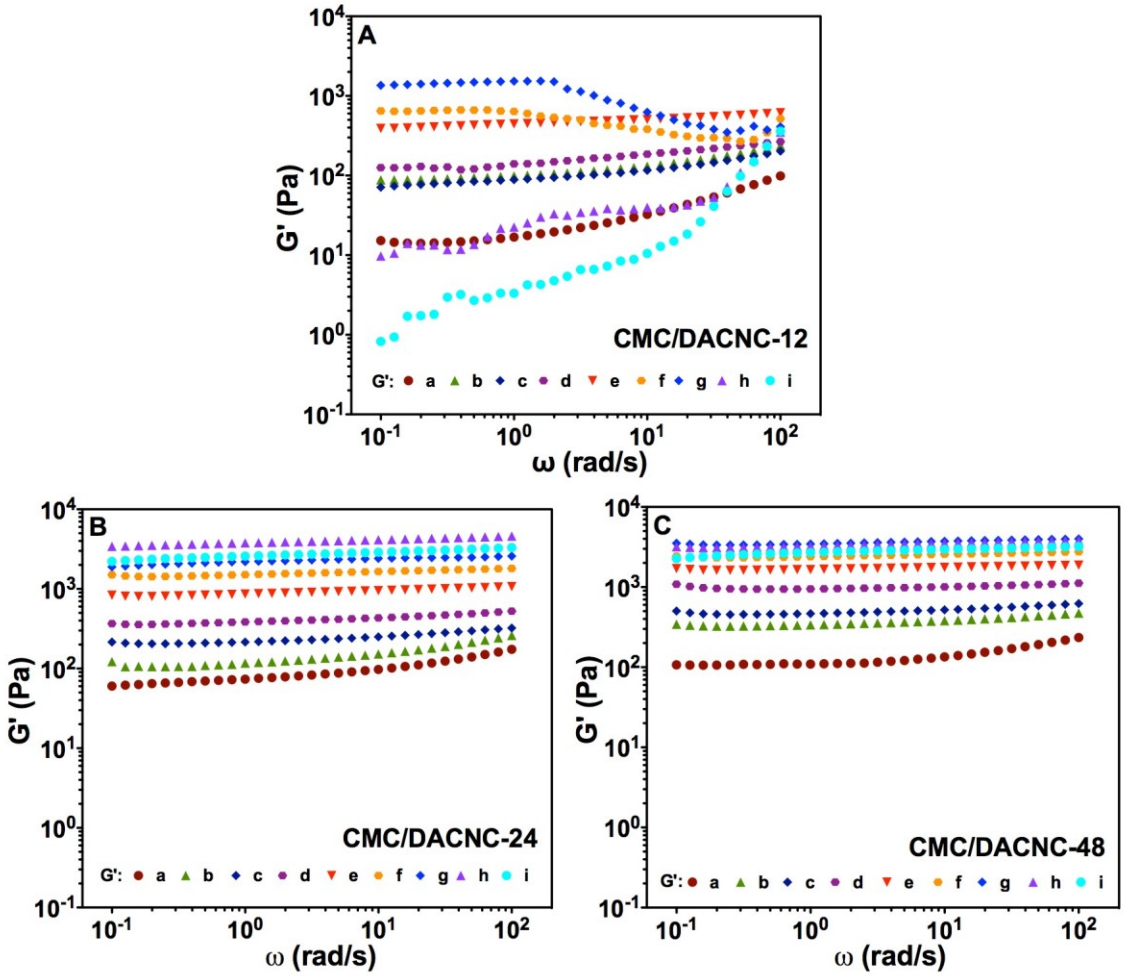

Figure 4-6. Frequency sweep of the (A) CMC/DACNC-12 hydrogel, (B) CMC/DACNC-24 hydrogel, and (C) CMC/DACNC-48 hydrogel at different molar ratios of amine groups from CMC to aldehyde groups from DACNC: (a) MR = 5, (b) MR = 4, (c) MR = 3, (d) MR = 2, (e) MR = 1, (f) MR = 0.5, (g) MR = 0.33, (h) MR = 0.25, and (i) MR = 0.2.

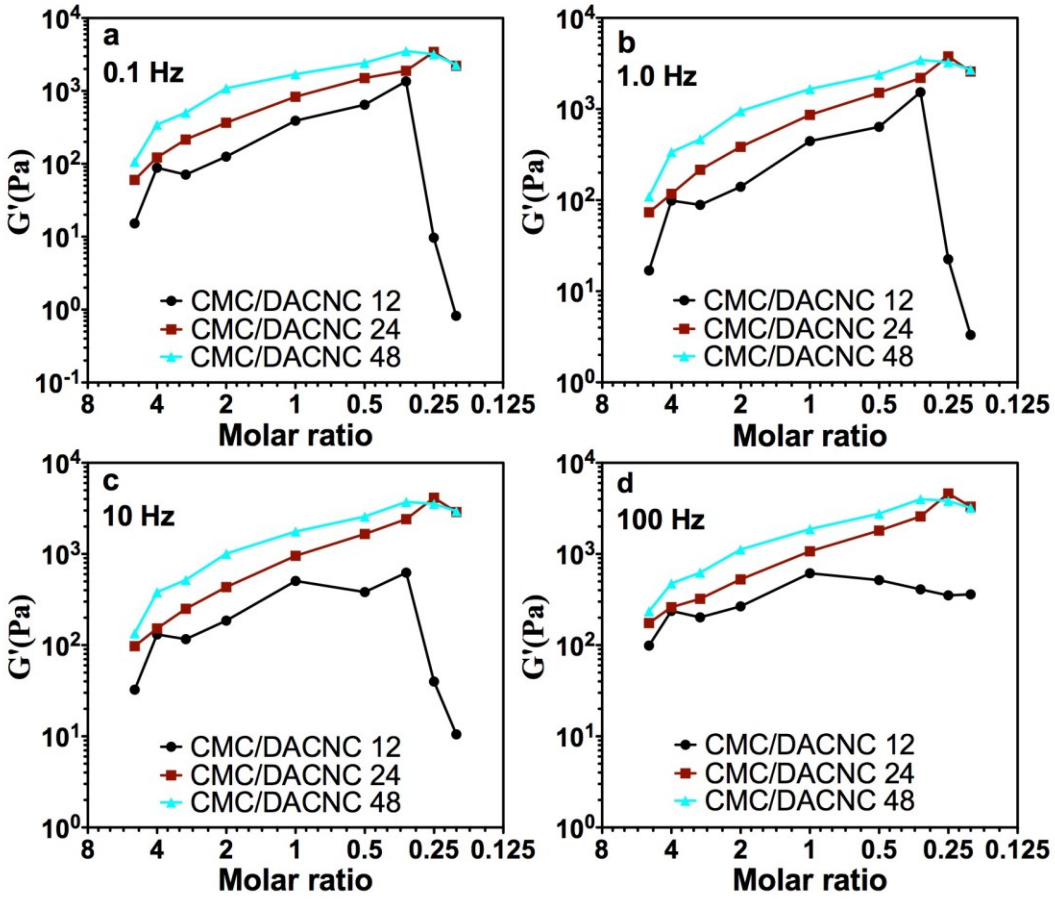

Figure 4-7. Molar ratio dependent viscoelastic properties of CMC/DACNC hydrogel at key frequencies. Storage modulus G' at different frequency (a) 0.1, (b) 1.0, (c) 10, and (d) 100 Hz VS molar ratio of amines in CMC to aldehydes in DACNC for CMC/DACNC-12, CMC-DACNC-24, CMC-DACNC-48 hydrogel.

4.3.3 Self-healing performance and injectable capacity

The self-healing ability of the CMC-DACNC-48 (MR = 2) hydrogel was confirmed by reforming the hydrogel from two separated pieces without any external stimuli and the healed hydrogel was obtained within 5 min at room temperature (**Figure 4-8**a). The re-formed hydrogel maintained its integrity even when it was stretched at both ends, indicating that the two separated hydrogels healed into an integrate hydrogel and it was strong enough to bear tensile stress.

Furthermore, rheological recovery test was used to quantitatively determine the self-healing capacity of the CMC/DACNC hydrogel. As shown in **Figure 4-8**b, the intersection point between the storage modulus (G') and loss modulus (G'') was at strain of 134%, which implies that the hydrogel was liquefied at a shear strain above the critical point. Afterwards, alternate continuous step-strain measurements were conducted to evaluate recovery of the hydrogel mechanical properties following network rupture at high strains. Storage modulus (G') recovered completely and instantaneously after a repeated strain decrease from 100%, 200%, and 800% to 1% (**Figure 4-8**c). When the CMC/DACNC hydrogels were subjected to high dynamic strains (200% and 800%), G' dropped to ~10 Pa, alone with the corresponding inversion of G' and G'' as a result of the collapse of the hydrogel network. When high strain was replaced by a low strain (1%), the hydrogel exhibited complete restoration of both G' and G'' immediately after strain-induced failure. All these results indicate that the network of the CMC/DACNC hydrogel exhibits rapid recovery when the hydrogel sustains oscillatory shear strain, which is attributed to the existence of the dynamic Schiff-base linkages. Schiff-base linkages as reversible covalent bonds exist in the dynamic networks of the CMC/DACNC hydrogel, which enables the hydrogel to possess self-healing and injectable ability. As diagrammatized in **Figure 4-4**b, rapidly breaking and reforming

of the reversible Schiff-base linkages make the CMC/DACNC hydrogel autonomously heal and maintain its integrity for long-term.

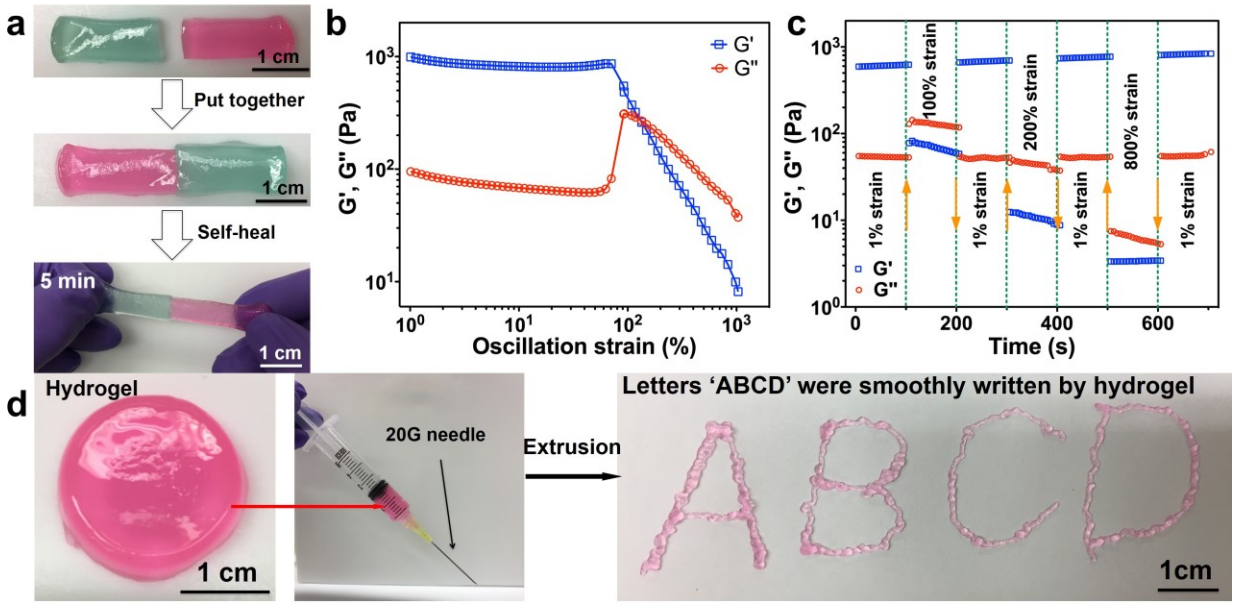

Figure 4-8. (a) Macroscopic photographs of self-healing process of the CMC/DACNC-48 (MR = 2) hydrogel. Two pieces of hydrogels with different color (red hydrogel was stained with rhodamine B and blue hydrogel was stained with methylene blue) were immediately brought into contact without any external intervention after exposing fresh interfaces. After five minutes, the healed hydrogel was stretched and no crack was observed, indicating that the two pieces healed into an integrate hydrogel. (b) Strain sweep and (c) alternate strain sweep of the CMC/DACNC-48 (MR = 2) hydrogel at frequency 10 rad s^{-1}. (d) Injectable process of the CMC/DACNC-48 (MR = 2) hydrogel. The hydrogel stained with rhodamine B passed through the needle without clogging, and the extrusive hydrogel was used as 'ink' to write letters 'ABCD' smoothly.

Surface-modified cellulose nanocrystals have been widely induced into hydrogel either as reinforcement agent or cross-linker to improve their mechanical properties. However cellulose nanocrystal crosslinked self-healing hydrogels have only been reported very recently with limited effort yet.[16, 26, 240-242] For example, Shao and co-workers reported a self-healing hydrogel composed of furyl-modified cellulose nanocrystal (CNC-F) and dimaleimide poly(ethylene glycol) (Mal-PEG-Mal), which heals via thermally reversible covalent Diels-Alder bond after incubating in 90 °C under nitrogen.[242] Besides, a self-healing hydrogel, consisting of cellulose acetoacetate, hydroxypropyl chitosan, and amino-modified cellulose nanocrystals, heals after 1 h under acidic conditions (pH 3.5) via the re-formation of the dynamic covalent enamine bonds between amino groups and acetoacetyl.[241] The CMC/DACNC hydrogel prepared in this study could heal within five minutes at room temperature without any stimuli. The large-aspect ratio and specific surface area of DACNC raise massive active junctions in the hydrogel network to help recover the broken Schiff-based linkages rapidly. This highly active aldehyde groups in DACNCs is easy and quick to re-crosslink with amine groups in CMC chain. In addition, the shear-thinning behavior of the hydrogel was visualized by successful injecting CMC/DACNC hydrogel through a narrow 20 G needle (**Figure 4-8**d). In contrast to sheets and membranes-based burn wound healing dressings, the injectable self-healing CMC/DACNC hydrogel could be easily injected to irregular wound beds and rapidly molded into the shape of wound to fully cover the large and irregular wound area.

4.3.4 Fluid absorption capacity

Hydrogels used for wound healing, especially for burn and scald wounds, should have high fluid absorption capacity to remove wound exudates and maintain a moist environment for the wound sites.[231, 243] The swelling ability was investigated by immersing the CMC/DACNC-48 (MR = 2) hydrogels into distilled water for different periods of time. As shown in **Figure 4-9**, after seven

hours of incubation, the hydrogel was stable and still maintained its integrity in water, which was different from the conventional 'soft' chains comprised self-healing hydrogels whose structure couldn't remain in one piece upon soaking. Analogously, Yang et al reported self-healing hydrogels, composed of carboxymethyl cellulose-hydrazide (CMC-$NHNH_2$) and dextran-aldehyde (Dextran-CHO) 'soft' chains with rigid CNCs or modified CNCs, could keep their structure better than unfilled polymeric hydrogels.[26] Moreover, the hydrogel reached high swelling ratio of 350% at the equilibrium state, which was higher than the swelling ratio (260%) of the CMC-$NHNH_2$/Dextran-CHO/aldehyde modified CNCs-based self-healing hydrogels.[26] The integrated structure and high water uptake ratio of CMC/DACNC hydrogel rely on two factors. Rigid rod-liked DACNCs induced physical "obstruction effect". The DACNCs was trapped and entangled in the hydrogel network, which restricted the mobility of the 'soft' CMC chains. On the other hand, the formation of a network structure with linkages among the DACNCs may provide another "locking effect" to maintain the structure of the hydrogel network, the aldehyde groups in DACNCs cross-linked with amine groups in CMC chain, which reduced free volume and chain mobility within the hydrogel, inhibiting water penetration, adhesion and uptake while maintain a rigid and compact hydrogel structure.[244] Both effects from rigid rod-liked DACNCs contribute to the integrated hydrogel structure and high water uptake ratio. The high-water absorption while still maintaining the hydrogel integrity is crucial for uses as wound dressing to remove the large amounts of excessive exudates in a long duration.

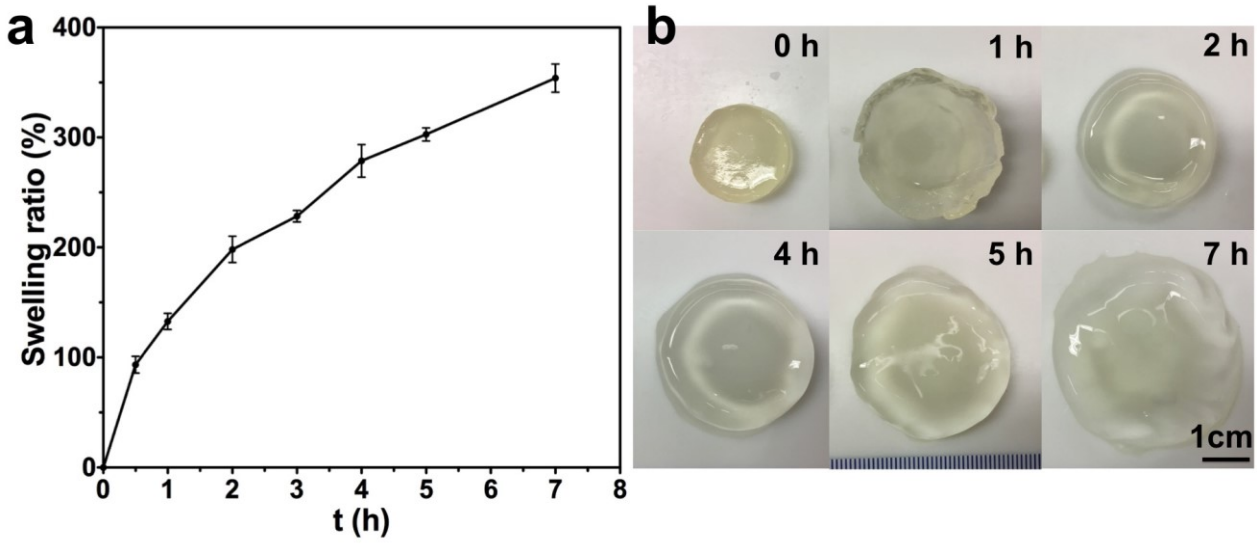

Figure 4-9. (a) Swelling kinetics of the CMC/DACNC-48 (MR = 2) hydrogels soaked in distilled water for different time, and (b) photographs of swollen hydrogel immersed into distilled water for 0, 1, 2, 4, 5, and 7 hours.

4.3.5 On-demand dissolution of hydrogel in amino acid solution

Usually, the burn wound healing dressings are surgically and mechanically removed from the wound, which causes additional injury to the newly formed tissue and it is painful without analgesia, while the anesthetics prevent wounds from healing.[231] The hydrogel with on-demand dissolvable property can eliminate the need for mechanical and surgical debridement and alleviate pain at wound dressing changes. The on-demand dissolution of the hydrogel by amino acid was investigated and results were showed in **Figure 4-10**. Amino acids can shift the equilibrium of Schiff base, leading to the decomposition of the hydrogel.[86, 245] In addition, amino acid is beneficial for wound and has been widely used for diet supplements to enhance wound healing.[246] Specifically, glycine was applied as a model amino acid and the CMC/DACNC-48 (MR = 2) hydrogel was incubated in glycine aqueous solution (100 mg/mL) at room temperature. The hydrogel completely dissolved after one hour of incubation (**Figure 4-10**a). Furthermore, the

quantitative rheological measurements were used for real time study of the dissolution behavior. A time sweep was run in which the CMC/DACNC-48 (MR = 2) hydrogel was exposed to glycine aqueous solution. As shown in **Figure 4-10**b, the storage modulus of hydrogel decreased with time, indicating the hydrogel dissolved progressively. When in contact with air, the hydrogel storage modulus remained unchanged and no hydrogel dissolution was observed. Similarly, the storage modulus of hydrogel just slightly decreased because of swelling when contacting with water. These results verified that the ability of the CMC/DACNC hydrogel to be dissolved on-demand is satisfying and the hydrogel is promising as an ideal alternative to debridement of the wound dressing. The on-demand dissolution was induced by Schiff-base transfer between the Schiff-base linkages present in the hydrogel network and an exogenous solution with amine groups.[86] More specifically, the equilibrium of Schiff-base reactions shifted by the addition of glycine in this work. Amine groups in free amino acid are more reactive than those in CMC to react with aldehyde groups on DACNC. Thus, glycine acts as a competitor of CMC to react with the aldehyde groups on DACNC, which resulted in the CMC/DACNC hydrogels break down and dissolve.

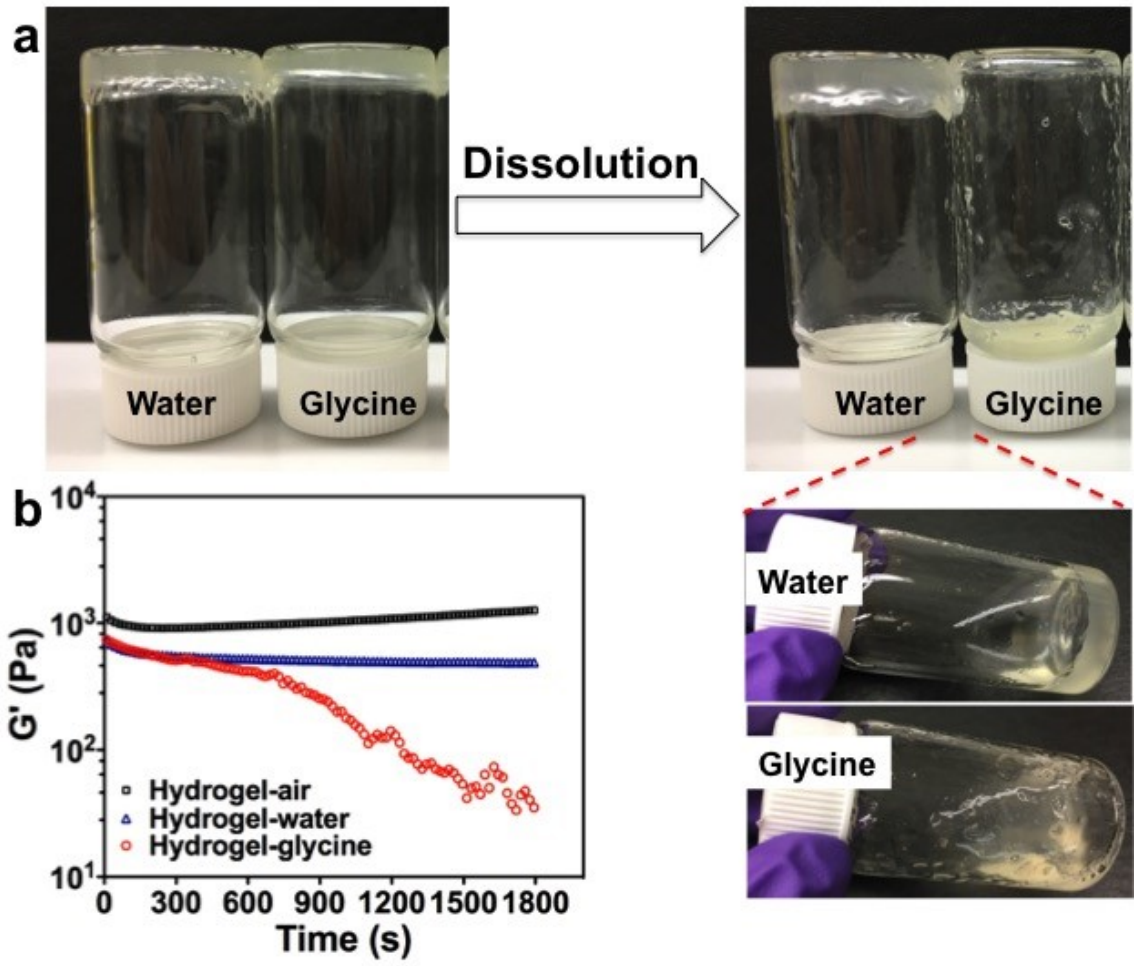

Figure 4-10. On-demand dissolution of the CMC/DACNC-48 (MR = 2) hydrogel: (a) Photographs of the dissolution of the hydrogel after treatment with water and a glycine solution (100 mg/mL, pH 6.3), (b) time sweep of hydrogel exposed to water and glycine solution.

4.3.6 *In vitro* cytotoxicity and 3D cell encapsulation

Biocompatibility is an important property for wound dressing materials. Preliminary *in vitro* cytotoxicity of the hydrogel and on-demand dissolved hydrogel solution was evaluated using MTT assay with normal adult human primary dermal fibroblasts, which has been widely used to investigate the cytotoxicity and biocompatibility of materials.[247] After cells were attached to the well bottom, hydrogel disks were introduced into the wells. **Figure 4-11** shows the cell viability

was 88.6 ± 11.1% and 89.9 ± 11.6% after 24 h when the cells were exposed to 100 μL complete growth media with 2.5 mg hydrogel and 5.0 mg hydrogel disks, respectively. Then we further tested the cytotoxicity of the dissolved hydrogel solution by MTT assay. The result shows that the cell viability was as high as 98.1 ± 8.0% after 24 h of cell exposure. These results suggest that the CMC/DACNC-48 (MR = 2) hydrogel and dissolved hydrogel solution are relatively nontoxic with good potential for biomedical applications.

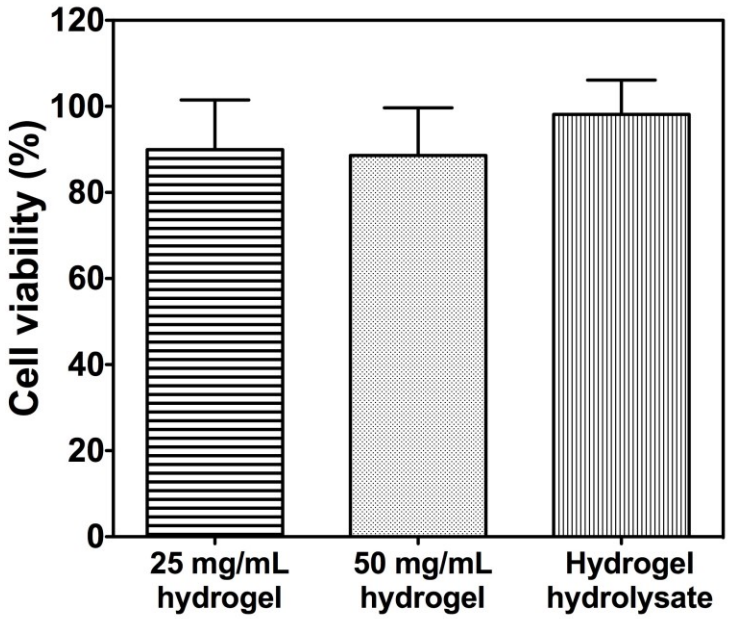

Figure 4-11. Cell viability of hydrogel and dissolved hydrogel product.

The ability of hydrogel to absorb massive liquid while maintain the hydrogel integrity is crucial for extracellular matrix (ECM) materials to support cell growth. In addition, cell spreading and migration destroy the hydrogel matrix, but self-healing capacity of the reversible hydrogel enables the recovery of the broken network and prolongs the lifetime of the hydrogel matrix. Thus, we performed the three-dimensional (3D) encapsulation of fibroblasts to test the feasibility of the CMC/DACNC hydrogel for cell growth. Fibroblasts were suspended in the DACNC solution

followed by addition of CMC to form hydrogels. Uniform cell distribution and excellent cell viability (98.6 ± 6.4%, **Figure 4-12**a) were confirmed by hydrogel observation using confocal microscopy. The cell viability was as high as 97.8 ± 4.2% and 96.7 ± 5.4% after one- and four-days encapsulation, respectively (**Figure 4-12**b-c). After seven days of incubation, not only the cell viability remained high (97.3% ± 5.2%), but also the cell numbers jumped from 2×10^5 cell/mL in the beginning to 7×10^5 cell/mL on day 7 (**Figure 4-12**d). The cell viabilities in different culture day have no significant difference, which demonstrated the excellent cytocompatibility of the hydrogels. After incubated for seven days, the hydrogel was dissolved by glycine solution. The polymer solution with free cells was cultured in the tissue culture plates for another 12 h. The free fibroblasts attached to the plate bottom and exhibited normal cell morphology (**Figure 4-12**c), further confirming good cytocompatibility and capacity to support fibroblasts growth of the CMC/DACNC hydrogel.

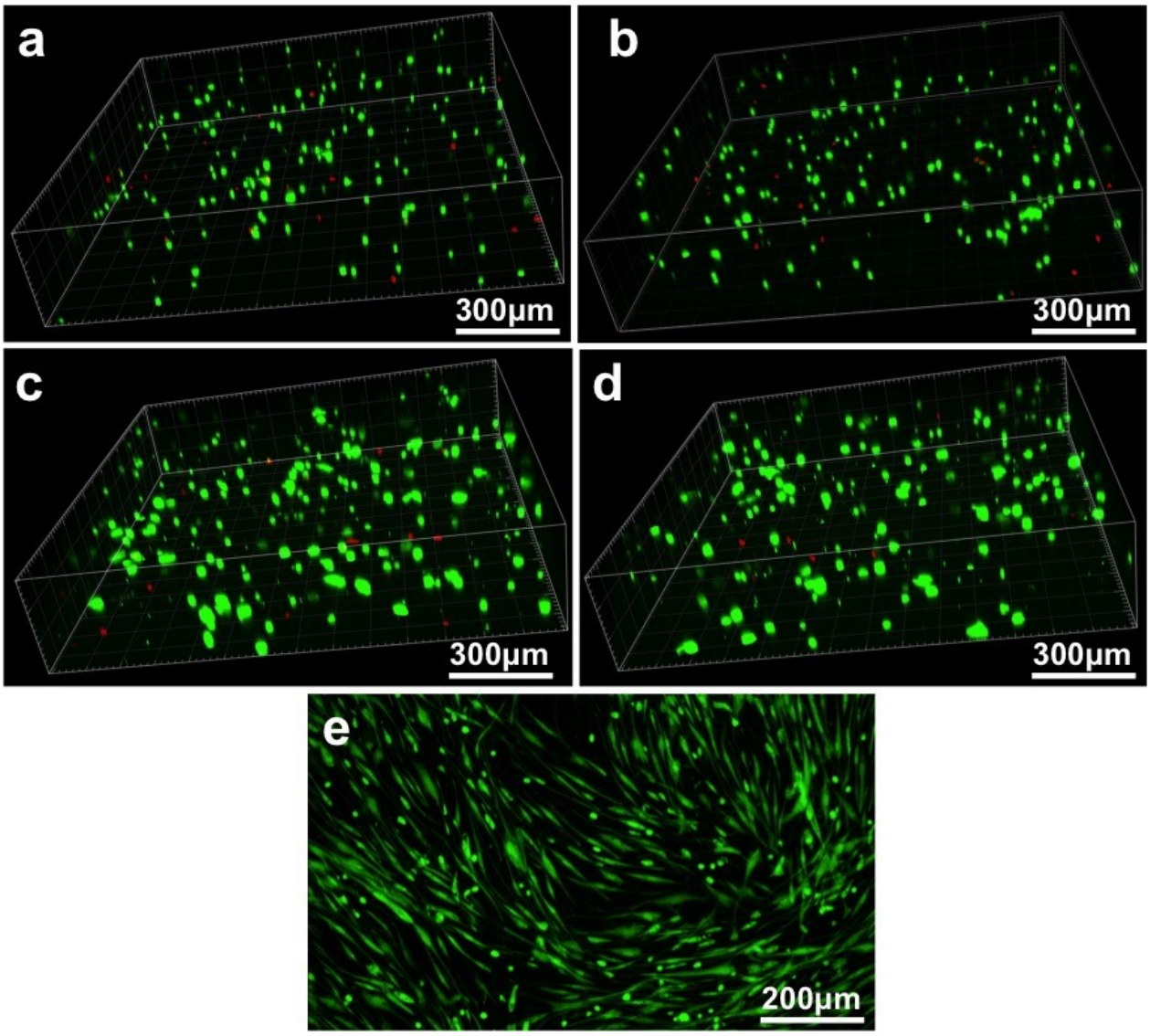

Figure 4-12. Cell encapsulation within the CMC/DACNC-48 (MR = 2) hydrogel scaffolds: Representative 3D images of encapsulated cells inside hydrogel network after (a) 0 day, (b) 1 day, (c) 4 day, and (d) 7 day encapsulation (green and red dots mean live and dead cells, respectively). There were *ca.*98% of cells survived after one week in culture. (e) The released fibroblasts from 3D cell encapsulation were cultured on tissue culture plates for 12 h. The free fibroblasts attached to the plate bottom and exhibited normal cell morphology.

4.3.7 Burn wound healing effect

In the animal model, deep partial thickness skin burn wounds were created on the dorsal area of SD rats which extended fully through the epidermis and dermis layers of skin. The CMC/DACNC hydrogel was injected into the wound to fully cover the wound bed. **Figure 4-13**a showed the photographs of burn wounds during healing process for (1) control group, (2) gauze group and (3) hydrogel group, and (4) D-hydrogel group, respectively. For group (3), CMC/DACNC-48 (MR = 2) hydrogels were injected into the wound beds followed by surgical removal, whereas for group (4), the injected CMC/DACNC-48 (MR = 2) hydrogels were removed by on-demand dissolving using glycine solution. On day 0, the skin was typically splotchy red and burns were extended to the reticular region of the dermis layer, which is classified as a deep partial thickness burn. In all four groups, the burn wounds contracted with time (**Figure 4-13**b). The four groups had no significant effects on the wound size after two days treatment ($p < 0.05$). Difference occurred after four days treatment. On day 4 and 6, compared to the control group, wound size reduced more in the other three groups, but there was no significant difference between Gauze group and Hydrogel group. There was less than one quarter of unclosed wound area (22.1 ± 8.0%) in D-Hydrogel group after eight days of healing while it took ten days for Hydrogel group to reduce the wound area to 23.0 ±11.4%, 12 days for the Gauze group (26.0 ± 3.8%) and 14 days for the Control group (22.3 ± 5.9%), indicating that wounds in D-hydrogel group demonstrated a faster healing rate. On day 14, D-hydrogel group showed the smallest unclosed wound area (0.6 ± 2.7%) among all groups, lower than that of Gauze group (13.1 ± 5.4%) and Hydrogel group (6.3 ± 3.1%). There were no obvious wounds and only small line-liked wound in the D-Hydrogel group on day 14, which is comparable or better than most of polymeric hydrogels-based wound healing dressings. For example, about 5% unclosed wound area was identified on day 14 by using keratin-

chitosan/n-ZnO nanocomposite hydrogel wound dressing,[248] and 4.7% unclosed wound area on day 15 for hydrogel wound dressing made from gelatin, oxidized alginate and borax.[249]

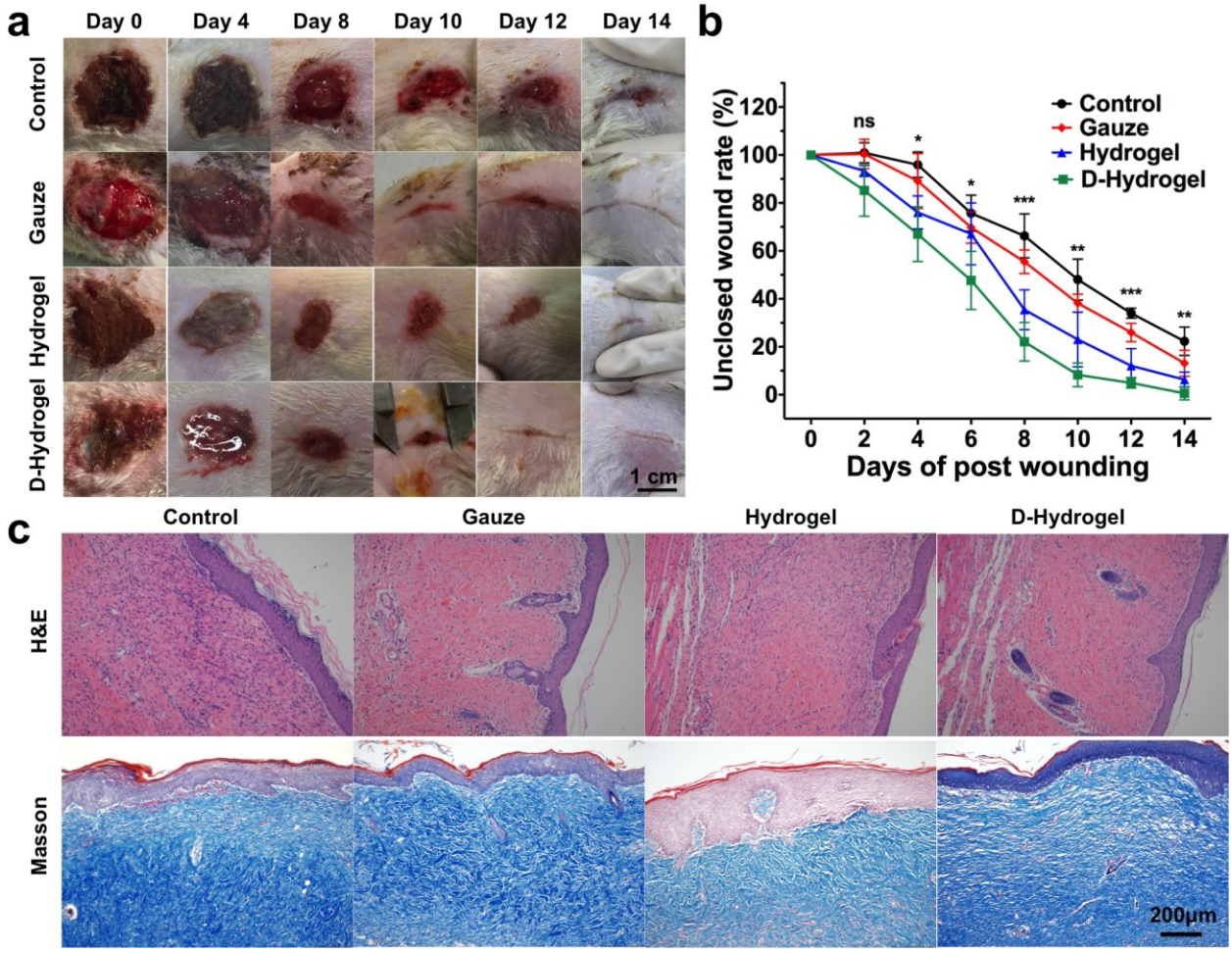

Figure 4-13. Wound healing progress: (a) Images of a representative wound site from each group taken on post-injury days 0, 4, 8, 10, 12, and 14. (b) Unclosed wound area rate of initial wound untreated or treated with petrolatum gauze, hydrogel, and hydrogel with glycine at day 0, 2, 4, 6, 8, 10, 12, and 14. Values are mean ± standard deviation for each group. ns $p > 0.05$, * $p \leq 0.05$, ** $p \leq 0.01$, *** $p \leq 0.001$. (c) H&E staining and Masson's trichrome staining of wounds at day 14.

Haemotoxylin and Eosin staining (H&E) and Masson trichrome staining were applied to further investigate wound repair of hydrogel on rats with deep partial thickness burn. **Figure 4-13**c displayed the histological results of the wounds in Control group, Gauze group, Hydrogel group, and D-Hydrogel group on postoperative day 14, respectively. As shown in the representative images of H&E stained wound, many hair follicles and blood vessels were observed in the Hydrogel and D-Hydrogel groups. In the Control and Gauze groups, however, no obvious cutaneous appendages regeneration was observed. Furthermore, collagen deposition after treatments was detected by Masson trichrome staining. In the D-Hydrogel group, wounds showed more densely packed collagen fibers with parallel arrangement, leading to less scar on the wound area. In contrast, collagen fibers were irregular in the other three groups. In summary, burn wounds in the D-Hydrogel group exhibit rapid skin regeneration and fewer visible scars compared with the Control, Gauze, and Hydrogel groups.

4.4 Conclusion

A novel injectable nanocomposite self-healing hydrogel was constructed by combining flexible CMC chain and rigid rod-like cellulose nanocrystal functionalized with aldehyde groups (DACNC). To achieve the CMC/DACNC nanocomposite hydrogel, the DACNCs of around 110 nm in length were fabricated through hydrolysis and periodate oxidation of wood cellulose. The CMC/DACNC hydrogels exhibit high self-healing efficiency (~ 5 min), injectability, good mechanical strength, and high equilibrium swelling ratio of 350% while maintaining the gel. Moreover, the hydrogel possesses unique on-demand dissolving ability by subjecting to amino acid solution, thereby enabling painless removal at wound dressing changes. Three-dimensional (3D) cell encapsulation demonstrated that the hydrogel has potential to be used as extracellular matrix to support cell growth with cell viability of 97.3% after seven days of incubation.

Importantly, the CMC/DACNC hydrogels could be injected and completely cover the large and irregular-shaped wounds to maintain a moist environment and absorb massive wound exudate, and then could be easily removed from the wound beds by on-demand dissolving the hydrogel. *In vivo* tests demonstrated that the self-healing hydrogel could effectively treat deep partial thickness burn wounds with only 0.6% wound area remaining unclosed after two weeks of healing without the formation of scars. In summary, this work presents a uniquely designed on-demand dissolvable nanocomposite self-healing hydrogel with multiple advantages and good potential as wound dressing materials for deep partial thickness burn patients.

Chapter 5

Stretchable and Tough Nanocomposite Hydrogels with Excellent Self-Recovery and Cytocompatibility

5.1 Introduction

Hydrogel, as a soft material, has been widely applied in the biomedical field due to its high water content, and similarity to the extracellular matrix. However, the insufficient mechanical properties and short lifetime of traditional hydrogels impede their applications. For example, artificial cartilage is expected to be as strong as natural cartilage, which provides the smooth load-bearing surfaces in freely moving joints. The structural deformation and mechanical strength reduction of cartilage are responsible for joint disorders.[250] Hydrogels with excellent mechanical properties as well as self-recovery and self-healing capacity could be employed as artificial cartilage and skeletal muscle tissue, because they can reform their structure after a break and restore their functions, thereby extending their lifetime in such load-bearing applications. Over the past decades, numerous strategies have been explored to enhance the mechanical properties of hydrogel by designing distinctive structure or introducing effective dissipation mechanism, such as nanocomposite hydrogel,[251-253] tetra-arm poly (ethylene glycol) hydrogel,[254] supramolecular hydrogel,[255-256] dual-crosslinked hydrogel, [257] and double-network hydrogel.[2, 123, 258] Particularly, double network (DN) hydrogels have drawn extensive attention recently due to their extraordinary mechanical performance. The DN hydrogels consist of a rigid and fragile first network and a ductile second network. The sacrificial bonds in the first network break to effectively dissipate energy, protect the second network and sustain stress, and the second network provides elasticity to the hydrogel.[2, 155, 259]

Polyacrylamide (PAAm) has been widely used to prepare hydrogels due to its hydrophilicity, non-toxicity and bio-inert nature, long chain lengths. PAAm also has a capacity to preserve their shape and mechanical properties. It is easy to adjust the mechanical, chemical and biophysical properties of PAAm hydrogels.[236] Hence, PAAm hydrogels have a wide-ranging applications, such as waste treatments,[260] controlled drug release,[261-262] and tissue engineering.[263] Until now, a lot of reports on DN hydrogel employing PAAm network as the second network to improve the elasticity of the hydrogel.[157] The cooperation of these two networks reinforces the hydrogel, leading to tough and elastic hydrogel. Unfortunately, the traditional covalently cross-linked DN hydrogels fail to restore their initial mechanical properties following loading and unloading cycle, since the covalent bonds in the first network can't be regenerated after a break.[264-265]

To address this issue, introducing a reversible network to replace sacrificial covalent bonds in the original irreversible covalent network both improves mechanical properties and generates self-recovery and self-healing ability.[264-266] Physically cross-linked bonds in the first network serve as the sacrificial bonds to dissipate energy when force is applied in the hydrogel, and then reform when the stress is released. Previously, Suo's group designed and prepared an alginate-Ca^{2+}/polyacrylamide DN hydrogel with ionically crosslinked alginate and covalently crosslinked polyacrylamide as the first and second network, respectively.[157] This hydrogel displays excellent stretchability and high fracture energy. However, the fracture strength of this DN hydrogel is below 160 kPa, and the hydrogel recovers only 74% of its first loading after being stored at 80 ℃ for one day. Following this work, a series of recoverable DN hydrogel consisting of thermos-reversibly physically crosslinked polysaccharide network as the first rigid network and covalent cross-linked polyacrylamide as the second elastic network were reported, such as κ-carrageenan/polyacrylamide DN hydrogel,[267-268] agar/polyacrylamide DN hydrogel,[269-271] and

xanthan gum/polyacrylamide DN hydrogel.[265] However, these DN hydrogels exhibit recovery and self-healing properties only under high temperature because the composites of the first network, such as *κ*-carrageenan, agar and xanthan gum, only re-dissolve at high temperature to reform the hydrogel. Although the broken bonds could be regenerated through re-heating and cooling the DN hydrogels, the requirement to prepare and recover the gels at high temperature extensively hampers their applications. Therefore, a stretchable and tough hydrogel that could self-recover and self-heal at ambient temperature without any external stimuli is more desirable.

Recently, our group reported a nanocomposite self-healing hydrogel composed of carboxymethyl chitosan (CMC) and dialdehyde cellulose nanocrystals (DACNCs).[140] DACNCs as both reinforcements and cross-linkers significantly reinforce the mechanical properties of hydrogels due to their rigid mechanical properties, large surface area, and high aspect ratios.[272-273] The amine groups in CMC react with the aldehyde groups in DACNC to generate reversible and dynamic Schiff-base linkages, which render the CMC/DACNC hydrogel self-healing at ambient temperature without any external stimuli. With these concerns in mind, we envisioned that the combination of CMC/DACNC reversible network with elastic polyacrylamide (PAAm) network might create a novel stretchable and tough hydrogel with self-recoverable and self-healable capacities in favor of reforming the structure of hydrogel after deformation and restoring their functions. Most importantly, these self-recoverable and self-healable functionalities can be achieved easily at ambient temperature without any external stimuli, which mimics the biological systems that could spontaneously self-repair following mechanical deformation.[274-275] Thus the tough and self-recoverable CMC/DACNC/PAAm hydrogel has potential applications towards load-bearing tissues, such as artificial cartilage and muscle tissue.

Herein, a novel double-network hydrogel consisting of Schiff-base linkages-based first network and covalent crosslinked PAAm second network was prepared. The effects of CMC percentage, polymer concentration, and DACNC concentration on mechanical properties of the hybrid hydrogel were investigated. In addition, the self-recovery, self-healing, swelling, and biocompatible properties of the CMC/DACNC/PAAm hybrid hydrogels were studied.

5.2 Experimental section

5.2.1 Materials

Chitosan (viscosity-average molecular weight: 12.4×10^5, degree of deacetylation: 72%) was purchased from Sigma-Aldrich (St. Louis, MO, USA). Spruce cellulose (bleached kraft pulp, $M_w = 4.10 \times 10^5$ g mol^{-1}) with α-cellulose content of 87.3 % was provided by Alberta Pacific Forest Industries Inc. (AB, Canada). Monomers acrylamide (AAm, for electrophoresis, ≥ 99% (HPLC), Sigma), *N, N'*-methylenebis (acrylamide) (MBAA, 99%, Sigma-Aldrich), free‑radical initiator ammonium persulfate (APS, ACS reagent, ≥ 98.0%, Sigma-Aldrich), polymerization accelerator tetramethyl-ethylenediamine (TEMED, electrophoresis grade, Fisher BioReagents). Primary dermal fibroblasts (Normal, Human, Adult, ATCC® PCS-201-012™), fibroblast basal medium (ATCC® PCS-201-030™), fibroblast growth kit-low serum (ATCC® PCS-201-041™), trypsin-EDTA for primary cells (ATCC® PCS-999-003™), and trypsin neutralizing solution (ATCC® PCS-201-004™) were purchased from American Type Culture Collection (ATCC, Manassas, VA, USA). Thiazolyl blue tetrazolium bromide (MTT, 98%), fluorescein diacetate (FDA), and prodidium iodide (PI, ≥ 94.0% (HPLC)) were purchased from Sigma-Aldrich.

5.2.2 Formation of CMC/DACNC/PAAm hybrid hydrogel

The preparation and characterization of carboxymethyl chitosan (CMC, amine group content: 0.285 mmol/g CMC) and dialdehyde cellulose nanocrystal (DACNC, aldehyde group content: 1.426 mmol/g DACNC) were reported in Chapter 4. Briefly, chitosan (10 g) dispersed in 120 g 50 wt.% NaOH aqueous solution was kept at -20 °C for 12 h. The frozen alkali chitosan was transferred to isopropanol (100 mL), and then sodium chloroacetate (35 g) was added in portions. Under vigorously mechanical stirring, the mixture reacted at room temperature for 2 h, and then at 60 °C for another 2 h to form CMC. Wood cellulose fibers (10.0 g) were hydrolyzed by sulfuric acid (100 mL, 65 wt.%) at 45 °C for 1 h to obtain cellulose nanocrystals (CNCs) and then the CNCs was oxidized by periodate oxidation ($NaIO_4$, 3.33 g) at room temperature for 48 h to obtain the DACNCs.

The CMC/DACNC/PAAm hybrid hydrogels were prepared by a one-pot method. CMC and acrylamide were first dissolved in distilled water with various CMC concentration (2, 3, 4, 5 wt.%) and polymer concentration (14, 18 wt.%), and stirred until a clear solution was obtained. This CMC and acrylamide solution of 10 g was then mixed with covalent cross-linker MBAA, thermo-initiator APS and polymerization accelerator TEMED (0.12%, 0.30%, and 0.3875% based on the amount of acrylamide, respectively), as well as 1 mL of 4 wt.% (or 2, 6, 8 wt.%) DACNC suspension. The mixture was transferred into the molds of a 1 mL syringe and 48-well plate, which was then put into an oven at 50 ℃ for 3 h to form the hydrogel. For comparison, the CMC/DACNC hydrogel was prepared by mixing 4 wt.% CMC solution and 4 wt.% DACNC suspension at room temperature. The PAAm hydrogel was prepared by mixing 14 wt.% acrylamide solution with MBAA, APS and TEMED, followed by treatment at 50 °C for 3 h.

5.2.3 Characterizations

To investigate the possible crosslinks in the hybrid hydrogel network, the Fourier transform infrared (FT-IR) spectra of CMC, DACNC, PAAm hydrogel, and the CMC/DACNC/PAAm hybrid hydrogel were collected by using a Nicolet 6700 Fourier transform infrared spectrophotometer (Thermo Fisher Scientific Inc., MA, USA). Hydrogel samples were frozen in liquid nitrogen and freeze-dried before testing. All samples were pressed to pellets with KBr. FT-IR spectra were recorded between 4000 and 800 cm^{-1} at a resolution of 4 cm^{-1}.

5.2.4 Mechanical tests

The mechanical properties of hydrogels were measured using an Instron 5967 universal testing machine (Instron Corp., MA, USA) at room temperature. Tensile tests of rod-like hydrogel samples (30 mm length and 4.78 mm diameter, prepared in the 1 mL syringe mold) were carried out using a 50 N load cell at a crosshead speed of 50 mm/min. The stress-strain curves were recorded, which were converted into stress-stretch curves, in which the stretch ratio (λ) = strain (ε) + 1. The tensile strength was equal to the maximum tensile stress, and the elastic modulus was the slope over 1.1-1.3 of stretch ratio from the stress-strain curve.

The unconfined compression tests of the cylindrical hydrogel samples (6 mm height and 11 mm diameter, prepared in the 48-well plate mold) were conducted by using the Instron equipped with a 5 kN load cell at a crosshead speed of 1 mm/min. The compressive stress-strain curves were recorded. Maximum stress (σ_{max}), strain (ε_{max}), and compressive modulus (E) were calculated from the compressive stress-strain curves. Maximum stress/strain was the stress/strain at fracture or until a strain of 90% since some hydrogels did not fracture. Compressive modulus refers to the average slope of the initial linear region (elastic range, ε = 0%-10%) of the stress-strain curve.

5.2.5 Self-healing test

The self-healing ability of the CMC/DACNC/PAAm hybrid hydrogels was first evaluated by macroscopic self-healing tests. The original rod-like hydrogel samples and pink color samples (stained with rhodamine B for better observation) were cut into halves, and immediately, the cut interfaces of each piece were brought to contact. The newly contacted hydrogels were sealed in plastic bags and put in a desiccator with saturated KCl solution to prevent water from evaporation, and stored at ambient temperature without any external stimuli. The new hydrogels were stretched from both ends to confirm that they were healed. To quantitatively measure the self-healing efficiency, the tensile tests of original and healed hydrogel samples were conducted as described in the mechanical test section. The self-healing efficiency was defined as the tensile strength of healed hydrogels divided by the original hydrogels. Besides, the microscopic observation was performed to assess the self-healing ability of the hybrid hydrogels. Cracks were created by a blade on the surface of hydrogel and observed under a microscope until the cracks disappeared.

5.2.6 Self-recovery test

To quantitatively measure the self-recovery rate, the tensile tests of original and recovered hydrogel samples were conducted as described in the mechanical test section. In a hysteresis measurement, the rod-like hydrogel samples were first stretched to various stretch ratios (λ = 2, 2.5, 3, or 3.5) and then unloaded. For the tensile recovery test, the hydrogel samples were first stretched to 3 times its initial length, and then unloaded to zero force. The hydrogel samples were then stored in a plastic bag at room temperature to prevent water from evaporation. The second loading and unloading was applied after different resting time (0.5, 1, 6, and 12 h). The recovery rate was defined as the dissipate energy of the second cycle divided by the first cycle. The dissipate energy during a cycle was estimated from the area under the loading-unloading curves. In the

compression recovery test, successive loading-unloading compressive tests were conducted 10 times under varying strain (70%, 85%, and 90%).

5.2.7 Water swelling test

The swelling ratio of the CMC/DACNC/PAAm hybrid hydrogel was measured using a gravimetric method at room temperature. In brief, the as-prepared cylindrical hydrogels (11 mm in diameter and 5 mm in height) were completely immersed in the distilled water (100 mL). The swollen hydrogels were weighed at designed time intervals until they reached swelling equilibrium. The swelling ratio of the CMC/DACNC/PAAm hybrid hydrogels was calculated as the following equation: $Swelling\ ratio\ (\%) = (W_i\text{-}W_0)/W_0 \times 100\%$, where W_i and W_0 refer the swollen weight and the initial weight of hydrogels, respectively.

5.2.8 *In vitro* cell compatibility

The preliminary *in vitro* cytotoxicity of the hybrid hydrogels was assessed by MTT assay. The hybrid hydrogel (200 g) was first immersed in 70% ethanol for 30 min, and then washed with PBS (pH 7.4) three times. Next, the hydrogel was washed with completed growth media and incubated for 30 min at 37 °C. The hybrid hydrogel was incubated in 10 mL completed growth media at 37 °C for 24 h to obtain the hydrogel extract. Normal adult human primary dermal fibroblasts were seeded in the 96-well plate at a density of 7500 cells/well (100 μL cell suspension each well, n = 6 per condition) and incubated at 37 °C for 24 h to allow the cells to adhere. Fibroblasts were treated with 100 μL different concentrations (0, 1, 5, 10, 50, 100%) of hydrogel extract and incubated at 37 °C for 24, 48, or 72 h. The hydrogel extract was discarded and the MTT solution (0.5 mg/mL in PBS, 100 μL) was added to cells and incubated for 4 h. The MTT solution was removed and 100 μL of DMSO was added into each well to dissolve the formazan crystals followed by measurement of the optical density at 570 nm using a microplate reader (SpectraMax,

Molecular Devices, USA). The cell viability was defined by the percentage of living cells with respect to the control cells.

To further confirm the biocompatibility of the hybrid hydrogels, the fibroblasts were directly seeded on the surface of the hydrogel. Briefly, the hydrogel (10 mm diameter, 1 mm thickness) was placed into the center of glass bottom microwell dish (MatTek Corporation, USA), and then cell suspension (1 mL, 75 000 cells/mL) was added above the hydrogel. After 3 days of incubation, the spent media was discarded, and cells were stained with FDA/PI solution (1 mL, 10 min).[103] The hydrogel was washed with PBS to remove excess dye and observed by a CLSM 710 Meta confocal laser scanning microscope (Carl Zeiss, Jena, Germany).

5.2.9 Statistical analysis

Experiments were replicated five times and the data are expressed as mean ± standard deviation (SD). Differences between treatments were determined via student's T-test and analysis of variance (ANOVA). The Post-hoc multiple-comparisons were evaluated by Duncan's multiple-range test. Statistical differences between samples were performed with a level of significance of $p < 0.05$.

5.3 Results and discussion

5.3.1 Synthesis and characterization of CMC/DACNC/PAAm hybrid hydrogel

Figure 5-1 illustrates the scheme to prepare the CMC/DACNC/PAAm hybrid hydrogel. CMC and monomer AAm were dissolved in distilled water to get a clear solution, and then cross-linker MBAA, initiator APS, and accelerator TEMED were added into the CMC/AAm solution, followed by adding DACNC suspension. Immediately, amine groups in CMC reacted with aldehyde groups in DACNC to generate the dynamic Schiff-base linkages, which served as the first and reversible covalently cross-linked CMC/DACNC network. Subsequently, the chemically cross-linked PAAm was formed under heating as the second network. As shown in the central pictures of **Figure 5-1**,

the CMC/DACNC/PAAm hybrid hydrogels were tough and could tolerate high-level deformations of knotting without any observable damage. Because of the adaptable gel-forming ability, the hybrid hydrogels can be readily adapted to different complex shapes, for example, maple leaf.

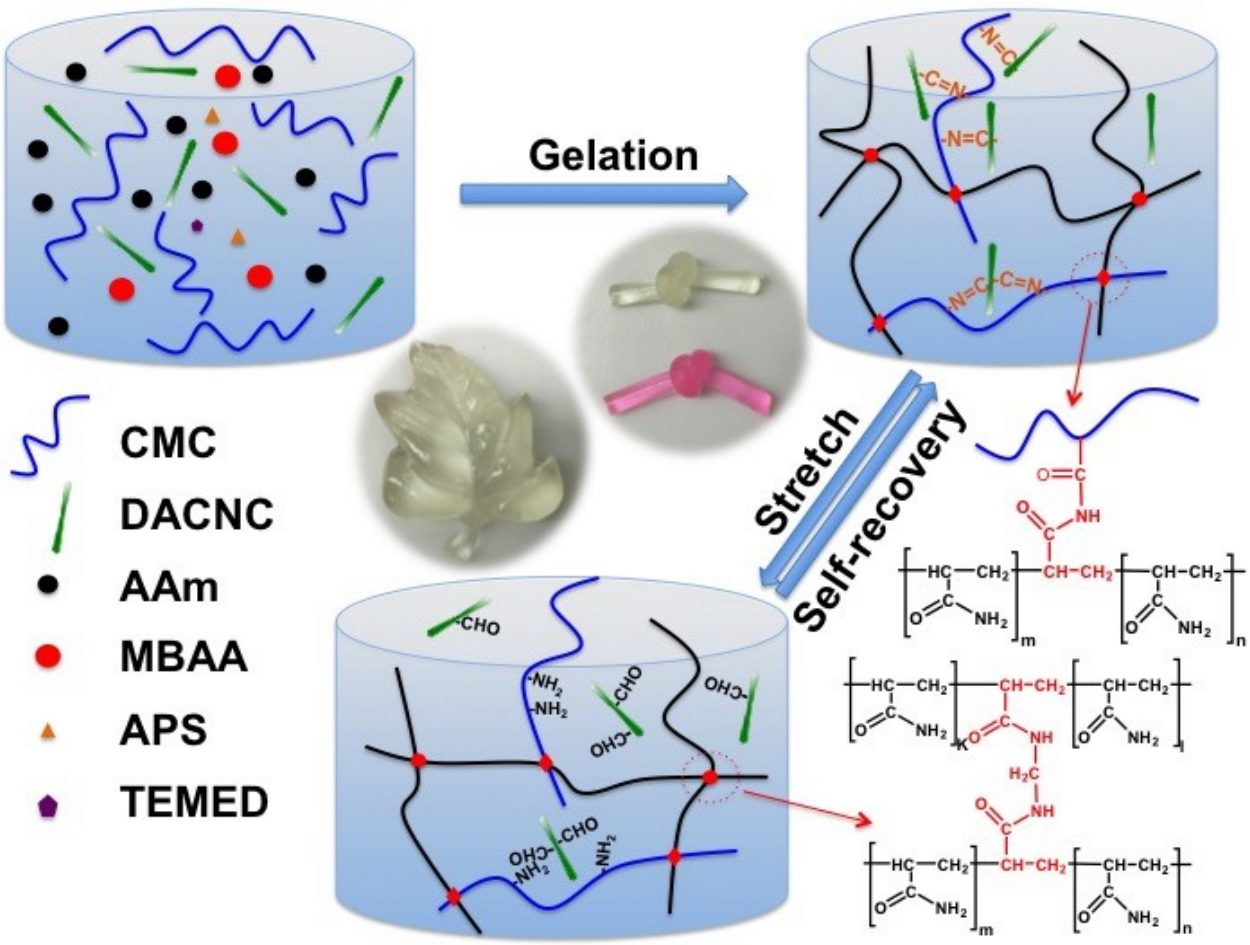

Figure 5-1. Schematics of preparation route for stretchable, tough and self-recovery CMC/DACNC/PAAm hybrid hydrogel.

As shown in **Figure 5-2**, the FT-IR spectrum of CMC exhibits characterized absorption peaks at 1602 cm^{-1} and 1411 cm^{-1}, corresponding to the stretching vibrations of asymmetric and symmetric carboxylic groups (-COO-), respectively, and the band at 1323 cm^{-1} was assigned to C-O

stretching.[276-278] The DACNC exhibited a broad peak at 3345 cm^{-1} (O-H stretching) and characteristic peaks at 1729 cm^{-1} (the aldehyde group), 1163 cm^{-1} and 1046 cm^{-1} (the asymmetric stretching vibration of C-O-C and C-OH stretching), respectively.[279] The peaks at 3360 and 3190 cm^{-1} in the spectrum of PAAm hydrogel were assigned to the stretching vibration of N-H, 1670 cm^{-1} to C=O stretching, 1612 cm^{-1} to N-H cm^{-1} deformation, 1414 cm^{-1} to C-N stretching, and 1123 cm^{-1} to $-NH_2$ in-plane rocking vibration.[280] In the spectrum of the CMC/DACNC/PAAm hybrid hydrogel, a band at 1666 cm^{-1} for imine stretching vibration (C=N) was observed, indicating that Schiff-base reactions had occurred.[15, 110] The peaks at 1587 cm^{-1} and 1274 cm^{-1} were assigned to amide bending vibration (N-H) and C-N stretching of secondary amide, respectively. Besides, the band around 3500-3100 cm^{-1} (O-H and N-H stretching vibration) becomes broader in the spectrum of CMC/DACNC/PAAm hybrid hydrogel, which was attributed to the formation of hydrogen bonds.[281] Thus, the hybrid hydrogels with double-networks of CMC/DACNC and PAAm were obtained.

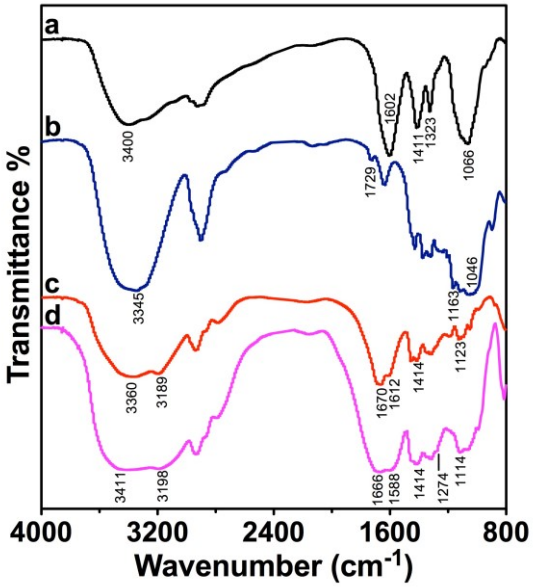

Figure 5-2. FT-IR spectra of (a) CMC powder, (b) DACNC powder, (c) PAAm single hydrogel, and (d) CMC/DACNC/PAAm hybrid hydrogel.

5.3.2 Mechanical properties

The CMC/DACNC/PAAm hybrid hydrogel exhibited excellent stretchability and high strength. As shown in **Figure 5-3**A, the hybrid hydrogel could be stretched to about four times of its original length, and the hybrid hydrogel could be repeatedly stretched as a rubber ribbon. After the force applied to the hydrogel was removed, the hydrogel immediately restored to its original shape, indicating its excellent elasticity. **Figure 5-3**B-E shows the tensile stress-stretch results of the CMC/DACNC/PAAm hybrid hydrogels. Under the same total polymer concentration, the stretch value (λ) of the hybrid hydrogel decreased with higher amount of the CMC in the hybrid hydrogel. In contrast, the fracture stress drastically enhanced when the percentage of CMC content increased from 2% to 4%, and then reached the plateau. There was no statistically significant difference in elastic modulus among hybrid hydrogels with 14% total polymer concentration, while the elastic moduli of hybrid hydrogels with 18% total polymer concentration increased with CMC content from 2 wt.% to 4 wt.% and then decreased. The stretch value, fracture stress and elastic modulus of the hybrid hydrogels with 18% total polymer concentration were higher than those with 14% total polymer concentration.

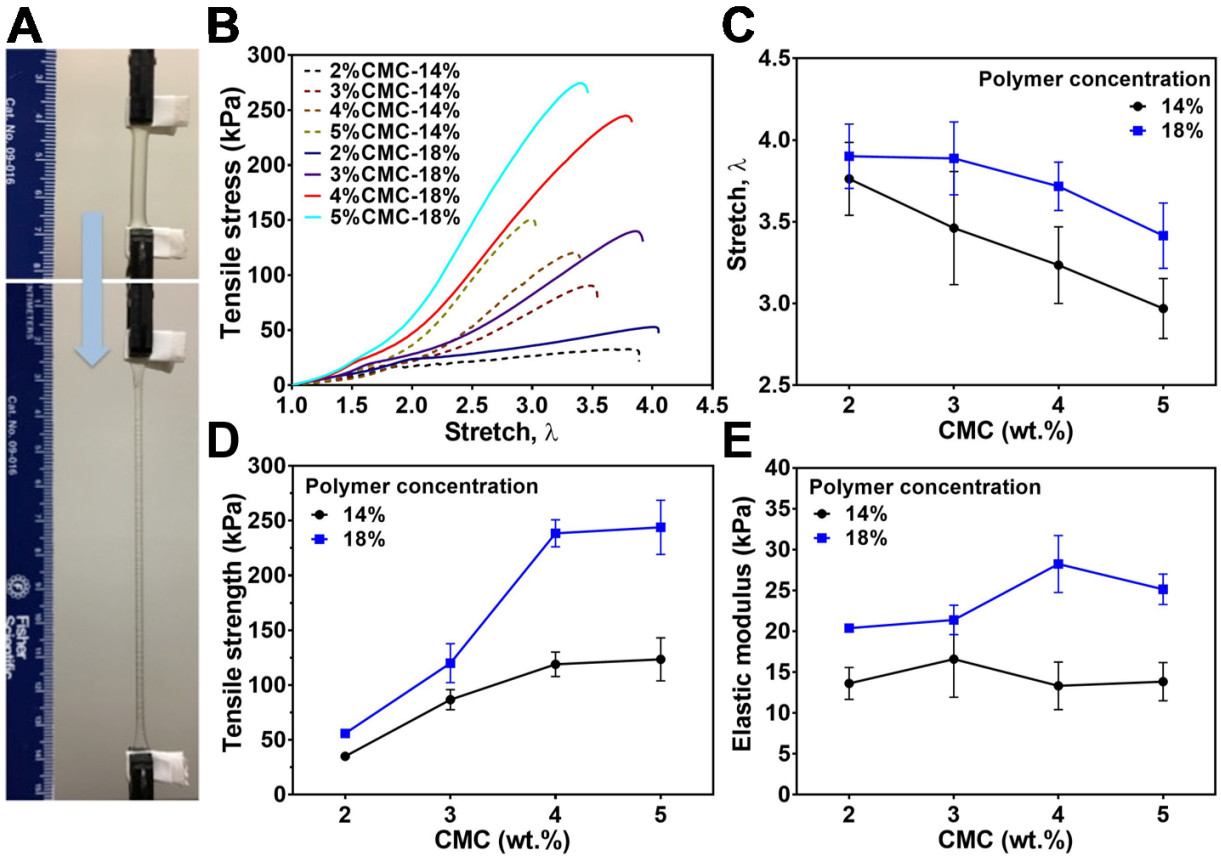

Figure 5-3. The effect of composition on tensile behavior of the CMC/DACNC/PAAm hybrid hydrogel. (A) A strip of hydrogel was fixed between the two clamps and the stretched hydrogel. (B) Representative tensile stress-stretch curves. (C) Stretch value. Stretch $\lambda = L/L_0 = \text{strain} + 1$, L_0 is the initial length and L is the length of stretched hydrogel, (D) Strength value. (E) Elastic moduli of hydrogels with various CMC content and polymer concentration. Each test was conducted by pulling the sample to rupture. (Values in Figures C, D, and E are Mean ± SD, $n \geq 5$). The CMC/DACNC/PAAm hybrid hydrogel was prepared by mixing 10 g CMC and AAm mixed solution, with MBAA, APS, TEMED and 1 g 4 wt.% DACNC suspension.

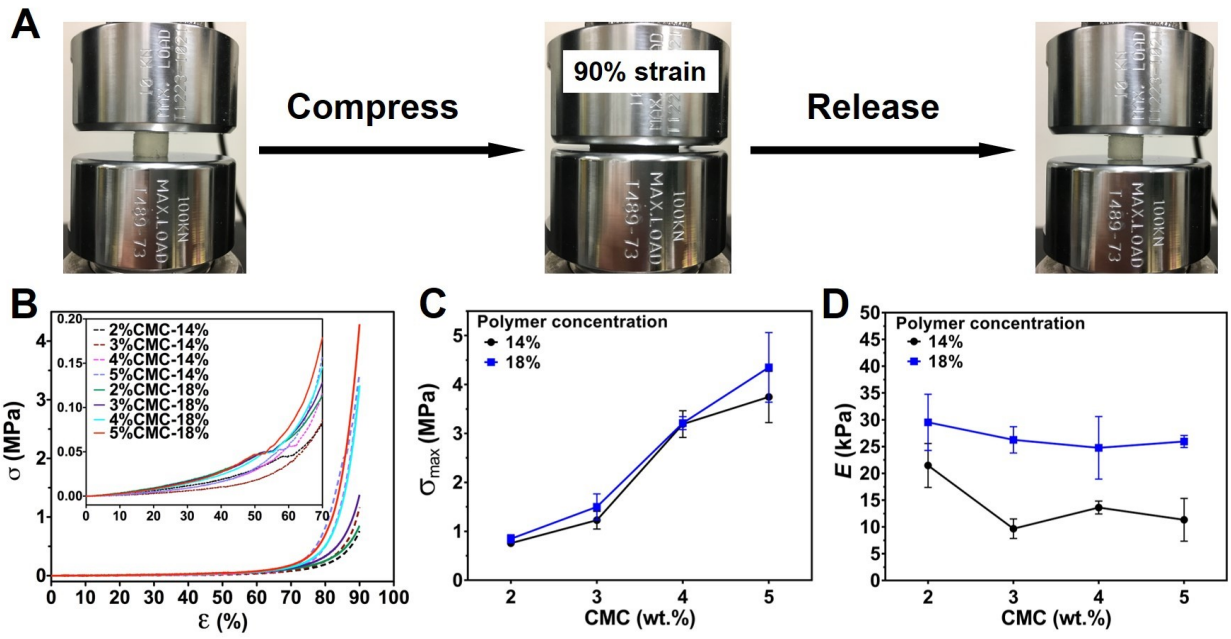

Figure 5-4. The effect of composition on compressive behavior of the CMC/DACNC/PAAm hybrid hydrogel. (A) Unconfined compressive test process of 4% CMC-18%-4% DACNC hybrid hydrogel. (B) Representative unconfined compression stress-strain curves. (C) Maximum compressive stress (σ_{max}), and (D) compressive modulus (*E*). The hybrid hydrogel was prepared by mixing 10 g CMC and AAm mixed solution, with MBAA, APS, TEMED, and 1 g 4 wt.% DACNC suspension. The hydrogel could return to its original shape after undergoing a compressive strain of 90% and relaxation.

In addition to the tensile properties, the CMC/DACNC/PAAm hybrid hydrogels also exhibited fantastic compression properties. The hybrid hydrogel did not fracture even when the compressive strain reached 90% (**Figure 5-4**A) and the test was stopped at 90% compressive strain in order to protect the machine. Results showed that the hybrid hydrogel could immediately recovered its original shape even if it was repeatedly compressed 50 times, suggesting that the hybrid hydrogel had good fatigue resistance. **Figure 5-4**B shows the typical compressive stress-strain curves of the

hybrid hydrogels. All samples did not break when the compressive strain reached up to 90%, so we defined the compressive stress at compressive strain 90% as the maximum compressive stress. The compressive stress and modulus of the hybrid hydrogels were summarized in **Figure 5-4**C and **Figure 5-4**D, respectively. The compressive stress of all samples slightly increased with increasing compressive strain until about 70%, but above this point, the compressive stress increased sharply. At the same total polymer concentration, the compressive stress (σ_{max}) at ε=90% increased with CMC%, whereas the modulus (*E*) decreased with CMC%. When CMC% was kept the same, σ_{max} and *E* of the hybrid hydrogels enhanced when the polymer concentration increased from 14% to 18%. The σ_{max} and *E* of hybrid hydrogel with 5% CMC and 18% total polymer were up to 4.4 ± 0.7 MPa and 25.9 ± 1.1 kPa, respectively. However, the 5% CMC solution was too viscous to handle. The gelation time of CMC/DACNC/PAAm hybrid hydrogel with 5% CMC and 18% total polymer concentration was too short to mix homogeneously. Based on the above tensile and compression results and ease of operation, the hybrid hydrogels with 4% CMC and 18% total polymer were selected for further tests.

The content of DACNC in the hybrid hydrogels may impact the mechanical properties of the hybrid hydrogels as it serves as both cross-linker and reinforcing reagent. Therefore, the hybrid hydrogels were prepared with DACNC of different concentration (2, 4, 6, 8%). With increasing DACNC from 2% to 8%, the tensile strength and elastic modulus gradually enhanced, while the stretch reached peak at 4%. At DACNC concentration of 8%, the maximum tensile strength (336.6 ± 49.9 kPa) and elastic modulus (80.7 ± 4.9 kPa) were obtained (**Figure 5-5**A-B), which were much higher than those of classic alginate/polyacrylamide DN hydrogels.[157] At the compressive stress of 90%, σ_{max} increased with the increasing concentration of DACNC, and reached 7.95 ± 0.69 MPa at 8% DACNC concentration (**Figure 5-5**C-D), which was comparable to the highly

mechanical agar/polyacrylamide DN hydrogels reported by Zheng's group (5 MPa compressive stress at 90% compressive strain).[264] The compressive modulus reached a plateau at 6% DACNC concentration.

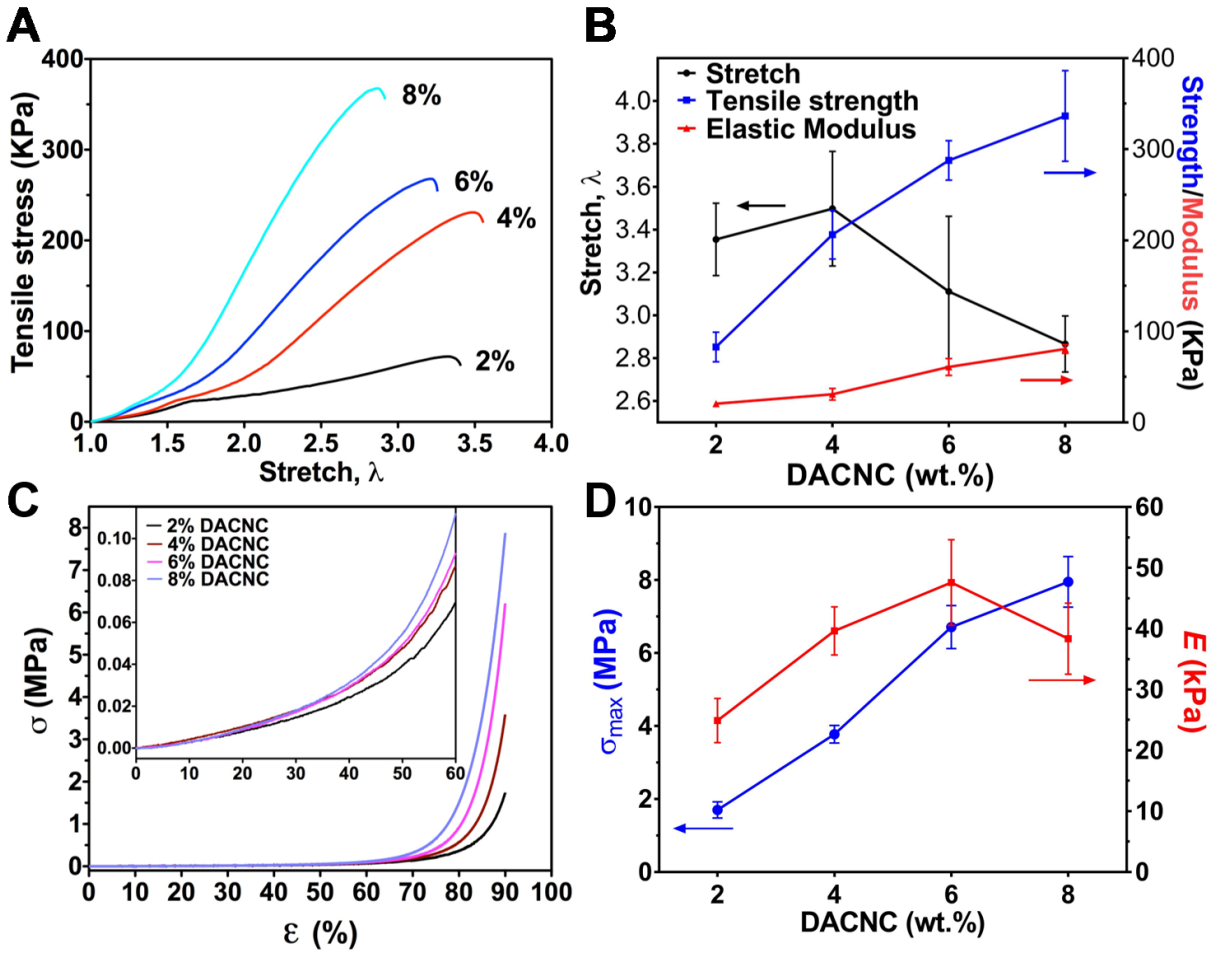

Figure 5-5. The effect of concentration of the nanocrosslinker DACNC on mechanical behaviors of the CMC/DACNC/PAAm hybrid hydrogel. (A) Representative tensile stress-stretch curves. (B) Stress, moduli, and stretch value. (C) Representative unconfined compression stress-strain curves. (D) Maximum compressive stress (σ max) and modulus (*E*). The CMC/DACNC/PAAm hybrid hydrogel was prepared by mixing 10 g CMC and AAm solution, with MBAA, APS, TEMED, and 1 g 4 wt.% (or 2, 6, 8 wt.%) DACNC suspension.

5.3.3 Hysteresis of the CMC/DACNC/PAAm hybrid hydrogel

Loading-unloading tensile tests with varying stretch ratios were conducted to assess the mechanical properties of the CMC/DACNCN/PAAm hybrid hydrogel by investigating the capability of energy dissipation. **Figure 5-6**A shows the typical loading-unloading curves of the CMC/DACNC/PAAm hybrid hydrogels at varying stretch ratios (λ = 2, 2.5, 3, 3.5), which exhibited an evident hysteresis loop and relatively small permanent deformation in every loading-unloading curve, revealing that the hybrid hydrogels could dissipate energy effectively. The dissipated energy per unit volume equals to the area between the loading and unloading curves of a hydrogel.[157] In addition, a more pronounced hysteresis was observed when the hybrid hydrogel was stretched to a larger ratio, which suggested that the energy dissipation increased with higher stretch ratio. As the stretch increased, the dynamic and reversible Schiff based linkages broke progressively and served as the sacrificial bonds to dissipate energy, while the covalent cross-linked PAAm network remained intact to stabilize the integral structure of the hybrid hydrogel,[157] so the CMC/DACNC/PAAm hybrid hydrogel exhibited obvious hysteresis and litter permanent deformation.

In the consecutive compressive tests (**Figure 5-6**B, C, and D), when the hybrid hydrogel was compressed by 70%, the hydrogel restored the initial strength and exhibited overlapping hysteresis loops under 10 cycles of the successive compressive loading-unloading tests. This complete recovery feature demonstrates that the covalent PAAm network has survived by reversibly breaking and reforming sacrificial bonds. However, the area of the hysteresis loop increased with higher compressive stain (85% and 90%), which implies that more energy was dissipated, mainly due to the cleavage of Schiff-base linkages between the CMC and DACNC. When the compressive strain increased to 85% and 90%, the hysteresis loop of the second cycle was smaller than that of

the first cycle, and the remaining cycles overlapped with the second cycle. This indicates that both the first and second networks are broken, because the covalent bonds in PAAm network may fracture and could not be reformed under ambient conditions.

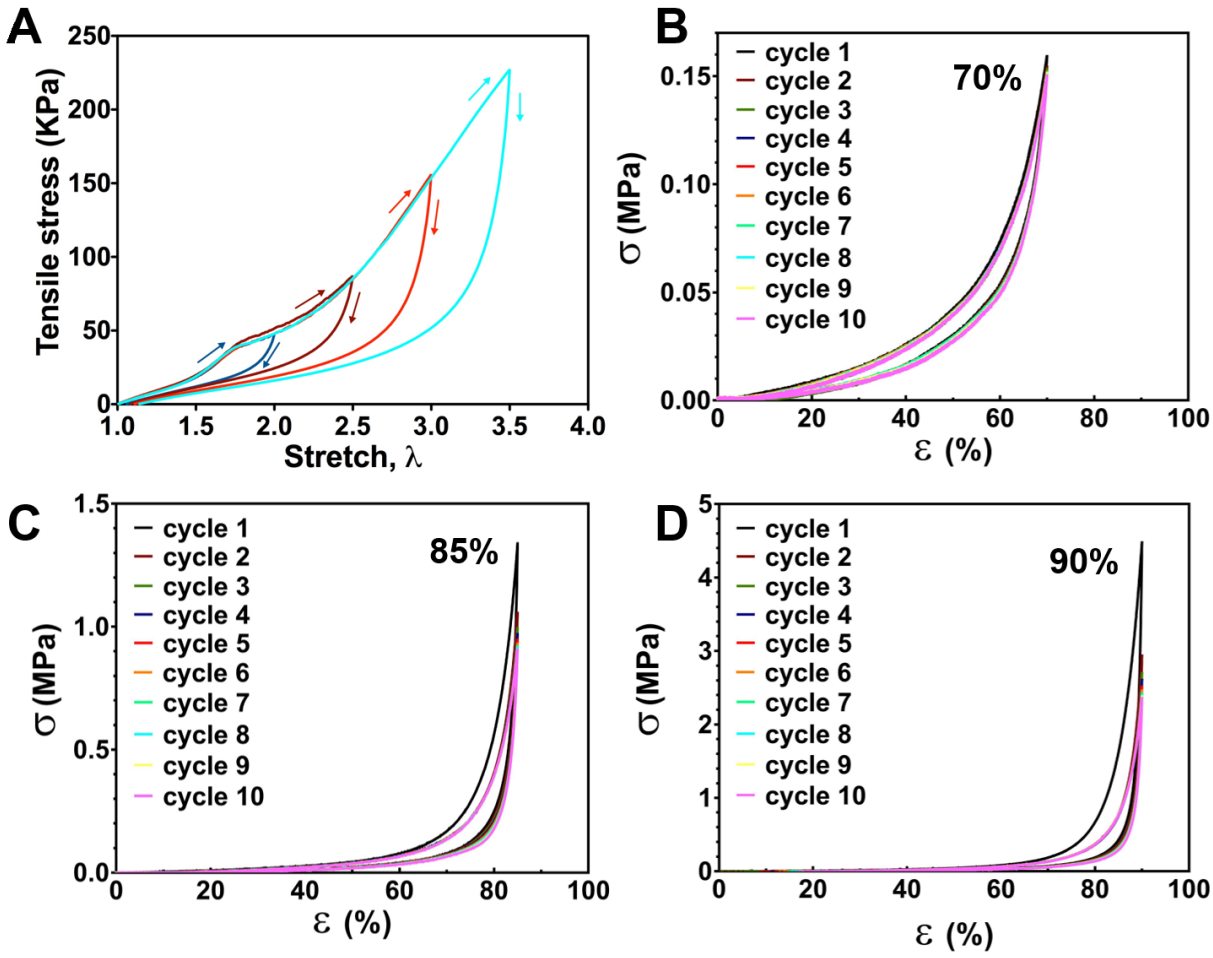

Figure 5-6. Cyclic tensile and compressive performance of 4% CMC-18%-4% DACNC hybrid hydrogel. (A) Samples of the hybrid hydrogel are subjected to a cycle of loading-unloading tensile test of varying maximum stretch (λ = 2, 2.5, 3, or 3.5) that is lower than the yielding strain of the hybrid hydrogel. Typical successive loading-unloading compression tests for 10 times at (B) 70% strain, (C) 85% strain, and (D) 90% strain.

5.3.4 Self-healing and self-recovery performances

The tough hydrogels with recoverability are promising for biomedical applications. The poor long-term mechanical stability of hydrogels employed for cell encapsulation results in unintended cell release and death,[8, 164] and a desirable engineered skeletal muscle tissue is expected to have adequate mechanical durability.[282-283] Considering that the CMC/DACNC network in the hybrid hydrogel was crosslinked via dynamic Schiff-base linkages, the self-healing behaviors of the hybrid hydrogel were investigated. The hydrogels were completely divided into two parts, and the self-healing was evaluated through macroscopic self-healing test by direct visual inspection and microscopic observation. The rod-liked hybrid hydrogels (one was stained with rhodamine B for better observation) were cut into half to expose fresh interfaces, and then the two fresh interfaces were brought together immediately (**Figure 5-7**A). The hydrogels were stored in a desiccator with saturated KCl solution to prevent water in hydrogel from evaporation. After 24 h at ambient temperature without any external stimuli, the combined hydrogel was healed to a whole piece and could sustain stretch. **Figure 5-7**B shows the optical microscope photos recording the self-healing process of the incision created by a scalpel. It was observed that the notch on the hydrogel could automatically heal within 2 h at ambient temperature without any external stimuli. Although the combined hydrogels could recover the macroscopic structure integrity, they couldn't completely restore the mechanical strength. The self-healing efficiency was about 8% after 24 h at room temperature, and it did not increase with longer time (**Figure 5-7**C), which was similar to the previous reports on double network (DN) hydrogel containing PAAm network. For example, κ-carrageenan/polyacrylamide DN hydrogels only recover almost 12% of its original stress after fracture even when the broken hydrogels were incubated in a bath of 90 ℃.[267] It was assumed that the healing process was due to the dynamic cleavage and regeneration of the reversible Schiff-

base linkages, but the broken covalently cross-linked polyacrylamide network in the hybrid hydrogel can't be regenerated.

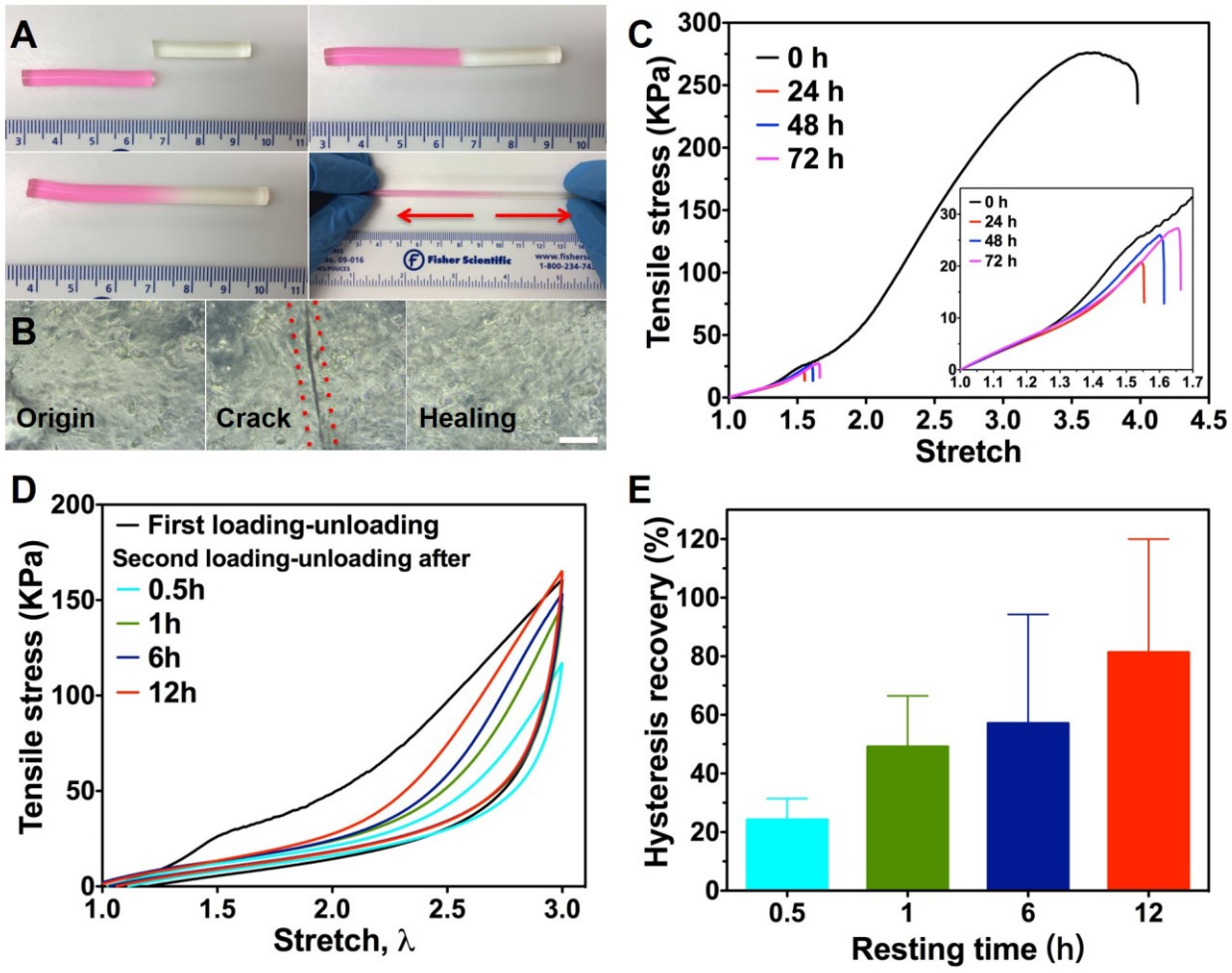

Figure 5-7. Self-healing performance of 4% CMC-18%-4% DACNC hybrid hydrogel: (A) Photographs of self-healing process. (B) Microscopic images of the self-healing process. (C) Tensile stress-strain curves of the original and healed hydrogels at various healing time. Scale bar: 500 μm. (D) Recovery of samples stored at room temperature for different durations of time: typical cyclic loading-unloading tensile test curve. (E) Recovery rate for the hydrogel after resting for 0.5, 1, 6, and 12 h at room temperature.

The CMC/DACNC/PAAm hybrid hydrogel couldn't completely self-heal when it was split to two parts, but it could recover small damage when the hydrogel was partially deformed. Therefore, we further conducted the loading-unloading tests to investigate the self-recovery properties of the hybrid hydrogels at room temperature without any external stimuli. The self-recovery properties of the CMC-DACNC/PAAm hybrid hydrogels were evaluated when the applied strain is lower than the yielding strain (λ_{max}). The ability of the CMC/DACNC/PAAm hybrid hydrogel to recover the initial dissipated energy was assessed by firstly stretching to a ratio of 3, and then the force was released to zero. Afterwards, the hybrid hydrogel samples were sealed into plastic bags to prevent water evaporation and stored at room temperature for a certain time, followed by a second loading-unloading test. As shown in **Figure 5-7**D-E, the area enclosed by the loading-unloading curves is defined as the dissipated energy of the cycle. The hybrid hydrogel in the second measurement after 0.5, 1, 6, 12 h could recover 24.2, 49.1, 71.4, and 81.3% in dissipated energy at $\lambda = 3$ and the recovery rate of the hybrid hydrogels increased with the longer resting time. An Alginate/PAAm hybrid hydrogel could only recover 74% at 80 ℃ after 1 day.[157] When the hybrid hydrogel was stretched, part of Schiff-base linkages were cleaved and energy was dissipated. Because of the dynamic and reversible nature of the Schiff-base linkages in the hybrid hydrogels, these bonds can be re-formed once the external load is removed, partially recovering the original mechanical properties. With longer resting time, more Schiff-base linkages could be re-established, which resulted in higher dissipated energy recovery rate of the hybrid hydrogels. Since only the reversible Schiff-base linkages were broken, they could quickly reform at room temperature even without any external stimuli, leading to the self-recovery of the internal damage of hydrogel network.

5.3.5 Toughening mechanisms of CMC/DACNC/PAAm hybrid hydrogel

The mechanical properties of the optimized CMC/DACNC/PAAm hybrid hydrogels with 4% CMC, 18% total polymer and 4% DACNC were compared with the CMC/DACNC hydrogels and PAAm hydrogels (**Figure 5-8**) to investigate the toughening mechanism of the CMC/DACNC/PAAm hybrid hydrogels. The percentage of CMC, DACNC and AAm in these hydrogels was kept the same as those in the CMC/DACNC/PAAm hybrid hydrogels. The CMC/DACNC hydrogel was too weak to be fixed by the clamps for tensile test. The tensile stress and stretch at rupture were 206.32 ± 26.93 kPa and 3.50 ± 0.27 for the CMC/DACNC/PAAm hybrid hydrogel, and 65.27 ± 9.58 kPa and 9.04 ± 0.96 for the PAAm hydrogel (**Figure 5-8**A, B, and C). The tensile stress of the hybrid hydrogel was almost three times that of PAAm hydrogel. Meanwhile, the CMC/DACNC hydrogel broke at a strain of 67.94 ± 3.64% with a compressive stress of 0.10 ± 0.02 MPa. The PAAm hydrogel exhibited a compressive stress of 0.70 ± 0.04 MPa when it was compressed by 90%. However, the CMC/DACNC/PAAm hybrid hydrogel possessed a compressive stress of 3.77 ± 0.24 MPa at the strain of 90% (**Figure 5-8**D, E, and F), which was 36 times and 5 times higher than those of the CMC/DACNC hydrogel and the PAAm hydrogel, respectively. In addition, the PAAm single hydrogel didn't recover its original shape after the force was released (**Figure 5-8**G, H, and I). These results suggested that the hybrid hydrogels were generated not only from a simple interpenetration of the CMC/DACNC hydrogel network and the PAAm hydrogel network, but also through a possible synergistic interaction of two networks, including entanglements of the polymers and covalent crosslinks formed between PAAm and DACNC and CMC (e.g. hydrogen bonds). As the rigid DACNC with large specific surface area and aspect ratio functions as both reinforcing filler and cross-linkers in the hybrid hydrogel network, its incorporation improved the hydrogel mechanical properties and self-healing capacity

of the first network crosslinked by the reversible Schiff-base linkages. Those results explained why the CMC/DACNC/PAAm hybrid hydrogels showed extraordinary mechanical properties. Moreover, the self-healing ability of the first network cross-linked by reversible Schiff-base linkages could improve fatigue resistance and self-recoverable property of the hybrid hydrogel. Small damage zones formed in the first network could accumulate to large damage, and macroscopic crack propagation can be produced.[264] The self-healing ability of the first network is beneficial to recovering the small damage zones and stopping the damage accumulation. After the Schiff-base linkages break, they can quickly reform between CMC and DACNC at room temperature even without any external stimuli, leading to the self-healing of the first network and repair of the internal damage of hydrogel network, thereby improving the mechanical properties and durability of hydrogel.

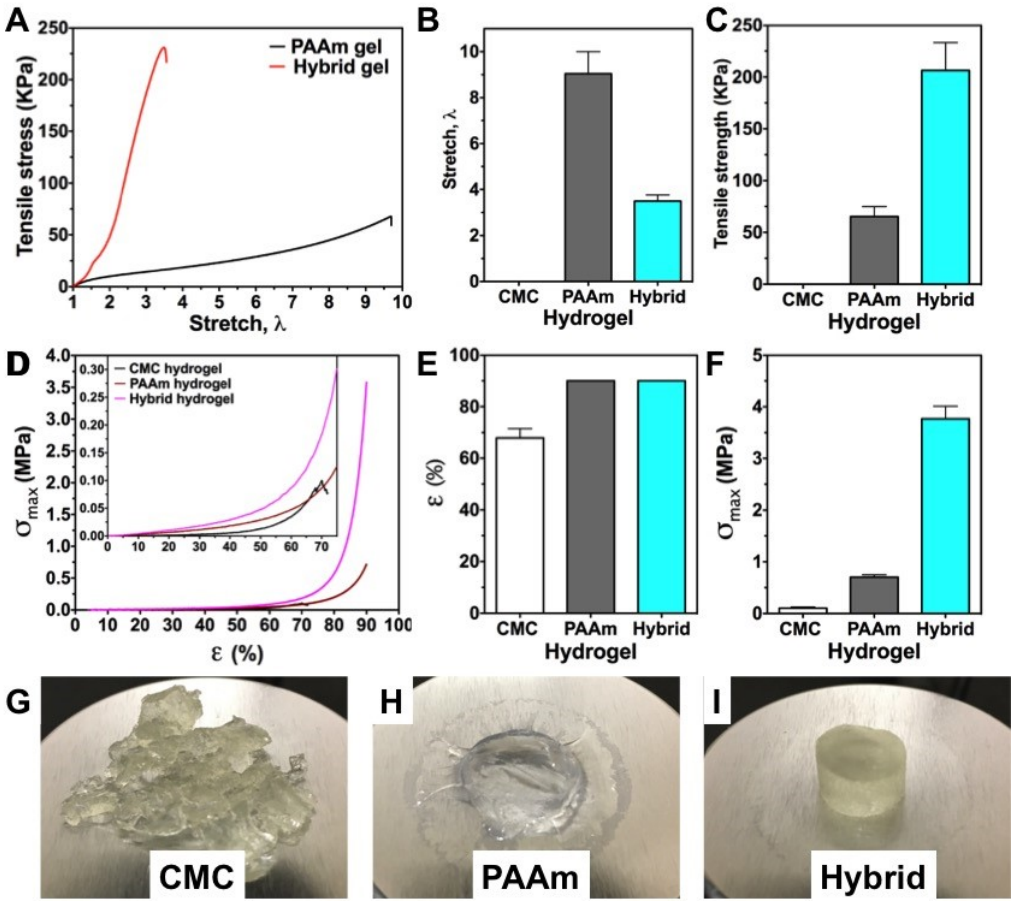

Figure 5-8. Mechanical behaviors of single and hybrid hydrogel: (A) Representative tensile stress-stretch curves. (B) Stretch value. (C) Tensile strength. CMC/DACNC single hydrogels are too mechanically weak to be fixed by the clamps for tensile test. (D) Representative compressive stress-strain curves. (E) Compressive strain until rupture or 90% strain. (F) Maximum compressive stress of the CMC/DACNC hydrogel, PAAm hydrogel, and CMC/DACNC/PAAm hybrid hydrogel. Hydrogel status after compression: (G) CMC/DACNC hydrogel, (H) PAAm hydrogel, (I) Hybrid hydrogel. 4%CMC-18%-4% DACNC hybrid hydrogel was tested as a representative hydrogel of the CMC/DACNC/PAAm hybrid hydrogel. For the CMC/DACNC single hydrogel and the PAAm single hydrogel, the contents of the CMC and acrylamide in the single hydrogel are identical to those in the CMC/DACNC/PAAm hybrid hydrogel.

5.3.6 Swelling behaviors

As shown in **Figure 5-9,** the hybrid hydrogels swelled in the first 24 h and then slowed down and finally reached equilibrium after approximately 120 h, when the swelling ratio reached 1556%, suggesting the swelling behavior of the hybrid hydrogel was in accord with the diffusion mechanism.[236] The DACNCs interacted with CMC and acted as nanofiller that occupy void space in the hybrid hydrogel network, leading to compact hydrogel. The combination of double-network and rigid DACNC in the hybrid hydrogel enabled the hybrid hydrogel to uptake large amounts of water and remain stable shape after equilibrium. The DACNCs occupation of the void space was important against hydrogel dissolution during swelling. This phenomenon was also observed in phosphate buffer. The high swelling ratio and stable shape after equilibrium suggested that the hybrid hydrogels could be applied as long-term drug delivery carrier, for example, loading antibiotic in the CMC/DACNC/PAAm hybrid hydrogel for anti-infection of the total hip arthrophasty.[284]

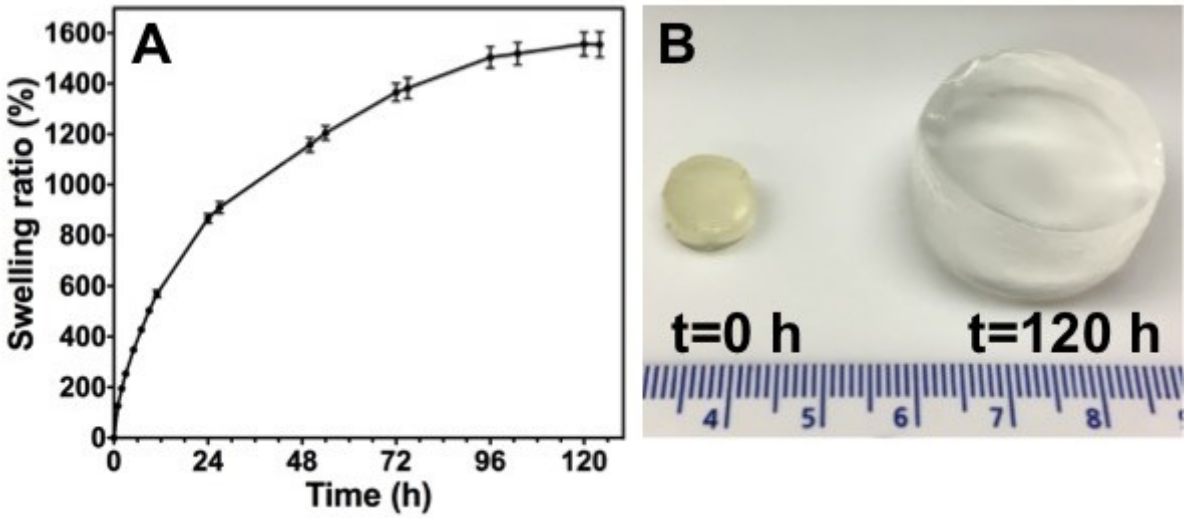

Figure 5-9. (A) Swelling ratio of CMC/DACNC/PAAm hybrid hydrogels that were incubated in distilled water at room temperature until swelling equilibrium. The error bars represent standard deviation (SD). (B) Pictures of the initial hydrogel and swollen hydrogel.

5.3.7 Cytocompatibility

There are different culturing methods to evaluate the *in vitro* cytotoxicity of biomaterials,[285] including direct contact, indirect contact and extract tests. The extract test evaluates the cytotoxicity of any leachable agents from the materials. In this study, *in vitro* cell viability of the extracted media leached from the hybrid hydrogels was evaluated by the MTT method using human primary dermal fibroblasts. The effect of the concentration of hydrogel extract and culture time on cell viability are shown in **Figure 5-10**A. All the samples showed cell viability higher than 86%. The cell viability of the hydrogel extract with different concentration for different culture time showed negligible differences. When the concentration of the hydrogel extraction reached up to 100%, which means the hydrogel extract was directly applied for test without dilution, the cell viability remained as high as 86.07 ± 4.64%, 89.26 ± 9.57%, 94.26 ± 4.03% after 1, 2, 3 days of culture, respectively. Usually, a material with cell viability higher than 80% is regarded to be noncytotoxic.[286] Then the fibroblasts were cultured on the hydrogel surface for three days. **Figure 5-10**B exhibits that the fibroblasts could grow well and spread on the surface of the hydrogel. These results suggest that the CMC/DACNC/PAAm hybrid hydrogel is relatively safe and could be potentially used for biomedical applications.

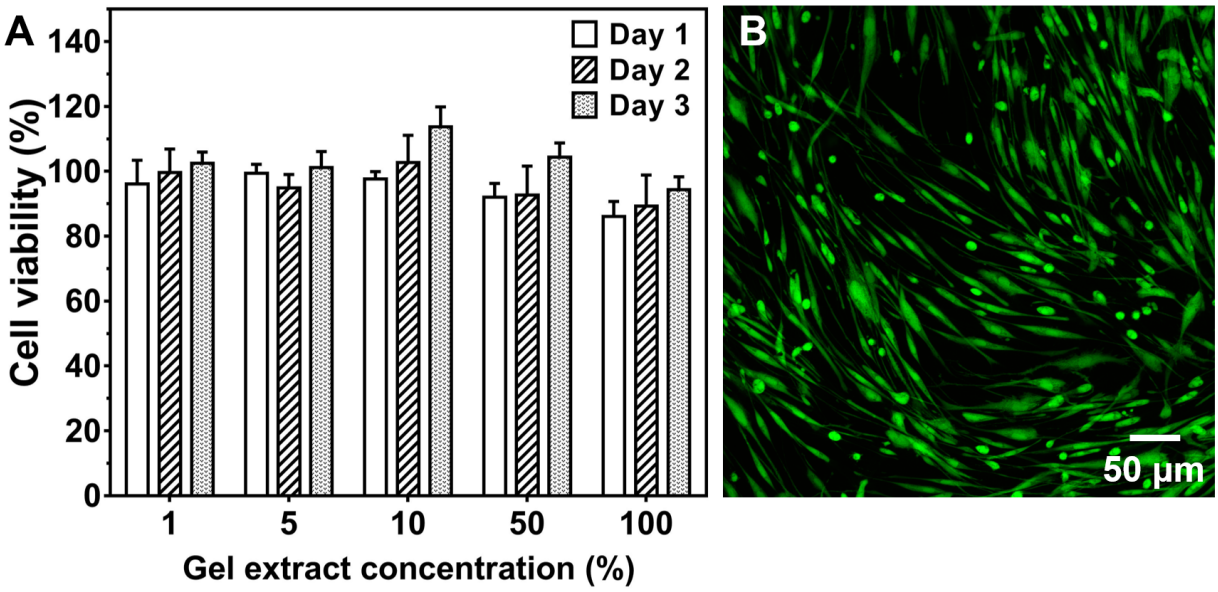

Figure 5-10. Cytotoxicity test of the CMC/DACNC/PAAm hybrid hydrogel: (A) Cell viability of hydrogel on day 1, day 2, and day 3. (B) Confocal fluorescent microscopy images of human primary dermal fibroblast cultured on the surface of hydrogel for three days.

5.4 Conclusion

This study introduces a biocompatible hydrogel that combines excellent mechanical properties and good self-recovery at room temperature without any external stimuli, which is important for fatigue resistance and extending its service life. A self-healing nanocomposite network collaborates with a chemically cross-linked elastic network to form a double-network hydrogel. The incorporation of rod-like rigid DACNC further strengthens the hydrogel, and DACNCs act as reinforcing agent and multifunctional cross-linker in the hybrid hydrogel network. The optimal hydrogel possesses high tensile strength (*ca.* 250 kPa), large elongation (> 4 times), ultrahigh compression strength (*ca.* 8 MPa), and good self-recovery (12 h at room temperature restore to 81.3%). Moreover, the CMC/DACNC/PAAm hybrid hydrogels exhibit good biocompatibility. The combination of great mechanical properties, self-recoverability and biocompatibility, along with a facile method of synthesis, empowers the hybrid hydrogel an ideal candidate for further biomedical applications, such as hydrogel contact lenses, and artificial cartilage.

Chapter 6

Mussel-Inspired Tissue-Adhesive, Moldable, and Self-Healing Nanocomposite Hydrogels

6.1 Introduction

Tissue adhesives are becoming increasingly popular in medical applications, such as sealing surgical incision, filling the wound cavity, and stopping bleeding, due to their fascinating features, including facile manipulation, less traumatic closure, no suture removal, less pain, and satisfying cosmetic result. The current commercial medical glues, such as synthetic glue cyanoacrylate and natural protein fibrin, have been widely applied in various surgical procedures. However the degradation products of cyanoacrylate are toxic,[173, 287] and fibrin exhibits poor adhesion to tissues in the presence of body fluid.[45, 288] Since most of cross-linked hydrogels containing a large amount of water do not exhibit strong adhesive strength to wet tissue surface, synthesis of adhesive materials with good biocompatibility and high wet adhesive strength remains a challenge.

Recently, mussel-inspired tissue adhesives have been developed as promising candidates due to their remarkable wet adhesion ability and biocompatible nature. Mussels can strongly attach to various surfaces under saline environment by mussel byssal.[289-290] The major functional components accounting for remarkable underwater adhesion are mussel foot proteins composed of catecholic amine acids, which can undergo oxidation and form effective adhesion interactions with solid substrates via a wide range of physical and chemical interactions.[22, 42] In particular, catechol group has high binding affinity to amine, thiol, and imidazole groups in tissue via strong covalent and noncovalent bonds formed through reactions such as Michael addition and Schiff-base formation.[24] Catechol conjugated polymers have significant potential in biomedical applications as tissue adhesives, but they are rarely employed to prepare self-healing hydrogels.

Self-healing hydrogels are promising biomaterials because they can autonomously repair physical damage and restore function, which prolongs their lifetime and cuts maintenance costs.[291]Self-healing hydrogels can be injected to irregular and deep wound beds through needle with very narrow gauge, followed by recovery to an integrated hydrogel at target sites.[89, 110] However, classic self-healing hydrogels usually lack tissue adhesive capacity, thus can move around the target area triggered by tissue and cell actions, causing in inflammation or damage to surrounding tissues.[8] Traditional tissue adhesives without self-healing ability normally adhere to the top surface of tissues. They are not capable of fully matching the wound contour that can be deep and irregularly shaped. Thus, the traditional tissue adhesives are not adequate as healing materials for deep wounds. For example, internal hemorrhaging is a leading cause of death after traumatic injury, the traditional adhesives cannot be used for incompressible wounds.[292] Combining the adhesion with self-healing capacity allows the hydrogel to be highly preferable as tissue adhesives due to their easy application and their viscoelastic nature resembling extracellular matrices. Adhesive self-healing hydrogels could be injected to wound beds to fully fill deep and irregular wounds and adhere to the tissues quickly with sufficient stability.

Hydrogels made out of natural renewable polymers are growing in popularity for their environmental friendliness, biodegradability, and biocompatibility.[186, 293] Among these bio-renewable polymers, cellulose and chitosan are the two most abundant organic polysaccharides on earth, and have been widely applied in biomedical fields ranging from wound healing to drug delivery and tissue engineering.[294-295] Chitosan is a naturally occurring polysaccharide derived from chitin and it has found wide biomedical applications, as it exhibits favorable properties of biocompatibility, biodegradability, tissue adhesion, hemostatic activity, anti-infection and antibacterial activities.[296-297] The primary amine groups endow chitosan with tissue adhesion, but

the tissue adhesion ability of cationic chitosan-based hydrogels is weak and short-lasting, because the electrostatic interactions and hydrogen bonds between chitosan and tissue surfaces are reversible.[45, 298] One of the most critical drawbacks regarding the use of chitosan as a functional biomaterial is its poor solubility in neutral aqueous solution. To address this issue, the Lee group reported that catechol-conjugated chitosan with low catechol substitution degree was soluble in acidic, neutral, and basic solutions.[45, 47] Moreover, amine groups and catechol groups have synergistic effects on adhesion, which is similar to mussel foot proteins composed of abundant positively charged amino acid residues and catechol motif.[46] Catechol-conjugated chitosan exhibits excellent solubility in neutral pH solutions and strong adhesiveness to the wet surface of tissue. Despite good adhesive strength of catechol-based adhesives, the use of chemical oxidants as cross-linkers like $FeCl_3$, $NaIO_4$, H_2O_2, or base buffer impairs the biocompatibility of the adhesives, and the long polymerization time hinders their practical applications, especially for use as an internal tissue adhesive.[299] Besides, the intermolecular crosslinking occurs at the expense of reducing adhesive strength, because they compete for catechol groups and amine groups. In this context, Ryu et al constructed a thermally sensitive tissue adhesive by crosslinking catechol-functionalized chitosan with thiol-terminated Pluronic F-127.[45] Nevertheless, the catechol-conjugate chitosan/Pluronic F-127 hydrogel could not be injected in a gel state.

Derived from cellulose, cellulose nanocrystals (CNCs) have rod-like shapes, which range between 0.1-3 μm in length and 3-70 nm in width.[273] CNCs have been widely entrapped within hydrogel matrices to improve its mechanical properties. It has been reported that incorporating CNCs into polymer matrix through the covalent bonding significantly improves the mechanical properties compared to simply adding the pristine CNCs as nanofillers.[16, 26, 240, 300-301] CNCs with surface modifications act as both reinforcing fillers and cross-linkers to improve the hydrogel. Aldehyde

modified CNCs crosslink with amines-rich polymers to form dynamic hydrogel network rapidly at room temperature because of the formation of reversible Schiff-base linkages between aldehyde groups and amine groups.

In this study, we crosslinked a catechol-conjugated chitosan (CHI-C) self-healing hydrogel using aldehyde modified cellulose nanocrystal (DACNC). Gelation occurred quickly at room temperature through dynamic Schiff-base linkages between amine groups from CHI-C and aldehyde groups from DACNC. The use of DACNC as crosslinker instead of oxidized catechols allowed for full exploitation of the bio-adhesive properties of catechol groups, as shown by the high adhesive strength evaluated by porcine skin lap shear tests. The enhanced mechanical strength of hydrogels was measured by rheological tests. In addition, the self-healing, injectable, and moldable behaviors were investigated by macroscopic observation.

6.2 Experimental section

6.2.1 Materials

Chitosan powder (Mw: 2.3×10^5 Da, degree of deacetylation: 87 %) was purchased from Zhejiang Golden-Shell Pharmaceutical Co., Ltd. (Zhejiang, China). Hydrocaffeic acid (HCA, 3-(3,4-Dihydroxyphenyl) propionic acid, 98+%) was purchased from Alfa Aesar (Ward Hill, MA, USA). 1-(3-Dimethylaminopropyl)-3-ethylcarbodiimide hydrochloride (EDC, 98+%) was purchased from Acros Organics (NJ, USA). *N*-Hydroxysuccinimide (NHS, 98%) was purchased from Sigma-Aldrich (St-Louis, USA). Spruce cellulose (bleached kraft pulp, M_w= 4.10×10^5 g mol^{-1}) with α-cellulose content of 87.3 % was kindly provided by Alberta Pacific Forest Industries Inc. (AB, Canada). All chemicals were of analytical grade.

6.2.2 Synthesis and characterizations of CHI-C

Catechol moieties were conjugated onto the chitosan backbone using EDC/NHS coupling reaction. The catechol-conjugated chitosan (CHI-C) was synthesized as previously reported with slight modification.[45, 47, 302] Briefly, chitosan (504.2 mg, 3 mmol amines) was hydrated in 5 mL 1 mol/L HCl solution, followed by slowly adding deionized (DI) water and adjusting pH to 5.0 with 6 mol/L NaOH solution. The final concentration of the chitosan solution was 1 wt.%. Afterwards, HCA (546.5 mg, 3 mmol) dissolved in 5 mL DI water was added into the chitosan solution. EDC (575.1 mg, 3 mmol) and NHS (345.3 mg, 3 mmol) were dissolved in 50 mL ethanol and DI water solution (1:1, v/v), and then the solution was added dropwise to the chitosan/HCA solution. The reaction mixture was stirred vigorously at room temperature for 10 h and its pH value was maintained at 5.0. To remove the unreacted residues, the crude CHI-C solution was dialyzed against acidified deionized water containing 10 mM NaCl for two days to inhibit oxidation of catechol groups and then deionized water for half day to neutralize the solution. The resulting solution was freeze-dried to obtain CHI-C powder, which was stored in a moisture-free desiccator placed in a refrigerator (4 °C) before use. The final CHI-C product was a pale yellow fluffy powder. To synthesize CHI-C with different degrees of catechol conjugation, the same procedure was repeated with varying molar ratio of amine/HCA/EDC/NHS of 1:2:1:1 and 1:2:2:2. The chemical structure of CHI-C was analyzed by FT-IR and ^{1}H NMR. The amount of catechol groups in CHI-C was quantified by ultraviolet (UV)-vis spectrometer (SpectraMax, Molecular Devices, USA), measuring absorbance at 280 nm. Serially diluted solution of HCA (10, 20, 25, 40, 50 μg/mL) was used to obtain a calibration curve to determine the degree of catechol conjugation. According to the molar ratio of materials, the products were denoted as CHI-C1, CHI-C2, and CHI-C3,

respectively, and their catechol content in percentage and mmol catechol per gram CHI-C are listed in **Table 6-1**.

Table 6-1. The conditions applied for synthesizing various CHI-C and their corresponding catechol content.

Polymer	Molar ratio of amine: HCA: EDC: NHS	DOC* (%)	mmol Catechol/g CHI-C
CHI-C1	1:1:1:1	8.08	0.4436
CHI-C2	1:2:1:1	8.95	0.4913
CHI-C3	1:2:2:2	11.28	0.6197

*DOC means degree of catechol conjugation of CHI-C.

6.2.3 Synthesis of DACNC

The synthesis and characterization of dialdehyde cellulose nanocrystal (DACNC) was carried out according to our previous work (Chapter 4 in this thesis).[140] Briefly, wood cellulose fibers (10.0 g) were hydrolyzed with sulfuric acid (100 mL, 65 wt.%) at 45 ℃ for 1 h under continuous stirring. The hydrolysate was washed and centrifuged (10 000 g, 20 min) until the supernatant became turbid, followed by dialyzing (3.5 kDa MWCO) until the pH value of the CNC suspension increased to 3. The resulting CNC suspension was diluted to 333 g and ultrasonicated (10 min, ice-water bath) prior to periodate oxidation. A total of 3.33 g $NaIO_4$ was added into the above CNC suspension. The reaction container was covered by aluminum foil to protect from light. The mixture was stirred for 48 h at room temperature (22 ℃) before ethylene glycol (5 mL) was added quickly to quench the reaction. Finally, the oxidized product was dialyzed and lyophilized to obtain dialdehyde oxidized CNC (DACNC) and the DACNC powder was stored at 4 ℃ for further use. The aldehyde content of DACNC was 1.42 mmol/g, which was determined by elemental analyzer after oxime reaction.

6.2.4 Preparation of hydrogel

To prepare the CHI-C/DACNC hydrogel, CHI-C (300 mg) was dissolved in DI water (10 mL) to get a 3% CHI-C solution. DACNC (300 mg) powder was dispersed in DI water (10 mL) and heated at 80 ℃ for 4 h, followed by ultrasonicating to obtain 3% DACNC suspension.[224] A series of hydrogel with varying formulas were prepared by homogeneously mixing CHI-C solution and DACNC suspension. Gelation occurred quickly upon mixing and hydrogel formation was confirmed via the tilting method. The vials were inverted and the samples that did not flow were regarded as gel.[15] Nanocomposite hydrogel with different formulas was coded as CHI-Cx/DACNC-a/b, where x and a/b mean the type of CHI-C, volume ratio of CHI-C solution to DACNC suspension, respectively.

6.2.5 Characterizations

Fourier transform infrared (FT-IR) spectra of chitosan powder, CHI-C1 powder, CHI-C2 powder, CHI-C3 powder, and dried CHI-C/DACNC hydrogel were recorded using KBr disks on a Nicolet 6700 spectrophotometer (Thermo Fisher Scientific Inc., Waltham, MA). The scans were carried out in the spectral range varying from 800 cm^{-1} to 4000 cm^{-1} with a resolution of 4 cm^{-1}. Proton nuclear magnetic resonance (^1H NMR) spectra of the chitosan (100 mg/mL in 2% DCl/D_2O), CHI-C1, CHI-C2, and CHI-C3 (100 mg/mL in D_2O) were recorded on an Agilent/Varian 400 MHz spectrometer. Stock solutions of CHI-C1, CHI-C2, CHI-C3 (2 mg/mL) and chitosan (10 mg/mL in 0.1M HCl) were prepared and diluted to 0.4 mg/mL with their corresponding solvent. The absorbance of chitosan, CHI-C1, CHI-2, and CHI-C3 solution (0.4 mg/mL) were measured from 200 nm to 500 nm using a UV-vis spectrophotometer (SpectraMax, Molecular Devices, USA).

6.2.6 Rheological studies

To understand the viscoelastic properties of the hydrogels, rheological studies were performed on a DHR-3 rheometer (TA Instruments, DE, USA). All the experiments were carried out at 25 ℃ using a 40 mm parallel plate with plate gap of 1.0 mm. The viscoelastic properties of CHI-C/DACNC hydrogel were tested immediately after gelation, but the pure CHI-C hydrogels were tested after 3 days of gelation to allow the autoxidation cross-linking in the CHI-C solution. Frequency sweeps were conducted at oscillation frequencies from 0.1-100 rad s^{-1} under a 1.0% strain level. Strain sweeps had a fixed oscillation frequency of 10 rad s^{-1} and variable applied strain of 1-1000%. To observe the damage–healing properties of the hydrogels, the storage modulus (G') and loss modulus (G'') of the hydrogel were measured by a continuous step change of the strain between high strain (200%, 500%) and 1% with a frequency of 10 rad/s.

6.2.7 Determination of hydrogel adhesion

The wet tissue adhesive properties were evaluated by porcine skin lap shear tests based on previously reported methods.[287, 303] The specimens were tensile tested in an Instron 5967 universal testing machine (Instron Corp., MA, USA) equipped with 50 N load cell under a crosshead speed of 5 mm min^{-1} and a gauge length of 50 mm. Fresh and shaved porcine skin without excess fat was obtained directly from a local market, and was cut into rectangular strips (50 mm long × 10 mm wide × 2 mm thick). Prior to test, the cut porcine skin pieces were washed with saline solution (0.9 wt.% NaCl), and soaked in PBS buffer solution (pH = 7.4) at 4 ℃ overnight to ensure the porcine skin samples remain moisturized. A total of 60 μL of CHI-C and DACNC solution was spread onto two pieces of porcine skin strips surface (1 cm × 1 cm), respectively, followed by addition of $NaIO_4$ solution (10 μL) on the porcine skip strip containing DACNC solution, and the molar ratio of catechol to IO_4^- was adjusted to 1:0 and 1:1. Then the two pieces of porcine skin strips were

immediately pressed together by hand. Following this, the adhered porcine skin pieces were pulled apart by the universal testing machine. The lap-shear adhesion strength (Pa) was calculated by dividing the maximum load (N) by the area of the adhesive overlap (m^2).

6.2.8 Self-healing test

The self-healing performance of the CHI-C/DACNC hydrogel was investigated with both macroscopic and quantitative methods using the CHI-C3/DACNC-1/1 hydrogel as an example. In the macroscopic observation test, two disk-shaped hydrogels (diameter = 10 mm) were prepared and one was stained with methylene blue. Subsequently, the two hydrogels were cut in half. Finally, the two different colored semicircular hydrogels were put together to heal at room temperature without any external stimuli, and pictures were taken to record the self-healing process of the hydrogel. In addition, the rheological analysis of the hydrogel was carried out to monitor quantitatively the self-healing process of the CHI-C/DACNC hydrogel. Elastic response of the hydrogel was analyzed through strain amplitude sweep. Based on the strain amplitude sweep results, the continuous step strain measurements were carried out to study the rheology recovery behavior of the hydrogel.

6.2.9 Injectability and moldability assay

To further observe the capability to be injected after gelation of CHI-C/DACNC hydrogels, the hydrogel was prepared, loaded into a syringe with a 23-G needle, and extruded through the needle directly into a plate or maple leaf shape mold. Photos and video were taken to record the process of injection and appearance of the united hydrogel.

6.2.10 Statistical analysis

All experiments were performed at least in three independent batches. Data were represented as the mean ± standard deviation (SD). For data in figures, error bars are standard deviations.

Statistical evaluation was conducted with Student's t-test and analysis of variance (ANOVA). The multiple-comparisons were evaluated by Duncan's multiple-range test. Statistical differences among samples were determined with a level of significance as $p < 0.05$.

6.3 Results and discussion

6.3.1 Synthesis and characterization of CHI-C/DACNC hydrogel

The adhesive and self-healing hydrogels were derived from naturally occurring polymers including chitosan and cellulose. First, catechol-conjugated chitosan (CHI-C) was synthesized by grafting the hydrocaffeic acid (HCA) to the chitosan backbone via a carbodiimide coupling reaction using EDC and NHS (**Figure 6-1**A). The conjugation of HCA to chitosan was confirmed by ^{1}H NMR, as indicated by the presence of catechol proton-specific peaks at around 6.7 ppm (**Figure 6-1**B). In addition, the functional groups and chemical bonds of CHI-C were identified by FT-IR (**Figure 6-1**C). Compared with chitosan, the characteristic absorption of CHI-C located at 1560 cm^{-1} was attributed to aromatic C=C ring stretching vibrations, which was consistent with the main vibration modes of catecholic moiety. These results suggested that HCA was conjugated successfully to the chitosan backbone by forming an amide bond between carboxylic acid group (-COOH) in HCA and primary amine group ($-NH_2$) in chitosan. Finally, the UV-vis profiles of the CHI-C show a broad band peak around 280 nm, which was the characteristic peak of the catechol moiety (**Figure 6-1**D). No absorption was observed around 400 nm for catechol-quinone, which suggested that the oxidation of catechol was absent. The degree of catechol substitution (DOC) onto chitosan backbone was quantitatively determined by UV-vis absorbance to be 8.1% (CHI-C1), 9.0% (CHI-C2), and 11.3% (CHI-C3), corresponding to 0.44, 0.50, and 0.62 mmol catechol/g CHI-C, respectively. Chitosan is only soluble in acidic solution, while CHI-C prepared in this study exhibit excellent solubility in a neutral pH solution, which is beneficial for the applications under

physiological conditions. Second, dialdehyde cellulose nanocrystal (DACNC) was prepared by oxidizing cellulose nanocrystal obtained from the acidic hydrolysis of wood cellulose. The structure and morphology of DACNC were described in Chapter 4.

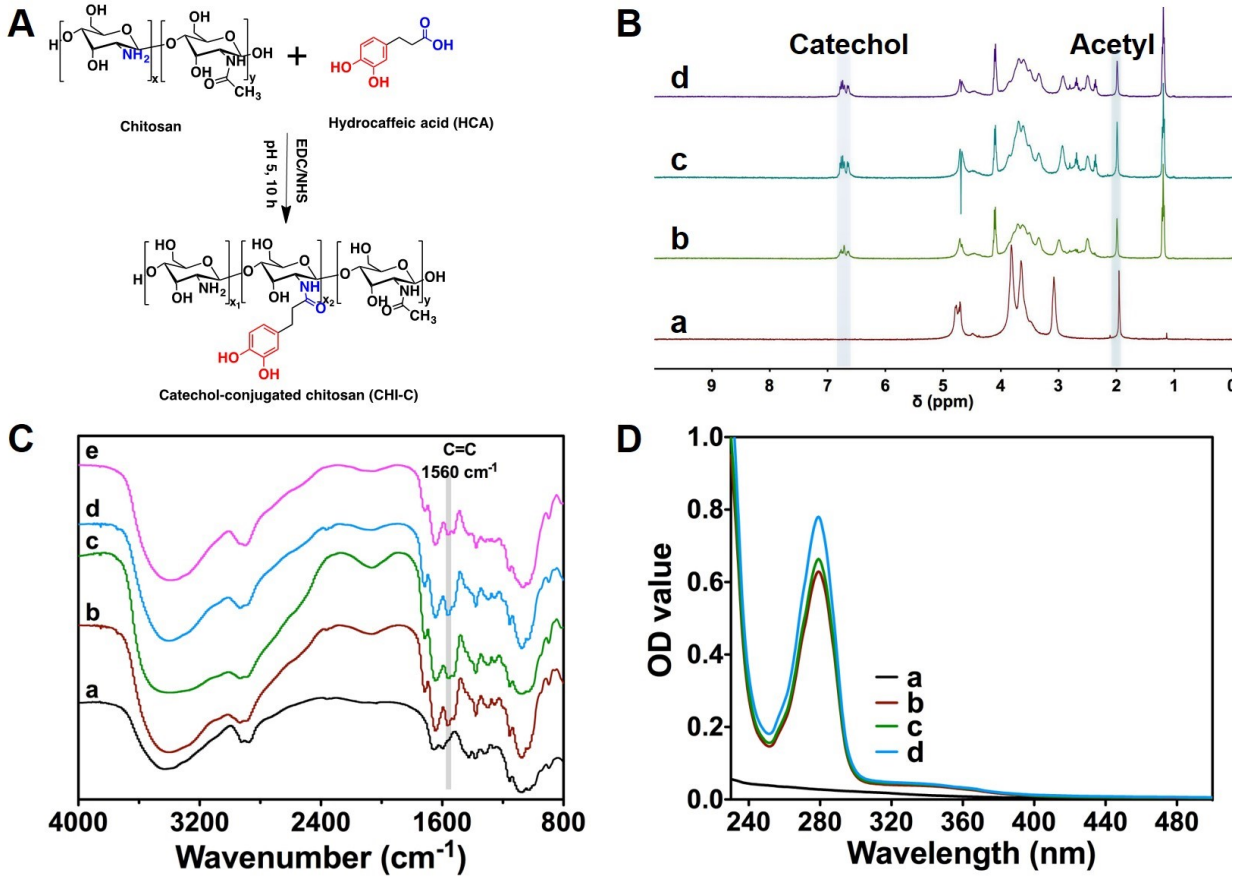

Figure 6-1. Properties of CHI-C: (A) Scheme of synthesis of catechol-conjugated chitosan. (B) ^{1}H NMR spectra of (a) chitosan, (b) CHI-C1, (c) CHI-C2, (d) CHI-C3. (C) FT-IR spectra of (a) chitosan, (b) CHI-C1, (c) CHI-C2, (d) CHI-C3, (e) CHI-C/DACNC hydrogel. (D) UV-vis profiles of the catechol conjugated chitosan showing increased intensity of the peak around 280 nm with increasing degree of substitution.

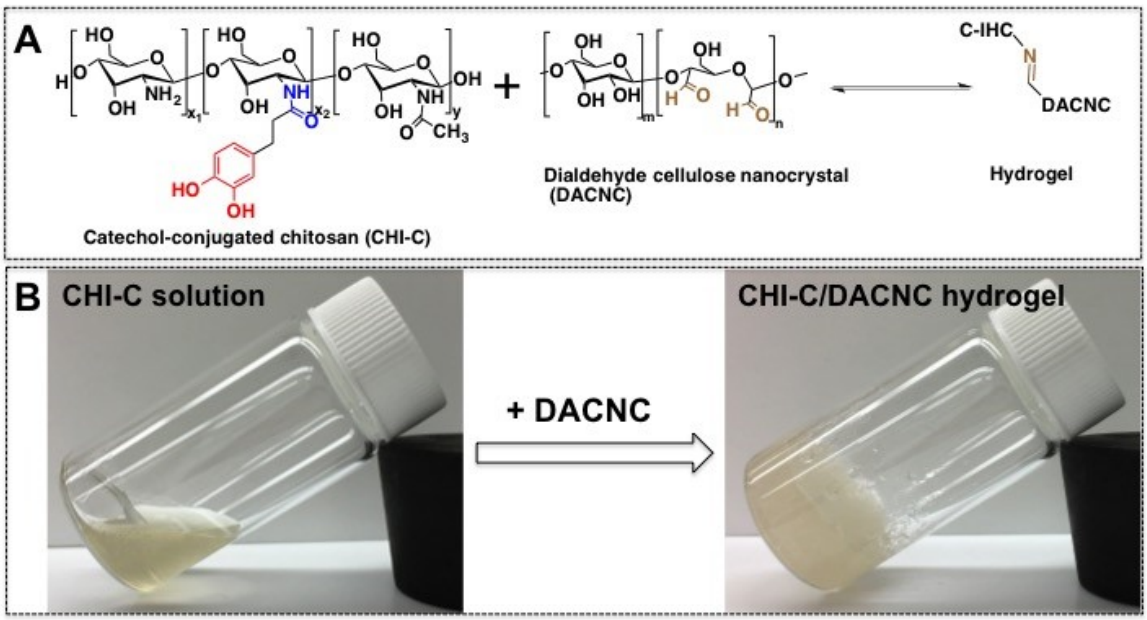

Figure 6-2. (A) Scheme of synthesis of CHI-C/DACNC hydrogel. (B) Pictures of CHI-C3/DACNC-1/1 hydrogel formation.

As shown in **Figure 6-2**, a series of CHI-C/DACNC hydrogels containing various formulas were prepared by homogeneously mixing CHI-C aqueous solution with DACNC aqueous suspension at room temperature. Upon mixing CHI-C and DACNC, a CHI-C/DACNC hydrogel was rapidly formed via the dynamic covalent Schiff-base linkages between amine groups from CHI-C and aldehyde groups from DACNC (**Figure 6-2**A). FT-IR was used to confirm the cross-linking, with a characteristic peak at 1644 cm^{-1} corresponding to the newly formed Schiff-base linkages.

6.3.2 Rheological properties

The mechanical properties of the hydrogels were investigated by dynamic frequency sweep rheological tests. **Figure 6-3**A-C shows the storage modulus (G') and loss modulus (G'') of the hydrogels with different catechol conjugation degree of CHI-C and mass ratio of CHI-C to DACNC (M = 1/0, 1/0.2, 1/0,5, 1/1, 1/2, and 1/3) as a function of frequency. The CHI-C and DACNC solution formed gel rapidly, so the G' and G'' of CHI-C/DACNC hydrogels (M = 1/0.2,

1/0,5, 1/1, 1/2, and 1/3) were measured immediately after mixing and gelation. However, the intra-molecular cross-linking between catechol and amine groups in CHI-C occurred very slowly, thus the G' and G'' of pure CHI-C hydrogel were measured after three days of gelation. All of the CHI-C/DACNC hydrogels exhibited higher G' than G'' over the frequency range, indicating that the hydrogel behaved as viscoelastic solids. The quantitative analysis results of G' were summarized in **Figure 6-3**D. Regarding the same mass ratio of CMC to DACNC, CHI-C2/DACNC hydrogels have higher storage modulus than those of CHI-C1/DACNC hydrogels, followed by CHI-C3/DACNC hydrogels. This result suggests the hydrogel's strength increased with increasing catechol content until reaching a plateau, then decreased with further increase in catechol conjugation degree. Excessive substitution of catechol groups resulted in less amino groups for hydrogel crosslinking, leading to reduced hydrogel strength. For the hydrogels containing the same CHI-C, with the addition and increase of DACNC content in CHI-C polymer, the storage modulus of the hydrogels increased steeply from 41-55 Pa at mass ratio of 1/0, to 669-1402 Pa at a mass ratio of 1/1, and then slightly dropped when mass ratio continuously decreased from 1/1 to 1/3. This behavior is probably because at low concentration of DACNC, the crosslinking density between CHI-C and DACNC increased with the addition of DACNC, which acts as both reinforcing nanofiller and crosslinker, thus resulted in higher G'. However, excessive DACNCs tended to aggregate to reduce their dispersion, resulting in the decrease of active junctions in the hydrogel network and cross-linking density of hydrogel.[26, 236] There was no significant difference in G' among the pure CHI-C1, CHI-C2, and CHI-C3 hydrogels. Even though the CHI-C alone formed gel at room temperature by intramolecular crosslinking between oxidized catechol groups and amine groups in CHI-C, the G' of pure CHI-C hydrogel (~50 Pa) was much lower than that of CHI-C/DACNC hydrogel. Both chemical and physical crosslinking have been involved in CHI-C

hydrogel preparation. CHI-C underwent intermolecular crosslinking under oxidative conditions via the transformation of catechol to o-quinone, which subsequently reacted with catechol groups and amine group presented by molecules nearby mainly through Michael-type addition and Schiff-base formation. Besides, reversible physical crosslinking, including hydrogen bonding, π-π stacking, π-cation interaction, and metal coordination, also contribute to the hydrogel network formation. Once DACNC was mixed with CHI-C, the Schiff-base linkages formed quickly between amine groups of CHI-C and aldehyde groups of DACNC. The addition of DACNC not only shortened the gelation time, but also dramatically increased the hydrogel strength. Rapid gelation and high hydrogel strength are essentially required for practical applications of hydrogels as tissue adhesives. Moreover, the intra-molecular crosslinking of CHI-C consumes catechol groups, which reduces the amount of catechol groups required for adhesion. However, the formation of CHI-C/DACNC hydrogel doesn't need the catechol groups, which can save the catechol groups for adhesion. Therefore, CHI-C cooperated with DACNC to synthesize fast-gelling and strong hydrogels with strong adhesiveness

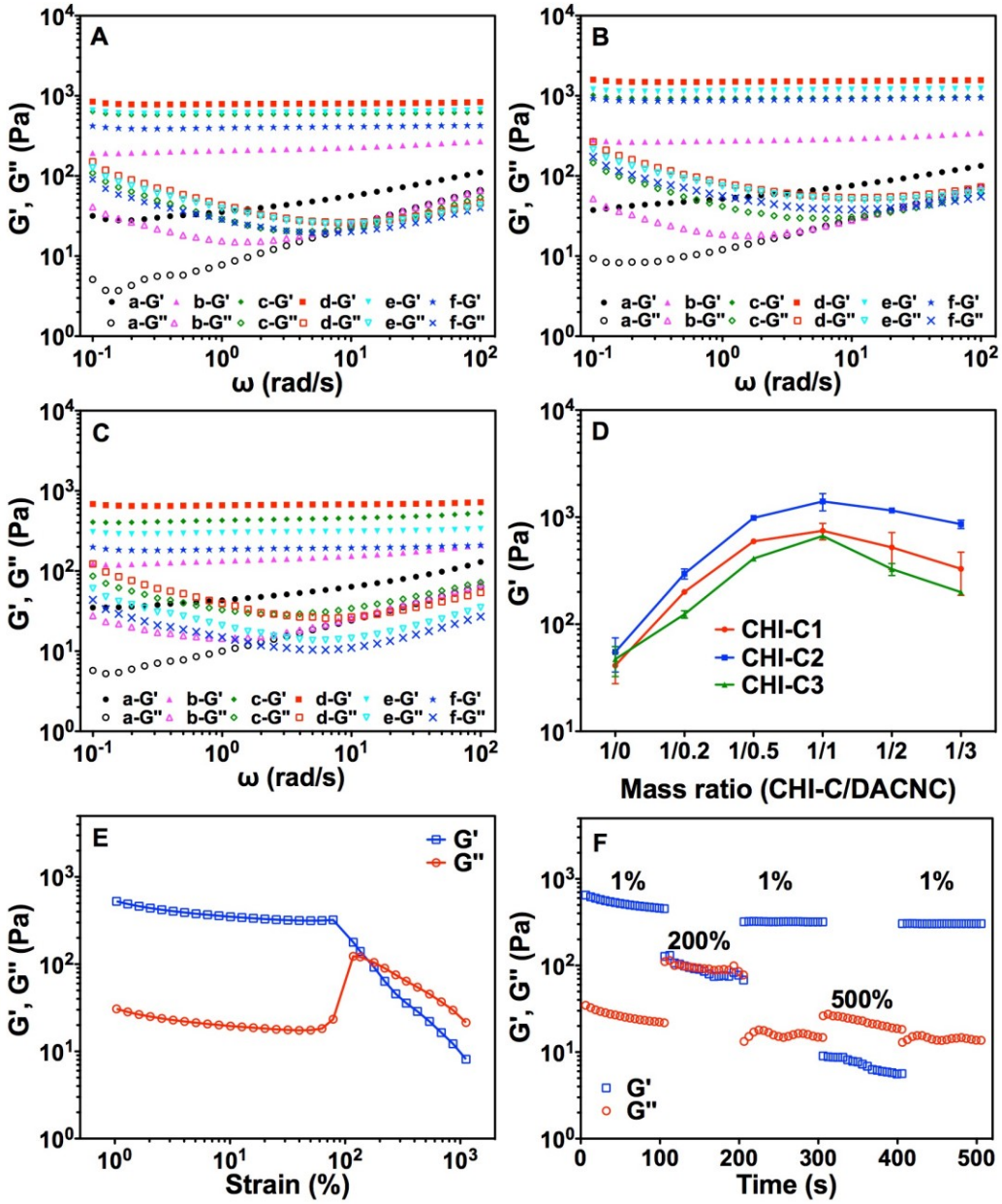

Figure 6-3. The rheological properties of CHI-C/DACNC hydrogel. Effect of mass ratio of CHI-C to DACNC on the strength of the hydrogels formed by (A) CHI-C1, (B) CHI-C2, (C) CHI-C3 with DACNC: mass ratio of (a)1/0, (b)1/0.2, (c) 1/0.5, (d) 1/1, (e) 1/2, (f) 1/3. (D) The storage moduli (G') of hydrogel with different mass ratio of CHI-C to DACNC: (a)1/0, (b)1/0.2, (c) 1/0.5, (d) 1/1, (e) 1/2, (f) 1/3. The data were extracted from the plateaus of variation of storage moduli versus angular frequency (1 rad/s to 10 rad/s). (E) The G' and G'' of the hydrogel from strain

amplitude sweep (γ = 1%–1000%) at a fixed angular frequency (10 rad/s). (F) The G' and G'' of the hydrogel when alternate step strain switched from small strain (γ = 1.0%) to large strain (γ = 200% and 500%) at a fixed angular frequency (10 rad/s). Each strain interval was kept as 100 s.

6.3.3 Self-healing performance

The self-healing behavior of the CHI-C/DACNC hydrogel was assessed by macroscopic observation and rheological recovery tests. Taking the CHI-C3/DACNC (1/1) as an example, as shown in **Figure 6-4**A-C, two hydrogel disks with different color were cut in half, and then two semicircles were brought together at room temperature without any external stimuli. It was observed that the two semicircles healed into one single hydrogel disk, which could be held up under the force of gravity. The cut hydrogel healed together within one min, which was strong enough to withstand a stretch along the direction vertical to the cut surface without splitting. The main forces contributing to the rapid healing include both the dynamic Schiff-base linkage between the amine groups and aldehyde groups, and the reversible physical interactions in the hydrogel network. The self-healing efficiency was higher than most of that of self-healing hydrogels based on Schiff-base linkages and catechol-conjugated chitosan self-healing hydrogel crosslinked by metal ions. Zhang et al developed a self-healing hydrogel composed of chitosan and dibenzaldehyde-terminated telechelic poly(ethylene glycol) (DF-PEG), which formed hydrogel through Schiff-base linkages.[86] It took two hours for the chitosan/DF-PEG to heal. A mussel-inspired self-healing hydrogel crosslinked by iron ion (Fe^{3+}) took 45 min to recover its external structure.[304] Furthermore, a rheological recovery test was used to determine the self-healing performance of the hydrogel. From the results of strain amplitude sweep of CHI-C/DACNC hydrogel, the storage modulus (G') and the loss modulus (G'') curve intersect at the strain of 170%, indicating that the state of hydrogel is between gel and sol near this critical point. Based on the

strain amplitude sweep results, the continuous alternative step strain measurements were conducted to evaluate the rheological recovery behavior of the CHI-C/DACNC hydrogel. **Figure 6-3**F shows that as the oscillatory shear strain stepped from 1% to 200% and maintained for 100 s, the G' and G'' overlapped, while they immediately recovered their original values after the strain was back to 1%. Even at a larger dynamic strain of 500%, the G' of the hydrogel was dropped from 652 Pa to 9 Pa due to the collapse of the hydrogel network. While the strain was back to 1%, the G' of the hydrogel was returned rapidly to the initial value with the restoration of the hydrogel structure. All these results indicate that the CHI-C/DACNC hydrogel network exhibit rapid recovery capacity when the hydrogel is subjected to oscillatory shear strain due to the dynamic Schiff-base linkages.

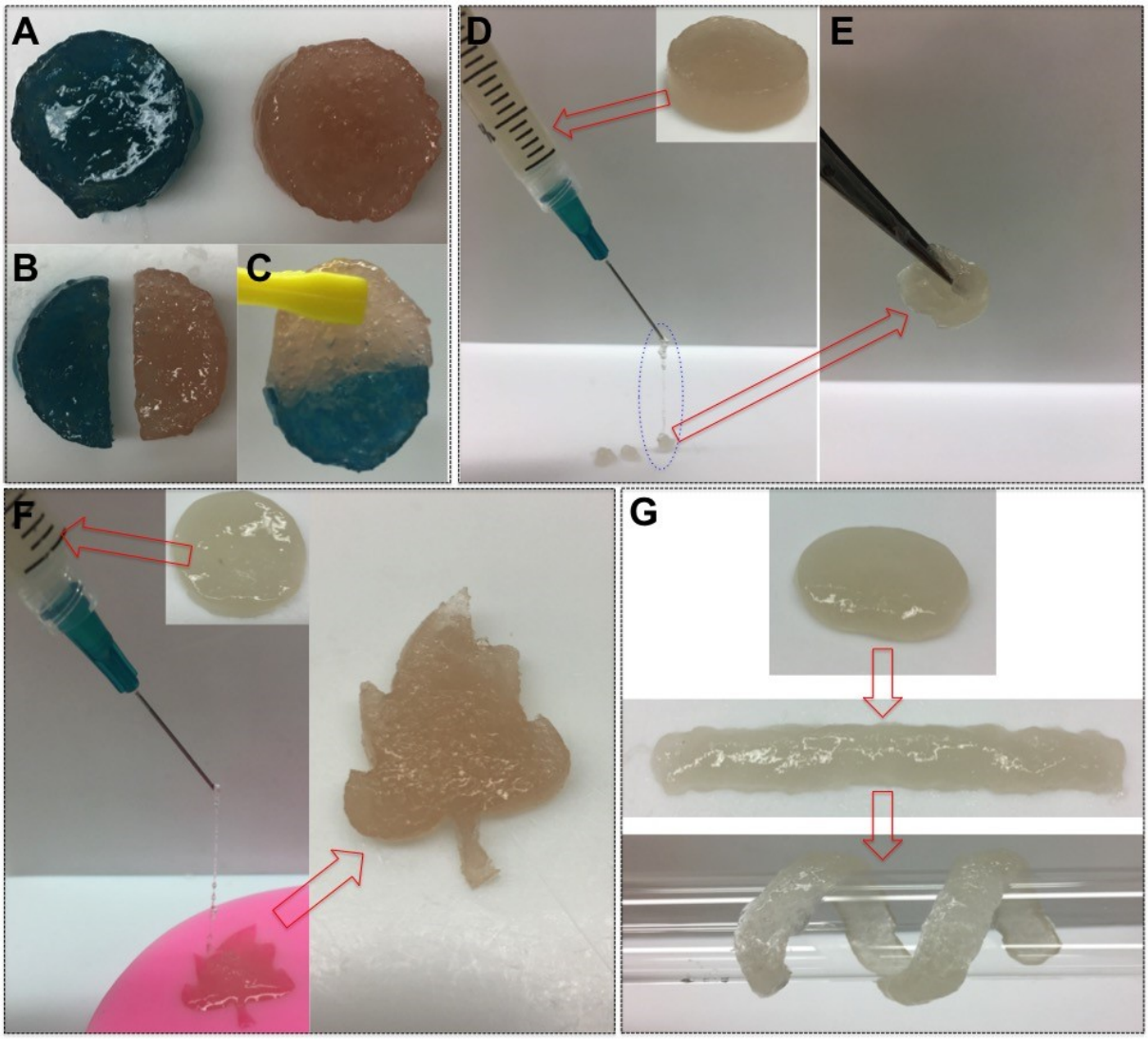

Figure 6-4. (A-C) Macroscopic self-healing behavior of CHI-C/DACNC hydrogel: (A) Two disk-shaped original hydrogels (one of the hydrogels was colored with a dye for clarity), (B) hydrogels were cut in half and then put together, (C) the hydrogels healed completely into one block immediately at room temperature without any external stimuli. Injectable performance of CHI-C/DACNC hydrogel: (D) The hydrogel was loaded into a syringe with a needle (23-gauge) and then was extruded directly through the needle without clogging, (E) the broken hydrogel fragments were reformed an integrate hydrogel immediately at room temperature without any stimuli. (F) and (G) The CHI-C/DACNC adhesive self-healing hydrogel could be molded into various shapes.

6.3.4 Injectable and moldable ability

Traditional hydrogels often fail to adapt to changing environmental conditions, which limits their practical application that require flow and injection. The self-healing hydrogels have good injectability because of the shear-thinning property. The CHI-C/DACNC hydrogel can be injected after gelation. **Figure 6-4**D-E shows that the hydrogel could be extruded through a 23 G needle without clogging and then the hydrogel fragments rapidly recovered the gel state and healed into an integrate hydrogel after injection. The dynamic Schiff-base linkages of the CHI-C/DACNC hydrogel network dissociated under pressure when the hydrogel was pushed out from the syringe. The hydrogel network broke, and then the broken hydrogel flowed like a liquid to pass through the narrow needle. Subsequently, the linkages re-associated and the broken hydrogel was recovered into an integrate hydrogel outside the syringe once the pressure was removed. These interactions can be readily broken and reformed, enabling the hydrogels to self-heal. These results suggest that the CHI-C/DACNC hydrogel could be applied by injection.

Moreover, the ability of the CHI-C/DACNC hydrogel to be molded into different shapes is shown in **Figure 6-4**F-G. As discussed above, the oscillatory rheology test shows that the hydrogel structural collapse at large shear strain (500%) was rapidly restored upon the removal of shear force. The ability of the hydrogel to rapidly restore their viscoelastic solid features allows fixing sequential shapes. The round hydrogel disk is able to mold into different shapes, such as maple leaf, strip, and helix shape. The reversible Schiff-base linkages in the network endow the hydrogel with the ability to rearrange their shape in response to applied stress because the self-healing hydrogels exhibit viscous flow under shear stress (shear-thinning property) and rapid recovery when the applied stress is relaxed (self-healing property). Rapid structure recovery allows the hydrogel to be played as dough and plasticine. These results demonstrate remarkable moldable

and self-healing properties of the CHI-C/DACNC hydrogel. Combined with injectability, this unique moldable characteristic is beneficial for materials employed in biomedical area to completely fill deep and irregular hollow shapes, such as junctions and wounds inside the body.

6.3.5 Wet tissue adhesion

Strong tissue adhesion would be favorable for the practical applications of the tissue adhesive. Therefore, the adhesive performance of the CHI-C/DACNC hydrogels was studied by wet pigskin lap shear test and macroscopic adhesion test. **Figure 6-5**A shows the wet lap shear adhesive strength of the CHI-C/DACNC hydrogels with different catechol conjugated degree of CHI-C and varying mass ratio of CHI-C to DACNC. The adhesive strength increases with the increasing of catechol conjugated degree and DACNC content. The adhesive strength of pure CHI-C1, CHI-C2, and CHI-C3 solution were 0.26 ± 0.08, 0.38 ± 0.17, and 0.55 ± 0.09 kPa, respectively, and they increased to 20.47 ± 1.89, 27.05 ± 2.90, and 37.90 ± 3.99 kPa at the mass ratio of 1/1. The adhesive strength of CHI-C3/DACNC (1/1) hydrogel was almost 70-fold higher that of CHI-C3/DACNC (1/0) hydrogel. The adhesive strength of CHI-C/DACNC hydrogel was higher than that of CHI-C/thiol-terminated Pluronic F-127 (Plu-SH) hydrogel (~15.0 kPa).[45] There are two steps to achieve adhesion—contact step and solidification step.[48]

Although the CHI-C solution could contact the surface of pigskin, the CHI-C solutions alone can't be solidified in a short time by themselves, resulting in negligible adhesive ability. However, with the addition of DACNC, the CHI-C solution solidified rapidly. The adhesiveness of the CHI-C hydrogel was attributed to the presence of sufficient free catechol groups and aldehyde groups in the hydrogel. Under physiological conditions, catechol groups of CHI-C were partially deprotonated and transformed to reactive catechol-quinone groups, which subsequently reacted with amine, thiol, and imidazole groups in extracellular matrix proteins and carbohydrates on the

surface of pigskin through Michael-type addition and Schiff-base formation.[24, 45] Schiff-base formation between the aldehyde groups from DACN and the amine groups on the pigskin surface also contributes to the adhesion.[305] In addition to those chemical crosslinking, various physical crosslinking, such as hydrogel bonding, π-π stacking, and π-cation interaction, also account for the adhesion.[23, 46] The formation of these bonds allowed catechol-conjugated chitosan to be stably attached to the pigskin surface for an extended period of time. Furthermore, the free catechol groups in the hydrogel network lead to intermolecular crosslinking, which results in further solidification of adhered CHI-C/DACNC hydrogel.

Figure 6-5B shows the effect of strong oxidant sodium periodate ($NaIO_4$) on the adhesive strength of the CHI-C/DACNC hydrogel. Once the sodium periodate was added into the CHI-C solution as a curing agent, catechol groups were immediately oxidized to catechol-quinone, which triggers intermolecular crosslinking and promotes the adhesion of pigskin.[306] Compared with pure CHI-C1, CHI-C2, and CHI-C3 solution, their corresponding adhesive strength were 9.18 ± 0.49, 9.13 ± 0.70, and 11.02 ± 2.63 kPa after the addition of sodium periodate, which were much higher than that of pure CHI-C solution. However, the addition of sodium periodate didn't make significant difference to the CHI-C/DACNC hydrogels. Moreover, $NaIO_4$ is substantially cytotoxic to cells.[307] These results suggest that replacing sodium periodate by DACNC in the adhesive hydrogel make the hydrogel more biocompatible considering that DACNC is biocompatible, and the sodium periodate presents the potential toxicity.

Furthermore, taking the CHI-C3/DACNC (1/1) hydrogel as an example, as a potential candidate for practical applications, the hydrogel exhibits the great adhesive performance on the skin surface of human body. As shown in **Figure 6-5**C-E, the hydrogel strip not only adheres to the finger surface, but also accommodates the finger movements and was easily peeled off without any

residue. Moreover, the CHI-C hydrogel could easily adhere to various solid materials, such as glass and plastic. The CHI-C/DACNC hydrogel exhibits effective adhesion on the various substrates. Even when the glass vial and plastic tube were vigorously shaken, the hydrogel still strongly adhered on their surface.

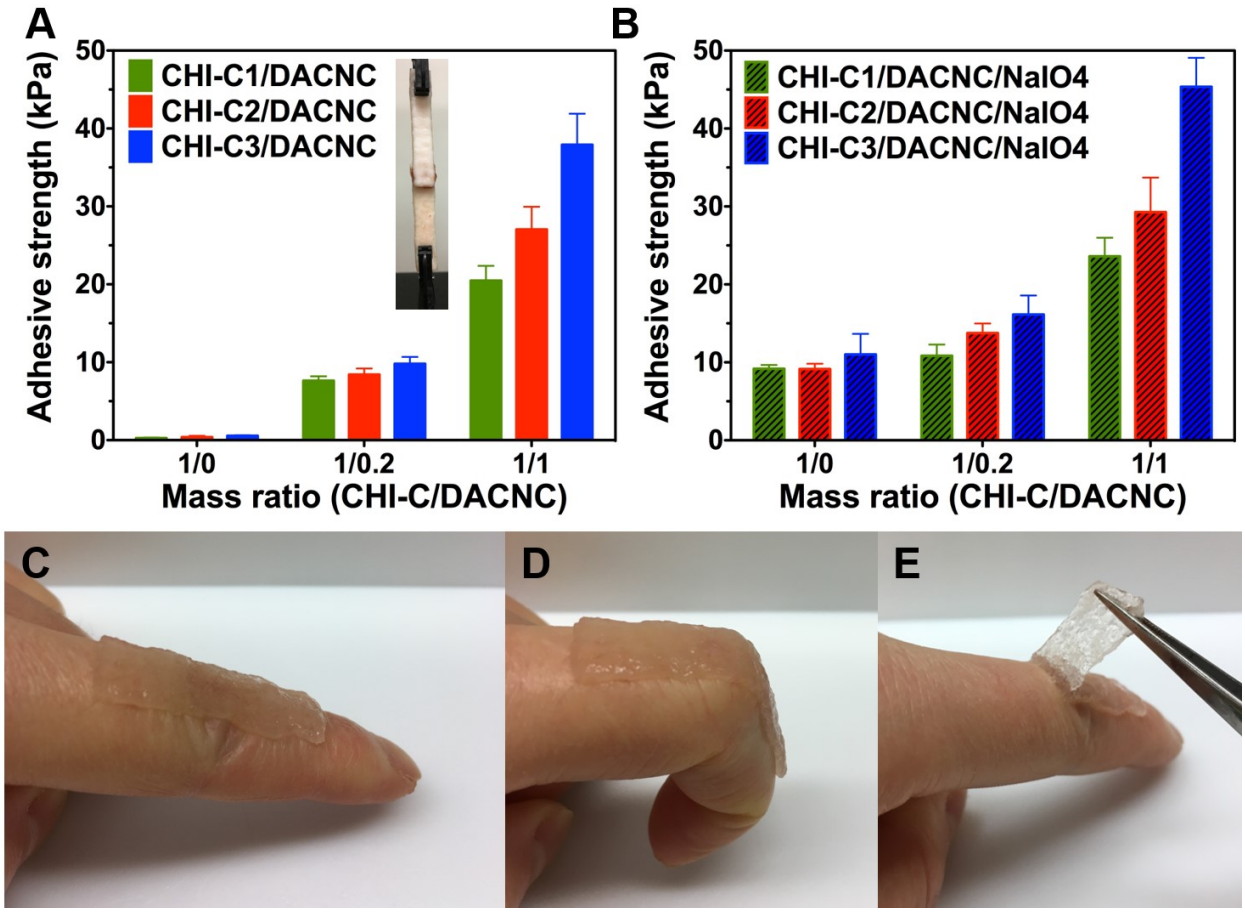

Figure 6-5. Lap-shear adhesion strength of (A) CHI-C/DACNC hydrogel, inset picture is the experimental setup for the adhesion strength tests on porcine skin, and (B) CHI-C/DACNC/NaIO4 hydrogel on porcine skin. All tests were conducted at room temperature after 1 h of adhesion. (C-D) A hydrogel film was adhered to a finger, which dynamically adapted to the figure surface and accommodated the finger movements, and (E) the hydrogel film was peeled from the skin easily.

6.4 Conclusion

In this study, a nanocomposite adhesive hydrogel with self-healing and moldable capacity was constructed by combining catechol-conjugated chitosan (CHI-C) and dialdehyde modified cellulose nanocrystals (DACNC). Due to the reversible Schiff-base linkages between the amine groups from CHI-C and aldehyde groups from DACNC, the hydrogel was endowed to be self-healing and injectable. DACNC acted as crosslinker and reinforcing filler in the hydrogel network, which inhibited the intermolecular crosslinking of CHI-C, sped up gelation, and improved the mechanical properties of the hydrogel. The cocktail of CHI-C and DACNC solution formed gel rapidly at room temperature without any cytotoxic oxidants, whereas the CHI-C solution became gel after 3 days. The storage modulus of CHI-C/DACNC hydrogel was almost 20 times as large as that of CHI-C hydrogel. Catechol group had high binding affinity to amine, thiol, and imidazole groups in the tissue via strong covalent and noncovalent bonds. In addition, aldehyde groups from DACNC could react with amine groups on the tissue surface by Schiff-base formation. This synergistically adhesion mechanism endowed the hydrogel with excellent tissue adhesive strength. The wet tissue adhesive strength of CHI-C/DACNC was as high as 37.90 ± 3.99 kPa, which was higher than the CHI-C hydrogel triggered by an oxidant. Additionally, the hydrogel could be molded to different shapes, restore from large strain deformation, and be injected through a syringe to adhere to irregularly shaped wounds.

Chapter 7

Conclusions and Perspectives

7.1 Summary and conclusions

Self-healing hydrogels are promising smart materials because of their capacity to autonomously heal upon damage, which prolongs their lifetime, reduces replacement costs, and improves product safety. Chitosan, partially deacetylated chitin, is a well-known biocompatible and biodegradable cationic polysaccharide used in biomedical applications. The abundant amino groups on chitosan are favorable to developing self-healing hydrogels based on reversible Schiff-base linkages. In addition, the chitosan based self-healing hydrogel can smoothly pass through the narrow needle and the broken hydrogel fragments can be reformed to a completely homogeneous hydrogel, suggesting good injectability. Thus, they can be injected in to irregular wound beds to stop bleeding and be used as a wound healing material. Despite these advancements, achieving chitosan-based self-healing hydrogels with both high self-healing efficiency and excellent mechanical performance has remained elusive because they are contradictory properties, making it difficult to optimize them simultaneously. Thus, novel self-healing hydrogels that have both good mechanical strength and high self-healing efficiency are required. In addition, tissue adhesive capacity is necessary for self-healing hydrogels to stably stay at designated sites, avoiding moving around to trigger inflammation or damage to surrounding tissues.

This research demonstrated that incorporation of aldehyde modified four-arm polyethylene glycol (PEG-BA) or oxidized cellulose nanocrystals (DACNC) into the chitosan-based self-healing hydrogel network could improve both self-healing performance and mechanical properties. The dynamic and reversible Schiff-base linkages in the hydrogel network endow the hydrogels with self-healing ability. The four-arm polymers behave as impenetrable space-filled spheres and have

small hydrodynamic size and low solution viscosity, so the four-arm polymers-based networks are more resistant to fracture than the equivalent two-arm polymers-based networks with the same average crosslink density, leading to strong hydrogel. DACNCs function as both cross-linkers to form hydrogel network with CMC and as nano-reinforcing fillers to strengthen the network. Gelation occurred within 2 min and storage modulus reached to approximately 3 kPa and rapidly self-healing process (5 mins at room temperature). The self-healing hydrogels could be injected to thoroughly cover the wounds of varying size, depth, shape and location. Additionally, the hydrogel could be painlessly removed from wounds by on-demand dissolution of the hydrogel with amino acid.

Afterwards, combining a self-healing network (CMC/DACNC) with an elastic network (polyacrylamide) improved the stretchability and toughness of hydrogels. The hybrid hydrogel could be repeatedly stretched to 4 times its initial length and had tensile strength of 244 kPa. Moreover, the hydrogels could be compressed to 90% of their initial height without any damage and rapidly recover to its original shape upon release of the load, and had the compressive strength up to 8 MPa, comparable to that of skeletal muscle tissue. In addition, at ambient temperature without any external stimuli, the deformed hydrogel recovered 81.3% of its dissipated energy.

Tissue adhesive ability is important to hydrogels applied in biomedical field. This feature was achieved by modifying chitosan with catechol moieties carrying adhesive capacity, and then catechol conjugated chitosan crosslinked with DACNC to prepare adhesive self-healing hydrogels. The wet tissue adhesive strength of CHI-C/DACNC was as high as 37.90 ± 3.99 kPa, which was higher than the CHI-C hydrogel triggered by oxidant.

The hydrogel exhibited good cytotoxicity and could be used as 3D cell carrier. Hemostatic capacity of the hydrogel was investigated in a rabbit liver model. The total blood loss and bleeding time

after applying the CMC/PEG-BA hydrogel without compression was 0.29 ± 0.11 g and 120 ± 10 s, respectively, which were much less than that of gauze. The CMC/PEG-BA self-healing hydrogel could be potentially used as a hemostatic material. The burn wound healing ability of the CMC/DACNC self-healing hydrogels was evaluated in deep partial thickness burn wounds using a rat model. The results indicated that 0.6% wound surface area remained unhealed without leaving visible scars after two weeks' healing with on-demand dissolvable hydrogel, much better than that of control group and gauze group (22.3% and 13.1%), indicating the highly efficient wound healing. This work opened a novel pathway to fabricate new self-healing hydrogels from natural polymers for burn wound healing to eliminate pain at wound dressing changes and scars, which are very important in the wound healing field.

7.2 Significance of this dissertation

This research aimed at developing new approaches for self-healing hydrogels in structure, functionality and application. Our efforts have been mainly dedicated to fabricating self-healing hydrogels with rapid self-healing process, high mechanical strength, and strong bio-adhesive ability using modified nature polymers including aldehyde modified polymeric crosslinker and water-soluble chitosan derivatives and applying them to fabricate self-healing, as well as exploring various potential biomedical applications.

The research described in Chapter 3-6 have addressed some unresolved issues in self-healing hydrogels. One issue is how to simultaneously improve the mechanical strength and self-healing efficiency, which are contrary properties. Previous work on self-healing hydrogels mainly focused on their healing efficiency instead of their mechanical properties, whereas the research work demonstrated in this dissertation provide many solutions to prepare self-healing hydrogels with both rapid self-healing process and high mechanical strength, including incorporating four-arm

polymers and cellulose nanocrystals into the hydrogel network, as well as combining a self-healing network to an elastic hydrogel network.

Self-healing hydrogels with shear-thinning capacity could be injected to target sites, but they could not remain at the target sites, especially for wet tissue surfaces. Therefore, the second long-standing issue regarding application of hydrogels is how to make the self-healing hydrogel adhere to the target sites. Inspired by the adhesion mechanism of mussels, we conjugated catechol moieties to chitosan and then applied it to prepare self-healing hydrogels. The resulted self-healing hydrogels could not only be injected to target sites, but also adhere to wet surfaces.

The increase of mechanical strength is beneficial for practical applications that require strong hydrogels. Most reports on self-healing hydrogel only focused on designing new hydrogels rather than to investigate their potential applications due to the weak mechanical properties and high cytotoxicity. In this context, the third issue surrounding hydrogels' application is how to develop multifunctional self-healing hydrogels to meet diverse needs in dynamic biomedical processes. All self-healing hydrogels developed in this research were facilely prepared and used, and biocompatible. Moreover, only water was used as the solvent to prepare these hydrogels. We applied the strong and rapidly self-healing hydrogel as the 3D cell carrier, hemostatic material, and wound healing dressing. The results exhibited that the CMC/PEG-BA self-healing hydrogel could reduce total blood loss and shorten bleeding time. The CMC/DACNC self-healing hydrogel could speed up deep partial thickness burn wound healing and prevent scar formation. The hydrogel could be injected to irregular and deep wound beds to fully fit the wounds. In addition, the hydrogel could be painlessly removed by on-demand dissolution, which alleviates pain for patients. Self-healing hydrogels demonstrated in this research presented a promising platform for a wide variety of biomedical applications requiring great injectable and biocompatible materials.

The self-healing hydrogels demonstrated in this dissertation were derived from natural polymers, including chitosan and cellulose. In terms of contribution of this research to industry, such as shellfish processing industry and forestry industry, the development of self-healing hydrogel based on natural polymers could transfer low-value resource to valuable products. It is well known that shellfish processing industry produces massive by-products. Disposal of these by-products can result in environmental and human health problems, which are world-wide concerns. Every year, approximately 6 ~ 8 million metric tons of discarded crustacean shells are produced globally. In the Canadian province of Newfoundland and Labrador alone, 40, 000 metric tons are discarded.[308] Crustacean shell wastes from shrimp, crab, and lobster contain quantities of chitin. The extraction of chitin from crustaceans' shells is a solution to minimize the waste and to produce valuable compounds which possess biological properties (e.g. anti-bacterial, anti-oxidant, anti-cancer, antioxidant, and immune-enhancing) with applications in various fields. Chitosan is the deacetylated derivative of chitin, which is the second most available polysaccharide following cellulose. Applying chitosan to prepare self-healing hydrogel can convert food by-products into high-value biomedical products. Furthermore, chitosan has been utilized to prepare hydrogel without self-healing ability. The incorporation of self-healing ability into chitosan hydrogels extended their functions and exploited new applications.

Cellulose is the most abundant biopolymer on the earth with a yield of 1.5×10^{12} tons per year.[52] Canada is the second largest country in the world with the forest or other wooded land making up 40% of its 979 million hectares.[309] The main component of wood is cellulose. Wood pulp fibers can undergo further chemical or mechanical treatments to produce a more useful class of materials, cellulose nanocrystals (CNCs). Currently, CNCs are commercially available in Canada. Modifying

CNCs with functional groups and applying modified CNCs in self-healing hydrogels could promote the application of CNCs.

7.3 Suggestions for future research

This research brings out some new strategies to develop multifunctional self-healing hydrogels, which pave the way for future studies on self-healing hydrogels. Nevertheless, there are still certain questions unanswered in the field of self-healing hydrogels.

Future work can be conducted to investigate the biocompatibility and safety of the CMC/DACNC/polyacrylamide hybrid hydrogels. The load-bearing of the hybrid hydrogels should also be improved, which can extend the application of the hybrid hydrogel.

The self-healing processes were only investigated *in vitro*. However, the body is complicated containing other components such as body fluid and blood, and the pH values are different in various tissues. All these may impact the self-healing process. It is also required to design the self-healing hydrogels according to specific practical applications.

In *in vivo* tests, the pristine self-healing hydrogels was applied without any cargos. Growth factors, drugs, and cells can be loaded into the self-healing hydrogels to improve their properties in future work. For example, thrombin can be encapsulated into the self-healing hydrogels to facilitate the hemostatic effect. Cells encapsulated in the self-healing hydrogels could live very well in the hydrogels and the self-healing hydrogels could be injected to target sites. Future work can be performed to study the effect of self-healing hydrogels on the cell proliferations via *in vivo* test. Cell-laden self-healing hydrogels can be injected to real microenvironment for investigation of the cell behaviors. Self-healing hydrogels with antibacterial capacity can also be designed to benefit wound healing.

References

(1) Haque, M. A.; Kurokawa, T.; Gong, J. P. Super Tough Double Network Hydrogels and Their Application as Biomaterials. *Polymer* **2012,** *53*, 1805-1822.

(2) Gong, J. P.; Katsuyama, Y.; Kurokawa, T.; Osada, Y. Double‐Network Hydrogels with Extremely High Mechanical Strength. *Adv. Mater.* **2003,** *15*, 1155-1158.

(3) Gong, J. P. Materials Both Tough and Soft. *Science* **2014,** *344*, 161-162.

(4) Stuart, M. A. C.; Huck, W. T.; Genzer, J.; Müller, M.; Ober, C.; Stamm, M.; Sukhorukov, G. B.; Szleifer, I.; Tsukruk, V. V.; Urban, M. Emerging Applications of Stimuli-Responsive Polymer Materials. *Nat. Mater.* **2010,** *9*, 101-113.

(5) De las Heras Alarcón, C.; Pennadam, S.; Alexander, C. Stimuli Responsive Polymers for Biomedical Applications. *Chem. Soc. Rev.* **2005,** *34*, 276-285.

(6) Van Vlierberghe, S.; Dubruel, P.; Schacht, E. Biopolymer-Based Hydrogels as Scaffolds for Tissue Engineering Applications: A Review. *Biomacromolecules* **2011,** *12*, 1387-1408.

(7) Lienemann, P. S.; Lutolf, M. P.; Ehrbar, M. Biomimetic Hydrogels for Controlled Biomolecule Delivery to Augment Bone Regeneration. *Adv. Drug Del. Rev.* **2012,** *64*, 1078-1089.

(8) Wang, H.; Heilshorn, S. C. Adaptable Hydrogel Networks with Reversible Linkages for Tissue Engineering. *Adv. Mater.* **2015,** *27*, 3717-3736.

(9) Yang, Y.; Ding, X.; Urban, M. W. Chemical and Physical Aspects of Self-Healing Materials. *Prog. Polym. Sci.* **2015,** *49*, 34-59.

(10) Wei, Z.; Yang, J. H.; Zhou, J.; Xu, F.; Zrínyi, M.; Dussault, P. H.; Osada, Y.; Chen, Y. M. Self-Healing Gels Based on Constitutional Dynamic Chemistry and Their Potential Applications. *Chem. Soc. Rev.* **2014,** *43*, 8114-8131.

(11) Taylor, D. L.; in het Panhuis, M. Self‐Healing Hydrogels. *Adv. Mater.* **2016,** *28*, 9060-9093.

(12) Kim, S. M.; Jeon, H.; Shin, S. H.; Park, S. A.; Jegal, J.; Hwang, S. Y.; Oh, D. X.; Park, J. Superior Toughness and Fast Self‐Healing at Room Temperature Engineered by Transparent Elastomers. *Adv. Mater.* **2018,** *30*, 1705145.

(13) Chaudhuri, O.; Gu, L.; Darnell, M.; Klumpers, D.; Bencherif, S. A.; Weaver, J. C.; Huebsch, N.; Mooney, D. J. Substrate Stress Relaxation Regulates Cell Spreading. *Nat. Commun.* **2015,** *6*, 6365.

(14) Chaudhuri, O.; Gu, L.; Klumpers, D.; Darnell, M.; Bencherif, S. A.; Weaver, J. C.; Huebsch, N.; Lee, H.-p.; Lippens, E.; Duda, G. N. Hydrogels with Tunable Stress Relaxation Regulate Stem Cell Fate and Activity. *Nat. Mater.* **2016,** *15*, 326-334.

(15) Wei, Z.; Yang, J. H.; Liu, Z. Q.; Xu, F.; Zhou, J. X.; Zrínyi, M.; Osada, Y.; Chen, Y. M. Novel Biocompatible Polysaccharide‐Based Self‐Healing Hydrogel. *Adv. Funct. Mater.* **2015,** *25*, 1352-1359.

(16) McKee, J. R.; Appel, E. A.; Seitsonen, J.; Kontturi, E.; Scherman, O. A.; Ikkala, O. Healable, Stable and Stiff Hydrogels: Combining Conflicting Properties Using Dynamic and Selective Three‐Component Recognition with Reinforcing Cellulose Nanorods. *Adv. Funct. Mater.* **2014,** *24*, 2706-2713.

(17) Seliktar, D. Designing Cell-Compatible Hydrogels for Biomedical Applications. *Science* **2012,** *336*, 1124-1128.

(18) Han, L.; Yan, L.; Wang, K.; Fang, L.; Zhang, H.; Tang, Y.; Ding, Y.; Weng, L.-T.; Xu, J.; Weng, J. Tough, Self-Healable and Tissue-Adhesive Hydrogel with Tunable Multifunctionality. *NPG Asia Mater.* **2017,** *9*, e372.

(19) Brubaker, C. E.; Kissler, H.; Wang, L.-J.; Kaufman, D. B.; Messersmith, P. B. Biological Performance of Mussel-Inspired Adhesive in Extrahepatic Islet Transplantation. *Biomaterials* **2010,** *31*, 420-427.

(20) Kan, Y.; Danner, E. W.; Israelachvili, J. N.; Chen, Y.; Waite, J. H. Boronate Complex Formation with Dopa Containing Mussel Adhesive Protein Retards pH-Induced Oxidation and Enables Adhesion to Mica. *PLoS ONE* **2014,** *9*, e108869.

(21) Lee, H.; Scherer, N. F.; Messersmith, P. B. Single-Molecule Mechanics of Mussel Adhesion. *Proc. Natl. Acad. Sci. U. S. A.* **2006,** *103*, 12999-13003.

(22) Lee, B. P.; Messersmith, P. B.; Israelachvili, J. N.; Waite, J. H. Mussel-Inspired Adhesives and Coatings. *Annu. Rev. Mater. Res.* **2011,** *41*, 99-132.

(23) Li, L.; Smitthipong, W.; Zeng, H. Mussel-Inspired Hydrogels for Biomedical and Environmental Applications. *Polym. Chem.* **2015,** *6*, 353-358.

(24) Shin, J.; Lee, J. S.; Lee, C.; Park, H. J.; Yang, K.; Jin, Y.; Ryu, J. H.; Hong, K. S.; Moon, S. H.; Chung, H. M. Tissue Adhesive Catechol‐Modified Hyaluronic Acid Hydrogel for Effective, Minimally Invasive Cell Therapy. *Adv. Funct. Mater.* **2015,** *25*, 3814-3824.

(25) Li, Y.; Wang, X.; Wei, Y.; Tao, L. Chitosan-Based Self-Healing Hydrogel for Bioapplications. *Chin. Chem. Lett.* **2017,** *28*, 2053-2057.

(26) Yang, X.; Bakaic, E.; Hoare, T.; Cranston, E. D. Injectable Polysaccharide Hydrogels Reinforced with Cellulose Nanocrystals: Morphology, Rheology, Degradation, and Cytotoxicity. *Biomacromolecules* **2013,** *14*, 4447-4455.

(27) Rinaudo, M. Chitin and Chitosan: Properties and Applications. *Prog. Polym. Sci.* **2006,** *31*, 603-632.

(28) Jayakumar, R.; Menon, D.; Manzoor, K.; Nair, S.; Tamura, H. Biomedical Applications of Chitin and Chitosan Based Nanomaterials-a Short Review. *Carbohydr. Polym.* **2010,** *82*, 227-232.

(29) Cheung, R.; Ng, T.; Wong, J.; Chan, W. Chitosan: An Update on Potential Biomedical and Pharmaceutical Applications. *Mar. Drugs* **2015,** *13*, 5156-5186.

(30) Zargar, V.; Asghari, M.; Dashti, A. A Review on Chitin and Chitosan Polymers: Structure, Chemistry, Solubility, Derivatives, and Applications. *ChemBioEng Rev.* **2015,** *2*, 204-226.

(31) LogithKumar, R.; KeshavNarayan, A.; Dhivya, S.; Chawla, A.; Saravanan, S.; Selvamurugan, N. A Review of Chitosan and Its Derivatives in Bone Tissue Engineering. *Carbohydr. Polym.* **2016,** *151*, 172-188.

(32) Xu, Y.; Li, Y.; Chen, Q.; Fu, L.; Tao, L.; Wei, Y. Injectable and Self-Healing Chitosan Hydrogel Based on Imine Bonds: Design and Therapeutic Applications. *Int. J. Mol. Sci.* **2018,** *19*, 2198.

(33) Fouda, M. M.; El-Aassar, M.; Al-Deyab, S. S. Antimicrobial Activity of Carboxymethyl Chitosan/Polyethylene Oxide Nanofibers Embedded Silver Nanoparticles. *Carbohydr. Polym.* **2013,** *92*, 1012-1017.

(34) Sogias, I. A.; Khutoryanskiy, V. V.; Williams, A. C. Exploring the Factors Affecting the Solubility of Chitosan in Water. *Macromol. Chem. Phys.* **2010,** *211*, 426-433.

(35) Alves, N.; Mano, J. Chitosan Derivatives Obtained by Chemical Modifications for Biomedical and Environmental Applications. *Int. J. Biol. Macromol.* **2008,** *43*, 401-414.

(36) Fei Liu, X.; Lin Guan, Y.; Zhi Yang, D.; Li, Z.; De Yao, K. Antibacterial Action of Chitosan and Carboxymethylated Chitosan. *J. Appl. Polym. Sci.* **2001,** *79*, 1324-1335.

(37) Lin, Y.-H.; Liang, H.-F.; Chung, C.-K.; Chen, M.-C.; Sung, H.-W. Physically Crosslinked Alginate/N, O-Carboxymethyl Chitosan Hydrogels with Calcium for Oral Delivery of Protein Drugs. *Biomaterials* **2005,** *26*, 2105-2113.

(38) Chen, S.-C.; Wu, Y.-C.; Mi, F.-L.; Lin, Y.-H.; Yu, L.-C.; Sung, H.-W. A Novel pH-Sensitive Hydrogel Composed of N, O-Carboxymethyl Chitosan and Alginate Cross-Linked by Genipin for Protein Drug Delivery. *J. Control. Release.* **2004,** *96*, 285-300.

(39) Chen, R.-N.; Wang, G.-M.; Chen, C.-H.; Ho, H.-O.; Sheu, M.-T. Development of N, O-(Carboxymethyl) Chitosan/Collagen Matrixes as a Wound Dressing. *Biomacromolecules* **2006,** *7*, 1058-1064.

(40) Anitha, A.; Rani, V. D.; Krishna, R.; Sreeja, V.; Selvamurugan, N.; Nair, S.; Tamura, H.; Jayakumar, R. Synthesis, Characterization, Cytotoxicity and Antibacterial Studies of Chitosan, O-Carboxymethyl and N, O-Carboxymethyl Chitosan Nanoparticles. *Carbohydr. Polym.* **2009,** *78*, 672-677.

(41) M Ways, T.; Lau, W.; Khutoryanskiy, V. Chitosan and Its Derivatives for Application in Mucoadhesive Drug Delivery Systems. *Polymers* **2018,** *10*, 267.

(42) Lee, H.; Dellatore, S. M.; Miller, W. M.; Messersmith, P. B. Mussel-Inspired Surface Chemistry for Multifunctional Coatings. *Science* **2007,** *318*, 426-430.

(43) Lee, H.; Lee, B. P.; Messersmith, P. B. A Reversible Wet/Dry Adhesive Inspired by Mussels and Geckos. *Nature* **2007,** *448*, 338-341.

(44) Lin, Q.; Gourdon, D.; Sun, C.; Holten-Andersen, N.; Anderson, T. H.; Waite, J. H.; Israelachvili, J. N. Adhesion Mechanisms of the Mussel Foot Proteins Mfp-1 and Mfp-3. *Proc. Natl. Acad. Sci. U. S. A.* **2007,** *104*, 3782-3786.

(45) Ryu, J. H.; Lee, Y.; Kong, W. H.; Kim, T. G.; Park, T. G.; Lee, H. Catechol-Functionalized Chitosan/Pluronic Hydrogels for Tissue Adhesives and Hemostatic Materials. *Biomacromolecules* **2011,** *12*, 2653-2659.

(46) Ryu, J. H.; Hong, S.; Lee, H. Bio-Inspired Adhesive Catechol-Conjugated Chitosan for Biomedical Applications: A Mini Review. *Acta Biomater.* **2015,** *27*, 101-115.

(47) Kim, K.; Ryu, J. H.; Lee, D. Y.; Lee, H. Bio-inspired Catechol Conjugation Converts Water-Insoluble Chitosan into a Highly Water-Soluble, Adhesive Chitosan Derivative for Hydrogels and Lbl Assembly. *Biomater. Sci.* **2013,** *1*, 783-790.

(48) Kim, K.; Kim, K.; Ryu, J. H.; Lee, H. Chitosan-Catechol: A Polymer with Long-Lasting Mucoadhesive Properties. *Biomaterials* **2015,** *52*, 161-170.

(49) Yang, J.; Stuart, M. A. C.; Kamperman, M. Jack of All Trades: Versatile Catechol Crosslinking Mechanisms. *Chem. Soc. Rev.* **2014,** *43*, 8271-8298.

(50) Sheikhi, A.; Hayashi, J.; Eichenbaum, J.; Gutin, M.; Kuntjoro, N.; Khorsandi, D.; Khademhosseini, A. Recent Advances in Nanoengineering Cellulose for Cargo Delivery. *J. Control. Release.* **2018,** *294*, 53-76.

(51) Trache, D.; Hussin, M. H.; Haafiz, M. M.; Thakur, V. K. Recent Progress in Cellulose Nanocrystals: Sources and Production. *Nanoscale* **2017,** *9*, 1763-1786.

(52) Klemm, D.; Heublein, B.; Fink, H. P.; Bohn, A. Cellulose: Fascinating Biopolymer and Sustainable Raw Material. *Angew. Chem. Int. Ed.* **2005,** *44*, 3358-3393.

(53) George, J.; Sabapathi, S. Cellulose Nanocrystals: Synthesis, Functional Properties, and Applications. *Nanotechnol. Sci. Appl.* **2015,** *8*, 45-54.

(54) O'sullivan, A. C. Cellulose: The Structure Slowly Unravels. *Cellulose* **1997,** *4*, 173-207.

(55) Bledzki, A.; Gassan, J. Composites Reinforced with Cellulose Based Fibres. *Prog. Polym. Sci.* **1999,** *24*, 221-274.

(56) Kargarzadeh, H.; Ahmad, I.; Abdullah, I.; Dufresne, A.; Zainudin, S. Y.; Sheltami, R. M. Effects of Hydrolysis Conditions on the Morphology, Crystallinity, and Thermal Stability of Cellulose Nanocrystals Extracted from Kenaf Bast Fibers. *Cellulose* **2012,** *19*, 855-866.

(57) Tang, J.; Sisler, J.; Grishkewich, N.; Tam, K. C. Functionalization of Cellulose Nanocrystals for Advanced Applications. *J. Colloid Interface Sci.* **2017,** *494*, 397-409.

(58) Lu, P.; Hsieh, Y.-L. Preparation and Properties of Cellulose Nanocrystals: Rods, Spheres, and Network. *Carbohydr. Polym.* **2010,** *82*, 329-336.

(59) Kaboorani, A.; Riedl, B. Surface Modification of Cellulose Nanocrystals (CNC) by a Cationic Surfactant. *Ind. Crops Prod.* **2015,** *65*, 45-55.

(60) Cao, Y.; Zavattieri, P.; Youngblood, J.; Moon, R.; Weiss, J. The Relationship between Cellulose Nanocrystal Dispersion and Strength. *Constr. Build. Mater.* **2016,** *119*, 71-79.

(61) Diesendruck, C. E.; Sottos, N. R.; Moore, J. S.; White, S. R. Biomimetic Self‐Healing. *Angew. Chem. Int. Ed.* **2015,** *54*, 10428-10447.

(62) Cremaldi, J. C.; Bhushan, B. Bioinspired Self-Healing Materials: Lessons from Nature. *Beilstein J. Nanotechnol.* **2018,** *9*, 907-935.

(63) Paul-Victor, C.; Dalle Vacche, S.; Sordo, F.; Fink, S.; Speck, T.; Michaud, V.; Speck, O. Effect of Mechanical Damage and Wound Healing on the Viscoelastic Properties of Stems of Flax Cultivars (Linum Usitatissimum L. Cv. Eden and Cv. Drakkar). *PLoS ONE* **2017,** *12*, e0185958.

(64) White, S. R.; Sottos, N.; Geubelle, P.; Moore, J.; Kessler, M. R.; Sriram, S.; Brown, E.; Viswanathan, S. Autonomic Healing of Polymer Composites. *Nature* **2001,** *409*, 794–797.

(65) Zwaag, S. Self Healing Materials: An Alternative Approach to 20 Centuries of Materials Science, Springer Science+ Business Media BV Dordrecht, The Netherlands: 2008.

(66) Saunders, L.; Ma, P. X. Self‐Healing Supramolecular Hydrogels for Tissue Engineering Applications. *Macromol. Biosci.* **2019,** *19*, 1800313.

(67) Liu, Y.; Hsu, S.-h. Synthesis and Biomedical Applications of Self-Healing Hydrogels. *Front. Chem.* **2018,** *6*, 1-10.

(68) Li, Q.; Liu, C.; Wen, J.; Wu, Y.; Shan, Y.; Liao, J. The Design, Mechanism and Biomedical Application of Self-Healing Hydrogels. *Chin. Chem. Lett.* **2017,** *28*, 1857-1874.

(69) Loebel, C.; Rodell, C. B.; Chen, M. H.; Burdick, J. A. Shear-Thinning and Self-Healing Hydrogels as Injectable Therapeutics and for 3D-Printing. *Nat. Protoc.* **2017,** *12*, 1521-1541.

(70) Kretlow, J. D.; Klouda, L.; Mikos, A. G. Injectable Matrices and Scaffolds for Drug Delivery in Tissue Engineering. *Adv. Drug Del. Rev.* **2007,** *59*, 263-273.

(71) Tseng, T. C.; Tao, L.; Hsieh, F. Y.; Wei, Y.; Chiu, I. M.; Hsu, S. h. An Injectable, Self‐Healing Hydrogel to Repair the Central Nervous System. *Adv. Mater.* **2015,** *27*, 3518-3524.

(72) Rosales, A. M.; Anseth, K. S. The Design of Reversible Hydrogels to Capture Extracellular Matrix Dynamics. *Nat. Rev. Mater.* **2016,** *1*, 15012.

(73) Wei, Z.; Gerecht, S. A Self-Healing Hydrogel as an Injectable Instructive Carrier for Cellular Morphogenesis. *Biomaterials* **2018,** *185*, 86-96.

(74) Highley, C. B.; Rodell, C. B.; Burdick, J. A. Direct 3D Printing of Shear‐Thinning Hydrogels into Self‐Healing Hydrogels. *Adv. Mater.* **2015,** *27*, 5075-5079.

(75) Paul, W.; Sharma, C. P. Chitosan and Alginate Wound Dressings: A Short Review. *Trends Biomater. Artif. Organs* **2004,** *18*, 18-23.

(76) Boateng, J. S.; Matthews, K. H.; Stevens, H. N.; Eccleston, G. M. Wound Healing Dressings and Drug Delivery Systems: A Review. *J. Pharm. Sci.* **2008,** *97*, 2892-2923.

(77) Qu, J.; Zhao, X.; Liang, Y.; Zhang, T.; Ma, P. X.; Guo, B. Antibacterial Adhesive Injectable Hydrogels with Rapid Self-Healing, Extensibility and Compressibility as Wound Dressing for Joints Skin Wound Healing. *Biomaterials* **2018,** *183*, 185-199.

(78) Ding, F.; Li, H.; Du, Y.; Shi, X. Recent Advances in Chitosan-Based Self-Healing Materials. *Res. Chem. Intermed.* **2018,** *44*, 4827–4840.

(79) Wang, Y.; Adokoh, C. K.; Narain, R. Recent Development and Biomedical Applications of Self-Healing Hydrogels. *Expert Opin. Drug Deliv.* **2018,** *15*, 77-91.

(80) Yang, Y.; Urban, M. W. Self-Healing Polymeric Materials. *Chem. Soc. Rev.* **2013,** *42*, 7446-7467.

(81) Ong, S.-Y.; Wu, J.; Moochhala, S. M.; Tan, M.-H.; Lu, J. Development of a Chitosan-Based Wound Dressing with Improved Hemostatic and Antimicrobial Properties. *Biomaterials* **2008,** *29*, 4323-4332.

(82) Rao, S. B.; Sharma, C. P. Use of Chitosan as a Biomaterial: Studies on Its Safety and Hemostatic Potential. *J. Biomed. Mater. Res. B* **1997,** *34*, 21-28.

(83) Peluso, G.; Petillo, O.; Ranieri, M.; Santin, M.; Ambrosic, L.; Calabró, D.; Avallone, B.; Balsamo, G. Chitosan-Mediated Stimulation of Macrophage Function. *Biomaterials* **1994,** *15*, 1215-1220.

(84) Jayakumar, R.; Prabaharan, M.; Kumar, P. S.; Nair, S.; Tamura, H. Biomaterials Based on Chitin and Chitosan in Wound Dressing Applications. *Biotechnol. Adv.* **2011,** *29*, 322-337.

(85) Miguel, S. P.; Ribeiro, M. P.; Brancal, H.; Coutinho, P.; Correia, I. J. Thermoresponsive Chitosan-Agarose Hydrogel for Skin Regeneration. *Carbohydr. Polym.* **2014,** *111*, 366-373.

(86) Zhang, Y.; Tao, L.; Li, S.; Wei, Y. Synthesis of Multiresponsive and Dynamic Chitosan-Based Hydrogels for Controlled Release of Bioactive Molecules. *Biomacromolecules* **2011,** *12*, 2894-2901.

(87) Zhang, Y.; Yang, B.; Zhang, X.; Xu, L.; Tao, L.; Li, S.; Wei, Y. A Magnetic Self-Healing Hydrogel. *Chem. Commun.* **2012,** *48*, 9305-9307.

(88) Xie, W.; Gao, Q.; Guo, Z.; Wang, D.; Gao, F.; Wang, X.; Wei, Y.; Zhao, L. Injectable and Self-Healing Thermosensitive Magnetic Hydrogel for Asynchronous Control Release of Doxorubicin and Docetaxel to Treat Triple-Negative Breast Cancer. *ACS Appl. Mater. Interfaces* **2017,** *9*, 33660-33673.

(89) Yang, B.; Zhang, Y.; Zhang, X.; Tao, L.; Li, S.; Wei, Y. Facilely Prepared Inexpensive and Biocompatible Self-Healing Hydrogel: A New Injectable Cell Therapy Carrier. *Polym. Chem.* **2012,** *3*, 3235-3238.

(90) Zhu, C.; Zhao, J.; Kempe, K.; Wilson, P.; Wang, J.; Velkov, T.; Li, J.; Davis, T. P.; Whittaker, M. R.; Haddleton, D. M. A Hydrogel‐Based Localized Release of Colistin for Antimicrobial Treatment of Burn Wound Infection. *Macromol. Biosci.* **2017,** *17*, 1600320.

(91) Li, Y.; Wang, X.; Fu, Y.-n.; Wei, Y.; Zhao, L.; Tao, L. Self-Adapting Hydrogel to Improve the Therapeutic Effect in Wound-Healing. *ACS Appl. Mater. Interfaces* **2018,** *10*, 26046-26055.

(92) Yang, L.; Li, Y.; Gou, Y.; Wang, X.; Zhao, X.; Tao, L. Improving Tumor Chemotherapy Effect Using an Injectable Self-Healing Hydrogel as Drug Carrier. *Polym. Chem.* **2017,** *8*, 5071-5076.

(93) Hsieh, F.-Y.; Han, H.-W.; Chen, X.-R.; Yang, C.-S.; Wei, Y.; Hsu, S.-h. Non-Viral Delivery of an Optogenetic Tool into Cells with Self-Healing Hydrogel. *Biomaterials* **2018,** *174*, 31-40.

(94) Hsieh, F.-Y.; Tao, L.; Wei, Y.; Hsu, S.-h. A Novel Biodegradable Self-Healing Hydrogel to Induce Blood Capillary Formation. *NPG Asia Mater.* **2017,** *9*, e363.

(95) Chen, G.; Ren, J.; Deng, Y.; Wu, X.; Huang, J.; Wang, G.; Zhao, Y.; Li, J. An Injectable, Wound-Adapting, Self-Healing Hydrogel for Fibroblast Growth Factor 2 Delivery System in Tissue Repair Applications. *J. Biomed. Nanotechnol.* **2017,** *13*, 1660-1672.

(96) Zhang, Y.; Fu, C.; Li, Y.; Wang, K.; Wang, X.; Wei, Y.; Tao, L. Synthesis of an Injectable, Self-Healable and Dual Responsive Hydrogel for Drug Delivery and 3D Cell Cultivation. *Polym. Chem.* **2017,** *8*, 537-544.

(97) Dong, R.; Zhao, X.; Guo, B.; Ma, P. X. Self-Healing Conductive Injectable Hydrogels with Antibacterial Activity as Cell Delivery Carrier for Cardiac Cell Therapy. *ACS Appl. Mater. Interfaces* **2016,** *8*, 17138-17150.

(98) Qu, J.; Zhao, X.; Ma, P. X.; Guo, B. pH-Responsive Self-Healing Injectable Hydrogel Based on N-Carboxyethyl Chitosan for Hepatocellular Carcinoma Therapy. *Acta Biomater.* **2017,** *58*, 168-180.

(99) Zhao, X.; Wu, H.; Guo, B.; Dong, R.; Qiu, Y.; Ma, P. X. Antibacterial Anti-Oxidant Electroactive Injectable Hydrogel as Self-Healing Wound Dressing with Hemostasis and Adhesiveness for Cutaneous Wound Healing. *Biomaterials* **2017,** *122*, 34-47.

(100) Guo, B.; Qu, J.; Zhao, X.; Zhang, M. Degradable Conductive Self-Healing Hydrogels Based on Dextran-Graft-Tetraaniline and N-Carboxyethyl Chitosan as Injectable Carrier for Myoblast Cell Therapy and Muscle Regeneration. *Acta Biomater.* **2019,** *84*, 180-193.

(101) Karimi, A. R.; Khodadadi, A. Mechanically Robust 3D Nanostructure Chitosan-Based Hydrogels with Autonomic Self-Healing Properties. *ACS Appl. Mater. Interfaces* **2016,** *8*, 27254-27263.

(102) Karimi, A. R.; Khodadadi, A.; Hadizadeh, M. A Nanoporous Photosensitizing Hydrogel Based on Chitosan Cross-Linked by Zinc Phthalocyanine: An Injectable and pH-Stimuli Responsive System for Effective Cancer Therapy. *RSC Adv.* **2016,** *6*, 91445-91452.

(103) Huang, W.; Wang, Y.; Chen, Y.; Zhao, Y.; Zhang, Q.; Zheng, X.; Chen, L.; Zhang, L. Strong and Rapidly Self‐Healing Hydrogels: Potential Hemostatic Materials. *Adv. Healthc. Mater.* **2016,** *5*, 2813-2822.

(104) Khan, M.; Koivisto, J. T.; Hukka, T. I.; Hokka, M.; Kellomäki, M. Composite Hydrogels Using Bioinspired Approach with *in situ* Fast Gelation and Self-Healing Ability as Future Injectable Biomaterial. *ACS Appl. Mater. Interfaces* **2018,** *10*, 11950-11960.

(105) Chen, G.; Yu, Y.; Wu, X.; Wang, G.; Ren, J.; Zhao, Y. Bioinspired Multifunctional Hybrid Hydrogel Promotes Wound Healing. *Adv. Funct. Mater.* **2018,** *28*, 1801386.

(106) Wei, Z.; Zhao, J.; Chen, Y. M.; Zhang, P.; Zhang, Q. Self-Healing Polysaccharide-Based Hydrogels as Injectable Carriers for Neural Stem Cells. *Sci. Rep.* **2016,** *6*, 37841.

(107) Wei, Z.; Lewis, D. M.; Xu, Y.; Gerecht, S. Dual Cross‐Linked Biofunctional and Self‐Healing Networks to Generate User‐Defined Modular Gradient Hydrogel Constructs. *Adv. Healthc. Mater.* **2017,** *6*, 1700523.

(108) Ding, F.; Shi, X.; Wu, S.; Liu, X.; Deng, H.; Du, Y.; Li, H. Flexible Polysaccharide Hydrogel with pH‐Regulated Recovery of Self‐Healing and Mechanical Properties. *Macromol. Mater. Eng.* **2017,** *302*, 1700221.

(109) Chen, J.; Li, S.; Zhang, Y.; Wang, W.; Zhang, X.; Zhao, Y.; Wang, Y.; Bi, H. A Reloadable Self‐Healing Hydrogel Enabling Diffusive Transport of C‐Dots across Gel-Gel Interface for Scavenging Reactive Oxygen Species. *Adv. Healthc. Mater.* **2017,** *6*, 1700746.

(110) Lü, S.; Gao, C.; Xu, X.; Bai, X.; Duan, H.; Gao, N.; Feng, C.; Xiong, Y.; Liu, M. Injectable and Self-Healing Carbohydrate-Based Hydrogel for Cell Encapsulation. *ACS Appl. Mater. Interfaces* **2015,** *7*, 13029-13037.

(111) Cho, I. S.; Ooya, T. An Injectable and Self-Healing Hydrogel for Spatiotemporal Protein Release Via Fragmentation after Passing through Needles. *J. Biomater. Sci. Polym. Ed.* **2018,** *29*, 145-159.

(112) Chen, H.; Cheng, J.; Ran, L.; Yu, K.; Lu, B.; Lan, G.; Dai, F.; Lu, F. An Injectable Self-Healing Hydrogel with Adhesive and Antibacterial Properties Effectively Promotes Wound Healing. *Carbohydr. Polym.* **2018,** *201*, 522-531.

(113) Qian, C.; Zhang, T.; Gravesande, J.; Baysah, C.; Song, X.; Xing, J. Injectable and Self-Healing Polysaccharide-Based Hydrogel for pH-Responsive Drug Release. *Int. J. Biol. Macromol.* **2019,** *123*, 140-148.

(114) Maity, S.; Datta, A.; Lahiri, S.; Ganguly, J. A Dynamic Chitosan-Based Self-Healing Hydrogel with Tunable Morphology and Its Application as an Isolating Agent. *RSC Adv.* **2016,** *6*, 81060-81068.

(115) Belali, S.; Emandi, G.; Cafolla, A. A.; O'Connell, B.; Haffner, B.; Möbius, M. E.; Karimi, A.; Senge, M. O. Water-Soluble, Neutral 3, 5-Diformyl-Bodipy with Extended Fluorescence Lifetime in a Self-Healable Chitosan Hydrogel. *Photochem. Photobiol. Sci.* **2017,** *16*, 1700-1708.

(116) Xu, C.; Zhan, W.; Tang, X.; Mo, F.; Fu, L.; Lin, B. Self-Healing Chitosan/Vanillin Hydrogels Based on Schiff-Base Bond/Hydrogen Bond Hybrid Linkages. *Polym. Test.* **2018,** *66*, 155-163.

(117) Liu, H.; Sui, X.; Xu, H.; Zhang, L.; Zhong, Y.; Mao, Z. Self‐Healing Polysaccharide Hydrogel Based on Dynamic Covalent Enamine Bonds. *Macromol. Mater. Eng.* **2016,** *301*, 725-732.

(118) Krogsgaard, M.; Hansen, M. R.; Birkedal, H. Metals & Polymers in the Mix: Fine-Tuning the Mechanical Properties & Color of Self-Healing Mussel-Inspired Hydrogels. *J. Mater. Chem. B* **2014,** *2*, 8292-8297.

(119) Yavvari, P. S.; Srivastava, A. Robust, Self-Healing Hydrogels Synthesised from Catechol Rich Polymers. *J. Mater. Chem. B* **2015,** *3*, 899-910.

(120) Yavvari, P. S.; Pal, S.; Kumar, S.; Kar, A.; Awasthi, A. K.; Naaz, A.; Srivastava, A.; Bajaj, A. Injectable, Self-Healing Chimeric Catechol-Fe Hydrogel for Localized Combination Cancer Therapy. *ACS Biomater. Sci. Eng.* **2017,** *3*, 3404-3413.

(121) Darabi, M. A.; Khosrozadeh, A.; Mbeleck, R.; Liu, Y.; Chang, Q.; Jiang, J.; Cai, J.; Wang, Q.; Luo, G.; Xing, M. Skin‐Inspired Multifunctional Autonomic‐Intrinsic Conductive Self‐Healing Hydrogels with Pressure Sensitivity, Stretchability, and 3D Printability. *Adv. Mater.* **2017,** *29*, 1700533.

(122) Kang, M.; Liu, S.; Oderinde, O.; Yao, F.; Fu, G.; Zhang, Z. Template Method for Dual Network Self-Healing Hydrogel with Conductive Property. *Mater. Des.* **2018,** *148*, 96-103.

(123) Wang, X.-H.; Song, F.; Qian, D.; He, Y.-D.; Nie, W.-C.; Wang, X.-L.; Wang, Y.-Z. Strong and Tough Fully Physically Crosslinked Double Network Hydrogels with Tunable Mechanics and High Self-Healing Performance. *Chem. Eng. J.* **2018,** *349*, 588-594.

(124) Wahid, F.; Zhou, Y.-N.; Wang, H.-S.; Wan, T.; Zhong, C.; Chu, L.-Q. Injectable Self-Healing Carboxymethyl Chitosan-Zinc Supramolecular Hydrogels and Their Antibacterial Activity. *Int. J. Biol. Macromol.* **2018,** *114*, 1233-1239.

(125) Azevedo, S.; Costa, A. M.; Andersen, A.; Choi, I. S.; Birkedal, H.; Mano, J. F. Bioinspired Ultratough Hydrogel with Fast Recovery, Self‐Healing, Injectability and Cytocompatibility. *Adv. Mater.* **2017,** *29*, 1700759.

(126) Li, S.; Wang, L.; Yu, X.; Wang, C.; Wang, Z. Synthesis and Characterization of a Novel Double Cross-Linked Hydrogel Based on Diels-Alder Click Reaction and Coordination Bonding. *Mater. Sci. Eng. C.* **2018,** *82*, 299-309.

(127) Chang, G.; Chen, Y.; Li, Y.; Li, S.; Huang, F.; Shen, Y.; Xie, A. Self-Healable Hydrogel on Tumor Cell as Drug Delivery System for Localized and Effective Therapy. *Carbohydr. Polym.* **2015,** *122*, 336-342.

(128) Zhang, Z.; Li, T.; Chen, B.; Wang, S.; Guo, Z. Self-Healing Supramolecular Hydrogel of Poly (vinyl alcohol)/Chitosan Carbon Dots. *J. Mater. Sci.* **2017,** *52*, 10614-10623.

(129) Konwar, A.; Kalita, S.; Kotoky, J.; Chowdhury, D. Chitosan–Iron Oxide Coated Graphene Oxide Nanocomposite Hydrogel: A Robust and Soft Antimicrobial Biofilm. *ACS Appl. Mater. Interfaces* **2016,** *8*, 20625-20634.

(130) Han, D.; Yan, L. Supramolecular Hydrogel of Chitosan in the Presence of Graphene Oxide Nanosheets as 2D Cross-Linkers. *ACS Sustain. Chem. Eng.* **2013,** *2*, 296-300.

(131) Jing, X.; Mi, H.-Y.; Napiwocki, B. N.; Peng, X.-F.; Turng, L.-S. Mussel-Inspired Electroactive Chitosan/Graphene Oxide Composite Hydrogel with Rapid Self-Healing and Recovery Behavior for Tissue Engineering. *Carbon* **2017,** *125*, 557-570.

(132) Li, Y.-K.; Guo, C.-G.; Wang, L.; Xu, Y.; Liu, C.-y.; Wang, C.-Q. A Self-Healing and Multi-Responsive Hydrogel Based on Biodegradable Ferrocene-Modified Chitosan. *RSC Adv.* **2014,** *4*, 55133-55138.

(133) Ren, Y.; Lou, R.; Liu, X.; Gao, M.; Zheng, H.; Yang, T.; Xie, H.; Yu, W.; Ma, X. A Self-Healing Hydrogel Formation Strategy Via Exploiting Endothermic Interactions between Polyelectrolytes. *Chem. Commun.* **2016,** *52*, 6273-6276.

(134) Harris, J. M. Poly (Ethylene Glycol) Chemistry: Biotechnical and Biomedical Applications, Springer Science & Business Media: 2013.

(135) Ding, F.; Wu, S.; Wang, S.; Xiong, Y.; Li, Y.; Li, B.; Deng, H.; Du, Y.; Xiao, L.; Shi, X. A Dynamic and Self-Crosslinked Polysaccharide Hydrogel with Autonomous Self-Healing Ability. *Soft Matter* **2015,** *11*, 3971-3976.

(136) Lopez-Perez, P. M.; da Silva, R. M.; Strehin, I.; Kouwer, P. H.; Leeuwenburgh, S. C.; Messersmith, P. B. Self-Healing Hydrogels Formed by Complexation between Calcium Ions and Bisphosphonate-Functionalized Star-Shaped Polymers. *Macromolecules* **2017,** *50*, 8698-8706.

(137) Drury, J. L.; Mooney, D. J. Hydrogels for Tissue Engineering: Scaffold Design Variables and Applications. *Biomaterials* **2003,** *24*, 4337-4351.

(138) Tan, H.; Chu, C. R.; Payne, K. A.; Marra, K. G. Injectable in Situ Forming Biodegradable Chitosan-Hyaluronic Acid Based Hydrogels for Cartilage Tissue Engineering. *Biomaterials* **2009,** *30*, 2499-2506.

(139) Zhao, X.; Li, P.; Guo, B.; Ma, P. X. Antibacterial and Conductive Injectable Hydrogels Based on Quaternized Chitosan-Graft-Polyaniline/Oxidized Dextran for Tissue Engineering. *Acta Biomater.* **2015,** *26*, 236-248.

(140) Huang, W.; Wang, Y.; Huang, Z.; Wang, X.; Chen, L.; Zhang, Y.; Zhang, L. On-Demand Dissolvable Self-Healing Hydrogels Based on Carboxymethyl Chitosan and Cellulose Nanocrystal for Deep Partial Thickness Burn Wound Healing. *ACS Appl. Mater. Interfaces* **2018,** *10*, 41076–41088.

(141) You, B.; Li, Q.; Dong, H.; Huang, T.; Cao, X.; Liao, H. Bilayered HA/CS/PEGDA Hydrogel with Good Biocompatibility and Self-Healing Property for Potential Application in Osteochondral Defect Repair. *J. Mater. Sci. Technol.* **2018,** *34*, 1016-1025.

(142) Sanchez-Sanchez, A.; Fulton, D. A.; Pomposo, J. A. pH-Responsive Single-Chain Polymer Nanoparticles Utilising Dynamic Covalent Enamine Bonds. *Chem. Commun.* **2014,** *50*, 1871-1874.

(143) Harrington, M. J.; Masic, A.; Holten-Andersen, N.; Waite, J. H.; Fratzl, P. Iron-Clad Fibers: A Metal-Based Biological Strategy for Hard Flexible Coatings. *Science* **2010,** *328*, 216-220.

(144) Holten-Andersen, N.; Harrington, M. J.; Birkedal, H.; Lee, B. P.; Messersmith, P. B.; Lee, K. Y. C.; Waite, J. H. pH-Induced Metal-Ligand Cross-Links Inspired by Mussel Yield Self-Healing Polymer Networks with near-Covalent Elastic Moduli. *Proc. Natl. Acad. Sci. U. S. A.* **2011,** *108*, 2651-2655.

(145) Phadke, A.; Zhang, C.; Arman, B.; Hsu, C.-C.; Mashelkar, R. A.; Lele, A. K.; Tauber, M. J.; Arya, G.; Varghese, S. Rapid Self-Healing Hydrogels. *Proc. Natl. Acad. Sci. U. S. A.* **2012,** *109*, 4383-4388.

(146) Nakahata, M.; Takashima, Y.; Yamaguchi, H.; Harada, A. Redox-Responsive Self-Healing Materials Formed from Host-Guest Polymers. *Nat. Commun.* **2011,** *2*, 511.

(147) Belali, S.; Karimi, A. R.; Hadizadeh, M. Cell-Specific and pH-Sensitive Nanostructure Hydrogel Based on Chitosan as a Photosensitizer Carrier for Selective Photodynamic Therapy. *Int. J. Biol. Macromol.* **2018,** *110*, 437-448.

(148) Yuk, H.; Zhang, T.; Parada, G. A.; Liu, X.; Zhao, X. Skin-Inspired Hydrogel-Elastomer Hybrids with Robust Interfaces and Functional Microstructures. *Nat. Commun.* **2016,** *7*, 12028.

(149) Dufresne, A. Interfacial Phenomena in Nanocomposites Based on Polysaccharide Nanocrystals. *Compos. Interfaces* **2003,** *10*, 369-387.

(150) Ooi, S. Y.; Ahmad, I.; Amin, M. C. I. M. Cellulose Nanocrystals Extracted from Rice Husks as a Reinforcing Material in Gelatin Hydrogels for Use in Controlled Drug Delivery Systems. *Ind. Crops Prod.* **2016,** *93*, 227-234.

(151) Savoie, D. Nanocrystalline Cellulose Is Breathing New Life into Canada's Forest Industry. https://www.universityaffairs.ca/news/news-article/nanocrystalline-cellulose-is-breathing-new-life-into-canadas-forest-industry/ (accessed Aug 31, 2011).

(152) Kim, U.-J.; Kuga, S.; Wada, M.; Okano, T.; Kondo, T. Periodate Oxidation of Crystalline Cellulose. *Biomacromolecules* **2000,** *1*, 488-492.

(153) Hu, J.; Quan, Y.; Lai, Y.; Zheng, Z.; Hu, Z.; Wang, X.; Dai, T.; Zhang, Q.; Cheng, Y. A Smart Aminoglycoside Hydrogel with Tunable Gel Degradation, on-Demand Drug Release, and High Antibacterial Activity. *J. Control. Release.* **2017,** *247*, 145-152.

(154) Dash, R.; Foston, M.; Ragauskas, A. J. Improving the Mechanical and Thermal Properties of Gelatin Hydrogels Cross-Linked by Cellulose Nanowhiskers. *Carbohydr. Polym.* **2013,** *91*, 638-645.

(155) Gong, J. P. Why Are Double Network Hydrogels So Tough? *Soft Matter* **2010,** *6*, 2583-2590.

(156) Nakajima, T.; Furukawa, H.; Tanaka, Y.; Kurokawa, T.; Osada, Y.; Gong, J. P. True Chemical Structure of Double Network Hydrogels. *Macromolecules* **2009,** *42*, 2184-2189.

(157) Sun, J.-Y.; Zhao, X.; Illeperuma, W. R.; Chaudhuri, O.; Oh, K. H.; Mooney, D. J.; Vlassak, J. J.; Suo, Z. Highly Stretchable and Tough Hydrogels. *Nature* **2012,** *489*, 133-136.

(158) Li, X.; Yang, Q.; Zhao, Y.; Long, S.; Zheng, J. Dual Physically Crosslinked Double Network Hydrogels with High Toughness and Self-Healing Properties. *Soft Matter* **2017,** *13*, 911-920.

(159) Gong, Z.; Zhang, G.; Zeng, X.; Li, J.; Li, G.; Huang, W.; Sun, R.; Wong, C. High-Strength, Tough, Fatigue Resistant, and Self-Healing Hydrogel Based on Dual Physically Cross-Linked Network. *ACS Appl. Mater. Interfaces* **2016,** *8*, 24030-24037.

(160) Jeon, I.; Cui, J.; Illeperuma, W. R.; Aizenberg, J.; Vlassak, J. J. Extremely Stretchable and Fast Self‐Healing Hydrogels. *Adv. Mater.* **2016,** *28*, 4678-4683.

(161) Shao, C.; Wang, M.; Chang, H.; Xu, F.; Yang, J. A Self-Healing Cellulose Nanocrystals-Poly (ethylene glycol) Nanocomposite Hydrogel Via Diels-Alder Click Reaction. *ACS Sustain. Chem. Eng.* **2017,** *5*, 6167-6174.

(162) Lee, J.; Song, B.; Subbiah, R.; Chung, J. J.; Choi, U. H.; Park, K.; Kim, S.-H.; Oh, S. J. Effect of Chain Flexibility on Cell Adhesion: Semi-Flexible Model-based Analysis of Cell Adhesion to Hydrogels. *Sci. Rep.* **2019,** *9*, 2463.

(163) Jin, R.; Teixeira, L. M.; Dijkstra, P. J.; Karperien, M.; Van Blitterswijk, C.; Zhong, Z.; Feijen, J. Injectable Chitosan-based Hydrogels for Cartilage Tissue Engineering. *Biomaterials* **2009,** *30*, 2544-2551.

(164) Yesilyurt, V.; Webber, M. J.; Appel, E. A.; Godwin, C.; Langer, R.; Anderson, D. G. Injectable Self‐Healing Glucose‐Responsive Hydrogels with pH‐Regulated Mechanical Properties. *Adv. Mater.* **2016,** *28*, 86-91.

(165) Sharabi, M.; Mandelberg, Y.; Benayahu, D.; Benayahu, Y.; Azem, A.; Haj-Ali, R. A New Class of Bio-Composite Materials of Unique Collagen Fibers. *J. Mech. Behav. Biomed. Mater.* **2014,** *36*, 71-81.

(166) Drury, J. L.; Dennis, R. G.; Mooney, D. J. The Tensile Properties of Alginate Hydrogels. *Biomaterials* **2004,** *25*, 3187-3199.

(167) Luo, F.; Sun, T. L.; Nakajima, T.; Kurokawa, T.; Zhao, Y.; Sato, K.; Ihsan, A. B.; Li, X.; Guo, H.; Gong, J. P. Oppositely Charged Polyelectrolytes Form Tough, Self‐Healing, and Rebuildable Hydrogels. *Adv. Mater.* **2015,** *27*, 2722-2727.

(168) Jenkins, L. E.; Davis, L. S. Comprehensive Review of Tissue Adhesives. *Dermatol. Surg.* **2018,** *44*, 1367-1372.

(169) Spotnitz, W. D. Fibrin Sealant: Past, Present, and Future: A Brief Review. *World J. Surg.* **2010,** *34*, 632-634.

(170) Edwards, S.; Parkinson, L. Is Fixing Pediatric Nail Bed Injuries with Medical Adhesives as Effective as Suturing?: A Review of the Literature. *Pediatr. Emerg. Care* **2019,** *35*, 75-77.

(171) Trott, A. T. Cyanoacrylate Tissue Adhesives: An Advance in Wound Care. *JAMA* **1997,** *277*, 1559-1560.

(172) Lehman, R. A.; Hayes, G. J. The Toxicity of Alkyl 2-Cyanoacrylate Tissue Adhesives: Brain and Blood Vessels. *Surgery* **1967,** *61*, 915-922.

(173) Leggat, P. A.; Smith, D. R.; Kedjarune, U. Surgical Applications of Cyanoacrylate Adhesives: A Review of Toxicity. *ANZ J. Surg.* **2007,** *77*, 209-213.

(174) Siedentop, K. H.; Park, J. J.; Shah, A. N.; Bhattacharyya, T. K.; O'Grady, K. M. Safety and Efficacy of Currently Available Fibrin Tissue Adhesives. *Am. J. Otolaryngol.* **2001,** *22*, 230-235.

(175) Mahdavi, A.; Ferreira, L.; Sundback, C.; Nichol, J. W.; Chan, E. P.; Carter, D. J.; Bettinger, C. J.; Patanavanich, S.; Chignozha, L.; Ben-Joseph, E. A Biodegradable and Biocompatible Gecko-Inspired Tissue Adhesive. *Proc. Natl. Acad. Sci. U. S. A.* **2008,** *105*, 2307-2312.

(176) Waite, J. H.; Qin, X. Polyphosphoprotein from the Adhesive Pads of *Mytilus Edulis*. *Biochemistry* **2001,** *40*, 2887-2893.

(177) Li, J.; Celiz, A.; Yang, J.; Yang, Q.; Wamala, I.; Whyte, W.; Seo, B.; Vasilyev, N.; Vlassak, J.; Suo, Z. Tough Adhesives for Diverse Wet Surfaces. *Science* **2017,** *357*, 378-381.

(178) Guvendiren, M.; Lu, H. D.; Burdick, J. A. Shear-Thinning Hydrogels for Biomedical Applications. *Soft Matter* **2012,** *8*, 260-272.

(179) Zhang, H.; Xia, H.; Zhao, Y. Poly (vinyl alcohol) Hydrogel Can Autonomously Self-Heal. *ACS Macro Lett.* **2012,** *1*, 1233-1236.

(180) Tibbitt, M. W.; Anseth, K. S. Hydrogels as Extracellular Matrix Mimics for 3D Cell Culture. *Biotechnol. Bioeng.* **2009,** *103*, 655-663.

(181) Wei, Z.; Yang, J. H.; Du, X. J.; Xu, F.; Zrinyi, M.; Osada, Y.; Li, F.; Chen, Y. M. Dextran‐Based Self‐Healing Hydrogels Formed by Reversible Diels-Alder Reaction under Physiological Conditions. *Macromol. Rapid Commun.* **2013,** *34*, 1464-1470.

(182) Li, Y.; Zhang, Y.; Shi, F.; Tao, L.; Wei, Y.; Wang, X. Modulus-Regulated 3D-Cell Proliferation in an Injectable Self-Healing Hydrogel. *Colloids Surf. B. Biointerfaces* **2017,** *149*, 168-173.

(183) Wedmore, I.; McManus, J. G.; Pusateri, A. E.; Holcomb, J. B. A Special Report on the Chitosan-Based Hemostatic Dressing: Experience in Current Combat Operations. *J. Trauma Acute Care Surg.* **2006,** *60*, 655-658.

(184) Kauvar, D. S.; Lefering, R.; Wade, C. E. Impact of Hemorrhage on Trauma Outcome: An Overview of Epidemiology, Clinical Presentations, and Therapeutic Considerations. *J. Trauma Acute Care Surg.* **2006,** *60*, S3-S11.

(185) McManus, J. G.; Eastridge, B. J.; Wade, C. E.; Holcomb, J. B. Hemorrhage Control Research on Today's Battlefield: Lessons Applied. *J. Trauma Acute Care Surg.* **2007,** *62*, S14.

(186) Hoffman, A. S. Hydrogels for Biomedical Applications. *Adv. Drug Del. Rev.* **2012,** *64*, 18-23.

(187) Hou, S.; Wang, X.; Park, S.; Jin, X.; Ma, P. X. Rapid Self‐Integrating, Injectable Hydrogel for Tissue Complex Regeneration. *Adv. Healthc. Mater.* **2015,** *4*, 1491-1495.

(188) Liu, H.; Liu, J.; Qi, C.; Fang, Y.; Zhang, L.; Zhuo, R.; Jiang, X. Thermosensitive Injectable *in-situ* Forming Carboxymethyl Chitin Hydrogel for Three-Dimensional Cell Culture. *Acta Biomater.* **2016,** *35*, 228-237.

(189) Suh, J.-K. F.; Matthew, H. W. Application of Chitosan-Based Polysaccharide Biomaterials in Cartilage Tissue Engineering: A Review. *Biomaterials* **2000,** *21*, 2589-2598.

(190) Rao, S. B.; Sharma, C. P. Use of Chitosan as a Biomaterial: Studies on Its Safety and Hemostatic Potential. *J. Biomed. Mater. Res.* **1997,** *34*, 21-28.

(191) Sakai, T.; Akagi, Y.; Matsunaga, T.; Kurakazu, M.; Chung, U. i.; Shibayama, M. Highly Elastic and Deformable Hydrogel Formed from Tetra‐arm Polymers. *Macromol. Rapid Commun.* **2010,** *31*, 1954-1959.

(192) Fujii, K.; Asai, H.; Ueki, T.; Sakai, T.; Imaizumi, S.; Chung, U.-i.; Watanabe, M.; Shibayama, M. High-Performance Ion Gel with Tetra-PEG Network. *Soft Matter* **2012,** *8*, 1756-1759.

(193) Naficy, S.; Brown, H. R.; Razal, J. M.; Spinks, G. M.; Whitten, P. G. Progress toward Robust Polymer Hydrogels. *Aust. J. Chem.* **2011,** *64*, 1007-1025.

(194) Akagi, Y.; Matsunaga, T.; Shibayama, M.; Chung, U.-i.; Sakai, T. Evaluation of Topological Defects in Tetra-PEG Gels. *Macromolecules* **2009,** *43*, 488-493.

(195) Chen, X.-G.; Park, H.-J. Chemical Characteristics of O-Carboxymethyl Chitosans Related to the Preparation Conditions. *Carbohydr. Polym.* **2003,** *53*, 355-359.

(196) Grover, G. N.; Braden, R. L.; Christman, K. L. Oxime Cross‐Linked Injectable Hydrogels for Catheter Delivery. *Adv. Mater.* **2013,** *25*, 2937-2942.

(197) Kumar, V. A.; Wickremasinghe, N. C.; Shi, S.; Hartgerink, J. D. Nanofibrous Snake Venom Hemostat. *ACS Biomater. Sci. Eng.* **2015,** *1*, 1300-1305.

(198) Kakuta, T.; Takashima, Y.; Nakahata, M.; Otsubo, M.; Yamaguchi, H.; Harada, A. Preorganized Hydrogel: Self‐Healing Properties of Supramolecular Hydrogels Formed by Polymerization of Host-Guest‐Monomers That Contain Cyclodextrins and Hydrophobic Guest Groups. *Adv. Mater.* **2013,** *25*, 2849-2853.

(199) Watarai, A.; Schirmer, L.; Thönes, S.; Freudenberg, U.; Werner, C.; Simon, J. C.; Anderegg, U. TGFβ Functionalized Starpeg-Heparin Hydrogels Modulate Human Dermal Fibroblast Growth and Differentiation. *Acta Biomater.* **2015,** *25*, 65-75.

(200) Mothe, A. J.; Tam, R. Y.; Zahir, T.; Tator, C. H.; Shoichet, M. S. Repair of the Injured Spinal Cord by Transplantation of Neural Stem Cells in a Hyaluronan-Based Hydrogel. *Biomaterials* **2013,** *34*, 3775-3783.

(201) Sharma, B.; Fermanian, S.; Gibson, M.; Unterman, S.; Herzka, D. A.; Cascio, B.; Coburn, J.; Hui, A. Y.; Marcus, N.; Gold, G. E. Human Cartilage Repair with a Photoreactive Adhesive-Hydrogel Composite. *Sci. Transl. Med.* **2013,** *5*, 167ra6.

(202) Kumar, M. R.; Muzzarelli, R. A.; Muzzarelli, C.; Sashiwa, H.; Domb, A. Chitosan Chemistry and Pharmaceutical Perspectives. *Chem. Rev.* **2004,** *104*, 6017-6084.

(203) Burns. World Health Organization.
http://www.who.int/violence_injury_prevention/other_injury/burns/en/

(204) Kowalske, K. J. Burn Wound Care. *Phys. Med. Rehabil. Clin.* **2011,** *22*, 213-227.

(205) Xu, H. L.; Chen, P. P.; ZhuGe, D. L.; Zhu, Q. Y.; Jin, B. H.; Shen, B. X.; Xiao, J.; Zhao, Y. Z. Liposomes with Silk Fibroin Hydrogel Core to Stabilize bFGF and Promote the Wound Healing of Mice with Deep Second‐Degree Scald. *Adv. Healthc. Mater.* **2017,** *6*, 1700344.

(206) Rowan, M. P.; Cancio, L. C.; Elster, E. A.; Burmeister, D. M.; Rose, L. F.; Natesan, S.; Chan, R. K.; Christy, R. J.; Chung, K. K. Burn Wound Healing and Treatment: Review and Advancements. *Crit. Care* **2015,** *19*, 243.

(207) Madaghiele, M.; Demitri, C.; Sannino, A.; Ambrosio, L. Polymeric Hydrogels for Burn Wound Care: Advanced Skin Wound Dressings and Regenerative Templates. *Burns Trauma* **2014,** *2*, 153-161.

(208) How Often Should I Change Dressing on a Wound. World Care Society. http://woundcaresociety.org/how-often-should-i-change-dressing-on-a-wound (accessed September 6, 2015).

(209) Mohanty, A. K.; Misra, M.; Drzal, L. Sustainable Bio-Composites from Renewable Resources: Opportunities and Challenges in the Green Materials World. *J. Polym. Environ.* **2002,** *10*, 19-26.

(210) Rosenberg, A.; Fogarty, M.; Sissenwine, M.; Beddington, J.; Shepherd, J. Achieving Sustainable Use of Renewable Resources. *Science* **1993,** *262*, 828-829.

(211) Olivetti, E. A.; Cullen, J. M. Toward a Sustainable Materials System. *Science* **2018,** *360*, 1396-1398.

(212) Duan, B.; Huang, Y.; Lu, A.; Zhang, L. Recent Advances in Chitin Based Materials Constructed Via Physical Methods. *Prog. Polym. Sci.* **2018,** *82*, 1-33.

(213) Croisier, F.; Jérôme, C. Chitosan-Based Biomaterials for Tissue Engineering. *Eur. Polym. J.* **2013,** *49*, 780-792.

(214) Grishkewich, N.; Mohammed, N.; Tang, J.; Tam, K. C. Recent Advances in the Application of Cellulose Nanocrystals. *Curr. Opin. Colloid Interface Sci.* **2017,** *29*, 32-45.

(215) Lam, E.; Male, K. B.; Chong, J. H.; Leung, A. C.; Luong, J. H. Applications of Functionalized and Nanoparticle-Modified Nanocrystalline Cellulose. *Trends Biotechnol.* **2012,** *30*, 283-290.

(216) Xie, D.-y.; Qian, D.; Song, F.; Wang, X.-L.; Wang, Y.-Z. A Fully Bio-Based Encapsulant Constructed by Soy Protein and Cellulose Nanocrystal for Flexible Electromechanical Sensing. *ACS Sustain. Chem. Eng.* **2017,** *5*, 7063-7070.

(217) Sun, T.; Xu, P.; Liu, Q.; Xue, J.; Xie, W. Graft Copolymerization of Methacrylic Acid onto Carboxymethyl Chitosan. *Eur. Polym. J.* **2003,** *39*, 189-192.

(218) Chen, L.; Tian, Z.; Du, Y. Synthesis and pH Sensitivity of Carboxymethyl Chitosan-Based Polyampholyte Hydrogels for Protein Carrier Matrices. *Biomaterials* **2004,** *25*, 3725-3732.

(219) García-Zamora, J. L.; Sánchez-González, M.; Lozano, J. A.; Jáuregui, J.; Zayas, T.; Santacruz, V.; Hernández, F.; Torres, E. Enzymatic Treatment of Wastewater from the Corn Tortilla Industry Using Chitosan as an Adsorbent Reduces the Chemical Oxygen Demand and Ferulic Acid Content. *Process Biochem.* **2015,** *50*, 125-133.

(220) Hermanson, G. T. *Bioconjugate Techniques*, Academic press: 1996.

(221) Hjerde, R. J. N.; Vårum, K. M.; Grasdalen, H.; Tokura, S.; Smidsrød, O. Chemical Composition of O-(Carboxymethyl)-Chitins in Relation to Lysozyme Degradation Rates. *Carbohydr. Polym.* **1997,** *34*, 131-139.

(222) Sun, B.; Hou, Q.; Liu, Z.; Ni, Y. Sodium Periodate Oxidation of Cellulose Nanocrystal and Its Application as a Paper Wet Strength Additive. *Cellulose* **2015,** *22*, 1135-1146.

(223) Dash, R.; Ragauskas, A. J. Synthesis of a Novel Cellulose Nanowhisker-Based Drug Delivery System. *RSC Adv.* **2012,** *2*, 3403-3409.

(224) Kim, U.-J.; Wada, M.; Kuga, S. Solubilization of Dialdehyde Cellulose by Hot Water. *Carbohydr. Polym.* **2004,** *56*, 7-10.

(225) Jin, R.; Teixeira, L. M.; Krouwels, A.; Dijkstra, P. J.; Van Blitterswijk, C.; Karperien, M.; Feijen, J. Synthesis and Characterization of Hyaluronic Acid-Poly (ethylene glycol) Hydrogels via Michael Addition: An Injectable Biomaterial for Cartilage Repair. *Acta Biomater.* **2010,** *6*, 1968-1977.

(226) Wang, Y.; Chen, L. Cellulose Nanowhiskers and Fiber Alignment Greatly Improve Mechanical Properties of Electrospun Prolamin Protein Fibers. *ACS Appl. Mater. Interfaces* **2014,** *6*, 1709-1718.

(227) Huang, W.; Wang, Y.; Zhang, L.; Chen, L. Rapid Dissolution of Spruce Cellulose in H_2SO_4 Aqueous Solution at Low Temperature. *Cellulose* **2016,** *23*, 3463-3473.

(228) Singh, M.; Kaushik, A.; Ahuja, D. Surface Functionalization of Nanofibrillated Cellulose Extracted from Wheat Straw: Effect of Process Parameters. *Carbohydr. Polym.* **2016,** *150*, 48-56.

(229) Yang, X.; Liu, G.; Peng, L.; Guo, J.; Tao, L.; Yuan, J.; Chang, C.; Wei, Y.; Zhang, L. Highly Efficient Self‐Healable and Dual Responsive Cellulose‐Based Hydrogels for Controlled Release and 3D Cell Culture. *Adv. Funct. Mater.* **2017,** *27*.

(230) Mukherjee, S.; Hill, M. R.; Sumerlin, B. S. Self-Healing Hydrogels Containing Reversible Oxime Crosslinks. *Soft Matter* **2015,** *11*, 6152-6161.

(231) Konieczynska, M. D.; Villa‐Camacho, J. C.; Ghobril, C.; Perez‐Viloria, M.; Tevis, K. M.; Blessing, W. A.; Nazarian, A.; Rodriguez, E. K.; Grinstaff, M. W. On‐Demand Dissolution of a Dendritic Hydrogel‐Based Dressing for Second‐Degree Burn Wounds through Thiol-Thioester Exchange Reaction. *Angew. Chem. Int. Ed.* **2016,** *55*, 9984-9987.

(232) Bu, Y.-z.; Sun, G.-f.; Zhang, L.-c.; Liu, J.-h.; Yang, F.; Tang, P.-f.; Wu, D.-c. POSS-Modified PEG Adhesives for Wound Closure. *Chin. J. Polym. Sci.* **2017,** *35*, 1231-1242.

(233) Ghobril, C.; Charoen, K.; Rodriguez, E. K.; Nazarian, A.; Grinstaff, M. W. A Dendritic Thioester Hydrogel Based on Thiol-Thioester Exchange as a Dissolvable Sealant System for Wound Closure. *Angew. Chem. Int. Ed.* **2013,** *52*, 14070-14074.

(234) Sirvio, J.; Hyvakko, U.; Liimatainen, H.; Niinimaki, J.; Hormi, O. Periodate Oxidation of Cellulose at Elevated Temperatures Using Metal Salts as Cellulose Activators. *Carbohydr. Polym.* **2011,** *83*, 1293-1297.

(235) Sirviö, J.; Liimatainen, H.; Niinimäki, J.; Hormi, O. Dialdehyde Cellulose Microfibers Generated from Wood Pulp by Milling-Induced Periodate Oxidation. *Carbohydr. Polym.* **2011,** *86*, 260-265.

(236) Zhou, C.; Wu, Q.; Yue, Y.; Zhang, Q. Application of Rod-Shaped Cellulose Nanocrystals in Polyacrylamide Hydrogels. *J. Colloid Interface Sci.* **2011,** *353*, 116-123.

(237) Discher, D. E.; Mooney, D. J.; Zandstra, P. W. Growth Factors, Matrices, and Forces Combine and Control Stem Cells. *Science* **2009,** *324*, 1673-1677.

(238) Nimmo, C. M.; Owen, S. C.; Shoichet, M. S. Diels-Alder Click Cross-Linked Hyaluronic Acid Hydrogels for Tissue Engineering. *Biomacromolecules* **2011,** *12*, 824-830.

(239) Bodenberger, N.; Paul, P.; Kubiczek, D.; Walther, P.; Gottschalk, K. E.; Rosenau, F. A Novel Cheap and Easy to Handle Protein Hydrogel for 3D Cell Culture Applications: A High Stability Matrix with Tunable Elasticity and Cell Adhesion Properties. *ChemistrySelect* **2016,** *1*, 1353-1360.

(240) Zhang, T.; Zuo, T.; Hu, D.; Chang, C. Dual Physically Cross-Linked Nanocomposite Hydrogels Reinforced by Tunicate Cellulose Nanocrystals with High Toughness and Good Self-Recoverability. *ACS Appl. Mater. Interfaces* **2017,** *9*, 24230-24237.

(241) Liu, H.; Li, C.; Wang, B.; Sui, X.; Wang, L.; Yan, X.; Xu, H.; Zhang, L.; Zhong, Y.; Mao, Z. Self-Healing and Injectable Polysaccharide Hydrogels with Tunable Mechanical Properties. *Cellulose* **2018**, 1-13.

(242) Shao, C.; Wang, M.; Chang, H.; Xu, F.; Yang, J. A Self-Healing Cellulose Nanocrystal-Poly (ethylene glycol) Nanocomposite Hydrogel Via Diels-Alder Click Reaction. *ACS Sustain. Chem. Eng.* **2017,** *5*, 6167-6174.

(243) Fan, Z.; Liu, B.; Wang, J.; Zhang, S.; Lin, Q.; Gong, P.; Ma, L.; Yang, S. A Novel Wound Dressing Based on Ag/Graphene Polymer Hydrogel: Effectively Kill Bacteria and Accelerate Wound Healing. *Adv. Funct. Mater.* **2014,** *24*, 3933-3943.

(244) Lin, N.; Dufresne, A. Supramolecular Hydrogels from in Situ Host–Guest Inclusion between Chemically Modified Cellulose Nanocrystals and Cyclodextrin. *Biomacromolecules* **2013,** *14*, 871-880.

(245) Zhou, L.; Chen, M.; Guan, Y.; Zhang, Y. Multiple Responsive Hydrogel Films Based on Dynamic Schiff Base Linkages. *Polym. Chem.* **2014,** *5*, 7081-7089.

(246) Barbul, A.; Lazarou, S. A.; Efron, D. T.; Wasserkrug, H. L.; Efron, G. Arginine Enhances Wound Healing and Lymphocyte Immune Responses in Humans. *Surgery* **1990,** *108*, 331-337.

(247) De Groot, C. J.; Van Luyn, M. J.; Van Dijk-Wolthuis, W. N.; Cadée, J. A.; Plantinga, J. A.; Den Otter, W.; Hennink, W. E. In Vitro Biocompatibility of Biodegradable Dextran-Based Hydrogels Tested with Human Fibroblasts. *Biomaterials* **2001,** *22*, 1197-1203.

(248) Zhai, M.; Xu, Y.; Zhou, B.; Jing, W. Keratin-Chitosan/n-ZnO Nanocomposite Hydrogel for Antimicrobial Treatment of Burn Wound Healing: Characterization and Biomedical Application. *J. Photochem. Photobiol. B: Biol.* **2018,** *180*, 253-258.

(249) Balakrishnan, B.; Mohanty, M.; Umashankar, P.; Jayakrishnan, A. Evaluation of an in Situ Forming Hydrogel Wound Dressing Based on Oxidized Alginate and Gelatin. *Biomaterials* **2005,** *26*, 6335-6342.

(250) Kerin, A.; Wisnom, M.; Adams, M. The Compressive Strength of Articular Cartilage. *Proc. Inst. Mech. Eng. H* **1998,** *212*, 273-280.

(251) Gao, G.; Du, G.; Sun, Y.; Fu, J. Self-Healable, Tough, and Ultrastretchable Nanocomposite Hydrogels Based on Reversible Polyacrylamide/Montmorillonite Adsorption. *ACS Appl. Mater. Interfaces* **2015,** *7*, 5029-5037.

(252) Haraguchi, K.; Takehisa, T. Nanocomposite Hydrogels: A Unique Organic-Inorganic Network Structure with Extraordinary Mechanical, Optical, and Swelling/De‐Swelling Properties. *Adv. Mater.* **2002,** *14*, 1120-1124.

(253) Fan, J.; Shi, Z.; Lian, M.; Li, H.; Yin, J. Mechanically Strong Graphene Oxide/Sodium Alginate/Polyacrylamide Nanocomposite Hydrogel with Improved Dye Adsorption Capacity. *J. Mater. Chem. A* **2013,** *1*, 7433-7443.

(254) Kamata, H.; Akagi, Y.; Kayasuga-Kariya, Y.; Chung, U.-i.; Sakai, T. "Nonswellable" Hydrogel without Mechanical Hysteresis. *Science* **2014,** *343*, 873-875.

(255) Guo, M.; Pitet, L. M.; Wyss, H. M.; Vos, M.; Dankers, P. Y.; Meijer, E. Tough Stimuli-Responsive Supramolecular Hydrogels with Hydrogen-Bonding Network Junctions. *J. Am. Chem. Soc.* **2014,** *136*, 6969-6977.

(256) Dai, X.; Zhang, Y.; Gao, L.; Bai, T.; Wang, W.; Cui, Y.; Liu, W. A Mechanically Strong, Highly Stable, Thermoplastic, and Self-Healable Supramolecular Polymer Hydrogel. *Adv. Mater.* **2015,** *27*, 3566-3571.

(257) Lin, P.; Ma, S.; Wang, X.; Zhou, F. Molecularly Engineered Dual‐Crosslinked Hydrogel with Ultrahigh Mechanical Strength, Toughness, and Good Self‐Recovery. *Adv. Mater.* **2015,** *27*, 2054-2059.

(258) Nakayama, A.; Kakugo, A.; Gong, J. P.; Osada, Y.; Takai, M.; Erata, T.; Kawano, S. High Mechanical Strength Double‐Network Hydrogel with Bacterial Cellulose. *Adv. Funct. Mater.* **2004,** *14*, 1124-1128.

(259) Webber, R. E.; Creton, C.; Brown, H. R.; Gong, J. P. Large Strain Hysteresis and Mullins Effect of Tough Double-Network Hydrogels. *Macromolecules* **2007,** *40*, 2919-2927.

(260) Akkaya, R.; Ulusoy, U. Adsorptive Features of Chitosan Entrapped in Polyacrylamide Hydrogel for Pb^{2+}, UO^{22+}, and Th^{4+}. *J. Hazard. Mater.* **2008,** *151*, 380-388.

(261) Mukhopadhyay, P.; Sarkar, K.; Bhattacharya, S.; Bhattacharyya, A.; Mishra, R.; Kundu, P. Ph Sensitive N-Succinyl Chitosan Grafted Polyacrylamide Hydrogel for Oral Insulin Delivery. *Carbohydr. Polym.* **2014,** *112*, 627-637.

(262) Mandal, B. B.; Kapoor, S.; Kundu, S. C. Silk Fibroin/Polyacrylamide Semi-Interpenetrating Network Hydrogels for Controlled Drug Release. *Biomaterials* **2009,** *30*, 2826-2836.

(263) von Buelow, S.; von Heimburg, D.; Pallua, N. Efficacy and Safety of Polyacrylamide Hydrogel for Facial Soft-Tissue Augmentation. *Plast. Reconstr. Surg.* **2005,** *116*, 1137-1146.

(264) Chen, Q.; Zhu, L.; Chen, H.; Yan, H.; Huang, L.; Yang, J.; Zheng, J. A Novel Design Strategy for Fully Physically Linked Double Network Hydrogels with Tough, Fatigue Resistant, and Self‐Healing Properties. *Adv. Funct. Mater.* **2015,** *25*, 1598-1607.

(265) Yuan, N.; Xu, L.; Wang, H.; Fu, Y.; Zhang, Z.; Liu, L.; Wang, C.; Zhao, J.; Rong, J. Dual Physically Cross-Linked Double Network Hydrogels with High Mechanical Strength, Fatigue Resistance, Notch-Insensitivity, and Self-Healing Properties. *ACS Appl. Mater. Interfaces* **2016,** *8*, 34034-34044.

(266) Deng, Y.; Hussain, I.; Kang, M.; Li, K.; Yao, F.; Liu, S.; Fu, G. Self-Recoverable and Mechanical-Reinforced Hydrogel Based on Hydrophobic Interaction with Self-Healable and Conductive Properties. *Chem. Eng. J.* **2018,** *353*, 900-910.

(267) Liu, S.; Li, L. Recoverable and Self-Healing Double Network Hydrogel Based on κ-Carrageenan. *ACS Appl. Mater. Interfaces* **2016,** *8*, 29749-29758.

(268) Liu, S.; Li, L. Ultrastretchable and Self-Healing Double-Network Hydrogel for 3D Printing and Strain Sensor. *ACS Appl. Mater. Interfaces* **2017,** *9*, 26429-26437.

(269) Chen, Q.; Zhu, L.; Zhao, C.; Wang, Q.; Zheng, J. A Robust, One‐Pot Synthesis of Highly Mechanical and Recoverable Double Network Hydrogels Using Thermoreversible Sol‐Gel Polysaccharide. *Adv. Mater.* **2013,** *25*, 4171-4176.

(270) Chen, Q.; Zhu, L.; Huang, L.; Chen, H.; Xu, K.; Tan, Y.; Wang, P.; Zheng, J. Fracture of the Physically Cross-Linked First Network in Hybrid Double Network Hydrogels. *Macromolecules* **2014,** *47*, 2140-2148.

(271) Chen, Q.; Wei, D.; Chen, H.; Zhu, L.; Jiao, C.; Liu, G.; Huang, L.; Yang, J.; Wang, L.; Zheng, J. Simultaneous Enhancement of Stiffness and Toughness in Hybrid Double-Network Hydrogels Via the First, Physically Linked Network. *Macromolecules* **2015,** *48*, 8003-8010.

(272) Miao, C.; Hamad, W. Y. Cellulose Reinforced Polymer Composites and Nanocomposites: A Critical Review. *Cellulose* **2013,** *20*, 2221-2262.

(273) Habibi, Y.; Lucia, L. A.; Rojas, O. J. Cellulose Nanocrystals: Chemistry, Self-Assembly, and Applications. *Chem. Rev.* **2010,** *110*, 3479-3500.

(274) Capadona, J. R.; Shanmuganathan, K.; Tyler, D. J.; Rowan, S. J.; Weder, C. Stimuli-Responsive Polymer Nanocomposites Inspired by the Sea Cucumber Dermis. *Science* **2008,** *319*, 1370-1374.

(275) Liu, J.; Tan, C. S. Y.; Yu, Z.; Lan, Y.; Abell, C.; Scherman, O. A. Biomimetic Supramolecular Polymer Networks Exhibiting Both Toughness and Self‐Recovery. *Adv. Mater.* **2017,** *29*, 1604951.

(276) Ge, J.; Yue, P.; Chi, J.; Liang, J.; Gao, X. Formation and Stability of Anthocyanins-Loaded Nanocomplexes Prepared with Chitosan Hydrochloride and Carboxymethyl Chitosan. *Food Hydrocoll.* **2018,** *74*, 23-31.

(277) Wahid, F.; Wang, H.-S.; Zhong, C.; Chu, L.-Q. Facile Fabrication of Moldable Antibacterial Carboxymethyl Chitosan Supramolecular Hydrogels Cross-Linked by Metal Ions Complexation. *Carbohydr. Polym.* **2017,** *165*, 455-461.

(278) Liu, M.; Min, L.; Zhu, C.; Rao, Z.; Liu, L.; Xu, W.; Luo, P.; Fan, L. Preparation, Characterization and Antioxidant Activity of Silk Peptides Grafted Carboxymethyl Chitosan. *Int. J. Biol. Macromol.* **2017,** *104*, 732-738.

(279) Xie, D.-Y.; Qian, D.; Song, F.; Wang, X.-L.; Wang, Y.-Z. A Fully Biobased Encapsulant Constructed of Soy Protein and Cellulose Nanocrystals for Flexible Electromechanical Sensing. *ACS Sustain. Chem. Eng.* **2017,** *5*, 7063-7070.

(280) Yuan, N.; Xu, L.; Zhang, L.; Ye, H.; Zhao, J.; Liu, Z.; Rong, J. Superior Hybrid Hydrogels of Polyacrylamide Enhanced by Bacterial Cellulose Nanofiber Clusters. *Mater. Sci. Eng. C.* **2016,** *67*, 221-230.

(281) Haafiz, M. M.; Hassan, A.; Khalil, H. A.; Khan, I.; Inuwa, I.; Islam, M. S.; Hossain, M. S.; Syakir, M.; Fazita, M. N. Bionanocomposite Based on Cellulose Nanowhisker from Oil Palm Biomass-Filled Poly (lactic acid). *Polym. Test.* **2015,** *48*, 133-139.

(282) Bhamra, T. S.; Tighe, B. J. Mechanical Properties of Contact Lenses: The Contribution of Measurement Techniques and Clinical Feedback to 50 Years of Materials Development. *Contact Lens and Anterior Eye* **2017,** *40*, 70-81.

(283) Bian, W.; Bursac, N. Engineered Skeletal Muscle Tissue Networks with Controllable Architecture. *Biomaterials* **2009,** *30*, 1401-1412.

(284) Hansen, E. N.; Adeli, B.; Kenyon, R.; Parvizi, J. Routine Use of Antibiotic Laden Bone Cement for Primary Total Knee Arthroplasty: Impact on Infecting Microbial Patterns and Resistance Profiles. *J Arthroplasty* **2014,** *29*, 1123-1127.

(285) Wang, M. O.; Etheridge, J. M.; Thompson, J. A.; Vorwald, C. E.; Dean, D.; Fisher, J. P. Evaluation of the in Vitro Cytotoxicity of Cross-Linked Biomaterials. *Biomacromolecules* **2013,** *14*, 1321-1329.

(286) Gehrmann, L.; Bielak, H.; Behr, M.; Itzel, F.; Lyko, S.; Simon, A.; Kunze, G.; Dopp, E.; Wagner, M.; Tuerk, J. (Anti-) Estrogenic and (Anti-) Androgenic Effects in Wastewater During Advanced Treatment: Comparison of Three in Vitro Bioassays. *Environ. Sci. Pollut. Res.* **2018,** *25*, 4094-4104.

(287) Zhu, W.; Peck, Y.; Iqbal, J.; Wang, D.-A. A Novel Dopa-Albumin Based Tissue Adhesive for Internal Medical Applications. *Biomaterials* **2017,** *147*, 99-115.

(288) Gibble, J.; Ness, P. Fibrin Glue: The Perfect Operative Sealant? *Transfusion* **1990,** *30*, 741-747.

(289) Waite, J. H. Nature's Underwater Adhesive Specialist. *Int. J. Adhes. Adhes.* **1987,** *7*, 9-14.

(290) Waite, J. H. Adhesion in Byssally Attached Bivalves. *Biological Reviews* **1983,** *58*, 209-231.

(291) Wu, D. Y.; Meure, S.; Solomon, D. Self-Healing Polymeric Materials: A Review of Recent Developments. *Prog. Polym. Sci.* **2008,** *33*, 479-522.

(292) Gaharwar, A. K.; Avery, R. K.; Assmann, A.; Paul, A.; McKinley, G. H.; Khademhosseini, A.; Olsen, B. D. Shear-Thinning Nanocomposite Hydrogels for the Treatment of Hemorrhage. *ACS Nano* **2014,** *8*, 9833-9842.

(293) Hoare, T. R.; Kohane, D. S. Hydrogels in Drug Delivery: Progress and Challenges. *Polymer* **2008,** *49*, 1993-2007.

(294) Zhu, Y.; Romain, C.; Williams, C. K. Sustainable Polymers from Renewable Resources. *Nature* **2016,** *540*, 354.

(295) Kumar, M. N. R. A Review of Chitin and Chitosan Applications. *React. Funct. Polym.* **2000,** *46*, 1-27.

(296) Dash, M.; Chiellini, F.; Ottenbrite, R. M.; Chiellini, E. Chitosan-a Versatile Semi-Synthetic Polymer in Biomedical Applications. *Prog. Polym. Sci.* **2011,** *36*, 981-1014.

(297) Anitha, A.; Sowmya, S.; Kumar, P. S.; Deepthi, S.; Chennazhi, K.; Ehrlich, H.; Tsurkan, M.; Jayakumar, R. Chitin and Chitosan in Selected Biomedical Applications. *Prog. Polym. Sci.* **2014,** *39*, 1644-1667.

(298) Grabovac, V.; Guggi, D.; Bernkop-Schnürch, A. Comparison of the Mucoadhesive Properties of Various Polymers. *Adv. Drug Del. Rev.* **2005,** *57*, 1713-1723.

(299) Xu, K.; Liu, Y.; Bu, S.; Wu, T.; Chang, Q.; Singh, G.; Cao, X.; Deng, C.; Li, B.; Luo, G. Egg Albumen as a Fast and Strong Medical Adhesive Glue. *Adv. Healthc. Mater.* **2017,** *6*, 1700132.

(300) Cudjoe, E.; Herbert, K. M.; Rowan, S. J. Strong, Rebondable, Dynamic Cross-Linked Cellulose Nanocrystal Polymer Nanocomposite Adhesives. *ACS Appl. Mater. Interfaces* **2018,** *10*, 30723–30731.

(301) Liu, H.; Li, C.; Wang, B.; Sui, X.; Wang, L.; Yan, X.; Xu, H.; Zhang, L.; Zhong, Y.; Mao, Z. Self-Healing and Injectable Polysaccharide Hydrogels with Tunable Mechanical Properties. *Cellulose* **2018,** *25*, 559-571.

(302) Shin, M.; Park, S.-G.; Oh, B.-C.; Kim, K.; Jo, S.; Lee, M. S.; Oh, S. S.; Hong, S.-H.; Shin, E.-C.; Kim, K.-S. Complete Prevention of Blood Loss with Self-Sealing Haemostatic Needles. *Nat. Mater.* **2017,** *16*, 147.

(303) Lu, D.; Wang, H.; Li, T. e.; Li, Y.; Dou, F.; Sun, S.; Guo, H.; Liao, S.; Yang, Z.; Wei, Q. Mussel-Inspired Thermoresponsive Polypeptide-Pluronic Copolymers for Versatile Surgical Adhesives and Hemostasis. *ACS Appl. Mater. Interfaces* **2017,** *9*, 16756-16766.

(304) Krogsgaard, M.; Behrens, M. A.; Pedersen, J. S.; Birkedal, H. Self-Healing Mussel-Inspired Multi-pH-Responsive Hydrogels. *Biomacromolecules* **2013,** *14*, 297-301.

(305) Murakami, Y.; Yokoyama, M.; Okano, T.; Nishida, H.; Tomizawa, Y.; Endo, M.; Kurosawa, H. A Novel Synthetic Tissue‐Adhesive Hydrogel Using a Crosslinkable Polymeric Micelle. *J. Biomed. Mater. Res. A* **2007,** *80*, 421-427.

(306) Zhang, H.; Bré, L. P.; Zhao, T.; Zheng, Y.; Newland, B.; Wang, W. Mussel-Inspired Hyperbranched Poly (amino ester) Polymer as Strong Wet Tissue Adhesive. *Biomaterials* **2014,** *35*, 711-719.

(307) Lee, C.; Shin, J.; Lee, J. S.; Byun, E.; Ryu, J. H.; Um, S. H.; Kim, D.-I.; Lee, H.; Cho, S.-W. Bioinspired, Calcium-Free Alginate Hydrogels with Tunable Physical and Mechanical Properties and Improved Biocompatibility. *Biomacromolecules* **2013,** *14*, 2004-2013.

(308) Chitocean Marine by-Product. http://www.chitocean.com/.

(309) Overview-Canada's Forests. Sustabinable Forest Management in Canada. https://www.sfmcanada.org/en/canada-s-forests.